DEVELOPMENT OF PASSIVE Q-SWITCHED AND MODE-LOCKED FIBER LASERS USING CARBON-BASED SATURABLE ABSORBERS

MOHD AFIQ BIN ISMAIL

THESIS SUBMITTED IN FULFILMENT OF THE REQUIREMENTS FOR THE DEGREE OF DOCTOR OF PHILOSOPHY

DEPARTMENT OF ELECTRICAL ENGINEERING

FACULTY OF ENGINEERING

UNIVERSITY OF MALAYA

KUALA LUMPUR

2015

UNIVERSITI MALAYA

ORIGINAL LITERARY WORK DECLARATION

Name of Candidate: MOHD AFIQ BIN ISMAIL (I.C/PassportNo:)

Registration/Matric No: KHA 110098

Name of Degree: DOCTOR OF PHILOSOPHY

Title of Project Paper/Research Report/Dissertation/Thesis ("this Work"):

DEVELOPMENT OF PASSIVE *Q*-SWITCHED AND MODE-LOCKED FIBER LASERS USING CARBON-BASED SATURABLE ABSORBERS

Field of Study: PULSED FIBER LASER

I do solemnly and sincerely declare that:

(1) I am the sole author/writer of this Work;
(2) This Work is original;
(3) Any use of any work in which copyright exists was done by way of fair dealing and for permitted purposes and any excerpt or extract from, or reference to or reproduction of any copyright work has been disclosed expressly and sufficiently and the title of the Work and its authorship have been acknowledged in this Work;
(4) I do not have any actual knowledge nor do I ought reasonably to know that the making of this work constitutes an infringement of any copyright work;
(5) I hereby assign all and every rights in the copyright to this Work to the University of Malaya ("UM"), who henceforth shall be owner of the copyright in this Work and that any reproduction or use in any form or by any means whatsoever is prohibited without the written consent of UM having been first had and obtained;
(6) I am fully aware that if in the course of making this Work I have infringed any copyright whether intentionally or otherwise, I may be subject to legal action or any other action as may be determined by UM.

Candidate's Signature Date

Subscribed and solemnly declared before,

Witness's Signature Date

Name:

Designation:

ABSTRACT

This thesis demonstrates various techniques for generating passive *Q*-switched and soliton mode-locked fiber laser using Erbium-doped fiber and Thulium-Bismuth doped fiber laser as gain mediums. The techniques for obtaining *Q*-switched and soliton mode-locked fiber laser includes nonlinear polarization rotation (NPR), semiconductor saturable absorber and carbon-based saturable absorber; specifically, single-walled carbon nanotubes (SWCNT), graphene and non-conductive graphene oxide paper.

A performance comparison is made between mode-locking using NPR technique and semiconductor saturable absorber. Based on the result, the semiconductor saturable absorber generates better quality of mode-locked pulse than using NPR.

A single-walled carbon nanotubes (SWCNT) in a sodium dedocyl sulfate (SDS) solution is deposited onto a fiber ferrule using dripping technique. Due to the high insertion loss, a *Q*-switched pulse ensues. After adding a 200 meter single mode fiber (SMF) into the laser cavity, the pulse energy is high enough to saturate the SWCNT saturable absorber. Consequently, a strong soliton mode-locked pulse is generated.

A simple and compact *Q*-switched fiber laser is demonstrated using graphene as saturable absorber. The saturable absorber is deposited onto a fiber ferrule by dripping a graphene solution and then is left to dry. A *Q*-switched pulse performances is compared between fiber lasers with one graphene saturable absorber and with two graphene saturable absorbers.

A highly ordered pyrolitic graphite (HOPG) is mechanically exfoliated using a scotch tape. The resulting graphene is transferred onto a fiber ferrule and inspected using Raman

spectroscopy. The transferred graphene has been identified as a single-layer. The ensuing pulsed fiber laser is a *Q*-switched, due to the large modulation depth of a single-layer graphene. A soliton mode-locked fiber laser is then generated by adding a 200 meter SMF. A soliton mode-locked is then demonstrated using Thulium-Bismuth doped fiber as gain medium.

In the sixth experiment, a novel non-conductive graphene oxide paper is introduced as a saturable absorber. The resulting soliton mode-locked fiber laser has a time-bandwidth product (TBP) value of 0.315. The mode-locked fiber laser has a low mode-locking threshold but the pulse gradually destroys the paper.

As a conclusion, this thesis shows the development of various techniques of generating *Q*-switched and mode-locked fiber, most notably using carbon based saturable absorber. This thesis also eases the focus on the saturable absorber, but instead, focusing on the cavity design to generate soliton mode-locked fiber lasers. Additionally, it introduces a non-conductive graphene oxide paper as a potential saturable absorber.

ABSTRAK

Tesis ini menunjukkan pelbagai teknik untuk menjana pasif *Q-switched* dan *soliton mode-locked* laser gentian optik menggunakan Erbium dan Thulium-Bismut sebagai medium aktif. Teknik-teknik untuk mendapatkan laser gentian optik *Q-switched* dan *soliton mode-locked* termasuk *nonlinear polarization rotation* (NPR), *saturable absorber* semikonduktor dan *saturable absorber* berasaskan karbon; terutamanya, *single-walled carbon nanotubes* (SWCNT), *graphene* dan kertas *graphene* oksida bukan konduktif.

Perbandingan prestasi dibuat antara *mode-locked* menggunakan teknik NPR dan *saturable absorber* semikonduktor. Berdasarkan keputusan, semikonduktor *saturable absorber* menjana *soliton mode-locked* dengan kualiti yang lebih baik daripada *soliton mode-locked* yang dijana menggunakan NPR.

Single-walled carbon nanotubes (SWCNT) dalam larutan natrium dedocyl sulfat (SDS) didepositkan ke atas permukaan simpai gentian optik menggunakan teknik titisan. Oleh kerana kehilangan sisipan yang tinggi, laser *Q-switched* terhasil. Selepas memasukkan 200 meter *single mode fiber* (SMF) ke dalam kaviti laser, tenaga nadi cukup tinggi untuk menepukan SWCNT *saturable absorber*. Oleh itu, *soliton mode-locked* yang kuat dihasilkan.

Q-switched laser gentian yang ringkas dan padat ditunjukkan menggunakan *graphene* sebagai *saturable absorber*. *Saturable absorber* didepositkan ke permukaan simpai gentian optik dengan menitis larutan *graphene* dan kemudian dibiarkan kering. Keupayaan laser denyut *Q-switched* dibandingkan antara laser gentian dengan satu *graphene saturable absorber* dan dengan dua *graphene saturable absorber*.

Highly ordered pyrolitic graphene (HOPG) dikupas secara mekanikal menggunakan pita pelekat. Dari situ, graphene dipindahkan ke satu simpai gentian optik dan diperiksa dengan menggunakan spektroskopi Raman. *Graphene* yang dipindahkan telah dikenal pasti sebagai lapisan tunggal. Oleh itu, terhasil laser denyut *Q-switched*, kerana kedalaman modulasi yang besar daripada satu lapisan *graphene*. *Soliton mode-locked* laser gentian optik kemudiannya dihasilkan dengan menambah SMF sepanjang 200 meter. Laser *soliton mode-locked* kemudian ditunjukkan menggunakan Thulium-Bismut sebagai medium aktif.

Dalam eksperimen yang ke-enam, kertas *graphene* oksida bukan konduktif yang novel diperkenalkan sebagai saturable absorber. Apa yang terhasil adalah laser gentian optik *soliton mode-locked* yang mempunyai nilai *time-bandwidth product* (TBP) 0.315. Laser gentian *mode-locked* mempunyai ambang yang rendah tetapi nadi secara beransur-ansur memusnahkan kertas.

Kesimpulannya, tesis ini menunjukkan perkembangan pelbagai teknik menjana *Q-swithced* dan *soliton mode-locked* laser, terutamanya menggunakan *saturable absorber* berasaskan karbon. Tesis ini juga mengurangkan penekanan pada *saturable absorber*, tetapi sebaliknya, memberi tumpuan kepada reka bentuk kaviti laser bagi menjana laser gentian optik *soliton mode-locked*. Selain itu, ia memperkenalkan kertas *graphene* oksida bukan konduktif sebagai *saturable absorber* yang berpotensi.

ACKNOWLEDGEMENTS

In the name of Allah, the Most Gracious, the Most Merciful.

"Nothing of me is original. I am the combined effort of everyone I've ever known."

-Chuck Palahniuk, Invisible Monsters

All praise be to Allah, for because of His Graciousness and Mercy, this thesis would not come into existence. I am extremely grateful for the assistance and guidance of Prof. Dr. Sulaiman Wadi Harun and Prof. Dr. Harith Ahmad. In truth, they've provided more than guidance and assistance, they've provided friendship when you need a friend and they've provided solace when you need a family.

I am also extremely grateful for the companionship and support of the other members of the lab. For because of their companionship and help, the lab is a home and the experiments are pleasures.

I am also extremely grateful for everything my family has given me.

To my beloved mother, Azizah Ab. Aziz, a thank you note would do you injustice. In spite of this, thank you. I could never ask for a better mother, ever.

To everyone and everything, thank you.

TABLE OF CONTENTS

Development of Passive *Q*-Switched and Mode-Locked Fiber Lasers Using Carbon-based Saturable Absorbers

LIST OF FIGURES

LIST OF TABLES

LIST OF SYMBOLS AND ABBREVIATIONS

EDFL	Erbium-Doped Fiber Laser
TBDFL	Thulium Bismuth-Doped Fiber Laser
SA	Saturable Absorber
NPR	Nonlinear Polarization Rotation
HOPG	Highly-Ordered Pyrolitic Graphite
CNT	Carbon Nanotubes
SWCNT	Single-Walled Carbon Nanotubes
MWCNT	Multi-Walled Carbon Nanotubes
GO	Graphene Oxide
dB	decibel
GVD	Group Velocity Dispersion
FWHM	Full-Width at Half Maximum
RFSA	Radio Frequency Spectrum Analyzer
TBP	Time-Bandwidth Product
GDD	Group Delay Dispersion
SPM	Self-Phase Modulation
PB	Photo Bleaching

PA	Photo-induced Absorption
TPA	Two-photon Absorption
3D	Three-Dimensional
1D	One-Dimensional
LASER	Light Amplification by Stimulated Emission of Radiation
MASER	Microwave Amplification by Stimulated Emission of Radiation
CW	Continues Wave
SAM	Self-Amplitude Modulation
n	refractive index
c	speed of light
ps	picosecond
fs	femtosecond
ASE	Amplified Spontaneous Emission
$h\nu$	photon energy
f_0	resonant frequency
ε	stored energy in the cavity
E_p	pulse energy
A	mode area
σ_L	emission cross section of the laser material

ΔR	modulation depth
η_{out}	output coupling efficiency
τ_p	pulse duration
T_R	cavity round-trip time
f_{rep}	repetition rate
g_0	small signal gain coefficient per resonator round trip
L_{tot}	total losses
L_p	parasitic losses
τ_L	upper-state lifetime of the gain medium
Δvg	gain linewidth
L	length
τ_{min}	shortest pulse duration obtainable
D_g	Gain dispersion
g	saturated amplitude coefficient
Ω_g	Half-Width at Half-Maximum of gain bandwidth in radians/second
Ω_m	loss modulation frequency in radians/second
2M	peak-to-peak modulation depth for amplitude loss coefficient
l	amplitude loss coefficient
ψ	phase shift

γA	absorber coefficient
q_0	maximum saturable amplitude loss coefficient
$I_{sat,A}$	saturation intensity
A_A	laser mode area in saturable absorber
D	dispersion parameter (half of the total group delay dispersion per cavity round trip)
δ_L	SPM coefficient
n_2	nonlinear refractive index
AL	laser mode area inside laser material
n_{eff}	effective refractive index
$\in_0$	permittivity in the vacuum
X^3	third-order nonlinear susceptibility
B_2	Group Velocity Dispersion
P_o	incident power
Ω	frequency of perturbation
K	wave number

CHAPTER 1

INTRODUCTION

1.1 BACKGROUND

The invention of laser in the 1960s has sparked various application in our lives. Fiber optics communication, built on the principles of laser and fiber optics, in particular, has enabled the transmission of information for thousands of kilometers. Lights pulses in fiber optics travel between continents, carrying signals, data, voice and visuals. In 2002, the fiber optic intercontinental networks spans 250,000 km of submarine communications cable, carrying 2.5 Tb of information per second.

Prior to the invention of laser, radio engineers use oscillators to generate the pure carrier frequency that are modulated onto input signal to be transmitted via radio waves. Radio oscillators drive antennas so they radiate coherent radio waves, which share that same frequency and stay in phase with one another. Therefore, in 1951, Bell Labs concluded that the only way to transmit information via light, is to have a coherent light source. Without coherent light source, Bell Labs pursued millimeter waveguide. Only in 1960, when laser was invented, Bell Labs and many others, took optical communication seriously.

However, the real stimulus in optical communication came in 1966. In 1966, Charles K. Kao and George Hockham from Standard Telecommunication Laboratories, U.K, reviewed the mode theory of electromagnetic propagation in a cylindrical dielectric structure. They identified a particular HE_{11} mode of a cladded glass fiber as a potential to perform

single-mode operation. By sufficiently reducing the core diameter, a single-mode operation can be achieved, therefore, removing the effects of multimode dispersion. The fiber optic of Kao and Hockham has a 1000 dB/km losses. As a comparison, coaxial cable only has losses of 5-10 dB/km. Today, a single-mode optical fiber, operating at 1550 nm, has an average loss of 0.22 dB/km. Charles K. Kao was awarded the Nobel Prize in Physics in 2009, for his *"groundbreaking achievements concerning the transmission of light in fibers for optical communication"*.

Carbon nanotube (CNT) and graphene are two carbon allotropes, which may bring another groundbreaking achievement in optics and communications. Carbon nanotube is a carbon allotrope with cylindrical nanostructure was discovered by Sumio Iijima of NEC Corporation. While Iijima was using a high resolution transmission electron microscope to study the soot made from by-products obtained during the synthesis of fullerenes by the electric discharge method, he noticed a molecular carbon tubes with diameters in the nanometer range. The carbon tubes were arranged in a seamless graphitic structure rolled up to form concentric cylinders. Electron microscopy reveals that each tube comprises of coaxial tubes of graphitic sheets, ranging in number from 2 up to 50. On each tube the carbon-atom hexagons are arranged in a helical fashion about the needle axis. The carbon nanotubes discovered by Iijima was later known as multi-walled carbon nanotube.

Graphene; a two-dimensional crystalline carbon allotrope, was discovered by Konstantin Novoselov and Andre Geim at the University of Manchester. Novoselov uses mechanical exfoliation technique (repeated peeling) of small mesas of highly oriented pyrolytic graphite. He managed to isolate a few, high quality layers of graphene films. The graphene layers were then transferred onto a 300 nm-thickness oxidized Si wafer. Under a microscope, Novoselov was able to identify the number of layer of a graphene film based on

the degree of contrast between the oxidized Si wafer and the graphene film itself. Further tests reveals that despite being several atoms thick, graphene shows remarkable electronic properties.

Due to their unique electronic and optical properties, carbon nanotube and graphene have attracted scientists to explore their potential. One of their optical properties is saturable absorption. Owing to their Pauli blocking property, carbon nanotube and graphene absorb light at low intensity, but transmit them at high intensity. Another interesting property is, carbon nanotube and graphene also are found to have fast relaxation time. Furthermore, the linear dispersion of the Dirac electrons ensures that graphene has an ultrawideband operability. As for carbon nanotube, because of the resonance energy depends on the tube diameter, carbon nanotube also has a wideband operability, although not as wide as graphene. In conclusion, saturable absorption, fast relaxation time and wideband operability are the factors that make carbon nanotube and graphene a suitable candidate for a saturable absorber.

Recently, many works have been focused on generating pulse laser for many industrial and communication applications through *Q*-switching and mode-locking approaches. Techniques of generating *Q*-switched or mode-locked laser are generally divided into two; active and passive. Active technique involved power operated modulator inside the cavity. Passive mode-locking, on the other hand, generates mode-lock or *Q*-switch pulse by using saturable absorber. A saturable absorber is a passive device that absorbs light when the intensity is low, but transmit them at high intensity. In other words, the degree of absorption of a saturable absorber decrease as light intensity increase. Nonlinear Polarization Rotation (NPR) is a passive mode-locking technique that particularly suits fiber laser. By using fiber compatible waveplates and polarizer, an artificial saturable absorber action can be achieved. A saturable absorber can also be made by using semiconductor materials. The semiconductor

materials must have a bandgap that corresponds to the operating wavelength. In the case of 1550 nm, GaInNAs and InGaAsP have been useful. However, compared to graphene and carbon nanotubes saturable absorber, semiconductor saturable absorber has limited operating bandwidth.

1.2 PROJECT MOTIVATIONS

Mode-locked and *Q*-switched fiber laser have become a useful tool in a number of applications. Since mode-locked laser was introduced in the 1960s with Nd:glass (Stetser & Demaria, 1966), it has come a long way from being in the picoseconds to attoseconds (Yoshitomi, Kobayashi, Takada, Kakehata, & Torizuka, 2005) pulsewidth. The trend in mode-locked laser is seems to be aiming at getting shorter pulse duration and higher repetition rate. On the other hand, journal publications in *Q*-switched laser appear to be aiming at acquiring higher peak power.

There are several techniques of generating mode-locked and *Q*-switched fiber laser. Using semiconductor saturable absorber is perhaps the most widespread and conventional technique. Semiconductor saturable absorber can be integrated into a fiber laser cavity, thus eliminate the need for free-space optics and other bulky element. Moreover, semiconductor saturable absorber aids in self-starting of the mode-locking and *Q*-switching processes. However, the weaknesses of semiconductor saturable absorber are that they are easily susceptible to damage and they have narrow operating bandwidth.

Other than semiconductor saturable absorber, the nonlinear polarization rotation (NPR) technique is also capable of generating a mode-locked and *Q*-switched fiber laser (Hideur et al., 2001). The most interesting saturable absorber materials perhaps come from

carbon nanotubes and graphene. These two carbon allotropes have saturable absorption properties, fast relaxation time and broadband operability. There are several ways of incorporating carbon nanotubes and graphene into a fiber laser cavity; film (Vittorio Scardaci et al., 2008; Z. Sun et al., 2010), optical deposition (Martinez, Fuse, Xu, & Yamashita, 2010), using tapered fiber (Song, Morimune, Set, & Yamashita, 2007), mechanical exfoliation (Martinez, Fuse, & Yamashita, 2011) and by spraying them onto a substrate (S. Yamashita et al., 2004).

Although the concepts of pulsed laser has been introduced in the in the 1960s, in Malaysia, the field of pulsed fiber laser is relatively unexplored. Best known to the author, the earliest published result on mode-lock fiber laser is in 2011 (Moghaddam, Harun, Akbari, & Ahmad, 2011). The author saw this as a challenge and a chance. The challenge of pursuing this field in Malaysia meant that help is scarce. However, if succeed, the author can establish himself as an expert in this field in Malaysia. This serves as one of the motivations for the author to pursue the work. The author also wish to add to the existing understanding of how mode-locked and *Q*-switched fiber laser work.

The author starts by comparing the performance of mode-lock fiber laser using nonlinear polarization rotation (NPR) technique and semiconductor saturable absorber. Published journals on mode-locked fiber laser rarely compare these two techniques. The author saw this as a start of his learning curve, to familiarize himself with mode-locked laser theory and experiment. Nonlinear polarization technique relies on Kerr effects to generate pulse while semiconductor saturable absorber, which uses the Pauli blocking property of a semiconductor materieal, is the easiest way to generate mode-locked fiber laser. Both techniques are distinctively different.

When carbon nanotubes and graphene become a popular subject in photonics, the author was interested to utilize them as saturable absorber. At that time, carbon nanotubes and graphene are mostly made into a film to be integrated into a fiber laser cavity. Although this technique is easy to imitate, the disadvantage is that there are no two films that are identical. Two research groups could be doing the same process of making a carbon nanotubes or graphene film, but the properties of these films will not be exactly the same. Therefore, it is difficult to identify the parameters that could define a working carbon nanotubes or graphene film. After an extensive reading and experimenting, the author understands that the design of mode-locked and *Q*-switched fiber laser does play a role. Since most of the carbon nanotubes and graphene saturable absorber are made of film, the author decided to take a different path. The author focuses on generating mode-lock pulse by changing the design of the fiber laser. The lack of understanding of the importance of design in initiating mode-lock fiber laser is another motivation for the author to explore the field. As a result, the author was successful in creating a new technique of saturable absorber called dripping technique.

Because the journal publications in carbon nanotubes and graphene film are too many, the author need to find something novel in-order to publish. By keeping abreast with the latest development in graphene processing, the author was able to identify a non-conductive graphene paper as a potential saturable absorber. The desire to be unique is another motivation for the author.

1.3 PROJECT OBJECTIVES

Based on the motivations, the project objectives are as follows:-

1. To utilize graphene and carbon nanotubes as saturable absorber
2. Provide understanding regarding passive mode-locked fiber laser using Nonlinear Polarization Rotation (NPR) and semiconductor saturable absorber
3. Present new technique and perspective in generating passive mode-locked fiber laser using carbon nanotubes and graphene as saturable absorber.
4. Generate a mode-locked fiber laser using a single-layer graphene (by mechanical exfoliation) saturable absorber
5. Explore other types of graphene saturable absorber.

1.4 ORIGINAL CONTRIBUTIONS

The major contributions of this research project are summarized as below:-

1. Provide understanding regarding mode-locked fiber laser using nonlinear polarization technique and semiconductor saturable absorber:

   The comparison between mode-lock fiber laser by nonlinear polarization rotation (NPR) technique and semiconductor saturable absorber is presented in Chapter 3. The result show that the pulsewidth differ significantly between these two techniques. Nonlinear polarization rotation technique gives a pulsewidth of 1.11 ps. By inserting a semiconductor saturable absorber in the cavity, the resultant pulsewidth is 0.58 ps. Kelly sidebands were prominent in the resultant optical spectrum of the nonlinear polarization rotation but less prominent in the optical spectrum of the semiconductor saturable absorber. Although both fiber lasers generate mode-locked pulse, the resultant pulsewidth and optical spectrum vary.

2. Created “dripping technique” for creating carbon nanotubes/graphene saturable absorber:

   Conventional techniques of incorporating a carbon nanotubes/graphene saturable absorber are film, optical deposition, mechanical exfoliation and spraying. All of these techniques have their own advantages and disadvantages. Of all the techniques, film is the most popular because of its simplicity. However, if the only concern is creating mode-locked fiber laser, dripping technique is much simpler than film. Dripping technique can not only create mode-locked pulse but also can create *Q*-

switched pulse. The advantage of dripping technique is that it eases the processing part, instead it focuses on forcing mode-locking through increasing the pulse energy.

3. Successfully generated *Q*-switched and mode-locked fiber lasers using a single-layer graphene by mechanical exfoliation:

   The author successfully isolate a single layer graphene by mechanical exfoliation to be used to generate *Q*-switched and mode-locked fiber lasers. Although there have been publications that use graphene saturable absorber by mechanical exfoliation, but best known to the author, those graphene saturable absorber were not a single-layer graphene. However, there was also a journal publication that uses a single-graphene layer film as saturable absorber. Two experiments in this thesis have confirmed that a single-layer graphene saturable absorber require a large pulse energy to be saturated. Consequently, the author was able to draw a conclusion that a single-layer graphene has a large modulation depth.

4. Introduced a non-conductive graphene oxide paper as saturable absorber:

   A non-conductive graphene oxide paper has been demonstrated by the author as capable of becoming a saturable absorber for generating mode-locked fiber laser. The advantage and disadvantage of a non-conductive graphene paper saturable absorber are also discussed.

1.5 OVERVIEW OF THESIS

This thesis consists of six main chapters. In these chapters, a comprehensive study of *Q*-switched and mode-locked fiber laser are presented. The current chapter is dedicated to a brief introduction to all aspects of pulsed fiber laser as well as motivations and contributions.

The second chapter gives more comprehensive details on the history of laser and fiber optics in addition to an approximate guide on laser principles and properties. This chapter emphasizes on *Q*-switch, mode-lock, carbon nanotubes and graphene. It gives detail description on *Q*-switch and mode-lock techniques, with uncomplicated mathematics. This chapter also elaborates on the photonics properties of carbon nanotubes, graphene and graphene oxide, which makes them suitable as saturable absorber.

Chapter three is divided into two main sub-chapters. In the first sub-chapter, it gives a comparison between a mode-locked fiber lasers generated using nonlinear polarization rotation technique and semiconductor saturable absorber. The first sub-chapter concludes with the performance comparison between the two techniques. In the second sub-chapter, it demonstrates a *Q*-switched and mode-locked by using carbon nanotubes. The carbon nanotubes saturable absorber is deposited onto a fiber ferrule using dripping technique. The second sub-chapter aims to prove that by altering the design of the fiber laser, a *Q*-switched and mode-locked operation can be achieved.

Chapter four is divided into two sub-chapters. The first sub-chapter describes a *Q*-switched fiber laser using graphene saturable absorbers. Two different saturable absorbers were fabricated by dripping a graphene solution onto fiber ferrule. Next, their performance is compared in-terms of their resultant *Q*-switched lasers. The second sub-chapter describes a single-layer graphene saturable absorber made by using mechanical exfoliation technique.

The single-layer graphene acts as a saturable absorber for generating *Q*-switched and mode-locked Erbium-doped fiber lasers. Another experiment in the second sub-chapter describes a Thulium Bismuth-doped fiber laser which also uses a single-layer graphene as saturable absorber. Chapter four have several conclusions; a compact and simple *Q*-switched fiber laser can be made using graphene as saturable absorber, a single-layer graphene has a very large modulation depth and graphene saturable absorber also works in the 2μm region.

Chapter five demonstrate the usability of a non-conductive graphene oxide paper as saturable absorber. It also discussed on the advantages and disadvantages of graphene oxide paper as saturable absorber.

Chapter six provide the summary, analysis and review of all results obtained in the study. Chapter six ends with modest recommendations for future works. Attached in the appendix are selected published journal papers during the duration of the study.

Below is the list of publications and conferences during the study is conducted.

Publications

1. **Ismail, M. A.**, Tan, S. J., Shahabuddin, N. S., Harun, S. W., Arof, H., & Ahmad, H. (2012). Performance comparison of mode-locked erbium-doped fiber laser with nonlinear polarization rotation and saturable absorber approaches. *Chinese Physics Letters*, *29*(5), 054216.
2. Harun, S. W., **Ismail, M. A.**, Ahmad, F., Ismail, M. F., Nor, R. M., Zulkepely, N. R., & Ahmad, H. (2012). A *Q*-switched erbium-doped fiber laser with a carbon nanotube based saturable absorber. *Chinese Physics Letters*, *29*(11), 114202.

3. **Ismail, M. A.**, Harun, S. W., Zulkepely, N. R., Nor, R. M., Ahmad, F., & Ahmad, H. (2012). Nanosecond soliton pulse generation by mode-locked erbium-doped fiber laser using single-walled carbon-nanotube-based saturable absorber. *Applied Optics*, *51*(36), 8621-8624.
4. **Ismail, M. A.**, Ahmad, F., Harun, S. W., Arof, H., & Ahmad, H. (2013). A *Q*-switched erbium-doped fiber laser with a graphene saturable absorber. *Laser Physics Letters*, *10*(2).
5. Harun, S., **Ismail, M.**, & Ahmad, H. (2014). Soliton Mode-Locked Erbium-Doped Fiber Laser Using Non-Conductive Graphene Oxide Paper.

Conference

1. Harun, S. W., Ahmad, H., **Ismail, M. A.**, & Ahmad, F. (2013, April). *Q*-switched and soliton pulses generation based on carbon nanotubes saturable absorber. In *Electronics, Communications and Photonics Conference (SIECPC), 2013 Saudi International* (pp. 1-4). IEEE.

CHAPTER 2

LITERATURE REVIEW

2.1 HISTORY OF LASER AND FIBER OPTICS

2.1.1 LASER

The idea of Light Amplification by Stimulated Emission of Radiation (LASER) was first mooted by Albert Einstein in 1916. In his "On the Quantum Theory of Radiation" (1917), Einstein proposed hypotheses on the radiative exchange of energy; the interaction between matter and radiation by means of absorption and emission. Kramers (1924) further expanded the theory by Einstein, introducing the term "negative dispersion", which exhibit resemblance to Einstein's "negative absorption". Kopfermann and Ladenburg (1928); Ladenburg (1928) later provide experimental evidence by pumping neon gas with high current densities. In his doctoral thesis, Fabrikant (1940), suggested that population inversion should lead to light wave amplification. However, Fabrikant did not pursue the theory. Owing to the wartime invention of microwave, Lamb and Retherford (1947), have found a way to excite molecular hydrogen from the ground state, thus, making inverse population a reality.

Gordon, Zeiger, and Townes (1955) have successfully created Microwave Amplification Stimulated Emission of Radiation (MASER) which is the predecessor of laser. The device can be utilized as a microwave amplifier, microwave spectrometer and an oscillator. Maser "utilizes a molecular beam in which molecules in the excited state of a microwave transition is selected. Interaction between these excited molecules and a

microwave field produces additional radiation and hence amplification by stimulated emission". The oscillation of maser also proved theoretically and experimentally monochromatic. Many scientist who are working in maser wish to extend the amplification and stimulation in the infrared and optical region. In 1957, Ali Javan (1957) published a paper describing a theory on three-level maser.

The breakthrough in laser was achieved by Maiman (1960). He had created the first laser by using ruby crystal as gain medium. In his experiment, a 1-cm ruby crystal was irradiated with high power flash lamp. The result is a narrow emission at the wavelength at 6929 Å. After that, more lasers were created such as helium-neon (A. Javan, Bennett, & Herriott, 1961), semiconductor (Hall, 1963) and CO_2 (Patel, 1965). Table 2.1 summarizes the milestones in laser fundamentals and technology.

Table 2.1 : Milestones in laser (Reproduced from Renk, 2012)

Year	Name; Milestone
1865	James Clerk Maxwell; Maxwell's equations
1888	Heinrich Hertz; generation and detection of electromagnetic waves
1900	Max Planck; quantization radiation in a cavity
1905	Albert Einstein; quantization of radiation
1905	Niels Bohr; quantization of the energy states of an atom
1917	Albert Einstein; interaction of radiation with an atom; spontaneous and and stimulated emission

Table 2.1, continued : Milestones in laser (Reproduced from Renk, 2012)

1923	Henryk A. Kramers; influence of stimulated emission on the refractive index of atomic gasses containing excited atoms.
1928	Rudolf Ladenburg; observation of an influence of stimulated emission on the refractive index of a gas of neon atoms excited by electron collisions in a gas discharge
1951	Charles H. Townes; idea of a maser
1954	Charles H. Townes; ammonia maser (frequency 23.870 GHz, wavelength 1.25 cm). Nicolai Basov, Aleksandr Prokhorov; idea of a maser in parallel to the development in the U.S.A and realization of ammonia laser.
1956	Nicolaas Bloembergen; proposal of the three-level maser (leading to solid state masers in other laboratories
1958	Arthur L. Schawlow, Charles H. Townes; proposal of infrared and optical masers (lasers) including the formulation of the threshold condition of laser oscillation. Aleksandr Prokhorov; general description of the principle of optical masers (lasers)
1959	Nicolai Basov; proposal of semiconductor laser
1960	Theodore Maiman; ruby laser (694 nm)
1960	Ali Javan; helium-neon laser (1.15 μm, later 633 nm)
1961	L. F. Johnson, K. Nassau; neodymium YAG laser
1962	Robert N. Hall; semiconductor laser.
1963	Herbert Kroemer; proposal of heterostructure laser.

Table 2.1, continued : Milestones in laser (Reproduced from Renk, 2012)

1964	C. Kumar N. Patel; carbon dioxide laser W. Bridges; argon ion laser
1966	Peter P. Sorokin and Fritz P. Schäfer; dye laser
1968	William T. Silfvast; metal vapor laser
1975	Basov; excimer laser
1977	John Madey, Luis Elias and coworkers; free-electron laser.
1979	J.C. Walling; alexandrite laser (first tunable solid state laser)
1982	P. Moulton; titanium-sapphire laser.
1991	M. Haase and coworkers; green diode laser (based on ZnSe)
1994	Federico Capasso, Jèrome Faist and coworkers; quantum cascade laser
1997	Shunji Nakamura and coworkers; blue diode laser (based on GaN)

2.1.2 FIBER OPTICS

In the 1950's and 1960's the demand for more resources to accommodate the ever increasing telephone calls meant that new alternative need to replace the existing copper cables. In United Kingdom, the number of installed telephones and the annual number of telephone calls doubled every five or six years over the entire period of 1915-1960. The number of telephone calls made in 1950 was 3000 million, in 1960; 4000 million, in 1970; 9000 million and in 1980; 19 000 million. Moreover, the telephone system is also used to carry data, video and other services. The existing network has difficulty in keeping up with the telephone demand and subsequently, other alternatives to copper wire and electric current

are being considered. Other means of communication such as microwave cables, microwave line-of-sight, satellites and over-moded millimeter waveguide were also taken into account.

The possibility of using an optical carrier wave for telecommunication began soon after the invention of the laser in 1960. The amount of information can be modulated onto a carrier wave is roughly proportional to its frequency. A shift from microwave to light waves could increase the carrier frequency by a factor of 100 000 and even if the bandwidth can be increased by in practice by 100 or 1000 times, the improvement is enormous compared to the existing system. Many laboratories began researching in optical communication as a possible source of carrier waves.

In a publication by Kao and Hockham (1966), they discussed in some detail the idea of communication by optical fibers. They reviewed the mode theory of electromagnetic propagation in a cylindrical dielectric surface and identified the HE_{11} mode of a cladded glass fiber as a potential. By reducing the core diameter sufficiently, single-mode operation can be achieved, and the effects of multimode dispersion can be removed. Studied were also made of bending loss, radiation loss, launching of modes and jointing. Since the publication of the paper, many works had started on single-mode and multimode optical fibers. At the University of Southampton, where the work on multimode fiber started, the loss was brought down to 140 dB/km compared to the thousands of dB/km in earlier fiber bundles. In Standard Telecommunication Laboratories (STL), the work on single-mode fiber indicated that its inherent loss was probably below than 20 dB/km target.

Kapron, Keck, and Maurer (1970) at Corning Glass Works, USA, reported the fabrication of a single-mode fiber with 20 dB/km transmission loss. Many laboratories across the world suddenly became interested in fiber optics. Kapron et al. (1970) deposited a thin layer of titanium on the internal surface of a silica tube which had then been collapsed

and drawn into a fiber. Although the resultant fiber was too brittle to be of use, it had proved that it is possible to develop a cladded fibers based on silica. Previously, it was thought too difficult to find a cladding glass compatible with silica core. The solution presented by Corning made it possible to use the silica glass as fiber optics core and cladding. By inserting oxides; TiO_2, GeO_2, P_2O_3, Al_2O_3, the refractive index can be increased while B_2O_3 and F lower it.

With the problem with choosing the glasses for core and cladding has been tackled, laboratories around the world are concentrating on the process of manufacturing optical fiber. Bell Telephone Laboratories introduces a process which they called "modified chemical vapor deposition" or MCVD. Other variations of the process include outside deposition on mandrel (Corning, USA),plasma chemical-vapor deposition (Philips, The Netherlands) (Kuppers, Lydtin, & Meijer, 1977) and vapor axial deposition (Izawa, Kobayashi, Sudo, & Hanawa, 1977).

Fiber lasers have unique advantages. One of the advantages is that the pump radiation, which is introduced by a dichroic mirror or coupler, is limit to the core, as is the laser radiation generated so that there is very efficient coupling between the lasing ions, pump radiation and lasing radiation. Furthermore, the pump intensity is very high due to small core diameter. Fiber lasers are small, lightweight, robust, flexible and do not require optical bench stability. They can also be easily mode-locked, *Q*-switched, line narrowed and up-converted. Fiber lasers are replacing conventional lasers in many applications (Gambling, 2000).

2.2 LASER PRINCIPLES AND PROPERTIES

Lasers are generated by means of population inversion. An active medium is excited by pumping and the resultant radiation oscillates inside the laser resonator. After a threshold is reached, some percentage of the radiation are coupled out to produce laser. What makes the difference between a laser and a light bulb is the temporal and spatial coherence. A light bulb emits uncorrelated wave trains into all spatial directions, while a laser generates coherent waves and the waves can have a high directionality. Moreover, a laser can emit a coherent continuous wave (cw) or a coherent pulse train. Fig. 2.1 gives an illustration to explain the difference between cw laser, femtosecond (fs) laser and light bulb.

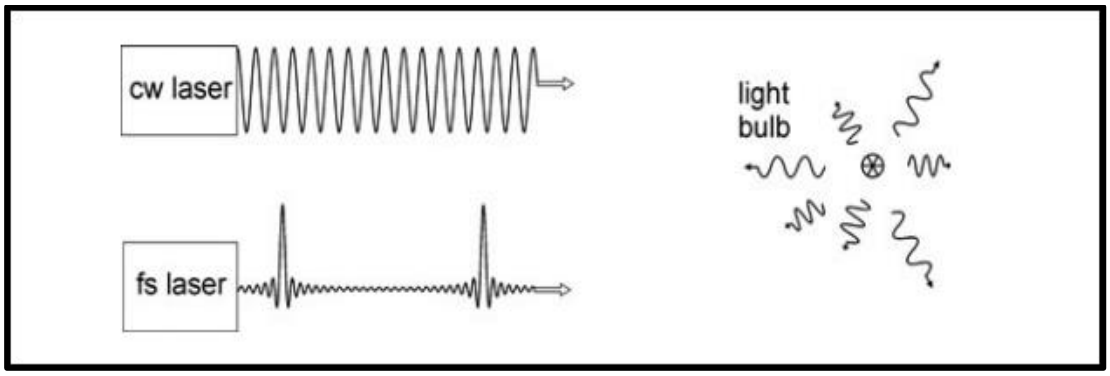

Fig. 2.1: cw laser, femtosecond (fs) laser and light bulb (Reproduced from Renk, 2012).

2.2.1 LASER PRINCIPLES

Laser radiation is generated by stimulated emission transition in an active medium (gain medium). By pumping the active medium, spontaneous photons are generated, which are then amplified to form an amplified spontaneous emission (ASE) as they propagate through the entire active medium. Fig. 2.2 depicts a simple laser setup, which consists of a laser resonator, active medium and pump system. Laser resonator consist of two mirrors; one

mirror with high reflectivity and the other has partial reflectivity. The mirror with partial reflectivity serves as the output coupler. The two mirrors also allow for feedback process inside the laser resonator. The ASE oscillates in the cavity to generate laser and a small portion of the oscillating light inside an optical resonator is coupled out as laser output at one of the mirror.

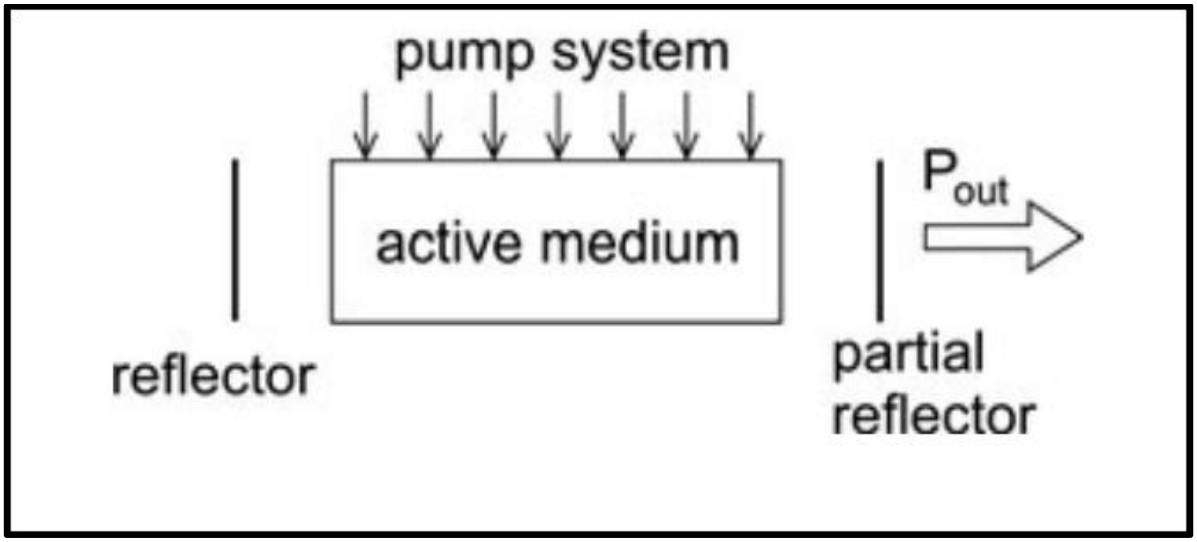

Fig. 2.2: A laser (Reproduced from Renk, 2012)

In order to create a stimulated emission, population inversion process is necessary. To simplify the concept of population inversion, we introduce a two discrete energy levels; E_1 and E_2. The following notation are also introduced to describe the process of population inversion.

- Level 2 (energy E_2) is the upper energy level.
- Level 1 (energy E_1) is the lower energy level.
- $E_{21} = E_2 - E_1$ = energy difference between the two levels
- N_2 = population of level 2 = density of excited two-level atomic systems
- N_1 = population of level 1 = density of the unexcited two-level atomic systems

Monochromatic electromagnetic radiation with frequency *v* can interact with two-level atomic system if Bohr's energy-frequency relation

$$hv = E_{21} = E_2 - E_1 \qquad \text{(Eq. 2.1)}$$

is satisfied. If the photon energy *hv* of the photons of the radiation field is equal to the energy difference E_{21}.

Two processes involve in the generation of laser; absorption and stimulated emission. In absorption, an electron absorb an incident photon; thus acquiring energy to jump from Level 1 to Level 2. When an electron decays from Level 2 to Level 1, without external influence, emitting a photon, the process is called spontaneous emission. Spontaneous emission emits photon that has no phase relation with other photons. When $N_2 < N_1$, the active medium behaves as an absorber. When an incident photon, with energy of E_{21} enters the active medium, the photon will be absorb. This process will provide energy that will enable the electron in Level 1 to be promoted to Level 2 ($1 \rightarrow 2$ transition). By pumping, we can raise the number of excited electrons. When $N_2 > N_1$, the condition is referred to as population inversion. Population inversion is essential for generating laser. When population inversion is reached, another photon with energy of E_{21} incident on the active medium, there is a finite probability that this wave will force the electron to undergo $2 \rightarrow 1$ transition. In this case, the energy E_{21} will be delivered in the form of electromagnetic wave that adds to the incident one. This phenomena is called stimulated emission. Stimulated emission will produce emission with the same phase and direction as the incident one (Renk, 2012; Svelto & Hanna, 1976; Träger, 2007).

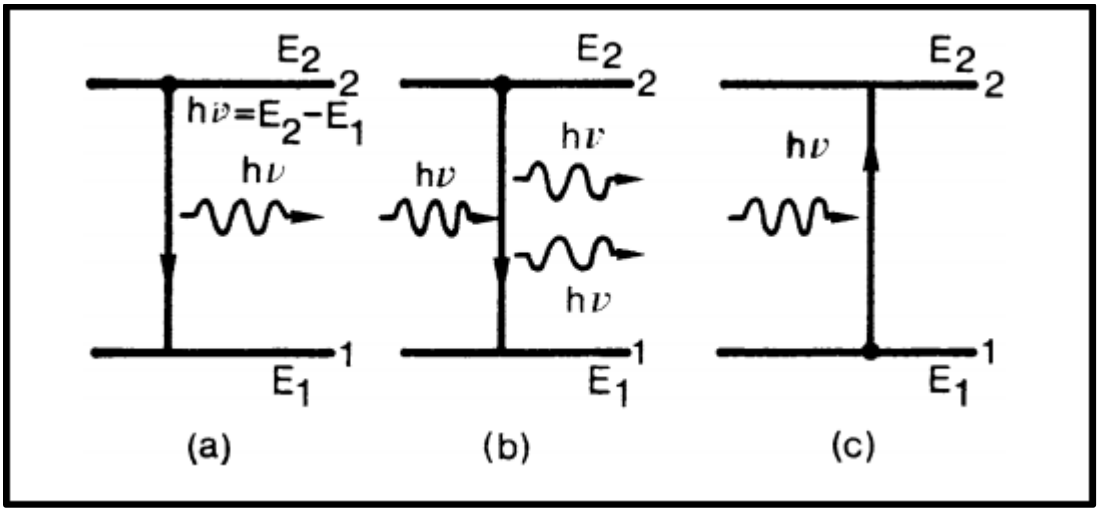

Fig. 2.3: Schematic illustration of (a) spontaneous emission, (b) stimulated emission, (c) absorption (Reproduced from Svelto & Hanna, 1976).

2.2.2 LASER PROPERTIES

Laser radiation has four main properties, namely; monochromaticity, coherence, directionality and brightness that separate them from ordinary light. Monochromaticity implies that the linewidth of a laser beam is much smaller compared with normal light. Because laser comes from one precise atomic transition, by the law of physics, a laser can only emit one wavelength (Svelto & Hanna, 1976; Träger, 2007). In general, coherence means that the laser waves are "in-phase" with one another at every point and time. Coherence in laser can be divided into spatial and temporal coherence. Spatial coherence means that there are correlation between different places (but not along the same wavefront. Correlation between the waves at one place at different times, or along the path of a beam at a single instant, are called temporal coherence (Lasers, 2014).

Referring to Fig. 2.2, directionality of a laser beam are due to the construction of the laser resonator. An active medium is placed inside an open optical resonator and therefore,

the laser beam preferentially occurs in the direction orthogonal to the two mirrors (Träger, 2007). The brightness of laser beam originated from the directionality and the capability of laser to emit a high optical power in a small solid angle of space. For the purpose of comparison, a laser of moderate power (e.g., a few miliwatts) has a brightness level of several orders of magnitude greater than the brightest conventional sources (Träger, 2007).

A fifth property of a laser may be considered; i.e. short time duration. Short time duration refers to the ability of lasers to produce short light pulse (Svelto & Hanna, 1976). By mode-locking a laser, it is possible to produce light pulses which has duration that is roughly equal to the inverse of the linewidth of the $2 \rightarrow 1$ transition. The pulse duration of a laser may be generated down to ~ 10 fs. The property of short time duration, which implies energy concentration in time, can, in a sense, be considered to be the counterpart of monochromaticity, which implies energy concentration in wavelength. Although lasers, in principle, be made monochromatic, only lasers with a broad linewidth, i.e. solid state or liquid lasers, may produce pulses of very short time duration (Svelto & Hanna, 1976).

2.3 *Q*-SWITCHING

The history of *Q*-switching starts as early as 1961, when Hellwarth (1961) foresee that a laser could emit short pulses if the loss of an optical resonator is rapidly switched from a high to low value. Collins and Kisliuk (1962) and McClung and Hellwarth (1962) produced the experimental evidence a year later. By controlling the *Q*-factor (quality factor) of a laser resonator, *Q*-switching allows the generation of laser pulses of short duration (from nanosecond to picosecond range) and high peak power. *Q*-factor is a dimensionless parameter that describes the measure of the strength of the damping of its oscillations. The *Q*-factor is given by

$$Q = \frac{2\pi f_0 \varepsilon}{P} \qquad \text{(Eq. 2.2)}$$

where f_o is the resonant frequency, ε is the stored energy in the cavity and $P = -\frac{dE}{dt}$ is the power dissipated. If the *Q* factor of a laser's cavity is abruptly changed from a low value to a high value, the laser will emit a pulse of light that is much more intense than the lasers's continues output. This technique is called *Q*-switching.

The operating mechanism is as follows; a shutter is introduced inside the laser cavity. When the shutter is closed, laser action cannot occur and the population inversion can reach a value far in excess of the laser threshold population. At this condition, the laser resonator loss is said to be high. The laser resonator switched to low loss when the shutter is now opened suddenly. At this moment laser will have a gain that greatly exceeds the losses, thus the stored energy will be released as a short burst of intense light (Ursula Keller, 2004). *Q*-switched operation can happen in a single- or in multiple- longitudinal cavity modes. However, in multiple-longitudinal cavity modes, the operation leads to mode-beating effects and increased timing jitter, making it less attractive (Spühler et al., 1999). There are two types of *Q*-switching; active and passive.

2.3.1 ACTIVE *Q*-SWITCHING

Active *Q*-switching uses modulation devices that change the cavity losses in accordance with an external control signal. Active *Q*-switches are divided into three categories; mechanical, electro-optical and acousto-optics. Mechanical *Q*-switches have been develop based on rotational, oscillatory or translational motion of optical components. The similarity between these techniques is that they inhibit laser action during the pump cycle by either blocking the light path, causing a mirror misalignment, or reducing the reflectivity of

one of the resonator mirrors. Towards the end of the pump pulse, when maximum energy has been stored in the active medium, a high *Q*-condition is established and a *Q*-switch pulse is emitted from the laser. Among the techniques is a spinning reflector technique that involves simply rotating one of the two resonant cavity reflectors so that parallelism of the reflectors occurs for only a brief instant in time. Rotating-mirror devices are simple and inexpensive. They are insensitive to polarization and consequently; birefringence effects. Therefore, more energy from the laser can be extracted under certain conditions as compared to electro-optic *Q*-switches. Fig. 2.4 depicts the diagram of a ruby laser using a spinning prism *Q*-switch.

2.3.1.1 MECHANICAL *Q*-SWITCHES

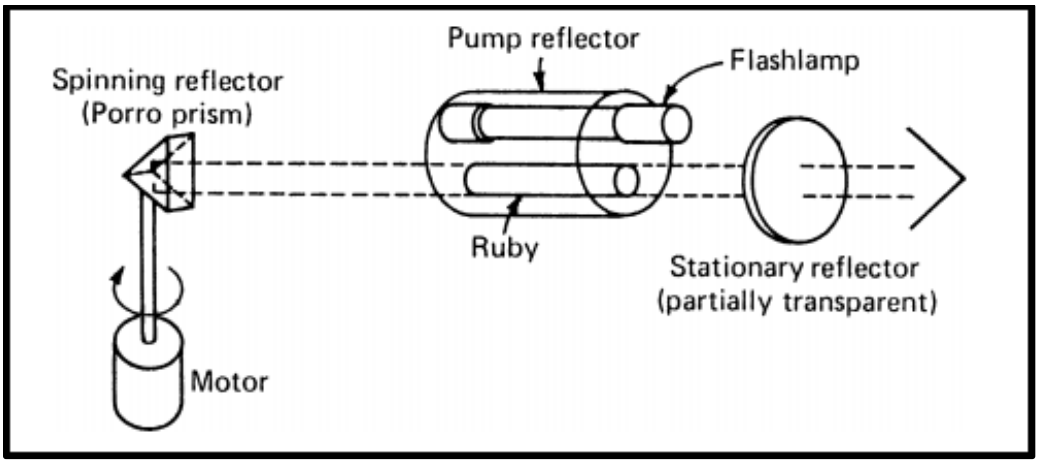

Fig. 2.4: Diagram of a ruby laser using a spinning prism *Q*-switch (Reproduced from Koechner, 2006).

However, the mechanical *Q*-switches suffer from the tendency to emit multiple pulses. Furthermore, the devices are very noisy and they require frequent maintenance due to the relatively short lifetime of the bearings. Because of these disadvantages, the rotating prism *Q*-switch has been replaced for visible and near infrared lasers by the acousto-optic *Q*-switch in cw pumped lasers (Koechner, 2006).

2.3.1.2 ELECTRO-OPTICAL *Q*-SWITCHES

An electronically controlled optical shutters can also be designed by exploiting the electro-optic effect in crystals or liquids. The electro-optic element becomes birefringent when exposed to an external field. Birefringence is also known as “double refraction” due to the nature of the medium that split the incident of light into two orthogonal direction. The two rays are known as “fast” and “slow” axes, both have different index of refraction. The two rays will travel at the same path, but different velocities. Therefore, the electro-optic effect causes a phase difference between the two beams. After travelling inside the medium, the combination of the two components will result in either elliptical, circular, or linearly polarized beam, depending on the voltage applied. For *Q*-switch operation, only two particular voltages leading to a quarter-wave and half-wave retardation are of interest as depicted in Fig. 2.5.

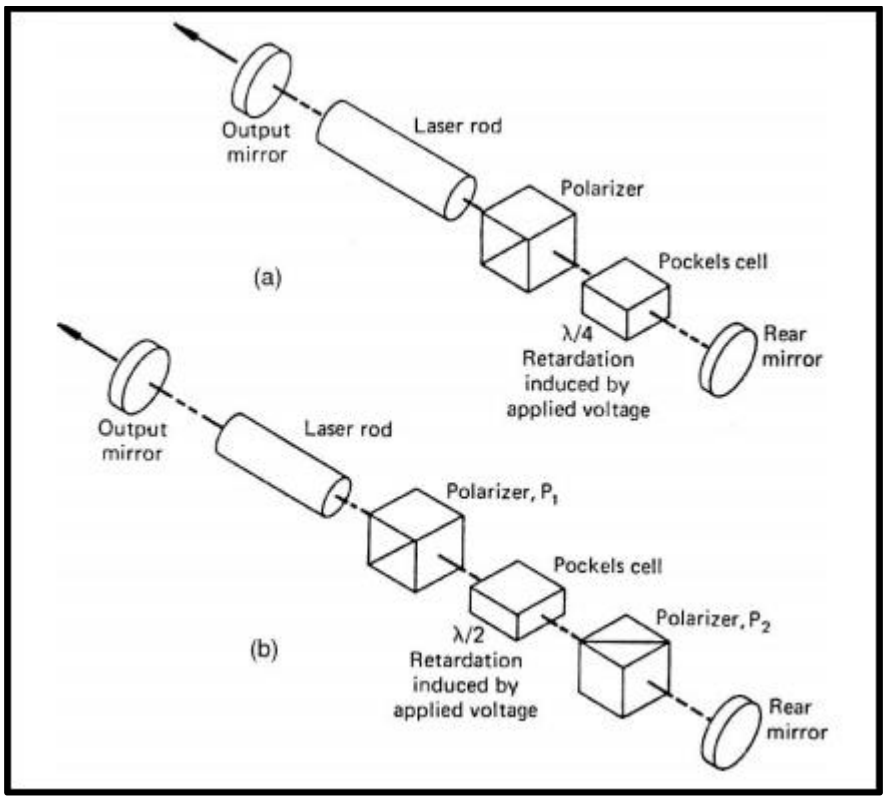

Fig. 2.5: Electro-optic *Q*-switch operated at (a) quarter-wave and (b) half-wave retardation voltage (Reproduced from Koechner, 2006)

In Fig. 2.5(a), the incident linearly polarized light is circular polarized after passing the cell and in Fig. 2.5(b) the output beam is linearly polarized, however, the plane of polarization has been rotated 90°. The Pockels cell contain an electro-optic crystal in which a refractive index change is produced by an externally applied electric field.

The operating mechanism of Fig. 2.5(a) is as follows; during the pump pulse, a voltage $V_{1/4}$ is applied to the electro-optic cell so that the linearly polarized light passed through the polarized is circularly polarized. After being reflected at the mirror, the radiation again passed through the electro-optic cell and then undergoes another λ/4 retardation, becoming linearly polarized but rotated 90° to its original direction. This radiation is ejected from the laser cavity by the polarizer, therefore preventing optical feedback. Towards the end

of the pump pulse, the voltage on the cell is switched off, allowing the polarizer-cell combination to pass a linearly polarized beam without loss. Oscillation within the cavity will build up, and after a short delay, a *Q*-switch pulse will be emitted from the cavity.

For Fig. 2.5(b), the electric voltage must first be applied to the cell to transmit the beam. The cell is located between two crossed polarizers. As before, polarizer P_1, which is located between the laser rod and the cell, is not required if the active medium emit polarized beam. During the pump pulse, with no voltage applied to the cell, the cavity *Q* is at a minimum due to crossed polarizers. At the end of the pump a voltage $V_{1/2}$ is applied to the cell, which causes a 90° rotation of the incoming beam. The light is therefore transmitted by the second polarizer P_2 and the cell, where it experience another 90° rotation. Light travelling toward the polarized P_1 has experience a 180° rotation and afterwards can be transmitted through P_1 (Koechner, 2006).

2.3.1.3 ACOUSTO-OPTIC *Q*-SWITCHES

Acoustic *Q*-switches introduces ultrasonic wave into a block of transparent optical material, usually fused silica. By switching on the acoustic field, a fraction of the energy of the main beam is diffracted out of the resonator, therefore introducing loss mechanism that prevents lase action. When the acoustic field is switched off, the full transmission of *Q*-switch cell can be reestablish and laser pulse is created. Fig. 2.6 below depicts an active *Q*-switch laser using acousto-optic *Q*-switch. The fused silica block to which a crystalline quartz of an $LiNbO_3$ transducer is bonded. Both transducer and the fused silica interface includes vacuum-deposited electrodes to allow for electrical connections. The ultrasonic wave is introduced into the *Q*-switch block by the piezoelectric transducer that converts electrical energy into ultrasonic energy. The laser returns to the high *Q*-state by switching off the driving voltage

to the transducer. Without ultrasonic wave propagating through the fused silica block, it returns to its usual state of high optical transmission and a *Q*-switch pulse is emitted.

Virtually all acousto-optic *Q*-switches a single-pass device. The acoustic wave generated by the transducer is absorbed after travelling across the interaction region. The role of the absorber is to prevent reflected acoustical waves from interfering with the incident light beam (Koechner, 2006).

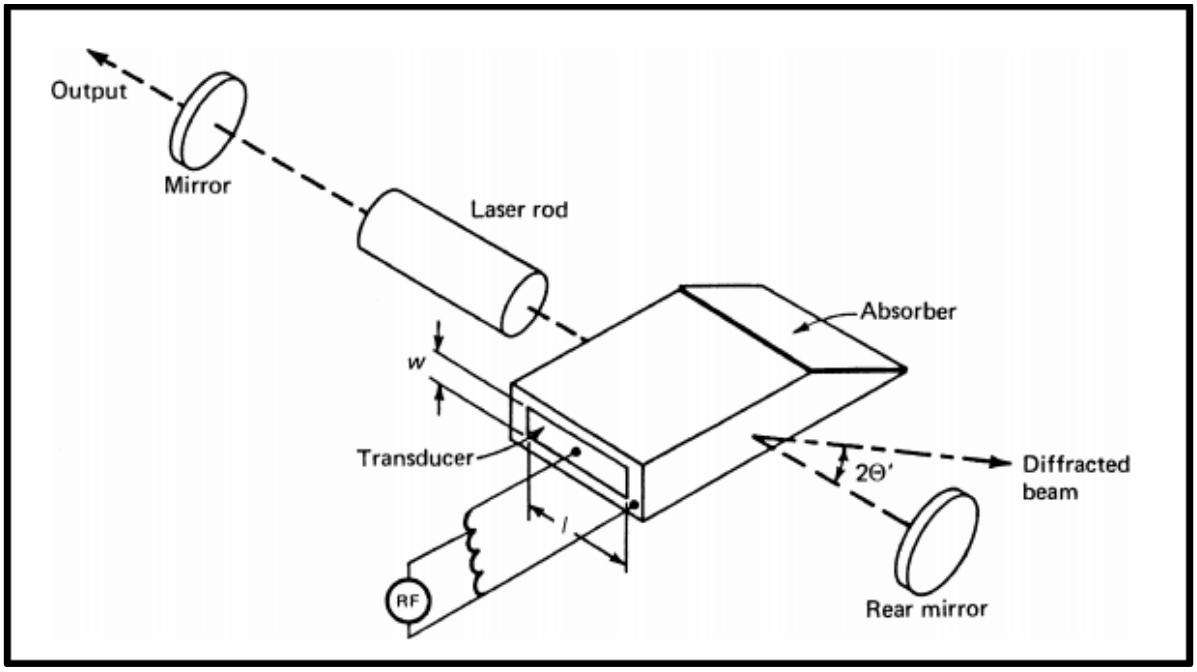

Fig. 2.6: Acousto-optic *Q*-switch (Reproduced from Koechner, 2006)

2.3.2 PASSIVE *Q*-SWITCHING

Besides active techniques, *Q*-switching pulse can also be realized using a passive techniques. In passive *Q*-switching, the laser resonator consist of a gain medium and an absorbing medium that acts as a saturable absorber. As the gain medium is pumped, it builds up stored energy and emit photons. After many round-trips, the photon flux begin to see gain, fixed loss and saturable loss in the absorber. If the gain medium saturates before the saturable

absorber, the photon flux may build, but the laser will not emit a short and intense pulse. On the contrary, if the photon flux builds up to a level that saturates the absorber before the gain medium saturates, the laser resonator will see a rapid reduction in the intracavity loss and the laser *Q*-switches and therefore, will emit a short and intense pulse of light (Welford, 2003).

Taking the Semiconductor Saturable Absorber Mirror (SESAM) model from Spühler et al. (1999) and J. Zayhowski and P. Kelley (1991). The SESAM model is flexible and applicable in wide parameter range. From the model, we show the pulse energy, pulse duration and repetition rate of a *Q*-switch laser as shown by Table 2.2 below.

Table 2.2 : *Q*-switch parameters taken from the SESAM model (Spühler et al., 1999; J. Zayhowski & P. Kelley, 1991).

Parameter	Model	Description	Eq.
Pulse energy	$E_p \approx \frac{h\nu_L}{\sigma_L} A\Delta R\eta_{out}$	$h\nu_L$: photon energy at lasing wavelength A: mode area σ_L: emission cross section of the laser material ΔR: modulation depth η_{out}: output coupling efficiency	(Eq. 2.3)
Pulse duration	$\tau_p \approx \frac{3.52T_R}{\Delta R}$	T_R : cavity round-trip time. ΔR : modulation depth	(Eq. 2.4)
Repetition rate	$f_{rep} \approx \frac{g_0 - (L_{tot} + \Delta R)}{2\Delta R\tau_L}$	g_0: small signal gain coefficient per resonator round trip L_{tot}: total losses ($L_{tot} = T_{out} + L_p$; where T_{out} is output coupler, L_p is parasitic losses) ΔR: modulation depth τ_L : upper-state lifetime of the gain medium	(Eq. 2.5)

From the SESAM model, *Q*-switch pulse can be divided into four phases, as depicted in Fig. 2.7. In phase 1, the absorber is in its unsaturated state. A pulse can start to develop as soon as the pump has lifted the gain more than $l + q_0$. The intracavity power, *P*, grows slowly, starting from spontaneous emission noise, until the intensity is enough to saturate the absorber. In phase 2, the SESAM is fully saturated. The power grows more quickly until the gain starts to deplete. The pulse maximum is reached when the net gain is zero. In phase 3, the gain further deplete. The net gain becomes negative and the intracavity power decays. Nevertheless, the pulse still extracts significant energy in this phase. In phase 4, after the absorber recovers (the absorber recovers more quickly than the gain), and the gain has to be pumped to the threshold level again before phase 1 of the subsequent pulse can start (Spühler et al., 1999).

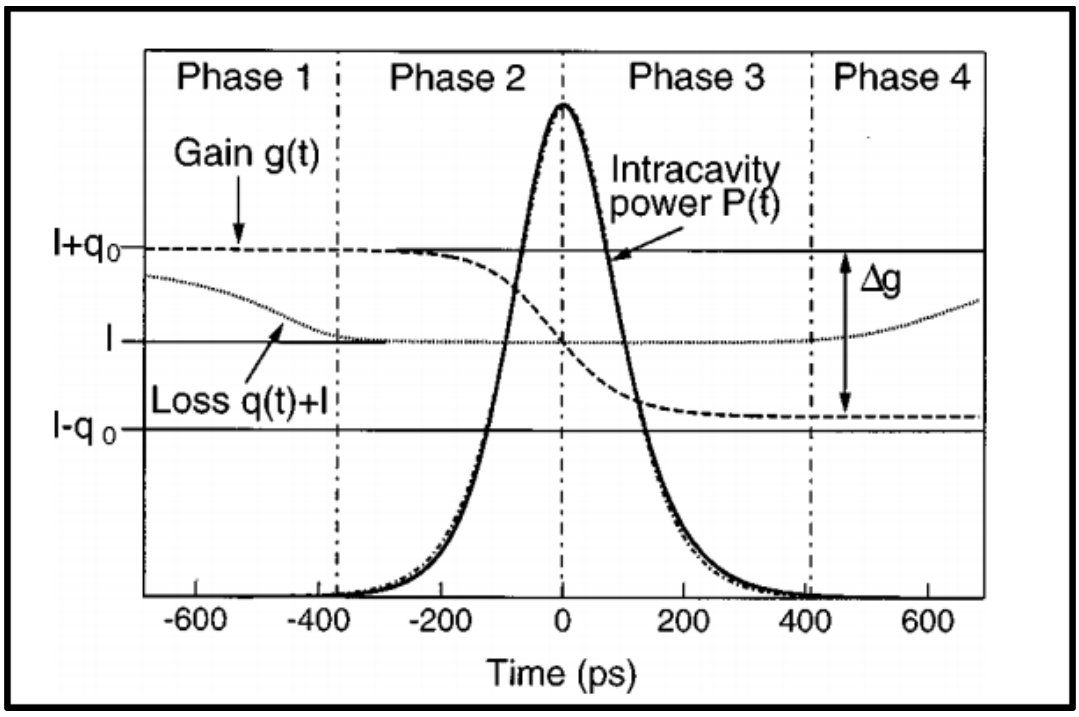

Fig. 2.7: Evolution of power, loss and gain on the time scale of the pulse width. As soon as the gain exceeds the loss, the power grows. The peak of the *Q*-switched pulse is reached when the gain equals the total losses. g: saturated intensity gain coefficient per resonator round-trip, l : total nonsaturable intensity loss coefficient per resonator round-trip, q : saturable intensity loss coefficient of the saturable absorber per cavity round-trip, q_0: unbleached intensity loss coefficient of the saturable absorber per cavity round-trip, Δg : gain coefficient between the beginning and the end of the pulse, (Reproduced from Spühler et al., 1999).

2.4 MODE-LOCKING

Mode-locking is a technique of generating an ultra-short pulse laser. The pulse duration range can be between picoseconds (10^{-12} s) to femtoseconds (10^{-15} s). An ultra-short pulse can be generated when all the longitudinal modes have a fixed phase relationship, hence

the term “mode-locking” or “phase-locking”. The fixed phase superposition between all the modes oscillating inside a laser cavity causes the cw laser to be transformed into a train of pulse. The number of longitudinal mode that can simultaneously lase are dependent on the gain linewidth, Δv_g and the frequency separation between modes. Under sufficiently strong pumping, we can expect that the number of modes oscillating in the cavity is given by

$$M = \frac{\Delta v_g}{c/2L} = \frac{2L}{c}\Delta v_g \qquad \text{(Eq. 2.6)}$$

where c is the speed of light and L is the length of a linear cavity. The shortest pulse duration that we can expect to obtain by a given gain linewidth is

$$\tau_{min} = \tau_M = \frac{2L}{cM} = \frac{1}{v_g} \qquad \text{(Eq. 2.7)}$$

From (Eq. 2.7), we can conclude that the shortest pulse that can be obtained is a reciprocal of gain linewidth (in Hz) (Milonni & Eberly, 2010).

Mode-locking involves periodic modulation of resonator loss. Once the resonator loss is modulated, all the laser modes phase can easily be fixed. The difference between cw and mode-locked laser is depicted in Fig. 2.8. In the time domain, a mode-locked laser generates an equidistance pulse train, with T_R defines the round-trip time of a pulse inside the laser cavity while pulse duration is indicated by τ_p. In the frequency domain, this resulted in a phase-locked frequency comb with constant mode-spacing, v_R, that is equal to $1/T_R$. The pulse duration, τ_p, is inversely proportional to the spectral width of the envelope of the frequency comb, Δv_p. Mode-locking in a frequency domain is homogeneously broadened laser normally lases at one axial mode at the peak of the gain. However, the periodic loss modulation transfers additional energy phase-locked to adjacent mode separated by the modulation frequency. This modulation frequency is normally referring to the cavity round-

trip frequency. Consequently, the frequency comb has an equidistance axial modes locked together in phase forms a short pulse in the time domain.

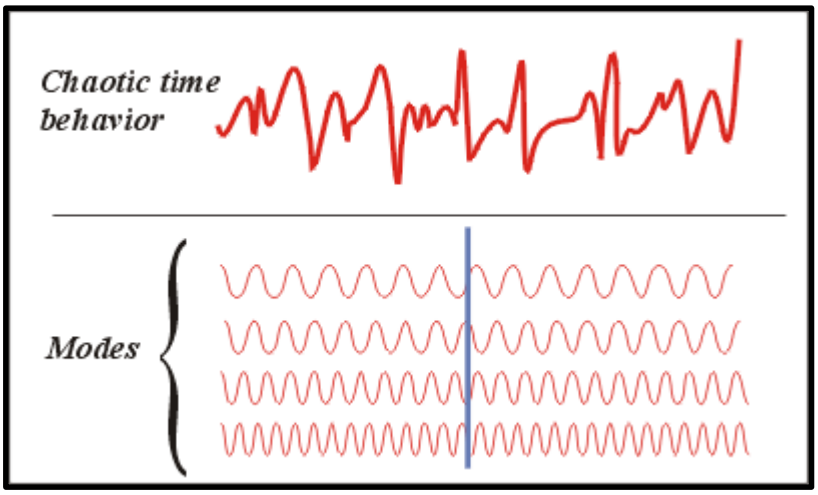

(a) CW

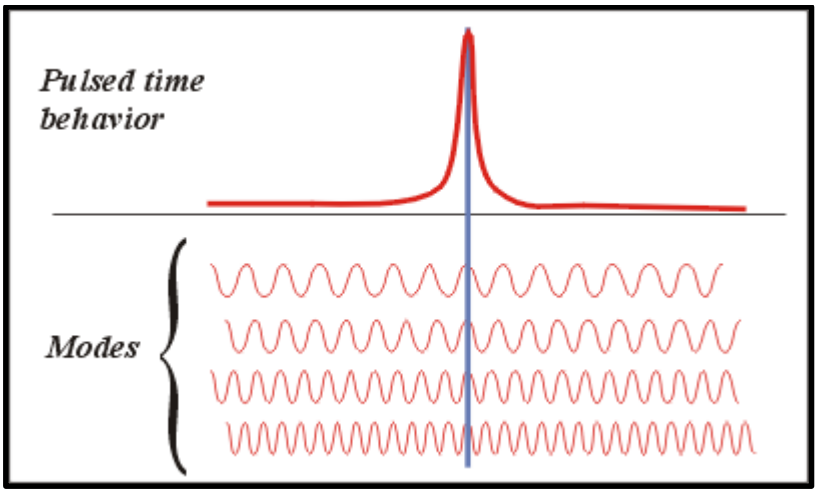

(b) Mode-locking

Fig. 2.8: CW (a) and mode-locking (b) operation in laser (Reproduced from International, 2013)

Mode-locked pulse in the time and frequency domains are depicted in Fig. 2.9 and Fig. 2.10, respectively (Ursula Keller, 2004). The fundamental repetition rate of a mode-lock laser is determined by its cavity length, as shown in the equations below.

$$\text{Repetition rate (for linear cavity)} = \frac{\text{c}}{2\text{Ln}} \qquad \text{(Eq. 2.8)}$$

$$\text{Repetition rate (for ring cavity)} = \frac{\text{c}}{\text{Ln}} \qquad \text{(Eq. 2.9)}$$

(Eq. 2.8) and (Eq. 2.9) are used for calculating fundamental repetition rate for linear and ring cavity respectively. *L*, *c* and *n* denotes the length of the cavity, speed of light and refractive index respectively. As the round-trip time, T_R, is the inverse of repetition rate, therefore, T_R is

$$T_R = \frac{\text{Ln (for ring cavity)or 2Ln (for linear cavity)}}{\text{c}} \qquad \text{(Eq. 2.10)}$$

depending on the cavity type. Under certain conditions, the repetition rate can be some integer multiple of the fundamental repetition rate. In this case, it is called harmonic mode-locking.

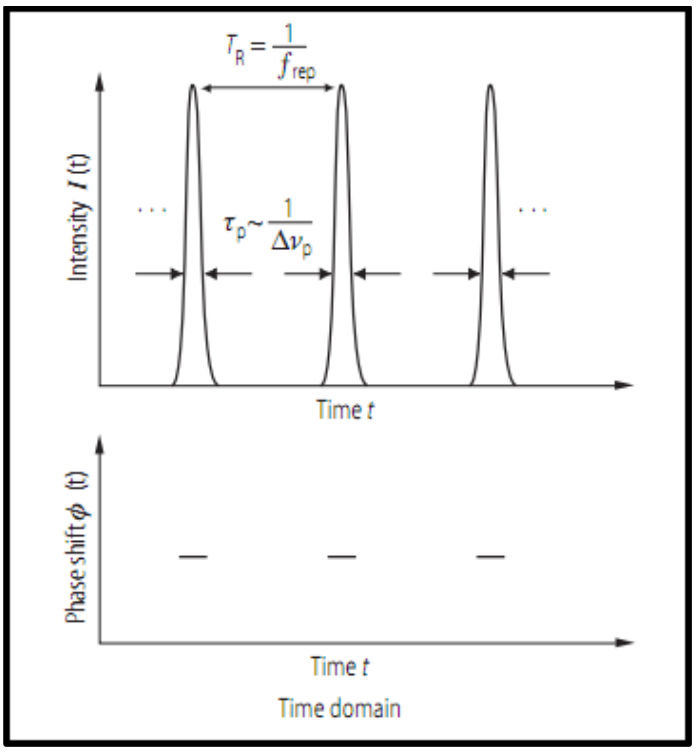

Fig. 2.9: Mode-locked pulse in the time domain (Reproduced from Ursula Keller, 2004)

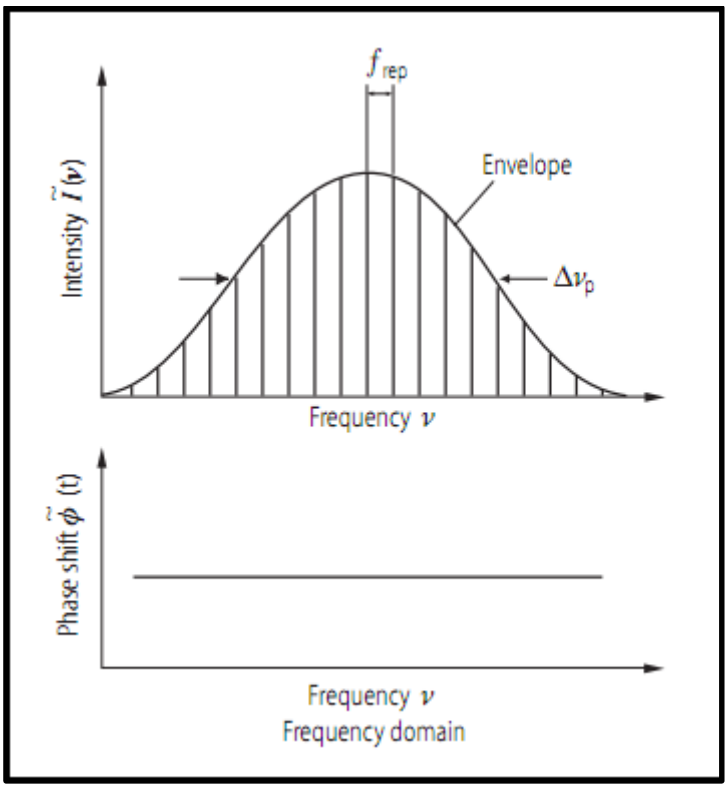

Fig. 2.10: Mode-locked pulse in the frequency domain (Reproduced from Ursula Keller, 2004).

Mode-locking techniques can be divided into three categories; active, passive and hybrid. Hybrid mode-locking combines active and passive mode-locking. Hybrid mode-locking uses active modulator to start mode-locking while passive mode-locking is utilized for pulse shaping. For the sake of brevity, here, we will only explain on active and passive mode-locking as shown in Fig. 2.11. Haus's master equation, introduced by Herman A. Haus (Duling III & Duling, 2006) is based on linearized different operators that described the temporal evolution of a pulse envelope inside the laser cavity. The master equation can be understood as a generalization of the nonlinear Schrödinger equation. It is often used to study soliton pulse phenomena. In general, the Haus master equation is a useful tool mainly for the study of simple situation, where analytical solution can be obtained, and as the basis for some

dynamic models (Ursula Keller, 2004; D. R. Paschotta, 2013). Table 2.3 summarize the linearized operators that model the change in the pulse envelope for each element in the laser cavity and their defining equations.

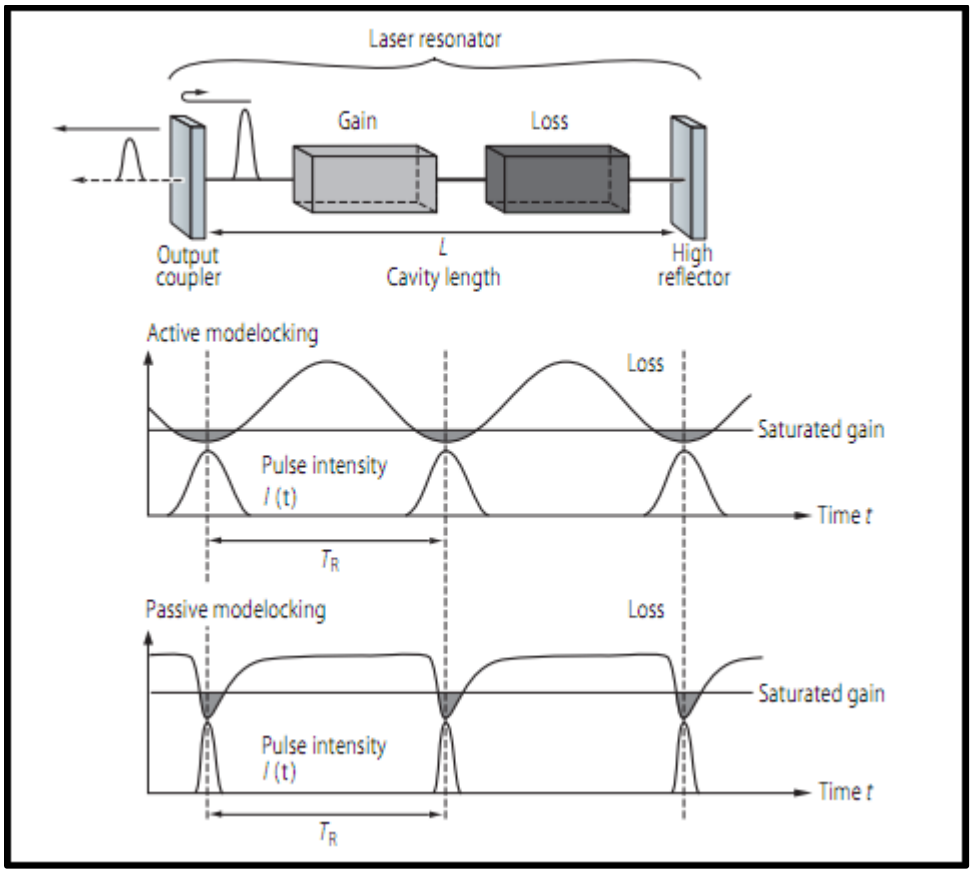

Fig. 2.11: Schematic laser cavity setup for active and passive mode-locking (Reproduced from Ursula Keller, 2004)

2.4.1 HAUS MASTER EQUATIONS

Haus's master equations are show in Table 2.3. Table 2.4 summarizes the predicted pulsewidth for different mode-locking techniques.

Table 2.3: Linearized operators that model the change in the pulse envelope *A(t)* for each element in the laser cavity and their defining equations. The pulse envelope is normalized such that $|A(z,t)^2|$ is the pulse power *P(z, t)* (Reproduced from Ursula Keller, 2004).

Laser cavity element	Linearized operator	New constants	Constant	Eq.
Gain	$\Delta A \approx \left[g + D_g \frac{\partial^2}{\partial t^2}\right]$	$D_g \equiv \frac{g}{\Omega_g^2}$	D_g: gain dispersion g: saturated amplitude coefficient Ω_g: HWHM of gain bandwidth in radians/seconds	(Eq. 2.11)
Loss modulator	$\Delta A \approx -M_s t^2 A$	$M_s \equiv \frac{M\omega_m^2}{2}$	ω_m: loss modulation frequency in radians/second $2M$: peak-to-peak modulation depth for amplitude loss coefficient	(Eq. 2.12)
Constant loss	$\Delta A \approx -lA$		l: amplitude loss coefficient	(Eq. 2.13)
Constant phase shift	$\Delta A \approx i\psi A$		ψ: phase shift	(Eq. 2.14)

Table 2.3, continued: Linearized operators that model the change in the pulse envelope *A(t)* for each element in the laser cavity and their defining equations. The pulse envelope is normalized such that $|A(z,t)^2|$ is the pulse power *P(z, t)* (Reproduced from Ursula Keller, 2004).

Fast saturable absorber	$\Delta A \approx \gamma_A \lvert A \rvert^2 A$	$\gamma_A \equiv \frac{q_0}{I_{sat,A} A_A}$	γ_A: absorber coefficient q_0: maximum saturable amplitude loss coefficient $I_{sat,A}$: saturation intensity A_A: laser mode area in saturable absorber	(Eq. 2.15)
Dispersion : 2nd order	$\Delta A \approx iD \frac{\delta^2}{\delta t^2} A$	$D \equiv \frac{1}{2} k_n^{"} z$	*D*: dispersion parameter (half of the total group delay dispersion per cavity round trip) $k_n^{"} = \frac{d^2 k_n}{d\omega^2}$	(Eq. 2.16)
Self-phase modulation (SPM)	$\Delta A \approx -i\delta_L \lvert A \rvert^2 A$	$\delta_L \equiv \frac{k n_2 z}{A_L}$	δ_L: SPM coefficient n_2: nonlinear refractive index A_L: laser mode area inside laser material (Note: Here we assume that the dominant SPM occurs in the laser material. Then *z* is equal to 2 times the length of the laser crystal in a standing-wave cavity)	(Eq. 2.17)

Table 2.4: Predicted pulse duration for the different mode-locking technique (Reproduced from Ursula Keller, 2004)

Mode-locking (ML) technique	Pulse shape	Pulse duration (FWHM)	Eq.
Active ML: Amplitude loss modulation	Gaussian	$\tau_p = 1.66 \times \sqrt[4]{\frac{D_g}{M_s}} = 1.66 \times \sqrt[4]{\frac{2g}{M}} \sqrt{\frac{1}{\omega_m \Omega_g}}$	(Eq. 2.18)
Passive ML: Slow saturable absorber and dynamic gain saturation	Soliton	$\tau_p \approx 1.76 \times \frac{4}{\pi} \frac{1}{\Delta v_g}$	(Eq. 2.19)
Slow saturable absorber for solid-state lasers and strongly saturated absorbers (S > 3)	Numerical simulations	$\tau_{p,min} \approx \frac{1.5}{\Delta v_g} \sqrt{\frac{g}{\Delta R}}$ for $\tau_A \leq 30\ \tau_p$	(Eq. 2.20)
Fast saturable absorber (FSA)	Soliton	$\tau_p = 1.76\ \frac{4D_g}{\gamma_A E_p}$ only transform-limited soliton pulses for a well-defined intracavity group delay dispersion (assuming negligible higher order dispersion): $\lvert D \rvert / \delta_L / \gamma_A$	(Eq. 2.21)

Table 2.4, continued: Predicted pulse duration for the different mode-locking technique (Reproduced from Ursula Keller, 2004).

Fully saturated ideal fast saturable absorber		$\tau_{p,min} = \frac{1.76}{\Omega_g}\sqrt{\frac{2g}{q_0}} \approx \frac{1.12}{\Delta v_g}\sqrt{\frac{g}{\Delta R}}$ for $\frac{\lvert D\rvert}{\delta_L} = \frac{D_g}{\gamma_A}$	(Eq. 2.22)
Soliton mode-locking	Soliton	$\tau_p = 1.76\,\frac{2\lvert D\rvert}{\delta_L E_p}$ Transform-limited soliton pulses for the total intracavity group delay dispersion (assuming negligible higher-order dispersion) $\tau_{p,min} = 1.7627\left(\frac{1}{\sqrt{6}\Omega_g}\right)^{3/4}{\phi_s}^{-1/8}\left(\frac{\tau_A g^{3/2}}{q_0}\right)^{1/4} \approx 0.45\left(\frac{1}{\Delta v_g}\right)^{3/4}\left(\frac{\tau_A}{\Delta R}\right)^{1/4}\frac{g^{3/8}}{{\phi_s}^{1/8}}$	(Eq. 2.23) (Eq. 2.24)

2.4.2 ACTIVE MODE-LOCKING

Active mode-locking is a mode-locking technique that achieved by using an active device that modulates the loss or the phase inside the laser resonator as indicated in Fig. 2.12. Acousto-optic modulator (Hunsperger, 2009) and electro-optic modulator (Maldonado, 1995) are among the widely used modulator for mode-locking. If the modulation frequency, ω_m, is synchronized with the cavity round-trip, T_R, ultrashort pulse can be generated. In other words, if the modulation frequency matches the frequency separation of the axial modes of the resonator. Therefore,

$$\omega_m = \frac{2\pi}{T_R} = \frac{\pi c}{n_{eff} L_o} \qquad \text{(Eq. 2.25)}$$

where, c is the speed of light, n_{eff} is the effective refractive index and L_o is the cavity length. However, (Eq. 2.25) is only applicable to linear cavity, as depicted in Fig. 2.12. For a ring cavity, has travelling waves as eigenmodes. In the case of ring cavity, the frequency separation of the axial modes is $2\pi c/(n_{eff} L_o)$.

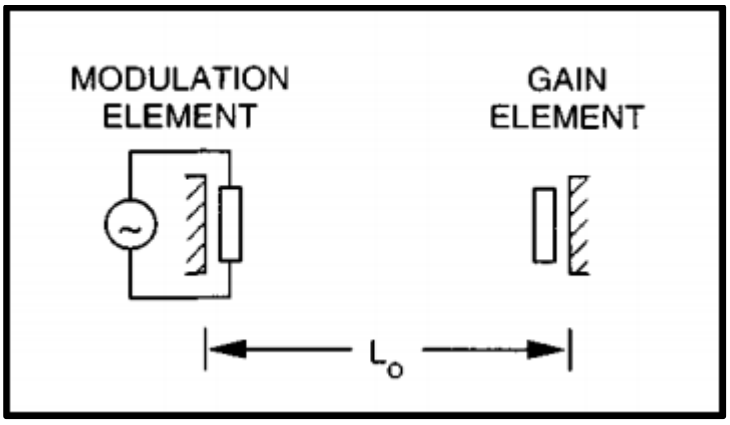

Fig. 2.12: Active mode-locking concept (Reproduced from Duling III & Duling, 2006).

Based on (Eq. 2.18), the pulse duration becomes shorter until the pulse shortening of the loss modulator, M_s, balances the pulse broadening due to gain dispersion, D_g. The only stable solution to this differential equation is a Gaussian pulse shape. The advantage of Haus master equation regarding active mode-locking is that no prior assumption has to be made for the pulse shape. The Haus master equation predicts a Gaussian pulse shape, which in principle justifies Kuizenga and Siegman's assumption previously (Kuizenga & Siegman, 1970a, 1970b). The pulse obtained by active mode-locking is typically shorter than the round trip time in the cavity. Fig. 2.13 shows the active mode-locking in the time-domain perspective. The periodic loss modulation provides a temporary window of gain. When gain exceeds the loss in the cavity, mode-locking pulse occurs, as depicted in Fig. 2.13.

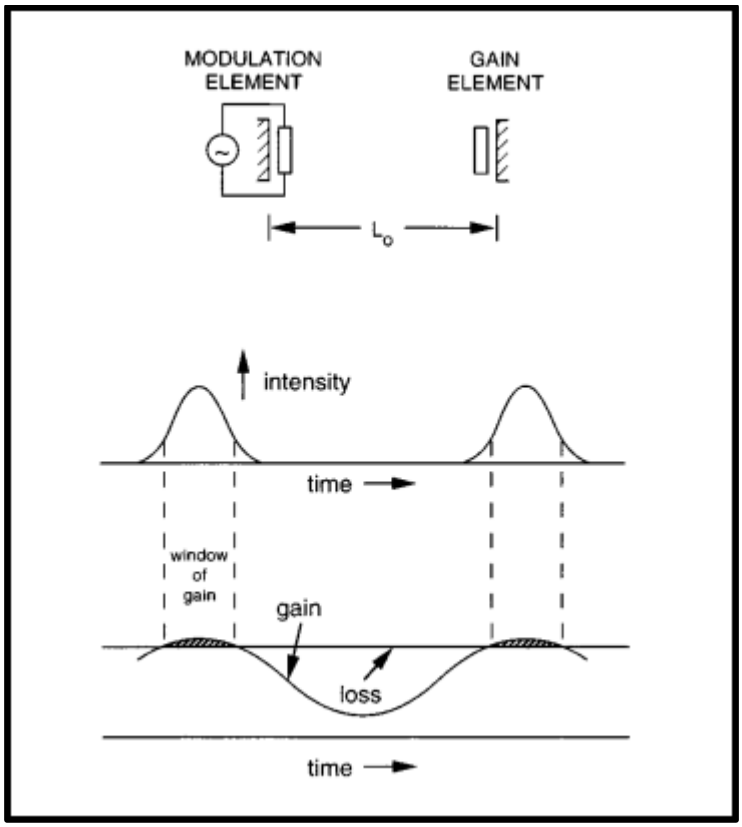

Fig. 2.13: Active mode-locking in the time-domain (Reproduced from Duling III & Duling, 2006).

2.4.3 PASSIVE MODE-LOCKING

Mode-locking also can be generated passively, where the pulse is generated without using any expensive electronics. Additionally, the pulse originate from fundamental mode-locking, therefore, every output pulse is a copy of the same single pulse that propagates back and forth inside the cavity. This is achieve through using saturable absorber or artificial saturable absorber such as Kerr lens mode-locking, nonlinear polarization rotation and additive-pulse mode-locking.

The saturable absorber would create some loss inside the laser cavity. The loss is relatively large for low intensities but small for a short pulse with high intensity. Therefore, a short pulse in the cavity produces loss modulation because of the high intensity at the peak of the pulse that saturates the absorber while low intensity wings (leading and trailing edges) would be absorbed by the saturable absorber. Thus, as the pulse propagates further inside the cavity, the pulse would saturates the gain to a level which is just enough to compensate the losses for the pulse itself, while other circulating low-intensity pulses die out because of their loss is more than their gain. As a result, as the pulse propagates further inside the cavity, it becomes cleaner and cleaner (Duling III & Duling, 2006; Ursula Keller, 2004; Nelson, Jones, Tamura, Haus, & Ippen, 1997).

The resultant pulse originates from the noise fluctuations inside the laser cavity. One noise spike is strong enough to saturate the absorber, therefore reduces its loss and amplified during the following cavity round trips. It will continue to grow until reaching a steady state where a stable pulse has been formed. In general, the pulse width obtained by passive mode-locking is shorter because the recovery time of a saturable absorber can be very fast, which resulted in a fast loss modulation. In comparison, the loss modulation of an active mode-

locking is significantly slower due to its sinusoidal loss modulation. As with active mode-locking, a passive mode-locked pulse is much shorter than the cavity round trip time.

The upper state lifetime of a rare-earth doped fiber is long (~ms), therefore, it does not react significantly with cavity round-trip time. Because they have a long upper state lifetime, the rare-earth doped fiber also is prone to *Q*-switching. Therefore, we need a fast saturable absorber to clean the leading and trailing edges of a mode-locked pulse (Nelson et al., 1997).

2.4.3.1 NONLINEAR POLARIZATION ROTATION (NPR)

Additive pulse mode-locking (APM) is a passive mode-locking technique that has its roots in bulk lasers. It utilizes a nonlinear interferometer to achieve pulse shortening. The pulse is split into two arms of the interferometer with nonlinear element placed in one arm. The pulses recombine at the beam splitter, thus, the pulse shortening occurs through the coherent addition of the self-phase modulated pulses. APM is an extremely fast artificial saturable absorber because it is based on self-phase modulation (SPM) from the Kerr effect in the glass. Therefore, APM should not impose a practical limit on the shortest pulse. APM has been extended to fiber laser, where pulse shortening is achieved through SPM and polarization controller. This kind of APM is especially convenient for fiber lasers, because rabbit-ear polarization controller and polarizers are all fiber-compatible (Herman A Haus, 2000).

Nonlinear polarization rotation (NPR) relies on Kerr effect that originated in the optical fiber in conjunction with polarizer to achieve artificial saturable absorber action and cause pulse shortening (Nelson et al., 1997). NPR maybe considered as APM due to the manipulation of optical Kerr effect in optical fiber (Dahlström, 1972; Stolen, Botineau, &

Ashkin, 1982). Two polarization states of the fiber corresponds to the excitation of an equivalent Mach-Zehnder fiber interferometer (French, 1995; H. A. Haus, Fujimoto, & Ippen, 1991; LaGasse, Liu-Wong, Fujimoto, & Haus, 1989). The result is a Kerr-induced nonlinear polarization rotation in a weakly birefringent optical fiber and polarization dependent loss (Ursula Keller, 2004). NPR relies on intensity-dependent rotation of elliptical polarization state in the optical fiber.

NPR can happen in an optical fiber when the initial polarization state is elliptical. The ellipse can be resolved into right-hand and left-hand circular polarization components of different intensities. Both circular components then accumulate different nonlinear phase shifts related to the intensity dependence of the refractive index $(n = n_0 + n_2 I)$, where n is the linear refractive index of a dispersive medium, n_0 is the initial refractive index, n_2 is the nonlinear refractive index and I is intensity. The polarization ellipse rotates as while maintaining its ellipticity and handedness. Owing to the small diameter of an optical fiber core, NPR is well suited for operation in optical fiber. The small diameter of fiber core allows light is concentrated in a small area, thus, leads to high intensity and therefore, producing high nonlinearity inside the optical fiber.

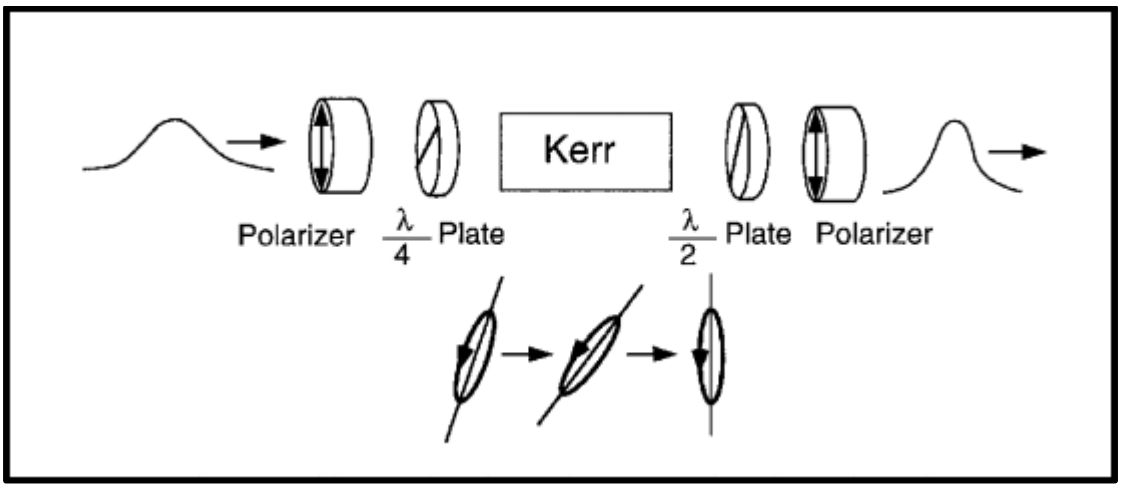

Fig. 2.14: Pulse shortening mechanism in P-APM. An initial pulse is linearly polarized and then made elliptically polarized by a quarter-wave plate. The light then passes through an optical fiber where ellipse rotation occurs and the peak of the pulse rotates more than the pulse wings. At the output of the fiber, the half-wave plate orients the pulse so that the peak of the pulse passes through the polarizer while the wings of the pulse are destroyed, therefore, pulse shortening occurs. The polarizer after the half-wave plate acts as analyzer (Reproduced from Herman A Haus, 2000; Nelson et al., 1997)

Fig. 2.14 shows how nonlinear polarization rotation can be used along with bulk polarization optics to achieve artificial saturable absorber and to mode-lock the laser. The mode-locking technique is also called polarization additive pulse mode-locking (P-APM) (Nelson et al., 1997). Linearly polarized light is transformed into elliptically polarized light which is then passed through an isotropic Kerr-medium. Elliptic polarization is rotated in the Kerr-medium by an intensity dependent angle. If the output light is again linearly polarized by an analyzer, the throughput of the system is intensity dependent. since the right- and left-hand circular polarization components acquire a differential nonlinear phase shift and are added together at the final polarizer (Nelson et al., 1997).

The rotation of elliptical polarization in an isotropic Kerr medium is best understood by writing the Kerr-polarization in terms of circular polarization components. If the medium responds instantaneously, the polarization can be written as

$$P_{\pm} = \epsilon_0 \frac{\chi^{(3)}}{2}\left(\left|E_{\pm}\right|^2 + 2|E_{\mp}|^2\right) E_{\pm} \qquad \text{(Eq. 2.26)}$$

where $\epsilon_0$is the permittivity in the vacuum, $\chi^{(3)}$ is third-order nonlinear susceptibility. The isotropic character of the medium dictates that a term of the form $E_{\mp}^2 E_{\pm}^*$ does not appear in the response. If such a term appear, the response would be sensitive to the relative phase between the electric field E_+ and E_-. But the relative phase determines the orientation of the E-field in the special case of a linear polarization with $|E_+| = |E_-|$. The Kerr response has to be independent of the polarization orientation in an isotropic medium. The factor of two in the cross phase modulation is a consequence of the instantaneous response.

It is clear that linear polarization and circular polarization acquire a simple phase shift due to the Kerr-polarization. Elliptic polarization is rotated. This rotation is exploited in the construction of an artificial saturable absorber with the use of an analyzer (Herman A Haus, 2000). The advantage of this technique is that it can operate at any wavelength, while the disadvantage is that any changes in the properties of the birefringence e.g. temperature, stress, pressure can affect the phase bias. Therefore, continues adjustment of polarization controller maybe necessary (French, 1995).

2.4.3.2 SEMICONDUCTOR SATURABLE ABSORBER

As the name suggest, semiconductor saturable absorber utilizes semiconducting materials to generate mode-lock pulse. Depending on the material, semiconductor offers

wide range of operating wavelength. The wavelength ranges from ≈ 400 nm in the UV using GaN-based materials to ≈ 2500 nm, in mid-infrared using GaInAsSb-based materials. Other semiconductor materials that can be used are AlGaAs (800 nm to 870 nm), InGaAs (870 nm to about 1150 nm), GaInNAs (1100 nm to 1500 nm) or InGaAsP (1500 nm range). Longer wavelength range for a given material composition may be obtained at the cost of increase defect concentration as a result of increased lattice mismatch to a given substrate material.

For InGaAs, GaAs and AlGaAs semiconductor materials systems, they are best-suited for wavelength between 800 nm to 1100 nm because of the near-perfect lattice match between GaAs and AlGaAs. InGaAs saturable absorbers have been grown on AlAs/GaAs Bragg mirrors and have been the material of choice for semiconductor saturable absorber mirror (SESAM) at ≈ 1000 nm operating wavelength. InGaAs saturable absorbers on AlAs/GaAs Bragg mirrors have been used at 1300 nm (Fluck, Braun, Gini, Melchior, & Keller, 1997; Fluck, Weingarten, Moser, Zhang, & Keller, 1996) and 1550 nm (Spuhler et al., 2003; Zeller et al., 2004) wavelengths.

GaInNAs has recently attracted a good intention for laser devices in the telecommunication wavelength range between 1300 nm to 1550 nm. Adding a few percent of nitrogen to InGaAs has given this combination of semiconductor materials two advantages; a redshift of the absorption wavelength and a reduction of the lattice mismatch to GaAs. The disadvantage is that the addition of nitrogen decreases the crystalline quality. Further study into the absorber properties and the mode-locking behavior revealed that GaInNAs SESAM has low saturation fluences and possess extremely low loss (Grange et al., 2005; Liverini et al., 2004; Schön et al., 2005). In 2003, GaInNAs 1500 nm SESAM is shown to mode-lock an Erbium-doped fiber laser (OG Okhotnikov, Jouhti, Konttinen, Karirinne, & Pessa, 2003) and in 2005; a solid-state laser (Rutz et al., 2005).

2.4.3.2 (a) SEMICONDUCTOR SATURABLE ABSORBER DYNAMICS

III-V semiconductor materials are well suited as absorber materials for ultrashort pulse generation. One advantage of semiconductor saturable absorber is that the semiconductor saturable absorber can be independently optimized from the laser cavity design. The semiconductor electronic structure and complex dynamics gives rise to strong interaction among optical excitations on ultrafast time scales. Despite the complexity, different time regimes can be discriminate in the evolution of optical excitation in semiconductors. These different time regimes are depicted in Fig. 2.15.

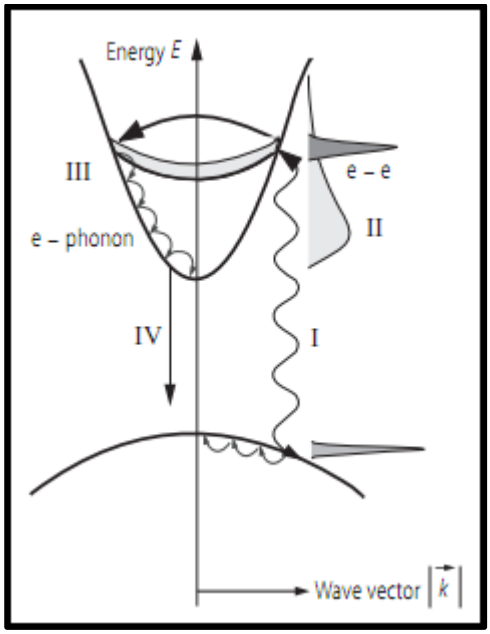

Fig. 2.15: Schematic dispersion diagram of a 2-band bulk semiconductor. Time regimes I-IV shows the dynamics after an optical excitation. e-e: electron-electron scattering. e-phonon: electron-phonon scattering (Reproduced from Ursula Keller, 2004)

Time regime I indicates that optical excitation with an ultrafast laser prepares the semiconductor in the coherent regime. In this regime, a well-defined phase relation exists between the optical excitation and the electric field of the laser pulse as well as among the

optical excitations themselves. As a result of the coherence among excitations in the semiconductor, macroscopic polarization (dipole moment density) arises. Information from the magnitude and decay of the polarization are useful in determining the properties of the semiconductor in the coherent regime. The irreversible decay of the polarization is due to scattering processes (i.e. electron-electron and electron-phonon scattering) and is usually expressed by the supposed dephasing or transversal relaxation time.

After the loss of coherence, ultrafast spectroscopy of semiconductor is only concerned with the dynamics of population (electron and hole distribution). In this incoherent regime, time regime II-IV in Fig. 2.15, can be distinguished. Scattering among charge carriers is mainly responsible for the redistribution of energy within the carrier distributions and for the formation of thermal distributions. Time regime II shows thermalization of electrons distribution where thermalization occurs through scattering among electrons. The exact thermalization time strongly depends on the carrier density, the excess photon energy with respect to the band edge and the type of carriers; mostly occurs on a time scale of 100 fs (Shah, 1999).

In general, the temperature of the carriers are different from the temperature of the lattice after themalization has completed. In Fig. 2.15, it is assumed that the carriers have a higher temperature than the lattice. In the same figure Fig. 2.15, it is schematically shown that the cooling of the carriers by the emission of phonon, i.e. the energy transfer to the lattices. Regime III is defined by cooling process. The time constants are typically in the picoseconds and tens of picosecond range.

Recombination defines the time regime IV in Fig. 2.15. The optically excited semiconductor returns to thermodynamics equilibrium by the recombination of electron-hole

pairs. These recombination processes is a low level of defect states semiconductor take place on a time scales of hundreds of picoseconds and longer.

Another ultrafast process happens if large densities of deep-level traps are incorporated in a semiconductor. Trapping of carriers into deep levels can proceed on sub-picosecond time scales (not shown in Fig. 2.15). Carrier trapping is an important process in a semiconductor saturable absorber application.

A typical Self-Amplitude Modulation (SAM) that occurs inside a semiconductor saturable absorber as shown in Fig. 2.16. Semiconductor saturable absorber applications in ultrashort pulse generation regularly require picosecond or sub-picosecond absorber recovery times (R. Paschotta & Keller, 2001). To obtain such short absorber recovery times, the optically excited carriers from the bands would have to be removed a few hundreds of femtoseconds to a few tens picoseconds after they have been created. However, intrinsic recombination processes are usually too slow to deplete the band states of a semiconductor on picosecond or sub-picosecond time scales. Hence, one generates defect states in the band gap which give rise to fast carrier trapping to deplete the bands. The trapping time determined by the density and the type of the traps. Higher trap densities give rise to faster trapping.

In conclusion, there are 4 time regimes in semiconductor saturable absorber complex dynamics. Time regimes I, II, III, IV corresponds 4 processes which are coherent regime, thermalization regime, cooling regime and recombination regime respectively. Thermalization typically happen in 100-fs time scale while carrier trapping proceeds on a time scales from a few hundreds of femtoseconds to tens of picoseconds. This resulted in Self-Amplitude Modulation (SAM) that is depicted in Fig. 2.16. Self-Amplitude Modulation (SAM) relates to the loss modulation used passive mode-locking as in Fig. 2.11 (Ursula Keller, 2004).

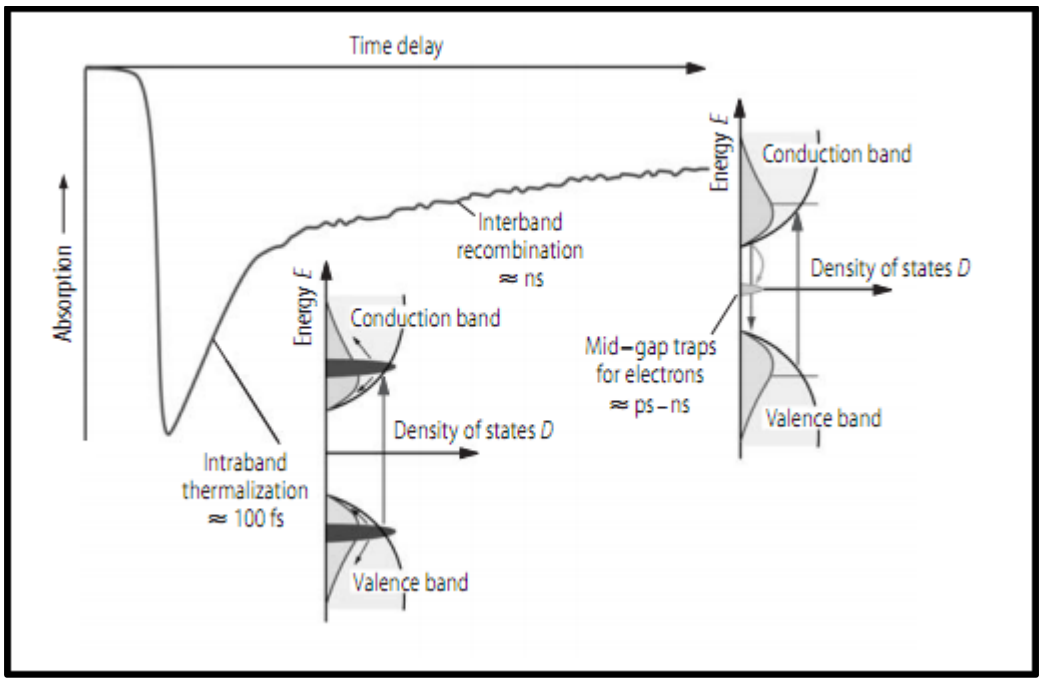

Fig. 2.16: Typical Self-Amplitude Modulation (SAM) observed in semiconductor saturable absorber. A semiconductor can absorb light if the photon energy is sufficient to excite carriers from the valence band to the conduction band. Under strong excitation, the absorption is saturated because the initial states of the pump transition are depleted while the final states are partially occupied. Within 60-300 fs after excitation, the carriers in each band themalize, and this leads to a partial recovery of the absorption. On a longer time scale – typically between a few ps and a few ns (depending on defect engineering), they will be removed by recombination and trapping. Both recombination and trapping. Both processes can be used for mode-locking (Reproduced from Ursula Keller, 2004).

2.4.3.3 SOLITON

Soliton has been discovered over many branches of physics. Soliton refers to a special kind of wave packets that can propagate undistorted over long distances. Soliton phenomena formed as a result of the interplay between the dispersive and nonlinear effects. In fiber optics, soliton has found a practical applications in the field of fiber-optic communications.

2.4.3.3 (a) MODULATION INSTABILITY

Many nonlinear system exhibit an instability that resulted in modulation of the steady state. This is due to the interplay between the nonlinear and dispersive effects. This phenomenon is referred to as the *modulation instability*. In the context of fiber optics, modulation instability requires anomalous dispersion and reveal itself as breakup of the cw or quasi-cw radiation into a train of ultrashort pulses (Boyd, Raymer, & Narducci, 1986; Hasegawa, 1984; Islam, Dijaili, & Gordon, 1988).

If we consider the light propagation inside the optical fiber, ignoring the losses, we are presented with

$$i\frac{\partial a}{\partial z} = \frac{\beta_2}{2}\frac{\partial^2 A}{\partial T^2} - \gamma|A|^2 A \qquad \text{(Eq. 2.27)}$$

(Eq. 2.27) is referred to as nonlinear Schrödinger (NLS) equation in the soliton literature. $A(\zeta,T)$ represents the amplitude of the field envelope, β_2 is the Group Velocity Dispersion (GVD) parameter, and the nonlinear parameter γ is responsible for Self-Phase Modulation (SPM). In the case of cw radiation, the amplitude A is independent of T at the input end of the fiber at $\zeta = 0$. Assuming that $A(\zeta,T)$ remains time independent during propagation inside the fiber, (Eq. 2.27) can be solved to obtain the steady-state solution

$$\bar{A} = \sqrt{P_0}exp(i\emptyset_{NL}) \qquad \text{(Eq. 2.28)}$$

where P_0 is the incident power and $\phi_{NL} = \gamma P_0 \zeta$ is the nonlinear phase shift induced by SPM. (Eq. 2.28) implies that a cw light is unchanged when it propagates through the fiber, except for acquiring a power-dependent phase shift (and for reduction in power in the presence of fiber losses).

Before making any conclusion, we must check whether the steady-state solution is able to withstand against small perturbations. In order to do this, a slight perturbation is introduced to the steady state such that

$$A = \left(\sqrt{P_0} + a\right) exp(i\emptyset_{NL}) \qquad \text{(Eq. 2.29)}$$

and examine the evolution of the perturbation *a(ζ, T)* using a linear stability analysis. Substituting (Eq. 2.29) in (Eq. 2.27) and linearizing in *a*, we obtain

$$i\frac{\partial a}{\partial z} = \frac{\beta_2}{2}\frac{\partial^2 A}{\partial T^2} - \gamma P_0(a + a^*) \qquad \text{(Eq. 2.30)}$$

This linear equation can be easily solved in the frequency domain. Nevertheless, because of the a^* term, the Fourier components at frequencies Ω and –Ω are coupled.

$$a(\zeta, T) = a_1\ exp/,[i(K\zeta - \Omega T)] + a_2 exp[-i(K\zeta - \Omega T)], \qquad \text{(Eq. 2.31)}$$

where *K* and *Ω* are the wave number and the frequency of perturbation, respectively. (Eq. 2.30) and (Eq. 2.31) provide a set of two homogeneous equations for a_1 and a_2. This set has a nontrivial solution only when *K* and *Ω* satisfy the following dispersion relation

$$K = \pm\frac{1}{2}|\beta_2\Omega|[\Omega^2 + sgn(\beta_2)\Omega_c^2]^{1/2} \qquad \text{(Eq. 2.32)}$$

where sgn(β_2) = ±1 depending on the sign of β_2,

$$\Omega_c^2 = \frac{4\gamma P_0}{|\beta_2|} = \frac{4}{|\beta_2|L_{NL}} \qquad \text{(Eq. 2.33)}$$

The nonlinear length L_{NL} is defined as $L_{NL} = 1/\gamma P_0$. Because of the factor exp $(i(\beta_0\zeta - \omega_0 t))$ has been factored out in

$$E(r,t) = \frac{1}{2}\hat{x}\{F(x,y)A(\zeta,t)\exp[i(\beta_0\zeta - \omega_0 t)] + c.c.\} \qquad \text{(Eq. 2.34)}$$

the actual wave number and the frequency of perturbation are $\beta_0 \pm K$ and $\omega_0 \pm \Omega$ respectively. Therefore, the two terms in (Eq. 2.31) represents two different frequency components, $\omega_0 + \Omega$ and $\omega_0 - \Omega$, that are present simultaneously.

The dispersion relation (Eq. 2.32) shows that steady-state stability depends critically on whether light experiences normal or anomalous GVD inside the fiber. In the case of normal GVD ($\beta_0 > 0$), the wave number K is real for all Ω, and the steady state is stable against small perturbations. In the case of anomalous GVD ($\beta_0 < 0$), K becomes imaginary for $|\Omega| < \Omega_c$, and the perturbation $a(\zeta, T)$ grows exponentially with ζ as seen from (Eq. 2.31). As a result, the cw solution (Eq. 2.28) is inherently unstable for $\beta_0 < 0$. This instability is referred to as modulation instability. The instability leads to a spontaneous temporal modulation of the cw beam and transforms it into a pulse train (Agrawal, 2006)

2.4.3.3 (b) SOLITON MODE-LOCKING

Soliton mode-locking implies that the pulse shaping is solely done by soliton formation; the balance of GVD and SPM at steady state, with no additional requirements for cavity stability regime. Soliton mode-locking does not depend on the transverse Kerr effect. Therefore, the mode-locking mechanism is not critically dependent on cavity design and no critical cavity stability regime is required. Soliton mode-locking basically works over the full cavity stability range.

In soliton mode-locking, an additional loss mechanism such as saturable absorber or an active modulator is essential to start the mode-locking process as well as stabilize the soliton pulse-forming process. In soliton mode-locking, the net gain window can remain open

for more than 10 times longer than the ultrashort pulse, depending on the specific laser parameter (Jung, Kärtner, Brovelli, Kamp, & Keller, 1995; Kartner, Jung, & Keller, 1996). Because the net gain window opening is 10 times longer than the ultrashort pulse, this relaxes the requirements on the saturable absorber. Therefore, we can obtain ultrashort pulses even in the 10 fs regime with semiconductor saturable absorbers that have much longer recovery times.

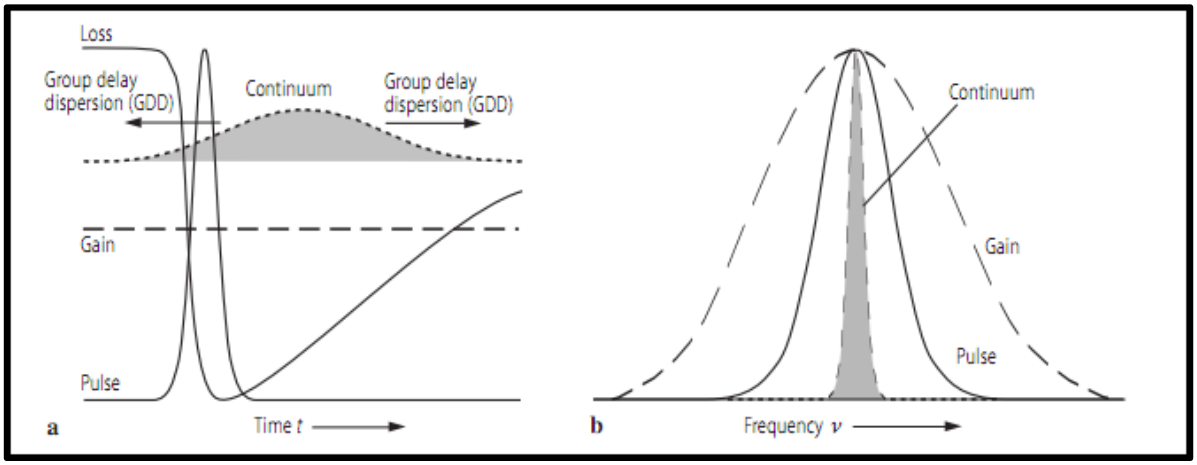

Fig. 2.17: Soliton mode-locking in (a) time and (b) frequency domain. In (a) the continuum pulse spreads in time due to GVD and experiences more loss in the relatively slow absorber, which is saturated by the shorter soliton pulse. However, in (b) the longer continuum pulse has a narrower spectrum and therefore experiences more gain than the spectrally broader soliton pulse. In normalized gain, soliton and continuum amplitudes , the continuum amplitude is the highest, followed by gain, then soliton (Reproduced from Ursula Keller, 2004)

Using slow saturable absorber as a starting and stabilizing mechanism for mode-locking, there remains a time window with the net round-trip gain behind the pulse. There is still net gain because the loss caused by the absorber is very small for the trailing edge (assuming a fully saturated absorber). Therefore, we might expect that the long net gain after

the pulse would destabilize the pulse. However, there is no shaping action of the absorber at the trailing edge of the pulse. This is because the weak pulses experience a temporal shift by the absorber, which limits the time in which noise behind the pulse can be amplified. The absorber attenuates mostly the leading wing of the pulse, as a result, the pulse center is shifting backwards in each cavity round trip. In other words, the pulse is constantly moving backward and swallows any noise growing behind itself. As a note, weak reflections in the laser cavity could generate weak satellite pulses behind the main pulse.

In soliton mode-locking, there is another factor that limits the above effect. The dispersion causes the background noise to temporally broaden and accordingly, it permanently loses the energy in those parts which made the noises drift into the time regions with net loss.

Soliton mode-locking can be expressed by using Haus master equation formalism, where we take into account GVD, SPM and slow saturable absorber *q(T, t)* that recovers slower than the pulse duration (refer to Fig. 2.17a) (Kärtner & Keller, 1995; Kartner et al., 1996)

$$\sum_i \Delta A_i = \left[-iD\frac{\partial^2}{\partial t^2} + i\delta_L|A\,(T,t)|^2\right] A\,(T,t) + \left[g - l + D_g\frac{\partial^2}{\partial t^2} - q\,(T,t)\right] A\,(T,t) = 0 \qquad \text{(Eq. 2.35)}$$

Here, *A(T, t)* is the slowly varying field envelope, *D* is the intracavity Group Delay Dispersion (GDD), $D_g = g/\Omega_g^2$ is the gain dispersion, Ωg is the Half-Width of Half-Maximum (HWHM) of gain bandwidth. The SPM coefficient δ is given by $\delta = (2\pi/\lambda_0 A_L) n_2 \ell_L$, where n_2 is the intensity dependent refractive index of the gain medium, λ_0 is the center wavelength of the pulse and A_L and ℓ_L is the effective mode area in the gain

medium and length of light path through the gain medium within one round-trip, respectively. g is the saturated gain and l is the round-trip losses. $q(T, t)$ is the response of the saturable absorber due to an ultrashort pulse.

The differential equation can be solved analytically using soliton perturbation theory. The first bracket term of the term determines the nonlinear Schrödinger equation for which the soliton pulse is a stable solution for negative GVD ($D < 0$) and positive SPM ($n_2 > 0$):

$$A(z,t) = A_0 \operatorname{sech}\left(\frac{t}{\tau}\right) e^{-i\phi_s(z)} \qquad \text{(Eq. 2.36)}$$

This soliton pulse propagates without distortion through a medium with negative GVD and positive SPM. The positive effect of SPM cancels the negative effect of dispersion. The FWHM soliton pulse duration is given by $\tau_p = 1.7627 \cdot \tau$ and the time-bandwidth product (TBP) is $\Delta\tau_p \upsilon_p = 0.3148$. $\phi_s(z)$ is the phase shift of the soliton as it propagates along the z-axis.

For a given negative of dispersion and an intracavity pulse energy, E_p, the pulse duration is given by

$$\tau_p = 1.7627 \frac{2|D|}{\delta_L E_p} \qquad \text{(Eq. 2.37)}$$

In (Eq. 2.37) in the pulse duration is a product of balance between dispersion and SPM with pulse energy.

This soliton pulse losses energy due to gain dispersion and losses in the cavity. Gain dispersion and losses can be assumed as a perturbation to the nonlinear Schrödinger equation in which a soliton is a stable solution (i.e. the second bracket term in (Eq. 2.35). The lost energy, is called continuum in soliton perturbation theory, is originally contained in a low-

intensity background pulse, which experiences negligible SPM, but spreads in time due to GDD (refer toFig. 2.17). In soliton mode-locking, a stable soliton pulse is formed for all GDD values as long as the continuum loss is larger than the soliton loss (Kartner et al., 1996) or the pulses break up to become into two of more pulses (Au, Kopf, Morier-Genoud, Moser, & Keller, 1997). When there is no pulse break up, the minimal pulse duration is given when the loss for the continuum pulse becomes equal to the loss of the soliton pulse. When the soliton pulse is stable, the saturated gain is equal to the loss

$$g = l + l_s \; with \; l_s = \frac{D_g}{3\tau^2} + q_0 \frac{E_{sat,A}}{E_p}\left[1 - exp\left(-\frac{E_p}{E_{sat,A}}\right)\right] \qquad \text{(Eq. 2.38)}$$

where l is the total saturated amplitude loss coefficient per cavity round trip and l_s is the additional loss experienced by the soliton due to gain filtering (i.e. the first term of (Eq. 2.38) and the amplitude loss coefficient for saturation of the slow saturable absorber (i.e. the second term of (Eq. 2.38). Soliton perturbation theory then determine the round trip loss of the continuum pulse (Kartner et al., 1996). The continuum is spread in time due to dispersion and thus experience enhanced loss in the recovering absorber that has been saturated by the much shorter soliton pulse.

Therefore, we can predict the minimum pulse duration for soliton pulse (Kärtner & Keller, 1995; Kartner et al., 1996)

$$\begin{aligned} \tau_{p,min} &= 1.7627\left(\frac{1}{\sqrt{6}\Omega_g}\right)^{3/4} \phi_s^{-1/8}\left(\frac{\tau_A g^{3/2}}{q_0}\right)^{1/4} \\ &\approx 0.45\left(\frac{1}{\Delta v_g}\right)^{3/4}\left(\frac{\tau_A}{\Delta R}\right)^{1/4}\frac{g^{3/8}}{\phi_s^{1/8}} \end{aligned} \qquad \text{(Eq. 2.39)}$$

where ϕ_s is the phase shift of the soliton per cavity round trip, Δv_g is the FWHM gain bandwidth and $\Delta R \approx 2q_0$. In (Eq. 2.39) we assume a fully saturated slow saturable absorber

and a linear approximation for the exponential decay of the slow saturable absorber. However, (Eq. 2.39) does not indicate when the soliton pulse would break up into two solitons which would occur if the saturable absorber is too strongly saturated.

In soliton mode-locking, the dominant pulse formation process is due to the balance between positive SPM and negative dispersion inside the cavity. The pulse duration is given by (Eq. 2.37). From (Eq. 2.37), it shows that pulse duration has a linear relationship with the negative GDD inside the laser cavity. In soliton mode-locking, an unchirped soliton pulse can be obtained for all dispersion levels as long as the stability requirement against the continuum is fulfilled. Higher-order dispersion only increase the pulse duration, therefore, it is undesirable and assumed to be compensated.

Solitons alone are not stable. The continuum pulse is much longer and thus experiences only the gain at line center, while the solitons reveal an effectively lower average gain because of its larger bandwidth. Therefore, the continuum shows a higher gain than soliton. After a sufficient built-up time, the continuum would actually grow until it reaches lasing threshold, and subsequently, destabilizing that soliton. Nevertheless, we can stabilize the soliton by introducing a relatively slow saturable absorber into the cavity. The absorber is fast enough to add sufficient additional loss for the growing continuum that spreads in time during its build-up phase so that it no longer reaches lasing threshold.

In conclusion, soliton shaping effects can allow for the generation of significantly shorter pulses, compared to cases without SPM and dispersion. The improvement is especially large for absorbers with a relatively low modulation depth and when the absorber recovery is not too slow. In this case, the absorber only needed to stabilize the solitons against the growth of the continuum while pulse shaping is done by the soliton effects. In general,

the absorber parameters are not critical. To obtain the desired pulse duration, we need to adjust the dispersion and SPM (Ursula Keller, 2004).

2.5 GRAPHENE

The Nobel Prize for physics in 2010 was awarded to Sir Professor Andre Geim and Sir Professor Konstantin Novoselov for their "*groundbreaking experiments regarding the two-dimensional material graphene"* (Novoselov et al., 2004). Graphene is a two-dimensional (2D), flat mononolayer of carbon atoms. The graphene lattice resembles a honeycomb lattice by sp^2 hybridization. The C-C bonds in the graphene constitute 2 inplane $\sigma(s, p_x, p_y)$ orbitals and $\pi(p_z)$ orbital perpendicular to the sheet (S. Yamashita, 2012). It is a basic building block for graphitic materials of all other dimensionalities. A 2D graphene can be wrapped up into 0D fullerenes, rolled into 1D carbon nanotubes or stacked on top of one another to form 3D graphite (refer to Fig. 2.18).

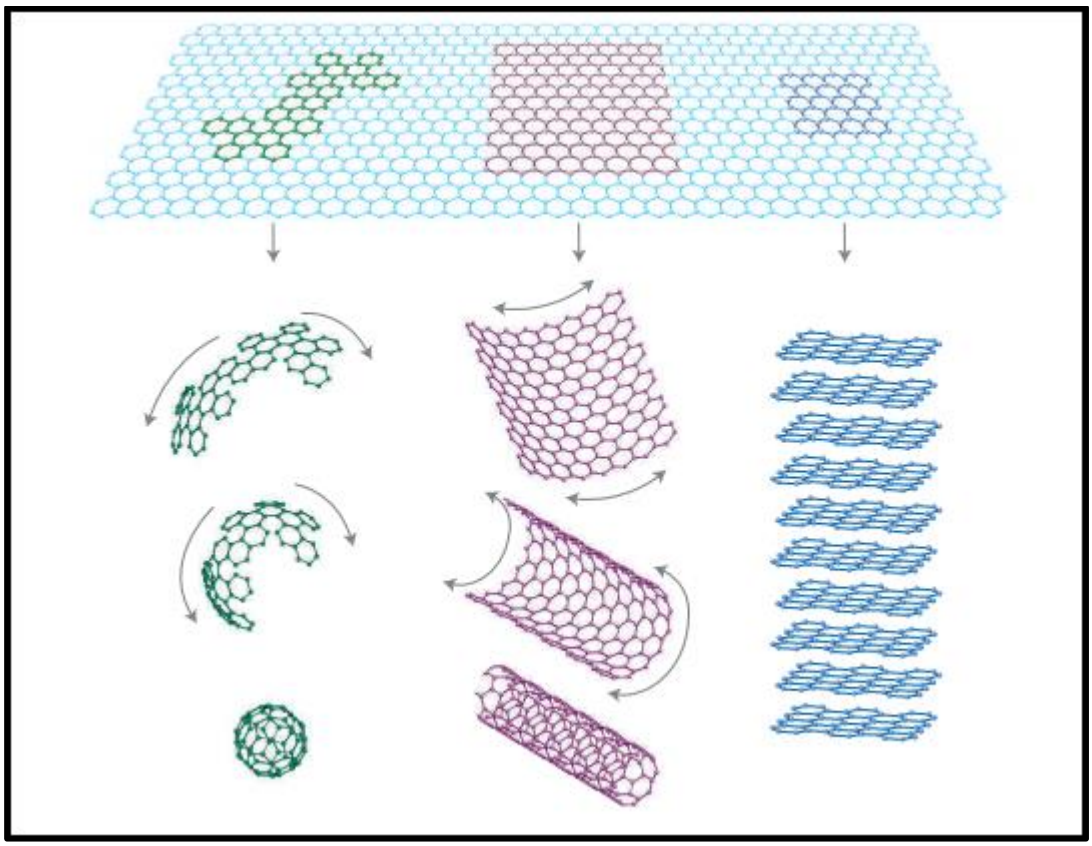

Fig. 2.18: Graphene is the basic building of all graphitic forms. Graphene can be wrapped up into 0D fullerenes, rolled into 2D carbon nanotube and stacked into 3D graphite (Reproduced from A.K. Geim & Novoselov, 2007).

Although the original definition of graphene is a “flat monolayer of carbon atoms”, it was shown that the electronic structure rapidly evolves with the number of layers, approaching 3D limit of graphite at 10 layers. Therefore, the term ‘graphene’ is still applicable to 10 layers of carbon atoms. Beyond 10 layers of graphene, the electronics properties resembles the electronics properties of graphite (Partoens & Peeters, 2006).

2.5.1 THE ELECTRONIC AND BAND STRUCTURE OF GRAPHENE

The structural flexibility of graphene can be traced to its electronic structure. The sp^2 hybridization between one *s* orbital and two *p* orbitals lead to a trigonal planar structure with a formation of a σ bond between carbon atoms that are separated by 1.42 Å. The σ band is responsible for the robustness of the lattice structure in all allotropes. Owing to the Pauli principle, these bands have a filled shell and therefore, form a deep valence band. The unaffected *p* orbital, which is perpendicular to the planar structure can bind covalently with the neighboring carbon atoms, leading to the formation of a π band. Since each *p* orbital has one extra electron, the π band is half filled (Neto, Guinea, Peres, Novoselov, & Geim, 2009).

Further observation of the band structure of graphene reveals three electronics properties that sparked such interest; the vanishing carrier density at Dirac point, the existence of pseudo-spin and the relativistic nature of its carriers. The band structure of graphene is shown in Fig. 2.19. The valance and conduction bands meet at high symmetry *K* points (Fig. 2.19). Because the conduction and valence band meet at a symmetry *K* point, graphene is considered as zero-gap semiconductors (or zero-overlap semimetals) (A.K. Geim & Novoselov, 2007). In intrinsic graphene, each carbon atom contributes one electron completely filling the valance band and leaving the conduction band empty. Therefore, the Fermi level, E_F, is situated precisely where the conduction and valence bands meet. These are known as the Dirac or charge neutrality points. Due to this unique band structure of graphene, the following are three important features which to a large extent define the nature of electron transport of this material.

- The occupied valance and empty conduction bands meet at Dirac point at which the density of states (DOS) is zero. Graphene is therefore best described as a zero-gap semiconductor, with vanishing DOS at the Dirac point but no energy gap between the valence and conduction bands.
- Close to the Fermi energy, the band structure of graphene can be described in terms of two inequivalent Dirac cones situated at *K* and *K'*. In order for an electron to scatter from *K* to *K'* requires a large momentum change. Electron transport in graphene can therefore be thought of as occurring in parallel through the *K* and *K'* Dirac cones. As such charge carriers in graphene have, as well as orbital and spin quantum numbers, a valley or pseudospin quantum number with a degeneracy of 2. The term pseudospin is used due to the analogy with real spin. Both however, are completely independent of one another.
- Close to the Dirac point, the graphene dispersion relation is linear in nature. This linear-dispersion relation is best described by the relativistic Dirac equation. In this description the charge carriers (electron and holes) are considered as massless Dirac fermions travelling with a group velocity of $v_F \approx 1 \times 10^6$ ms^{-1} (Warner, Schaffel, Rummeli, & Bachmatiuk, 2012)

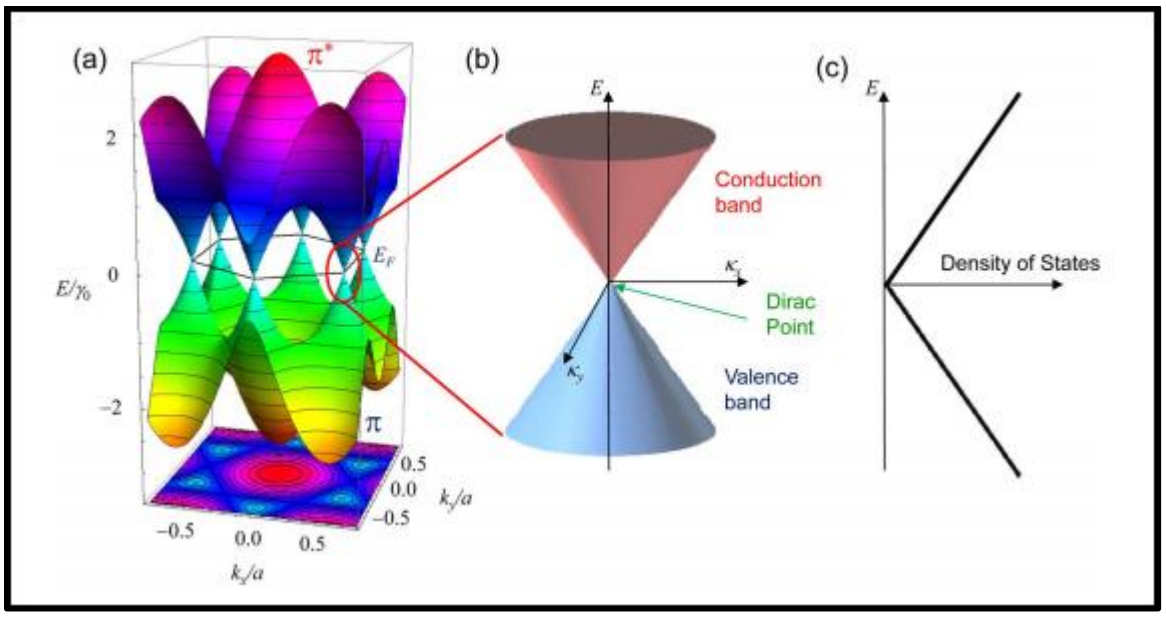

Fig. 2.19: Band structure of graphene. (a) Dispersion relation under tight-binding approximation, (b) Dirac cones near Dirac point, and (c) Density of states (DOS) near Fermi level (Reproduced from S. Yamashita, 2012)

2.5.2 OPTICAL PROPERTIES OF GRAPHENE

Apart from having a unique electronic properties, graphene also has several interesting optical properties. For example, graphene can be detected optically, despite being one atom thick (Blake et al., 2007; Casiraghi et al., 2007). The Dirac linear-dispersion relation implying that broadband application is possible. Third-order nonlinear photonics such as saturable absorption, originates from Pauli blocking (Qiaoliang Bao et al., 2009; Zhipei Sun, Daniel Popa, Tawfique Hasan, Felice Torrisi, Fengqiu Wang, EdmundJ R. Kelleher, et al., 2010), and graphene can be made luminesce by chemical and physical treatments (G. Eda et al., 2009; Gokus et al., 2009).

2.5.2.1 LINEAR OPTICAL ABSORPTION

Owing to the unique electronics properties, graphene is found to absorb a significant amount of incident light, despite being only one atom thick. The transmittance of a single-layer graphene is calculated to be

$$T = (1 - 0.5\pi\alpha)^{-2} \approx 1 - \pi\alpha \approx 97.7\% \qquad \text{(Eq. 2.40)}$$

where $\alpha = e^2/\hbar c \approx 1/137$ is the fine-structure constant. $\hbar$ is Plank constant, *c* is the speed of light and *e* is the electron charge (Nair et al., 2008). Graphene only reflects <0.1% of the incident light in the visible region, increasing to ~2% for ten layers. Therefore, we can assume that the optical absorption of graphene layers is relative to the number of layers, for each layer absorbing $A \approx 1 - T \approx \pi\alpha \approx 2.3\%$ over the visible spectrum (Nair et al., 2008). Because of the linear dispersion relation of graphene, graphene absorption is independent of wavelength (refer to Fig. 2.20) (Bonaccorso, Sun, Hasan, & Ferrari, 2010; S. Yamashita, 2012).

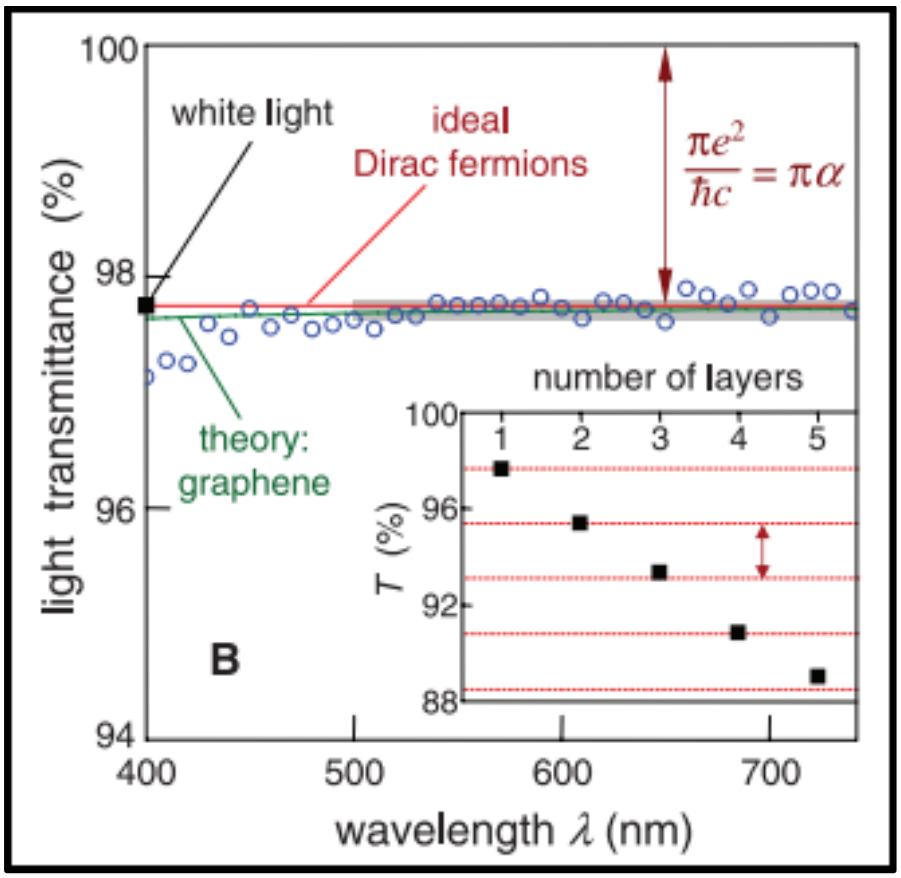

Fig. 2.20: Transmittance spectrum of single-layer graphene (open circles). Slightly lower transmittance for λ < 500 nm is probably due to hydrocarbon contamination. The red line is the transmittance expected for two-dimensional Dirac fermions, whereas the green curve takes into account a nonlinearity and triangular warping of graphene's electronics spectrum. The grey area indicates the standard error for the measurement. (Inset) Transmittance of white light as a function of the number of graphene layers (square) (Reproduced from Nair et al., 2008).

2.5.2.2 SATURABLE ABSORPTION

Interband excitation by ultrafast optical pulses produces a non-equilibrium carrier population in the valence and conduction bands. In time-resolved measurements (Breusing, Ropers, & Elsaesser, 2009), two relaxation timescales are observed; a faster one of ~100 fs

and a slower one, on picosecond timescale. The faster relaxation time is related to the carrier-carrier intraband collisions and phonon emission. The slower relation time corresponds to electron interband relaxation and cooling of hot phonons (Kampfrath, Perfetti, Schapper, Frischkorn, & Wolf, 2005; Lazzeri, Piscanec, Mauri, Ferrari, & Robertson, 2005).

The linear dispersion of the Dirac electrons denote that for excitation there will always be an electron-hole pair in resonance. If the relaxation times are shorter than the pulse duration, during the pulse, the electrons reach a stationary state and collisions put electrons and holes into thermal equilibrium at an effective temperature. The populations determine the electron and hole densities, total energy density and a reduction of photon absorption per layer, due to Pauli blocking.

For linear dispersions near the Dirac point, pair-carrier collisions cannot lead to interband relaxation, therefore conserving the total number of electrons and holes separately. Interband relaxation by phonon emission can occur only if the electron and hole energies are close to the Dirac point (within the phonon energy). For graphite flakes, the dispersion is quadratic and pair-carrier collisions can lead to interband relaxation. As a conclusion, in principle, single-layer graphene can provide the highest saturable absorption (Bao et al., 2010; González, Guinea, & Vozmediano, 1996; Z. Sun et al., 2010).

It is the saturable absorption property in graphene that is responsible for generating ultrashort pulses. Techniques of incorporating graphene SA into fiber laser includes graphene polymer composites (Qiaoliang Bao et al., 2009; Zhipei Sun, Daniel Popa, Tawfique Hasan, Felice Torrisi, Fengqiu Wang, Edmund J. R. Kelleher, et al., 2010), optical deposition (Martinez et al., 2010), mechanical exfoliation (Chang, Kim, Lee, & Song, 2010; Martinez et al., 2011), graphene nano-particles embedded in hollow core photonics crystal fiber (PCF)

(Lin, Yang, Liou, Yu, & Lin, 2013) and evanescent field interaction (Z. Q. Luo et al., 2012; Song, Jang, Han, & Bae, 2010).

2.5.2.3 LUMINESCENCE

Graphene can be made luminescence by inducing a bandgap through two techniques to modify the electronic structure of graphene. One technique is by cutting it into ribbons and quantum dots (Dössel, Gherghel, Feng, & Müllen, 2011)and the other technique is by chemical or physical treatments (Gokus et al., 2009; Stöhr, Kolesov, Pflaum, & Wrachtrup, 2010), to reduce the connectivity of the π-electron network. Individual graphene flakes can be made luminescent by mild oxygen plasma treatment as in Fig. 2.21(d), in which a uniform photoluminescence map and the corresponding elastic scattering image are compared. It is also possible to make hybrid structures by etching just the top layer, while making the underlying layers stay intact. The combination of photoluminescent and conductive layers could be used in sandwich light-emitting diodes. Luminescent graphene-based material has been made to cover the infrared, visible and blue spectral ranges (Bonaccorso et al., 2010; G. Eda et al., 2009; Gokus et al., 2009; Lu et al., 2009; X. Sun et al., 2008).

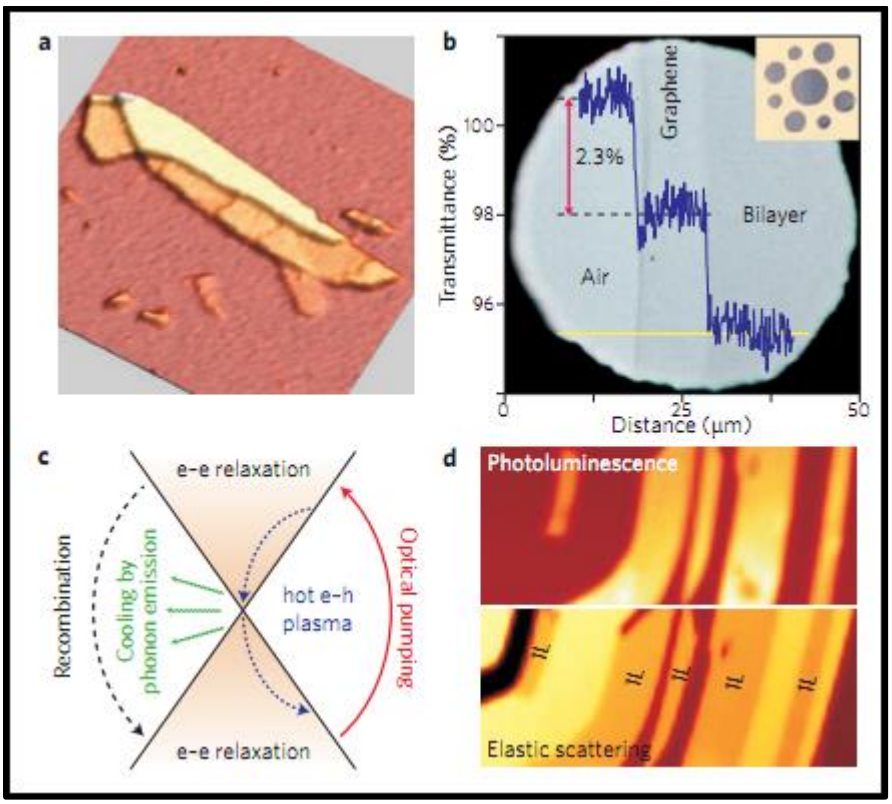

Fig. 2.21: The optical properties of graphene. a) Elastic light scattering (Rayleigh) image of a graphite flake with varying number of graphene layer. b) Light transmittance percentage according to graphene layers (inset: sample design for the experiment). c) Schematic of photoexcited electron kinetics in graphene, with possible relaxation mechanisms for the non-equilibrium electron population. d) Photoluminescence (top) and elastic scattering (bottom) images of oxygen-treated flake. 1L indicates a monolayer graphene (Reproduced from Bonaccorso et al., 2010)

2.6 GRAPHENE OXIDE (GO)

Graphite oxide (GO) has been synthesized as early as 1860 (Brodie, 1860). Due to the recent discovery of graphene (Novoselov et al., 2004), interest in graphene oxide was reignited. GO is a layered material consisting hydrophilic oxygenated graphene sheet

containing oxygen functional groups on their basal planes and edges (Dmitriy A. Dikin et al., 2007). The reason behind the renewed interest in graphene oxide lies in the difficulty of mass producing graphene. Although producing graphene is simple (mechanical exfoliation method), the method is labour intensive and there is little control over the size and shape of the flakes and their position on a wafer. Therefore, the method is deemed not suitable for producing graphene in mass quantity. Other methods of producing graphene were also invented, such as growth on SiC (Berger et al., 2006), Cu (Li et al., 2009), Ni (Kim et al., 2009) and other surfaces.

GO offers a route to producing graphene by mass quantities (Segal, 2009). While graphene is hydrophobic, GO that is sonicated in water leads to a stable colloidal suspension. The GO then can be further chemically reduced to graphene sheets. GO also has band gap which add to the advantage of GO to serve as important component in graphene-based electronics. By selectively oxidizing portions of graphene sheet, it is possible to isolate conductive regions and develop barrier layers for electronic devices. Another advantage of GO is its ability to change the electronic properties from semiconductor to insulator (Stewart & Mkhoyan, 2012).

Following complete exfoliation in water, GO sheets can be assembled into a paper-like material under a directional flow. The result is a material that is uniform and dark brown under transmitted white light and almost black in reflection when thicker than 5 μm. The material is called GO paper (Dmitriy A. Dikin et al., 2007).

2.6.1 ELECTRONIC AND BAND STRUCTURE OF GO

GO is often referred to as insulating and disordered analogue of the highly conducting crystalline graphene. Physicist is interested in the latter part, because of its unique electronic

structure with linear dispersion of Dirac electrons. Therefore, GO is an electronically hybrid material the showcases both conducting π-states from sp^2 carbon sites and a large energy gap (carrier transport gap) between the σ-states of its sp^3-bonded carbons. The ability to modify the ratio of sp^2 and sp^3 fraction by reduction chemistry can transform GO from insulator to a semiconductor and to a graphene-like semi-metal (Eda, Mattevi, Yamaguchi, Kim, & Chhowalla, 2009; Loh, Bao, Eda, & Chhowalla, 2010).

Due to its random distribution of epoxy and hydroxyl groups on the surface of graphene oxide, the electronic structure of GO is difficult to discuss in terms of a crystalline band structure model (Stewart & Mkhoyan, 2012). Lerf-Klinowski model, as shown in Fig. 2.22a, has been experimentally supported and generally accepted as a chemical arrangement of a single atomically thing layer of GO (He, Klinowski, Forster, & Lerf, 1998). Recently Gao, Alemany, Ci, and Ajayan (2009), has suggested a new insights into the structure of GO sheet as shown in Fig. 2.22b, with five- and six-membered lactol rings decorating the edges as well as esters of tertiary alcohols on the surface.

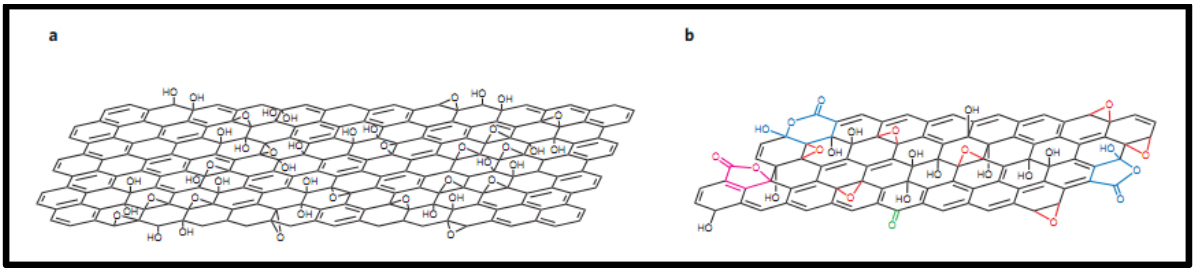

Fig. 2.22: a) the chemical structure of a single sheet of GO by Lerf-Klinowski model, b) the chemical structure of GO sheet as recently proposed by Gao *et al.* taking into account the five- and six-membered lactol rings (blue), ester of a tertiary alcohol (purple), hydroxyl (black) epoxy (red) and ketone (green) functionalities (Reproduced from Loh et al., 2010).

The presence of localized finite-sized molecular sp^2 clusters within an sp^3 matrix can lead to confinement of π- electrons in GO. The size of sp^2 clusters determines the local energy gap and thus, responsible for determining the wavelength of the emitted fluorescence. Due to a range of sp^2 cluster sizes are present in GO, the collective band structure has no signature features as depicted in Fig. 2.23. Several studies suggest that GO possesses an energy gap which can be tune by controlling the degree of oxidation or reduction as well as reversible absorption and desorption of oxygen atoms on the graphene (Jeong, Jin, So, Lim, & Lee, 2009; Z. Luo, Vora, Mele, Johnson, & Kikkawa, 2009; Shen et al., 2013; Tsuchiya, Terabe, & Aono, 2013).

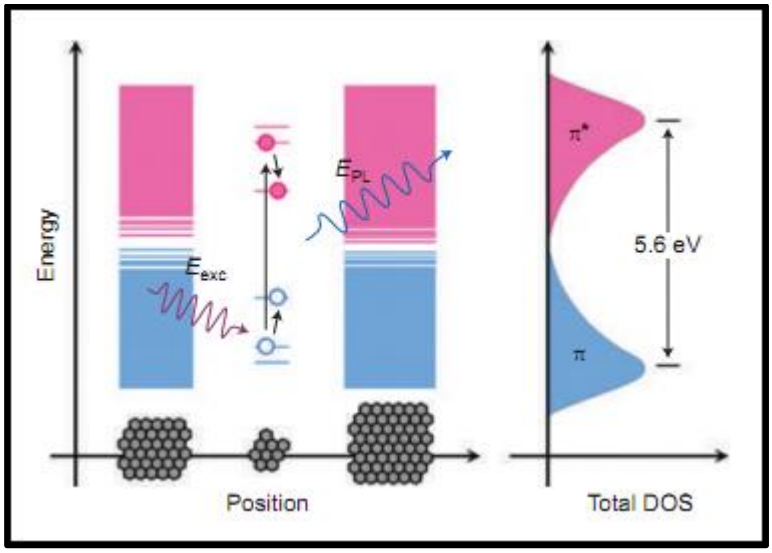

Fig. 2.23: Schematic band structure of GO (pink and blue indicates conduction and valence bands, respectively). Smaller sp^2 domains have a larger energy gap due to stronger confinement effect. Photogeneration of an electron-hole (e-h) pair on absorption of light (E_{exc}) followed by non-radiative relaxation and radiative recombination resulting in fluorescence (E_{PL}) is depicted. Black arrows denote the transitions of electrons and holes during this process. DOS is electronic density of states (Reproduced from Loh et al., 2010).

2.6.2 OPTICAL PROPERTIES OF GO

With its origin in graphene, GO is expected to possess the optical properties of graphene. Saturable absorption and flourescence are thought to be inherent in GO. However, due to the nonstoichiometric chemical composition of GO, it is difficult to determine the fundamental properties of GO such as energy band gap and optical properties.

2.6.2.1 PHOTO BLEACHING AND PHOTO ABSORPTION IN GO

Ultrafast carrier dynamics, Pauli blocking and large absorption bandwidth have made graphene an ideal ultrabroadband saturble absorber. Altering band gap as well as electrical and optical properties of graphene has become a subject of intensive research. Because of that, scientists have turn their attention to GO, which possesses heterogeneous chemical and electronic structures, with the fact that it can be processed in water.

Z.-B. Liu et al. (2011) have reported an observation of a heterogeneous nonlinear optical response contribution to the transient differential transmission in GO. By increasing the pump intensities, the transient optical response exhibits a crossover from bleaching to enhanced absorption as two-photon absorption (TPA) of sp^3 domains becomes more noticeable. At low pump intensity, the pump-induced change in transmission is dominated by photobleaching (PB). This characteristic is the result from Pauli blocking of the strong interband optical transitions in the sp^2 domains. As a result from Pauli blocking, saturable absorption occurs in GO.

In GO, the existence of oxygen-containing functional groups with C-O bonds results in a transformation of carbon atom from sp^2 to sp^3 hybridization. There is a large energy gap between σ states of its sp^3-bonded carbons in GO as in Fig. 2.24. At low pump intensity, the

optical transition in the sp^3 domains is forbidden, and the optical absorption decreases as state filling of the interband transition in the sp^2 domains dominates the transient response. At high intensity pump power, a fast photoinduced absorption (PA) that has a negative signal $\Delta T / T_0$ can be observed following the PB. Referring to the energy band gap structure of sp^3 domains in Fig. 2.24, we can conclude that TPA is dominating at high pump power intensity (Z.-B. Liu et al., 2011). The PA mechanism of GO at high intensity laser, makes the GO an excellent broadband optical limiter (an optical components that limits transmission of intense light).

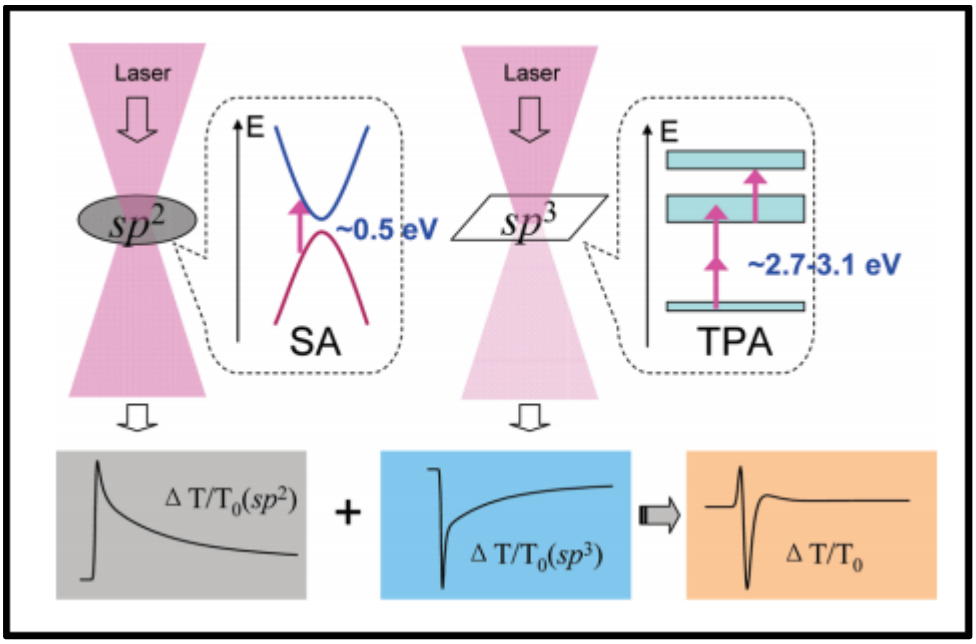

Fig. 2.24: Depiction of transient absorption in sp^2 and sp^3 domains; saturable absorption (SA) and two-photon absorption (TPA). The incident excitation induces a positive transient differential transmission in sp^2 domains due to SA and negative transient differential transmission in sp^3 domains due to TPA. The insets are the band gap structures of sp^2 domains (left) and sp^3 domains (right). The bottom shows that the combination of both transient differential transmission corresponds to sp^2 and sp^3 domains, respectively (Reproduced from Z.-B. Liu et al., 2011).

2.6.2.2 FLUORESCENCE IN GO

The absence of energy band gap in graphene implies that fluorescence is not possible unless assisted by phonons (Essig et al., 2010). In contrast to graphene, GO display evidence of near-infrared (NIR), visible and ultraviolet fluorescence as a consequence of the heterogeneous atomic and electronic structures (Cuong et al., 2010; Eda et al., 2010; Z. Luo et al., 2009; Pan, Zhang, Li, & Wu, 2010; Subrahmanyam, Kumar, Nag, & Rao, 2010).

The chemical versatility and tunability of GO alongside with easy process ability makes GO an attractive candidate for a wide range of applications. Strongly heterogeneous atomic and electronic structures of GO denote that fluorescence in GO arises from recombination of electron-hole pairs in localized electronic states originating from various possible configurations, rather than from band-edge transitions as is the case in typical semiconductors. While the exact mechanism that is responsible for fluorescence in GO is unclear, various groups have reported some key experimental observations and proposed different mechanisms.

Low-energy fluorescence in the red to NIR region in laterally nanosized GO aqueous suspensions have been reported by Sun and colleagues (Z. Liu, Robinson, Sun, & Dai, 2008; X. Sun et al., 2008). Z. Luo et al. (2009) published a comparable fluorescence properties for suspensions and solid samples containing as-synthesized GO with typical lateral dimension of 1-10 μm, implying that the lateral size of the sheets is not the main factor controlling the emission energy. Gokus et al. (2009) reported broad red to NIR fluorescence from an oxygen-plasma-treated, mechanically exfoliated graphene sample. The conclusion from these findings, from the fact that similar fluorescence properties can be observed from nanosized GO, as-synthesized GO and oxygen-plasma-treated graphene, suggest that the origin of fluorescence in GO is closely related.

An alternative explanation for fluorescence in GO has also been proposed by Pan et al. (2010), who used the hydrothermal route to cut GO sheets into blue-luminescent graphene quantum dots. From their analysis, emission from zigzag sites with a carbene-like triplet ground states described as $\sigma^1\pi^1$ has been proposed as possible explanation for the fluorescence. Moreover, previous observations of fluorescence from carbon nanoparticles and functionalized carbon nanotubes have been attributed to the presence of oxygen-containing functional groups (Loh et al., 2010).

2.7 CARBON NANOTUBE (CNT)

In 1991, Sumio Iijima, who was then a Senior Principle Researcher at NEC Corporation, published a paper in which he observed a graphitic carbon needles using an electron microscope (Iijima, 1991). Although traces of carbon nanotube can be found in ancient Damascus sabre steel from the seventeenth century (Reibold et al., 2006), Sumio Iijima, nonetheless, is often cited as the inventor of carbon nanotube.

In simple description, carbon nanotube (CNT) is a rolled-up graphene (refer to Fig. 2.18), whose typical diameter is ~1 nm and has a typical length of ~1 μm. Therefore, it is a long 1-D material. CNT can be classified into two categories; single-wall (SWCNT) and multiwall (MWCNT) (refer to Fig. 2.25). The CNT structure is determined by how the single-layer graphene is rolled, and defined by a single parameter; chirality. Chirality is expressed by a chiral vector $\mathbf{C_h}$, connecting two crystallographically equivalent sites (connecting points in rolling) of the 2-D graphene sheet. The chirality, $\mathbf{C_h}$ is define as

$$\boldsymbol{C}_h = n\boldsymbol{a}_1 + m\boldsymbol{a}_2 \equiv (n, m) \qquad \text{(Eq. 2.41)}$$

where $\mathbf{a}_1$ and $\mathbf{a}_2$ are the unit vectors of the hexagonal honeycomb lattice. The structure of any CNT can be defined by a pair of integers (*n, m*) the determined its chiral vector (Phaedon Avouris & Chen, 2006). Depending on the chiral vector, CNT can be classified as metallic or semiconducting. Fig. 2.26 show graphical example how chirality is determined.

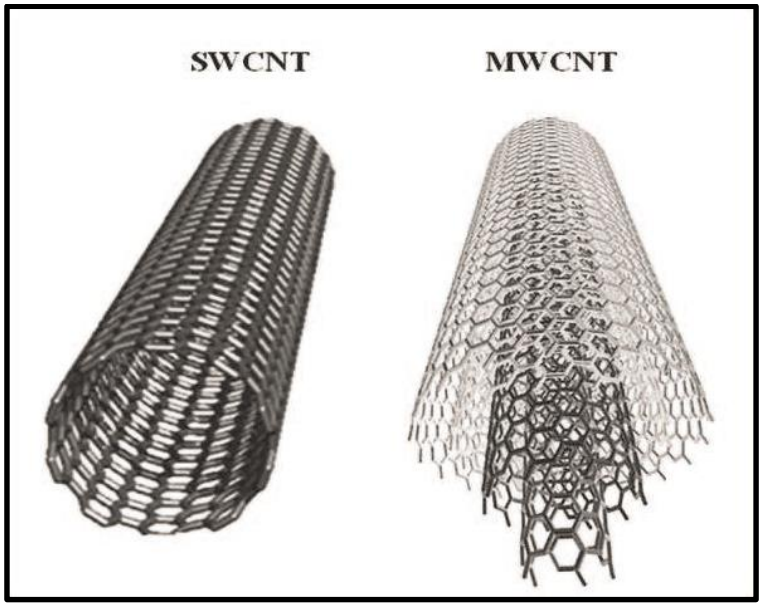

Fig. 2.25: SWCNT and MWCNT (Reproduced from Choudhary & Gupta, 2011)

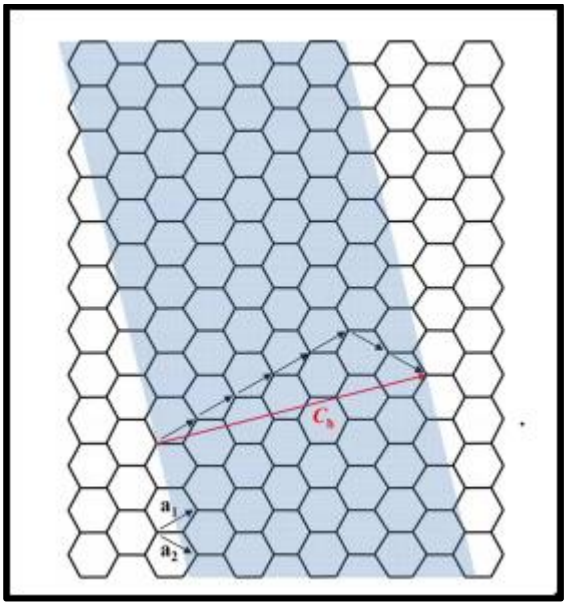

Fig. 2.26: Representation of the CNT structure through the folding of a graphene sheet. The chirality vector C_h of a (5,2) CNT is shown as an example (Reproduced from S. Yamashita, 2012).

If $n\text{-}m = 3k$ (k is integer) the CNT is classified as metallic CNT, and $n\text{-}m \neq 3k$ is for semiconducting CNT. Fig. 2.27 shows the band structure of metallic and semiconducting CNTs and their associated density of states (DOS).

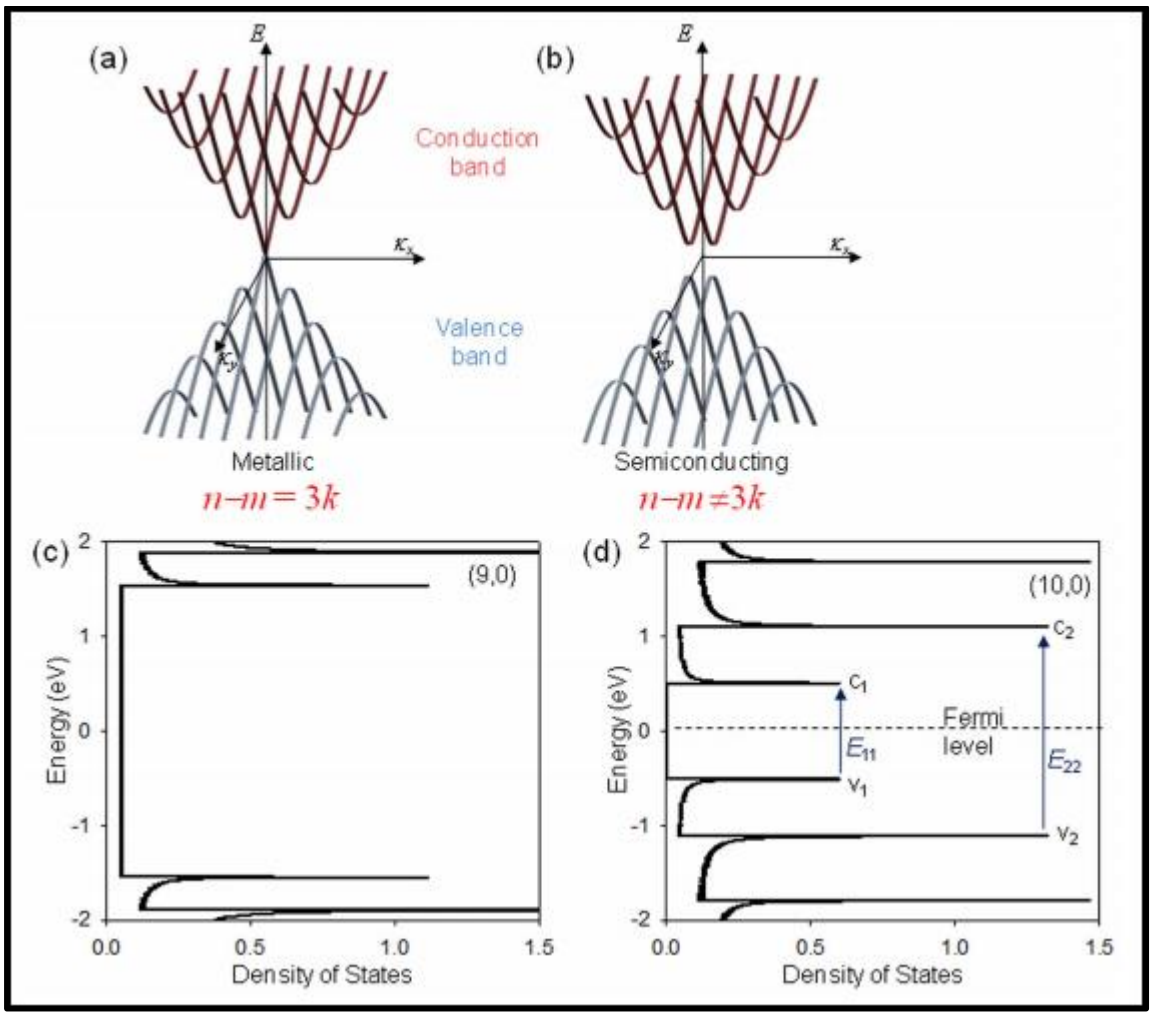

Fig. 2.27: Band structures and density of states of (a),(c) metallic CNT and (b),(d) semiconducting CNT (Reproduced from S. Yamashita, 2012).

2.7.1 ELECTRONIC AND BAND STRUCTURE OF SWCNT

The band structure of the "rolled-up" graphene can be assumed under a simple tight-binding model of Riichiro Saito, Fujita, Dresselhaus, and Dresselhaus (1992). In Riichiro Saito et al. (1992), CNT is considered as a roll of graphene layers. The unit cell of the sheet contains two carbon atoms, where each carbon atoms have four valence electrons. Therefore, the tight-binding model of (Riichiro Saito et al., 1992) resulted in eight bands; four valence bands and four conduction bands. One *s* orbital and two in-plane *p* orbitals of each carbon

atom are sp^2-hybridized. Due to the different symmetry of the sp^2-hybridized orbitals and p_z orbitals, the matrix elements of the Hamiltonian and the overlap matrix elements between such orbitals vanish. The sp^2-hybridized orbitals form the so-called σ valence bands and σ* conduction bands. The p_z orbitals of the carbon atoms, oriented perpendicular to the sheet (z-direction), form the π valence and the π* conduction band. As a result, the problem for the band structure of a graphite sheet conveniently splits into a problem for the σ and σ* bands, and a problem for the π and π* bands. The resulting band structure of graphene is characterized with π and π* bands degenerate at the ***K*** points in the hexagonal Brillouin zone of the sheet (Fig. 2.28).

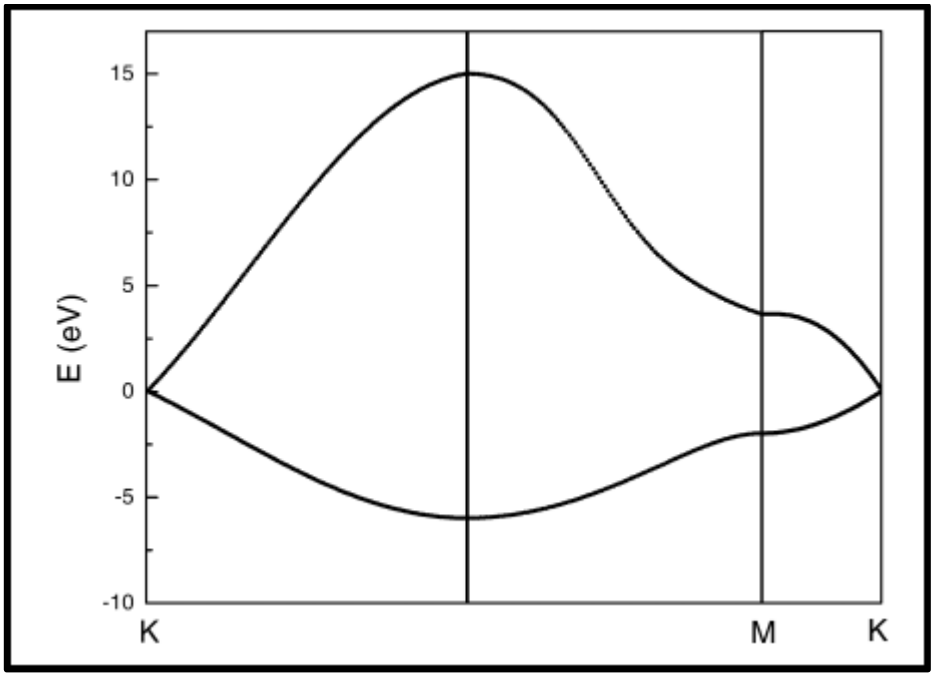

Fig. 2.28: The electronic band structure of a graphite sheet calculated within a π-band tight-binding model. The valence π and conducting π* bands show degeneracy at the *K* points in the Brillouin zone at the Fermi level (Reproduced from Popov, 2004).

The degenerate energy level corresponds to the Fermi energy, which shows that the graphene sheet is a zero-gap metal. By rolling-up graphene strip into cylindrical nanotube,

the band structure of the nanotube can be derived from that of the graphene sheet by the zone-folding method. However, this model completely ignores the curvature effect of CNTs (S. Yamashita, 2012). The one-dimensional (1D) band structure of a *(n, m)* nanotube is given by the zone-folding relation by use of the two-dimensional band structure of graphene (R Saito, 1998)

$$E_{k\mu} = E_{2D}\left(k\frac{\boldsymbol{K}_2}{|\boldsymbol{K}_2|} + \mu\boldsymbol{K}_1\right) \qquad \text{(Eq. 2.42)}$$

where k is the 1D wavevector ($-\pi/T < k < \pi/T$, T being the translation period of the nanotube) and μ is a discrete quantum number ($\mu = 1, 2, \ldots, N$ is the number of carbon pairs in the unit cell of the nanotube). The vectors $\boldsymbol{K_1}$ and $\boldsymbol{K}_2$ are expressed through the reciprocal lattice vectors $\boldsymbol{b}_1$ and $\boldsymbol{b}_2$ of the graphene sheet as

$$\boldsymbol{K}_1 = \frac{-t_2\boldsymbol{b}_1 + t_1\boldsymbol{b}_2}{N} \; and \; \boldsymbol{K}_2 = \frac{m\boldsymbol{b}_1 - n\boldsymbol{b}_2}{N} \qquad \text{(Eq. 2.43)}$$

The 1D band structure of a given SWCNT consists of the 2D band structure of the graphene sheet along N lines along $\boldsymbol{K}_2$ in the 2D Brillouin zone of the sheet. If for a given nanotube, one of these lines passes through a $\boldsymbol{K}$ point, the tube will have a finite energy gap. In the former case, the tube is metallic and in the latter case, it is semiconducting. In the folding-zone method, a tube is metallic if *n-m* is a multiple of 3 and semiconducting if *n-m* is not a multiple of 3 (Hamada, Sawada, & Oshiyama, 1992; Wilder, Venema, Rinzler, Smalley, & Dekker, 1998) (Fig. 2.31). As with other 1D systems, the electronics density of states is govern by van Hove singularities.

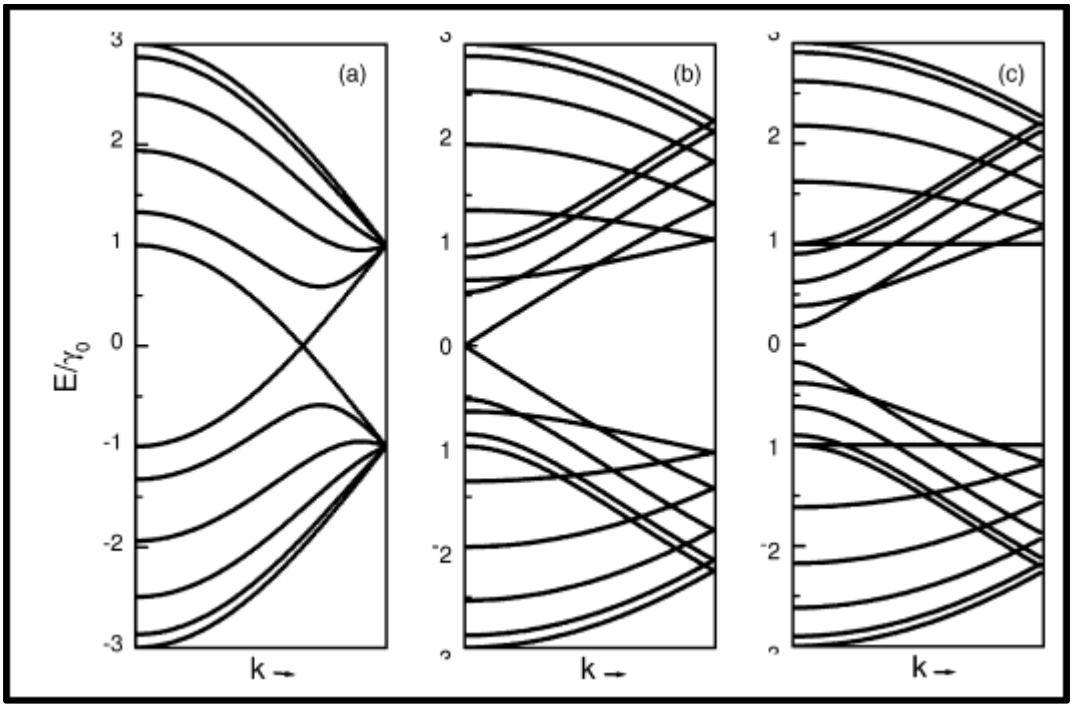

Fig. 2.29: Electronic band structure of nanotubes (a) (5, 5), (b) (9, 0) and (c) (10, 0) derived by zone-folding of the band structure of the graphene sheet; *a* is the nearest-neighbor C-C separation and $\gamma_0 = 2.9$ eV (Reproduced from Popov, 2004)

2.7.2 OPTICAL PROPERTIES OF CNT

Essentially a rolled-up graphene, most of the electronic properties of CNT are inherent of the unusual electronic properties of graphene.

2.7.2.1 OPTICAL ABSORPTION OF CNT

The semiconducting CNTs has peak absorption wavelength depending on the optical bandgaps. Typical CNT with diameter *d,* of 7-15 nm has a bandgap energy of 1.2-0.6 eV, corresponds to the optical wavelength of 1-2 μm. Thus, the peak absorption can be tuned by

choosing the appropriate diameter. However, since CNTs are a mixture of several or many kinds of semiconducting and metallic CNT as well as different diameter distribution, the absorption peak is determined by the mean tube diameter and the absorption bandwidth depends on the tube diameter distribution. Fig. 2.30 shows a transmission spectrum of a CNT sample. Although CNT is essentially a rolled-up graphene, the absorption of CNT is nonlinear.

The optical absorption in CNT is anisotropic because CNT only absorbs the light whose polarization is parallel to the axial direction of the tube, therefore, an aligned CNT sample is polarization dependent (Shinji Yamashita et al., 2006). In spite of this, since we use a randomly oriented CNT samples, the CNT is polarization independent (S. Yamashita, 2012).

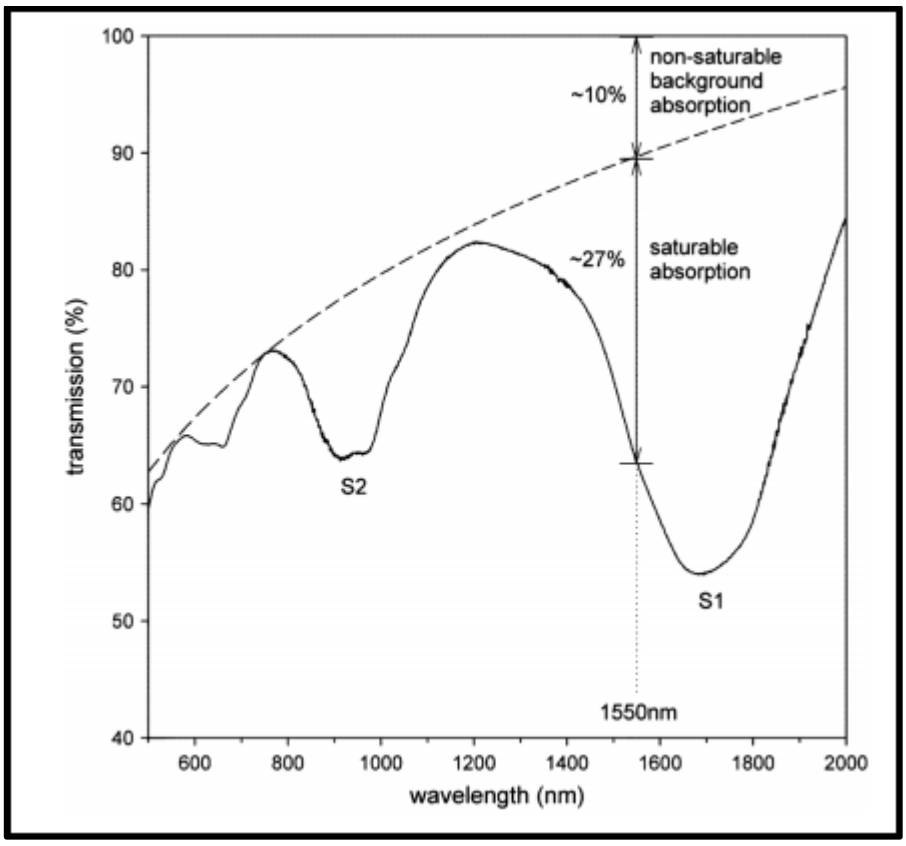

Fig. 2.30: CNT transmission spectrum showing saturable absorption and non-saturable background absorption (Reproduced from Set, Yaguchi, Tanaka, & Jablonski, 2004b).

2.7.2.2 ELECTROLUMINESCENCE AND PHOTOLUMINESCENCE IN CNT

The direct bandgap that exists in CNT suggest that they can be an efficient light absorbers and emitters. Studies regarding electroluminescence properties of SWCNT-polymer composites have been performed (Kazaoui et al., 2005; Z. Xu, Wu, Hu, Ivanov, & Geohegan, 2005). Electron and hole carriers in semiconductors can recombine by different sorts of mechanism. In most of the cases, the energy will be released as heat. Nevertheless, a fraction of the recombination events may involve the emission of a photon. The process is

called electroluminescence and is responsible for producing solid-state light sources such as light-emitting diodes (LED).

In order to fabricate LEDs or any other electroluminescent device, significant recombination of electrons and holes population is necessary. In ambipolar CNT-field effect transistor (CNT-FET), at an appropriate bias, electrons and holes can be simultaneously injected at the opposite ends of the CNT channel. The process allows electroluminescence to occur (Misewich et al., 2003). The radiation also has a characteristic energy that depends on the diameter and chirality of the excited CNT, (Phaedon Avouris & Chen, 2006).

The direct bandgap of a semiconducting CNT is responsible for the photoluminescence phenomena in CNT. An electron in a CNT absorbs excitation light via transition from v_2 to c_2 and creates another excitation (refer to Fig. 2.31). Electron and hole rapidly relax from c_2 to c_1 and from v_2 to v_1 states respectively. When plotting the emission wavelength as function of excitation wavelength, we can identify the chirality distribution, as depicted in Fig. 2.31. Luminescence can only be observed in isolated semiconducting CNTs because the bundled CNTs have rapid transfer process from semiconducting to metallic CNTs (Reich, Thomsen, & Maultzsch, 2008).

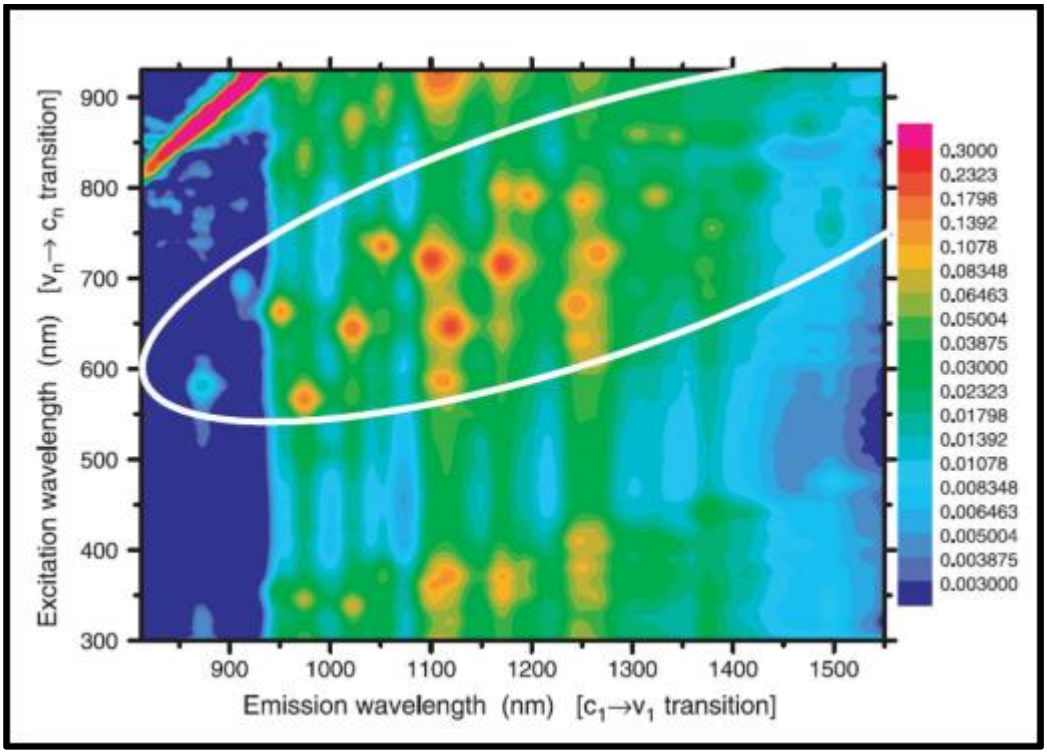

Fig. 2.31: Contour plot of fluorescence intensity versus excitation as a function of excitation and emission wavelength for a sample of SWCNTs (Bachilo et al., 2002)

2.7.2.3 SATURABLE ABSORBER

SWCNT has been utilized as saturable absorber (SA) for mode-locking fiber laser long before graphene. The first publication of SWCNT SA can be traced as early as 2003 (Sze Y Set et al., 2003). CNT can saturate with high-intensity light when the states of conduction band becomes full and the states at valence band becomes empty. Furthermore, the recovery time, τ is observed to be very fast.

In semiconducting CNT, the recovery time of E_{11} transition is an order of 1 ps, and the transition of E_{22} is in the order of 100 fs (refer to Fig. 2.27). Slower recovery in an order of several ps is also seen in the E_{11} transition. Several mechanisms are believed to be responsible for the fast relaxation have been proposed. These mechanisms are multi-phonon

emission (Ichida, Hamanaka, Kataura, Achiba, & Nakamura, 2002), tube-tube interaction (Tatsuura et al., 2003) and exciton-exciton annihilation (Ma, Hertel, Vardeny, Fleming, & Valkunas, 2008; Ma et al., 2004).

SWCNT SA can be incorporated in fiber laser in various ways. These techniques are spray coating (Set et al., 2004b; Sze Y Set et al., 2003), direct growth (S. Yamashita et al., 2004), optical deposition (Kashiwagi, Yamashita, & Set, 2009; Nicholson, Windeler, & DiGiovanni, 2007), polymer composite (Tawfique Hasan et al., 2009; Rozhin et al., 2006; Sakakibara, Rozhin, Kataura, Achiba, & Tokumoto, 2005), polymer fiber (Uchida, Martinez, Song, Ishigure, & Yamashita, 2009) and microfiber (Kashiwagi & Yamashita, 2009)

CHAPTER 3

Q-SWITCHED AND MODE-LOCKED ERBIUM-DOPED FIBER LASERS

3.1 INTRODUCTION

Fiber lasers are made possible by incorporating trivalent rare-earth ions such as neodymium, erbium and thulium into glass hosts. Since 1980's Erbium-doped fiber lasers (EDFLs) have gained widespread interest because the lasing wavelength at 1.55 μm, falls within the low-loss window of optical fiber, which is suitable for optical fiber communications (H Ahmad, Saat, & Harun, 2005; Tamura, Haus, & Ippen, 1992). They have numerous advantages such as simple doping procedures, low loss, compact, high reliability and high-output power.

Q-switched and mode-locked are two types of pulsed laser. Both are usually distinguished by the repetition rate, pulse duration and pulse energy. A *Q*-switched laser usually has much lower repetition rate (~kHz) and longer pulse duration (~ns to ~μs). Because of the lower repetition rate, pulse energy of *Q*-switched laser is larger than mode-locked laser. *Q*-switching is a technique of modulating the intracavity losses, also known as quality factor, *Q*. When the gain medium is pumped, it accumulates energy and emits photons. A loss modulator will initially inhibit the laser buildup in the cavity while the gain medium is being pump. When photon flux build-up to a level that saturates the saturable absorber before the gain medium, suddenly, the intracavity losses reduces and the laser

produces a short and intense pulse, known as *Q*-switch. This technique usually produces pulses with pulse duration equal to the duration of a few roundtrips in the cavity. Unlike mode-locking, the *Q*-switching pulse is not short enough to be affected by dispersion (Digonnet, 2001; Welford, 2003). Mode-locking is another technique of generating pulsed laser. It is usually characterized by a high repetition rate (~MHz to ~GHz) and shorter pulse duration (~ps to ~ fs). The term mode-locking describes the fixed phase relationship between all the longitudinal modes inside the laser cavity. Because of the fixed relationship between all the longitudinal modes inside the laser cavity, the pulse duration is shorter compared to *Q*-switch.

Both techniques can be realized using active and passive methods. An active method involves an external modulator; acousto-optic or electro-optic. These modulators act as a switch, which transmits and attenuates light from the laser; thus creating pulses. Passive methods also involves modulating the loss inside the cavity, usually using saturable absorber. Passive method can generate shorter pulses than active methods because the loss modulation is faster. Passive mode-locking (M. E. Fermann, Galvanauskas, & Sucha, 2002; M. E. Fermann, Galvanauskas, Sucha, & Harter, 1997; Ippen, 1994; Nelson et al., 1997) has several other techniques namely non-polarization rotation (NPR) (M. Fermann, Andrejco, Silberberg, & Stock, 1993; Komarov, Leblond, & Sanchez, 2005; Tamura et al., 1992), figure-of-eight (Iii, 1991; Richardson, Laming, Payne, Phillips, & Matsas, 1991; Seong & Kim, 2002), and semiconductor saturable absorber mirror (SESAM) (U. Keller, 2003; U. Keller et al., 1996; O. Okhotnikov, Grudinin, & Pessa, 2004).

In this chapter, *Q*-switched and mode-locked fiber lasers are demonstrated using various passive techniques. In the first section, mode-locked EDFLs is demonstrated using a highly concentrated Erbium-doped fiber (EDF) as the gain medium in a ring configuration

based on nonlinear polarization rotation (NPR) technique. A polarizer and a polarization controller (PC) are added into the cavity to act as an artificial saturable absorber (SA). The proposed laser generates soliton pulses with a repetition rate of 12 MHz, pulse-width of 1.11 ps and energy pulse of 0.0863 nJ. Mode-locked EDFL is also demonstrated using a semiconductor SA. By incorporating the SA in the ring cavity and substituting the polarized output coupler with normal coupler, the Kelly sidebands at the optical output of the laser is less prominent due to the high nonlinearity of the SA. With the SA, a cleaner pulse is obtained with a repetition rate of 11.3 MHz, pulse-width of 0.58 ps and pulse energy of 0.123 nJ.

In the second part of this chapter, it is demonstrated that the *Q*-switched and soliton mode-locked fiber lasers are generated using a homemade single-walled carbon nanotube saturable absorber (SWCNT SA). The SWCNT is incorporated into a ring cavity by dripping the SWCNT sodium dedocyl sulfate (SDS) solution onto the fiber ferrule. The SWCNT SA has a linear insertion loss of 3.61 dB. *Q*-switched fiber laser self-starts with repetition rate between 10.25 kHz to 41.87 kHz, depending on pump power. After adding 200 meter single-mode fiber (SMF), the fiber laser self-starts in soliton mode-lock operation. Resultant repetition rate is 907 kHz, pulse duration of 2.52 ps with signal-to-noise ratio (SNR) of 53.42 dB.

3.2 MODE-LOCKED EDFL USING NPR AND SEMICONDUCTOR SA

It is observed that there is a growing interest in mode-locked EDFLs in recent years due to their many applications in communication systems for time-division multiplexing (TDM) (Yamamoto, Yoshida, Tamura, Yonenaga, & Nakazawa, 2000), code-division

multiple access (CDMA) (Sardesai, Chang, & Weiner, 1998) and wavelength division-multiplexing (WDM) (Boivin, Wegmueller, Nuss, & Knox, 1999; De Souza, Nuss, Knox, & Miller, 1995). Mode-locked lasers have found their applications in high-resolution spectroscopy, THz pulse generation, optical clockworks, absolute distance measurements and many others (Diddams, Hollberg, Ma, & Robertsson, 2002; Diddams et al., 2000; Shioda, Mori, Sugimoto, Tanaka, & Kurokawa, 2009; Udem, Holzwarth, & Hansch, 2002).

Recently, a high concentration Erbium-doped fiber (EDF), IsoGain^{TM} has been commercially developed by FiberCore Co. Ltd. to provide the ultimate in cost-effectiveness for the EDF amplifier (EDFA), with typical C-band gain-lengths of only a few meters (H Ahmad et al., 2005). This fiber is actually more suited to reducing the exceptionally long doped fiber lengths required for effective L-band amplification. In this section, a mode-locked EDFL is demonstrated using a simple ring cavity structure with the IsoGain^{TM} EDF as the gain medium. The performance of the laser is investigated for two different mode-locking techniques; nonlinear polarization rotation (NPR) and semiconductor saturable absorber (SA). Since the gain medium is only a piece of 2.5 m long EDF, the cavity length of the EDFL is considered short and therefore stable clean pulses can be generated with a higher repetition frequency.

3.2.1 EXPERIMENTAL SETUP

Fig. 3.1 shows the configuration of the proposed laser, which is an all-fiber setup using commercially available components. It consists of a piece of 2.5 m long EDF, wavelength division multiplexers (WDMs), a 1550 nm polarization independent isolator, a PC, a transmission-type SA and a polarized 3 dB output coupler. The total length of the cavity is about 14.5 m, which comprises a 2.5 m long EDF and a 12 m long single mode fiber (SMF)

used in the other components. The EDF has an erbium ion concentration of 2000 ppm, a cut-off wavelength at 910 nm, a pump absorption rate of 24 dB/m at 980 nm and a dispersion coefficient of -21.64 ps/nm.km at λ=1550 nm. It is forward pumped using a 1480 nm laser diode via the WDM to provide amplification in the C-band region. The other part of the ring cavity uses a standard single mode fiber (SMF-28) with a dispersion coefficient of 17 ps/nm.km at λ=1545 nm. Therefore, the total cavity Group Velocity Dispersion (GVD) is 0.1499 ps/nm.km. This shows that the mode-lock fiber laser is working in the soliton region. A transmission-type semiconductor SA is used for the initiation and stabilization of mode-locking at around 1550 nm region. The SA is designed for transmission application and has a modulation depth, ΔT of 15%, saturation fluence of 300 $\mu J/cm^2$, nonsaturable loss of 10% and relaxation time constant of 2 ps. An isolator is used to ensure a unidirectional operation of the laser. A PC is used to adjust the polarization state and allows continuous adjustment of the birefringence within the cavity to balance the gain and loss for laser pulse generation. The experiment is also repeated without the semiconductor SA and the normal output coupler is substituted with a polarized output coupler wherein the mode-locking mechanism is based on NPR technique.

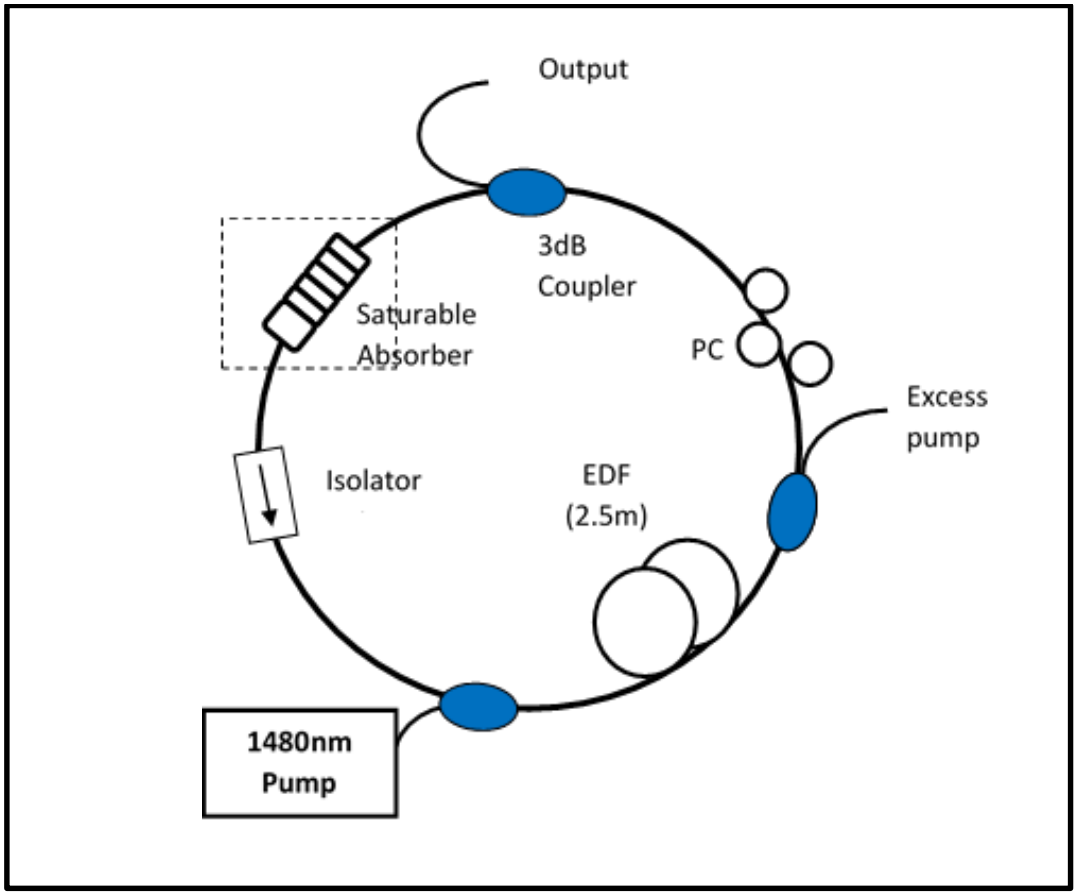

Fig. 3.1: Experimental setup consisting 1480 nm Laser Diode (LD); 2.5 meter of Erbium-Doped Fiber as gain medium; 1480/1550 nm Wavelength Division Multiplexer (WDM) to remove excess pump from 1480 nm LD; polarization controller (PC); 3-dB polarized output coupler/ 3-dB normal output coupler (OC); a 1550 nm polarization independent isolator and transmission-type saturable absorber (SA).

Fig. 3.2 compares the output spectrum of the mode locked EDFL with SA and NPR technique. As shown in the figure, both techniques are operating in the soliton regime. The soliton regime is apparent from the presence of Kelly sidebands. Kelly sidebands are less prominent in the saturable absorber optical spectrum because the saturable absorber has high nonlinearity. Without the SA, the proposed laser generates mode-locked pulses using a NPR effect in the cavity. The NPR relies on the Kerr effect in an EDF in conjunction with an

optical polarizer to produce artificial saturable absorber action. By setting the initial polarization ellipse and phase bias properly, pulse shortening can be attained. The NPR can occur in an optical fiber when the initial polarization state is elliptical. This elliptical state can be resolved into right- and left-hand circular polarization components of different intensities. These two circular components then experience different nonlinear phase shift related to the intensity dependence of the refractive index (Nelson et al., 1997; Stolen et al., 1982).

In a simple numerical simulation work of NPR, "changing the relative orientations of the wave plates is physically equivalent to adding a variable linear cavity phase delay bias to the cavity" (D. Y. Tang, Zhao, Zhao, & Liu, 2005). By properly choosing the linear cavity phase delay bias, which corresponds to appropriately selecting the orientations of the polarization controllers, soliton operation can be always obtained. With a fixed linear cavity phase delay bias but different values of gain, as long as the generated soliton pulse peak power is weaker than that of the polarization switching power of the cavity, stable uniform soliton pulse train can always is achievable (D. Y. Tang et al., 2005; D. Tang, Zhao, & Lin, 2005).

3.2.2 RESULT

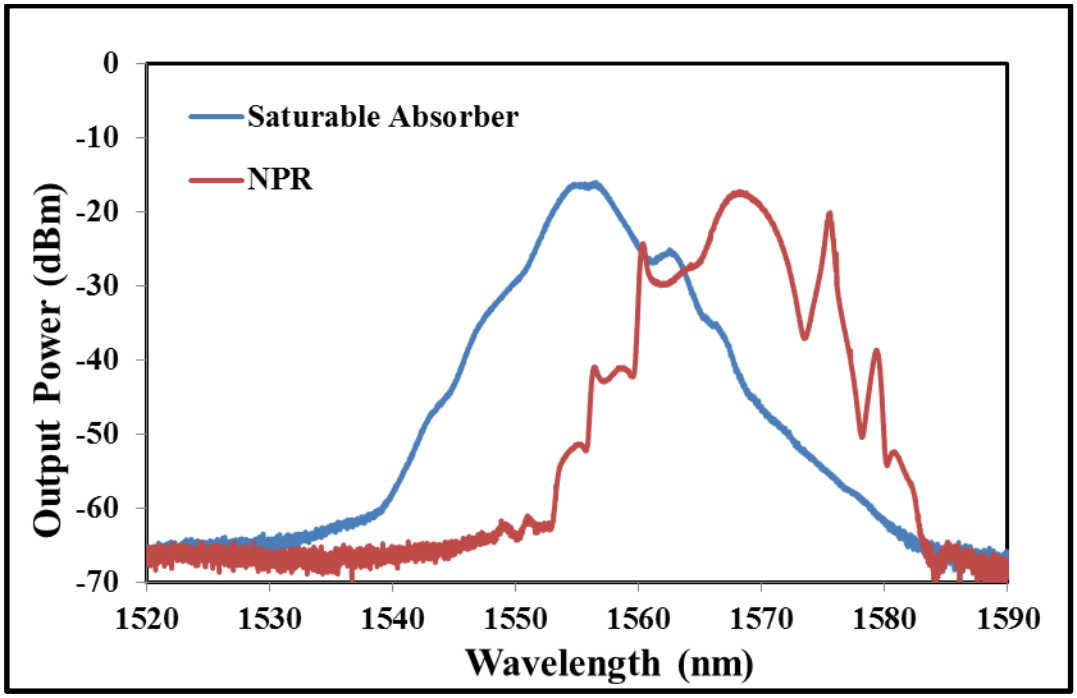

Fig. 3.2: Output spectrum of the proposed EDFL with NPR and SA operations.

On the other hand, SA introduces high loss at low intensity, but produces low loss at high intensity. As the intensity increases, the optical loss decreases. This phenomenon produces intensity modulation effect in the laser cavity, which in turn initiates mode-locking pulse.

As observed in Fig. 3.2, output spectrum peaks at 1568.2 nm and 1556.6nm for the respective NPR and SA operations. The 3 dB bandwidths of the output spectrum are obtained at 13.84 nm and 4.45 nm for NPR- and SA-based operation respectively. With maximum pump power of 136 mW, the average maximum output of 1.4 mW was achieved with the SA while NPR give an average output power of 1.036 mW. This gives pulse energy for SA and NPR of 0.123 nJ and 0.0863 nJ respectively.

Fig. 3.3 illustrates the autocorrelation trace of the output pulse of the laser with SA and NPR operations. By applying hyperbolic secant function fitting for both output curves, the pulse width of the laser is estimated to be 0.58 ps and 1.11 ps for the SA- and NPR-operation, respectively. The pulse-width of the NPR laser is nearly twice as broad as that of the pulse-width of the SA laser. This gives a Time-Bandwidth Product (TBP) of 1.874 and 0.32 for NPR and SA respectively. The ideal value for TBP is 0.32 for passive mode-lock laser. Hence, the NPR pulse is almost six times larger than the ideal value while the pulse from SA is exactly ideal. It is also noticed that the pulse from NPR is slightly unstable.

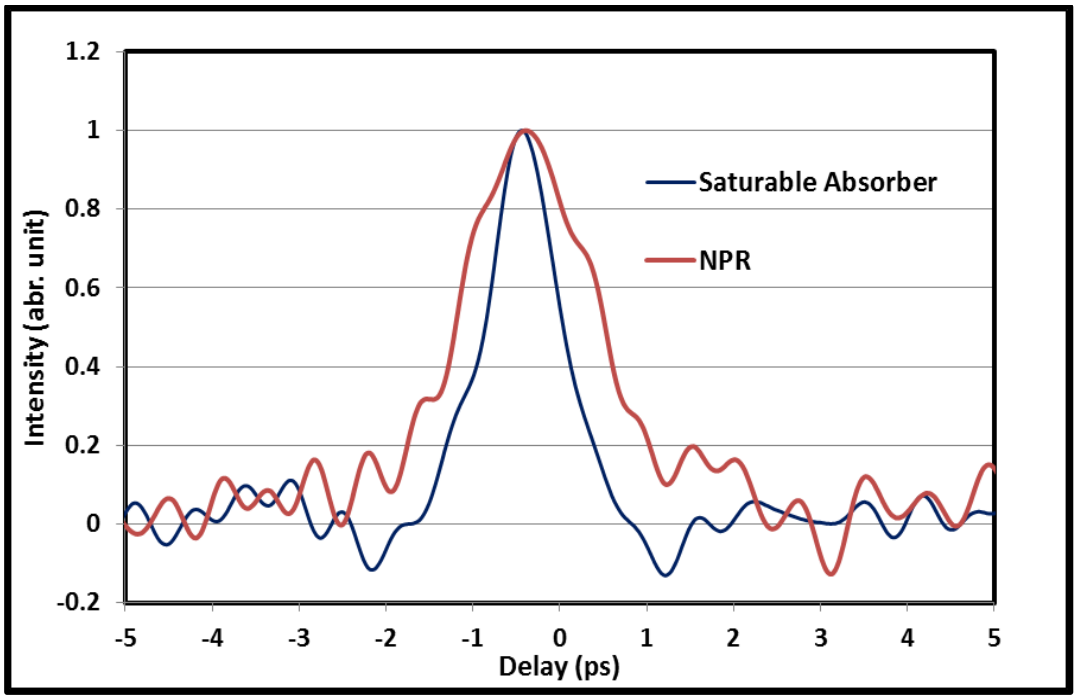

Fig. 3.3: Autocorrelation trace of the output pulse from both mode-locked EDFLs with SA and NPR approaches.

Fig. 3.4 shows the oscilloscope traces for both lasers. The repetition rate for the SA operation is determined at 11.3 MHz while the repetition rate for NPR operation is 12 MHz. Adding an SA to the fiber ring brings an extra length to the existing experimental setup. As

the result, the repetition rate for the SA operation is slightly more than that of NPR operated laser. Fig. 3.4 also illustrates that the pulse shape of the laser with SA is cleaner than the one generated by the NPR laser.

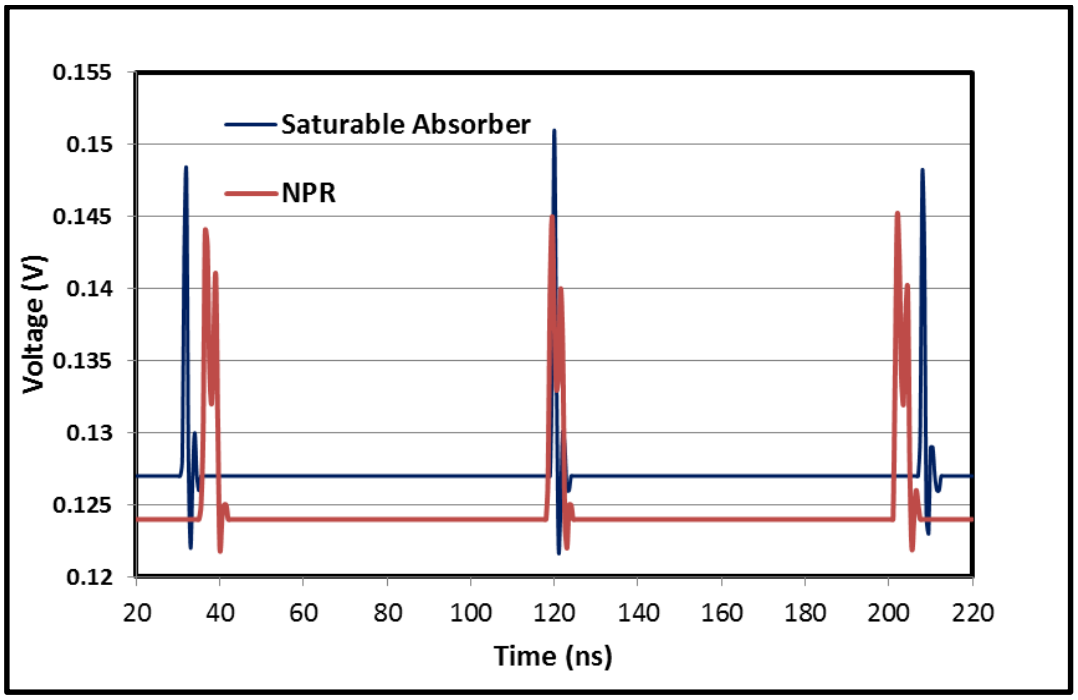

Fig. 3.4: Repetition rate observed from an oscilloscope for both SA and NPR lasers.

3.3 *Q*-SWITCHED AND MODE-LOCKED LASERS GENERATION USING A SINGLE-WALLED CARBON NANOTUBES SA

3.3.1 INTRODUCTION

The discovery of carbon nanotube (CNT) (Iijima, 1991) and graphene (Novoselov et al., 2004) have ignite the interest in passive *Q*-switched / mode-locked laser. Graphene and carbon nanotube is a one-dimensional (1-D) and two-dimensional (2-D) forms of carbon

allotrope. Both have remarkable photonics and optoelectronics properties (P. Avouris, Freitag, & Perebeinos, 2008; Bonaccorso et al., 2010; S. Yamashita, 2012). The saturable absorption property in both materials is utilized to produce *Q*-switched and mode-locked fiber lasers (H. Ahmad et al., 2012; D. Popa et al., 2011; Z. Sun, Hasan, & Ferrari, 2012). Among the advantages of CNT SA are fast recovery time (< 1 ps), compatible to optical fiber, polarization independent, tunable operating wavelength and bandwidth via diameter control and can work in transmission, reflection and bi-directional setup (S. Yamashita, 2012). Several methods of incorporating CNT SA into fiber laser have been developed; spraying (S.Y. Set, H. Yaguchi, et al., 2003; Set, Yaguchi, Tanaka, & Jablonski, 2004a), optical deposition (Kashiwagi et al., 2009; Nicholson et al., 2007), polymer composite (T. Hasan et al., 2009; V. Scardaci, Rozhin, Hennrich, Milne, & Ferrari, 2007) and film (Kivistö et al., 2009; Travers et al., 2011).

Dual-regime mode-locked and *Q*-switched EDFLs have been reported by several papers (Hideur et al., 2001; Lee et al., 2012; S. Set et al., 2003). Hideur et al. (2001) reported a switchable operating regime between continuous-wave (CW), *Q*-switched and mode-locked by controlling pump power and polarization state. Lee et al. (2012) combines passive *Q*-switching and active mode-locking to operate in both regimes while S. Set et al. (2003) uses CNT SA to produce passive mode-locking and *Q*-switching by increasing pump power.

In this section, a new technique for fabricating single-walled carbon nanotubes (SWCNTs) SA is proposed. SA is prepared by simply depositing SWCNTs sodium dedocyl sulfate (SDS) solution onto fiber ferrule. By incorporating the SA in the proposed EDFL setup, *Q*-switched and mode-locked EDFLs can be realized by adjusting cavity length.

3.3.2 FABRICATION AND CHARACTERIZATION OF THE SWCNTS SA

A homogeneous suspension solution was prepared by mixing 250 mg SWCNTs (99% pure, diameter of 1-2 nm and length of 3-30 μm) with 400 ml 1% sodium dedocyl sulfate (SDS) solution in deionized water and then ultrasonicating it for 30 minutes at 50 W. The solution was centrifuged at 1000 rpm to remove large particles of undispersed CNT to obtain dispersed suspension that is stable for weeks. The SWCNT SA was fabricated by dripping a SWCNT SDS solution onto a fiber ferrule using a pipette (refer to inset of Fig. 3.5). The droplet was left to dry at room temperature for 24 hours, before the fiber ferrule is mated to a clean ferrule via a connector.

Raman spectroscopy measurement was performed on the fiber ferrule which contains a droplet of SWCNT SDS solution. The spectroscopy was performed using laser excitation at 532 nm with 50x objective lens. The sample was exposed to 5% laser power for 20 seconds. Based on the Raman spectroscopy result, a peak at 1592 cm^{-1} is observed, indicating that the CNT is a semiconducting type. A very small peak at 174.7 cm^{-1} is also present in the spectroscopy result which gives information about the Radial Breathing Mode (RBM) of the SWCNTs. A 174.7 cm^{-1} at Raman shift gives an estimate SWCNT diameter to be ~1.4 nm (Jorio et al., 2003). The SWCNT SA linear insertion loss is measured to be 3.61 dB. This is slightly more than the recommended 3 dB maximum insertion loss by optical deposition technique (Martinez et al., 2010; Nicholson et al., 2007).

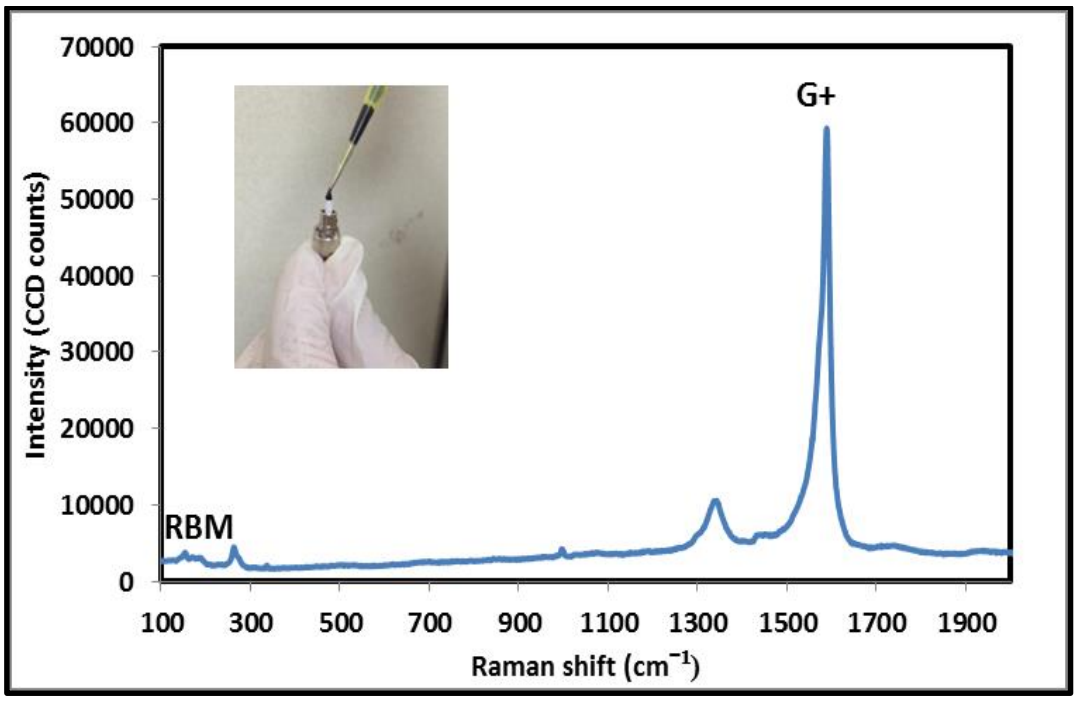

Fig. 3.5: Raman spectroscopy of SWCNT SA and SWCNT SA fabrication (inset).

3.3.3 *Q*-SWITCHED EDFL USING THE SWCNTS SA

Lasers operating in CW or quasi-CW mode have limited optical output power depending on the maximum available pump power. By concentrating the available energy in a single, short optical pulse, or in a periodic sequence of optical pulses transient laser behavior allows for higher peak power. *Q*-switching is a technique that enables the generation of a short optical pulse by sudden switching of the cavity *Q*-factor or the cavity loss. Compared to CW fiber lasers, *Q*-switched fiber lasers produce higher peak power, which are useful in numerous applications, such as industrial processing, remote sensing, range finding and medicine. As discussed earlier, active *Q*-switching is typically achieved by inserting an acoustic-optic or an electro-optic modulator into the cavity. On the other hand, passive *Q*-switching by means of SAs is a convenient technique to simplify the cavity design and eliminate the need for external *Q*-switching electronics. Semiconductor saturable absorber

mirrors (SESAMs) (R. Paschotta et al., 1999) can be used as the SA for the *Q*-switched fiber lasers. However, the fabrication of SESAMs requires very complex and costly processes. In this sub-section, a *Q*-switched EDFL is demonstrated using a comparatively simple and cost effective alternative technique based on SWCNTs SA.

Fig. 3.6 shows the experimental setup for the proposed *Q*-switched EDFL. It consists of a 4 m long EDF, two 1480/1550nm wavelength division multiplexer (WDM), a SWCNTs based SA, an optical isolator and a 20 dB output coupler in a ring configuration. The EDF is a commercial fiber with Erbium ion concentration of 2000 ppm, cut off wavelength of 920 nm and numerical aperture of 0.24. It is backward pumped by a 1480 nm laser diode (LD) with the maximum output power of 129 mW via the WDM. Another 1480/1550 WDM is used after the gain medium to dispose excess power from the LD. An isolator is used to ensure unidirectional propagation of light inside the cavity. The homemade SWCNT SA is placed between the isolator and the WDM to act as a *Q*-switcher. The output of the laser is tapped out of the cavity through a 1% port of the 20 dB coupler. The optical spectrum analyzer (OSA, Ando AQ6317B) is used for the spectral analysis of the *Q*-switched EDFL with a spectral resolution of 0.02 nm whereas the oscilloscope (OSC, Tektronix, TDS 3052C) is used to observe the output pulse train of the *Q*-switched operation via a 6 GHz bandwidth photo-detector. Except for the gain medium, the rest of the cavity uses a standard SMF-28 fiber. Total cavity length is 23 meter. The total cavity length of the ring resonator is measured to be around 23 m. All fiber components are spliced between each other. No Polarization Controller (PC) is used in the cavity. Furthermore, all optical components are polarization independent.

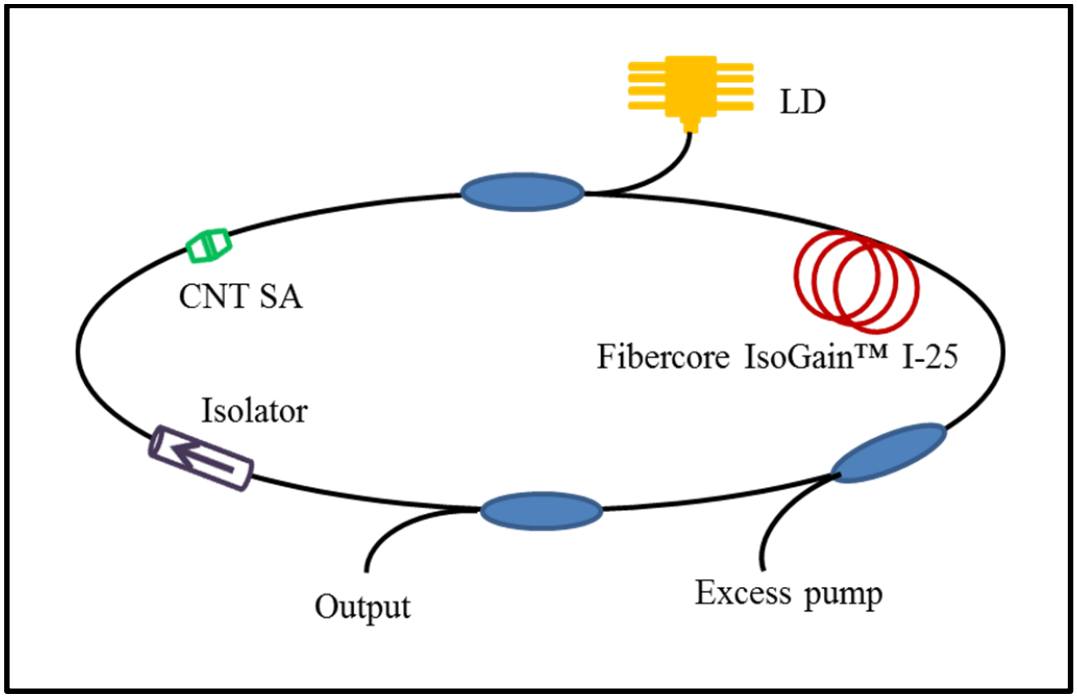

Fig. 3.6: Experimental setup for the proposed SWCNTs based *Q*-switched EDFL.

Stable and self-starting *Q*-switching operation is obtained just by adjusting the 1480 nm pump power over the threshold pump power of 30 mW. Fig. 3.7 compares the output spectra of the EDFL at three different pump powers; 30 mW, 80 mW and 129 mW. As shown in the figure, the laser operates at center wavelength of around 1571.6 nm. Spectral broadening is observed in the spectrum especially at a pump power of 80 mW, which corresponds to the minimum pulse width region. This is attributed to the Self-Phase Modulation (SPM) effect in the laser cavity. In the proposed *Q*-switched laser, the pulse width obtained is relatively long (in microsecond region) and thus it is difficult to group velocity dispersion (GVD) to have effect. Therefore only SPM-induced spectral broadening is obtained (Digonnet, 2001). The maximum Full-Width at Half-Maximum (FWHM) of 0.6 nm is obtained at 129 mW pump power.

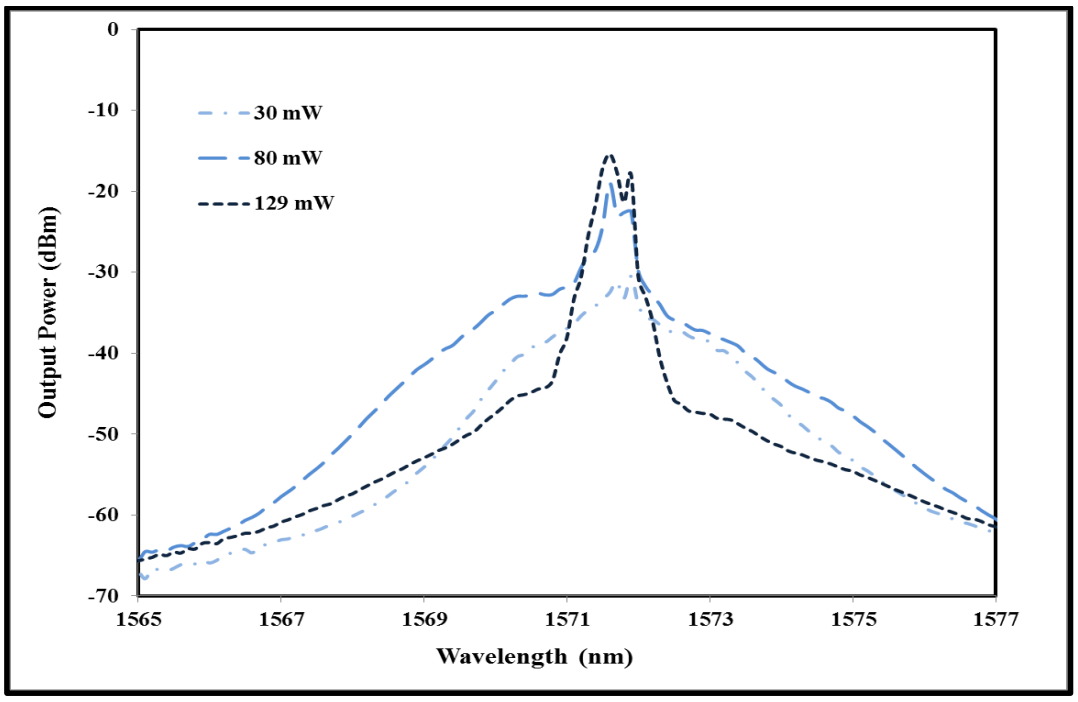

Fig. 3.7: Output spectra of the *Q*-switched EDFL at three different pump powers: 30 mw, 80 mW and 129 mW.

Fig. 3.8 shows the relationship between repetition rates and pulse durations with pump power. At the threshold pump power of 30 mW, the repetition rate and pulse duration are obtained at 10.25 kHz and 17.6 µs respectively. As pump power increases from 30 mW to 129 mW, the repetition rate increases linearly from 10.25 kHz to 41.87 kHz. This indicates that the repetition rate in *Q*-switched laser is a function of pump power. As pump power increases, more gain is provided to saturate the SA and thus increases repetition rate of the output laser. In contrast, pulse duration decreases from 17.6 µs to 10.92 µs as the pump power increases from 30 to 129 mW. However, the lowest pulse duration of 10.42 µs is achieved at 80 mW pump power. As the pump power increases from 80 mW to 129 mW, the pulse durations increase slightly before decreasing back at 129 mW. Hence, the minimum attainable pulse duration is 10.24 µs, which is related to modulation depth of the saturable absorber (Zayhowski & Dill Iii, 1994; J. J. Zayhowski & P. L. Kelley, 1991). Based on the

minimum attainable pulse duration, the modulation depth of the SWCNT SA is calculated to be around 3.7%. Fig. 3.9 shows the relationship between pulse energy and pump power in the proposed *Q*-switched EDFL. As the pump power increases, the average output power also increases, which give rise to pulse energy. It is obtained that the pulse energy can be increased from 2.23 nJ to 4.94 nJ by tuning the pump power from 30 to 80 mW, and from 4.94 nJ to 5.19 nJ when the pump power increases from 80 mW to 129 mW . The calculated average slope efficiency is 12% when the pump power increases from 30 mW to 80 mW. From 80 mW to 129 mW pump power, the calculated average slope efficiency is 16%. The pulse energy is saturated as the pump power is further increased above 80 mW.

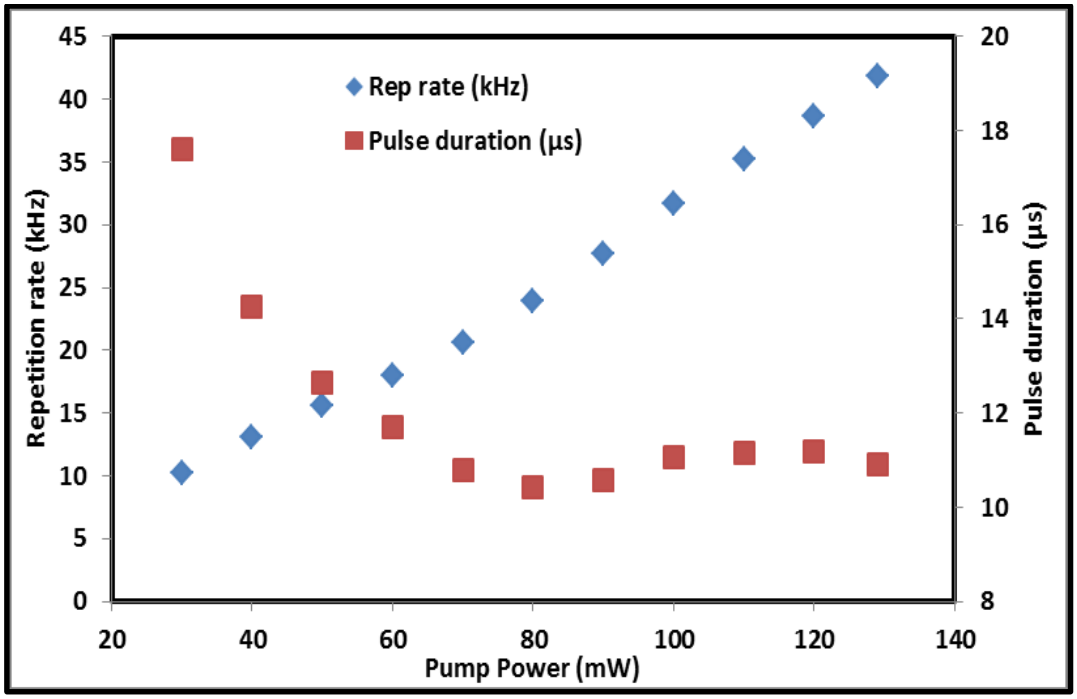

Fig. 3.8: Repetition rate and pulse duration relationships with pump power.

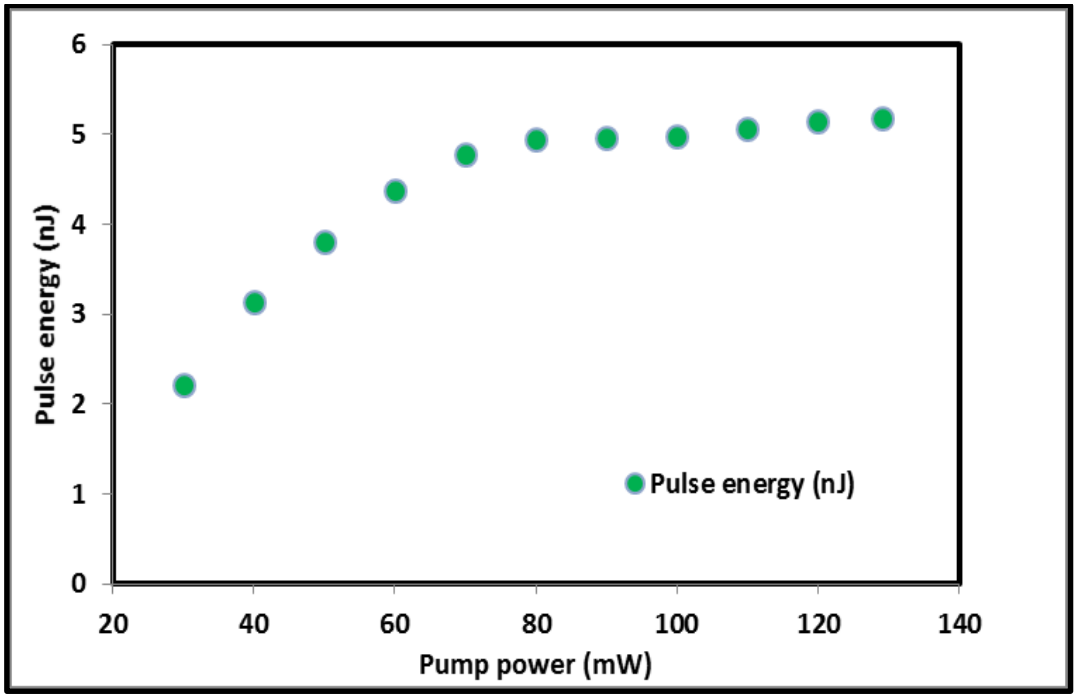

Fig. 3.9: Pulse energy against pump power

3.3.4 MODE-LOCKED EDFL USING THE SWCNTS SA

The previous laser setup of Fig. 3.6 is slightly modified to realize mode-locking operation. The experimental setup for proposed SWCNTs based mode-locked EDFL is shown in Fig. 3.10. Compared to the previous setup, a 200 m long SMF is added in the mode-locked setup to reduce the repetition rate of the output pulse and thus increase the pulse energy in the cavity. The improved pulse energy is sufficient enough to saturate the SA for mode-locking operation. The cavity consists of 4 m long EDF and a ~219 m long SMF-28 fibers with a dispersion of -21.64 ps nm^{-1} km^{-1} and 17 ps nm^{-1} km^{-1}, respectively at 1550 nm. This gives total cavity length of ~223 meter and a total Group Velocity Dispersion (GVD) of 3.6364 ps nm^{-1} km^{-1}. Therefore, soliton pulse train can be generated by the cavity. For pulse duration measurement, an autocorrelator with 25 fs resolution was used. The SNR is measured using Anritsu MS2667C Radio Frequency Spectrum Analyzer (RFSA).

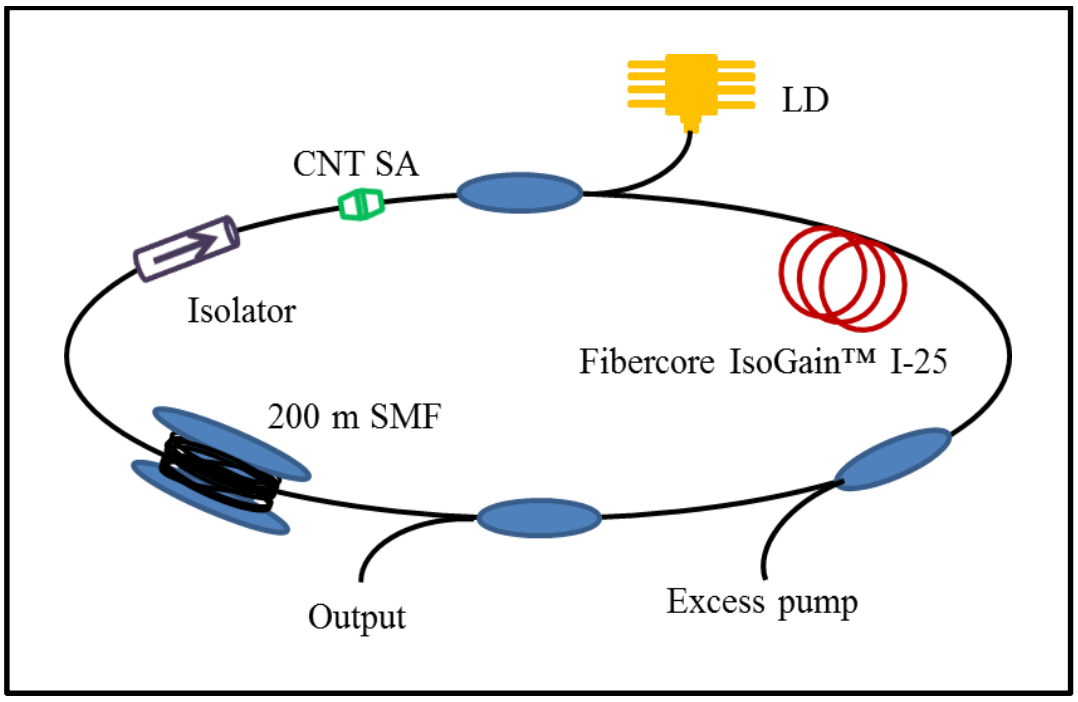

Fig. 3.10: Experimental setup for soliton mode-lock operation.

Soliton mode-locking operation self-starts at 56.75 mW without *Q*-switching instabilities. It is observed that the pulse state diminishes into continuous-wave (CW) when the pump power is below than 30 mW. The resultant repetition rate is 907 kHz, which corresponds to ~223 meter of cavity length. Fig. 3.11 shows output spectrum of the proposed mode-locked EDFL, which is obtained by incorporating SWCNTs SA in the laser cavity. As shown in the figure, the laser operates at a central wavelength, λ_C, of 1570.5 nm with 3-dB bandwidth of 1.080 nm. Compared to the *Q*-switched laser, the mode-locked laser operates at a shorter wavelength due to the incorporation of 200 m long SMF in the cavity, which increases the cavity loss. The operating wavelength shifts to shorter wavelength to acquire more gain to compensate the loss.

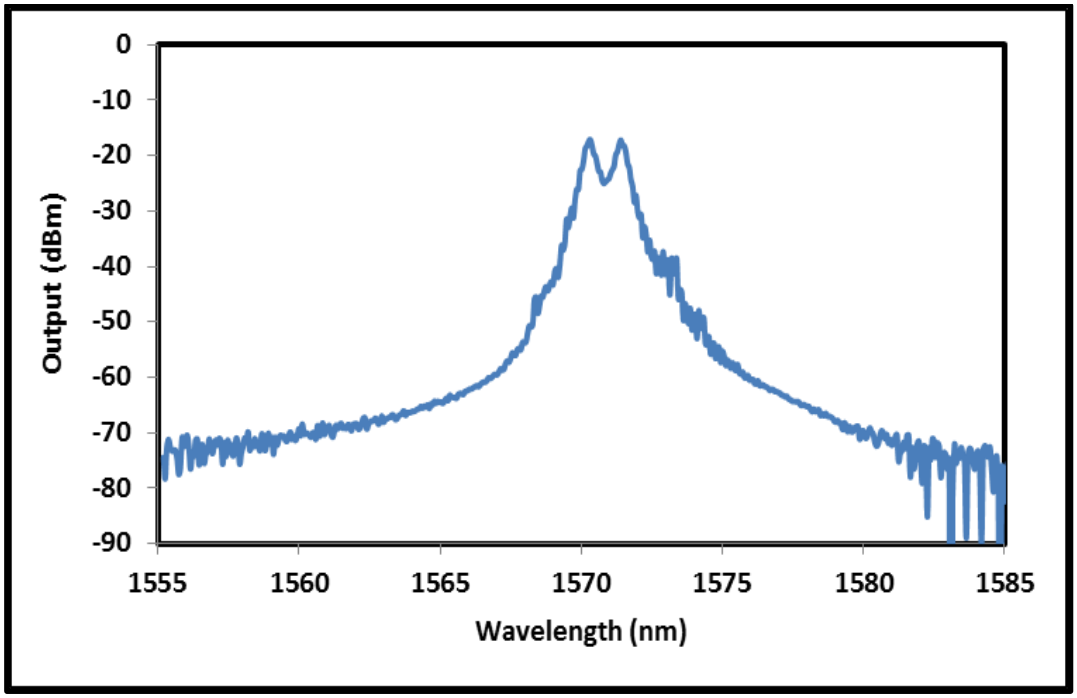

Fig. 3.11: Output spectrum of the proposed soliton mode-locked EDFL when the pump power is fixed at 129 mW.

Fig. 3.12 shows the typical pulse train of the mode-locked EDFL at pump power of 129 mW. As shown in the figure, the cavity round-trip time, T_R, is 1.1 µs, which in agreement with 907 kHz repetition rate. Fig. 3.13 shows the corresponding autocorrelation trace of the mode-locked pulse showing the pulse duration, T_{FWHM}, of 2.52 ps. The RF spectrum of the mode-locked laser is also investigated using a RF spectrum analyzer. Fig. 3.14 shows the result, which indicates a strong mode-locked pulse at frequency of 907 kHz. As shown in Fig. 3.14, SNR is obtained at 53.42 dB, which is limited by the available pump power. The average output power of the soliton mode-locked fiber laser is measured to be -6.54 dBm. Based on the 3 dB bandwidth of the output spectrum, a Time Bandwidth Product (TBP) of laser is calculated to be around 0.331, which shows the soliton pulse is slightly chirped.

Compared to sech^2 transform limited value of 0.315, this indicates that the pulse is very near to the ideal TBP value. When comparing between the leading edge and the trailing edge of the pulse from autocorrelation trace, the leading edge shows significant loss from the saturable absorber. On the contrary, the pulse trailing edge has negligible loss because the saturable absorber is fully saturated. This shows that the SWCNT SA is a slow SA (Paschotta & Keller, 2001), conforming to the semiconducting SWCNT obtained by Raman spectroscopy (refer to Fig. 3.5). A semiconducting CNT does not have fast recovery time (Reich, Thomsen, & Maultzsch, 2008).

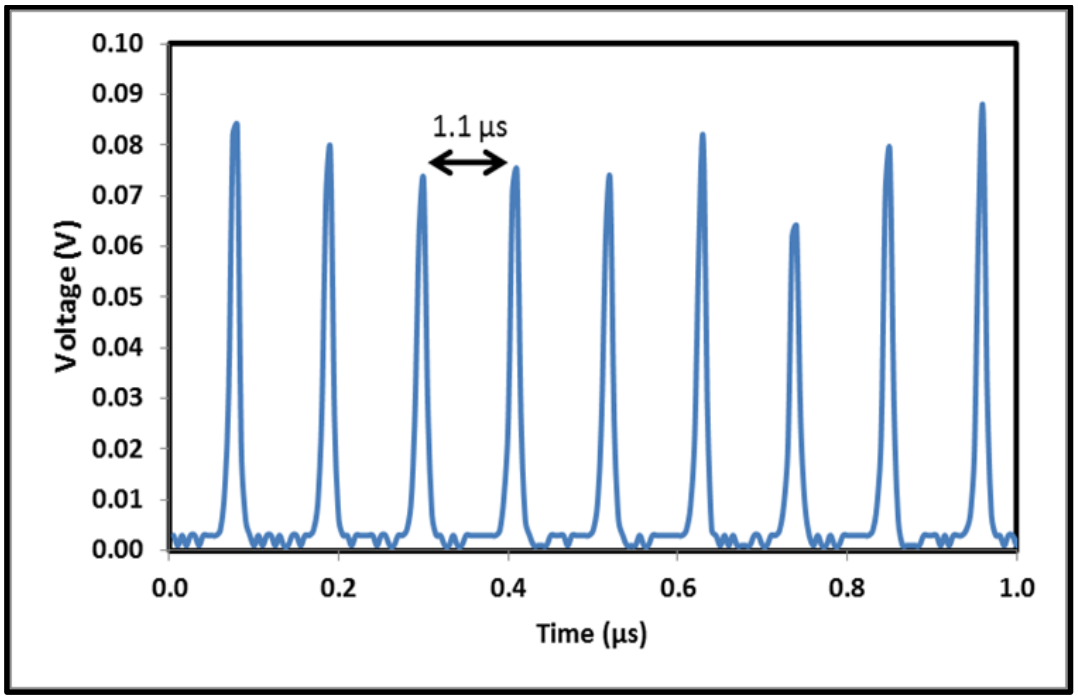

Fig. 3.12: OSC trace of mode-locked fiber laser

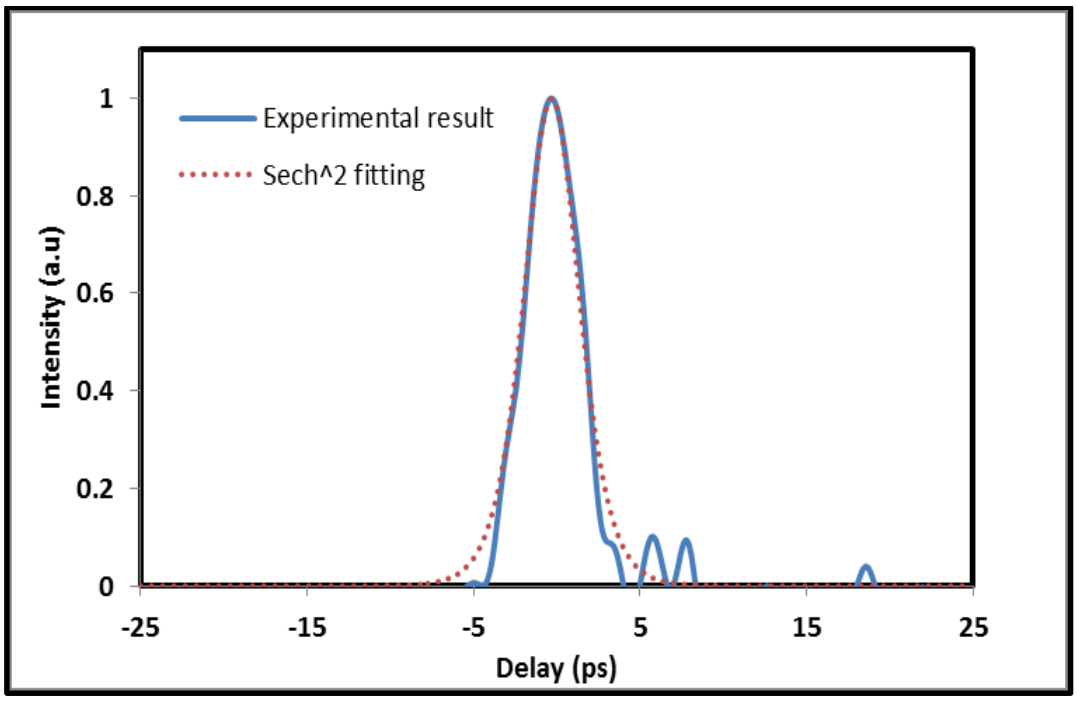

Fig. 3.13: Autocorrelation trace of mode-locked fiber laser at 129 mW

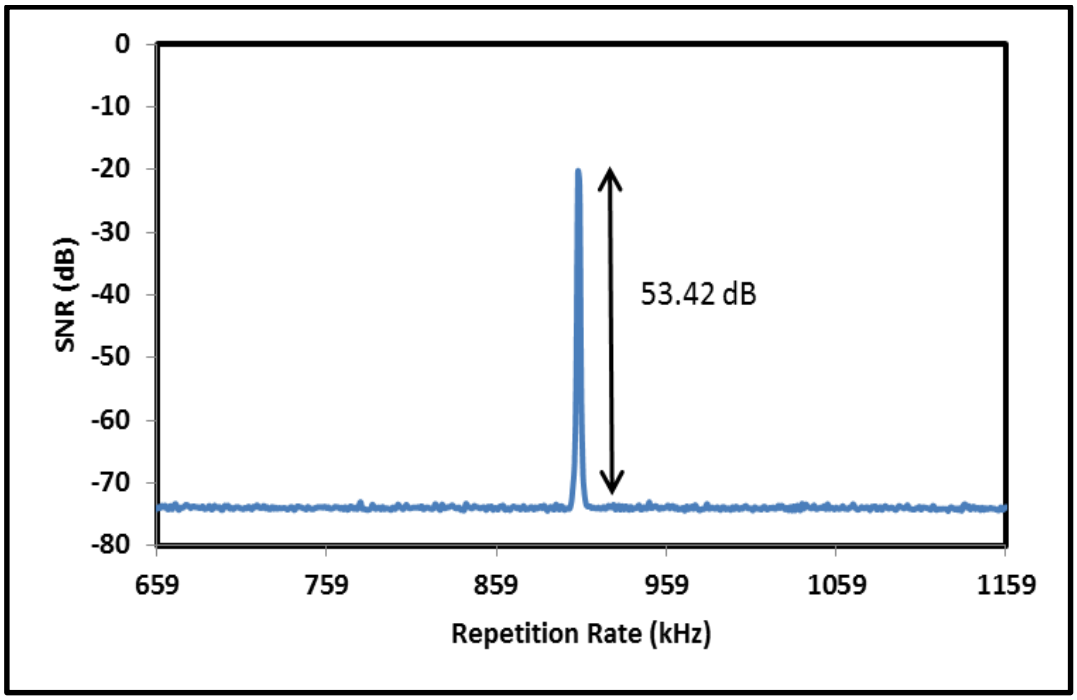

Fig. 3.14: RFSA trace of soliton mode-locked fiber laser at 129 mW.

Referring to Fig. 3.13, the autocorrelation trace does not follow exactly the $sech^2$ fitting. When mode-locked pulse self-start at 56.75 mW, the pulse shape does follow exactly the shape of the $sech^2$ fitting. However, in the RFSA, the SNR value is below the threshold value required to be qualified as mode-locked pulse. This is due to the 20 dB output coupler used in the experimental setup. Only 1% of the total energy that is circulating inside the cavity is extracted for measurement purpose.

Therefore, the pump power is increased to 129 mW to achieve a satisfactory SNR value. However, this, in turn, increase the pulse intensity in the autocorrelator. As a result, the pulse shape in the autocorrelator does not follow the $sech^2$ fitting.

3.4 SUMMARY

Q-switched and mode-locked fiber lasers have been demonstrated using various passive techniques. At first, mode-locked fiber lasers are successfully achieved using a 2 m long EDF as a gain medium based on two techniques, namely the NPR and semiconductor SA. Compared to NPR technique, it is found that the semiconductor SA is able to produce a cleaner pulse shape. Correspondingly, the pulse-width and pulse energy are also improved from 1.11 ps to 0.58 ps and 0.0863 nJ to 0.123 nJ, respectively by the use of the semiconductor SA. The TBP can also be enhanced from 1.874 to 0.32 with the use of semiconductor SA. This shows that the semiconductor SA performs better than NPR in generating mode-locked pulse.

A switchable *Q*-switched and soliton mode-locked fiber laser are then demonstrated using a SWCNT-based SA. The *Q*-switched EDFL is self-started in a 23 m long laser cavity to produce a pulse with repetition rate that can be widely tuned from 10.25 kHz to 41.87 kHz

by varying the pump power from 30 mW to 129 mW. It has a pulse width of 10.92 μs and pulse energy of 5.2 nJ at the maximum pump power of 129 mW. A 200 m long SMF is incorporated in the laser cavity to switch the EDFL into a self-start mode-locked fiber laser. The mode-locked EDFL produces a soliton pulse train with a repetition rate of 907 kHz, pulse duration of 2.52 ps and signal-to-noise ratio (SNR) of more than 53 dB.

CHAPTER 4

GRAPHENE SATURABLE ABSORBER FOR *Q*-SWITCHING AND MODE-LOCKING APPLICATIONS

4.1 INTRODUCTION

In the previous chapter, various *Q*-switched and mode-locked fiber lasers have been demonstrated using three different passive techniques; nonlinear polarization rotation (NPR), semiconductor saturable absorber (SA) and single-walled carbon nanotubes (SWCNTs) SA. Among these techniques, it is found that SWCNT is a comparatively simple and cost-effective technique especially for generating a mode-locking pulse train in an Erbium-doped fiber laser (EDFL) cavity. Unfortunately, when operating at a particular wavelength, the absorption wavelength of the SWCNTs is related to the diameter of the SWCNT. This, somehow, limit the operating wavelength of a SWCNT SA. Recently, graphene has also gained a tremendous attention for SA applications. This is due to the gapless linear dispersion of Dirac electron in graphene which allows an ultrabroadband operation. The graphene is a flat monolayer of carbon atom tightly packed into two dimensional (2-D) honeycomb lattice. It can be stacked to form 3D graphite, rolled to form 1D nanotube and wrapped to form 0D fullerenes (A. K. Geim, 2009). Nair et al. (2008) has demonstrated that despite being only one atom thick, graphene absorb a significant ($\pi\alpha$=2.3%) fraction of incident white light due to its unique electronic structure. The optical absorption is also found to be frequency

independent and proportional to the number of layers (S. Yamashita, 2012). Qiaoliang Bao et al. (2009) have recently reported that graphene can provide outstanding saturable absorption, where it has a much lower saturation intensity, larger saturable-absorption modulation depth and higher damage threshold compared to the SWCNTs.

Up to date, many techniques have been developed to integrate graphene into fiber devices to construct SAs for passive pulse construction. For instance, mode-locked Erbium-doped fiber laser with stable soliton-like pulse output was achieved using a graphene from a CVD process (Bao et al., 2010) . In this chapter, investigation and demonstration of the generation of various *Q*-switched and mode-locked fiber lasers using various homemade graphene SAs, which were newly developed. .

4.2 *Q*-SWITCHED ERBIUM-DOPED FIBER LASER WITH GRAPHENE SATURABLE ABSORBER OBTAINED BASED ON OPTICAL DEPOSITION

Graphene is an atomic-thin nano-scale material, which has unique electrical and optical properties that opens a new field of research in solid state physics and material science (Novoselov et al., 2004). It also exhibits linear optical absorption and saturable absorption properties, which are useful in generating ultra-short laser pulses (Qiaoliang Bao et al., 2009; Z. Sun et al., 2010). The linear dispersion of the Dirac electrons in graphene promises broadband applications while its saturable absorption property is the result of Pauli blocking (Kumar et al., 2009). At high intensity, the photo-generated carriers increase in concentration and cause the states near the edge of the conduction and valence bands to fill, thus, blocking further absorption. Band filling occurs because no two electrons can fill the same state. Consequently, saturable absorption is reached due to this Pauli blocking process. Moreover, the relaxation of carriers in a single layer graphene is ultrafast (200 fs) (Carbone

et al., 2011) . Other papers have included other factors that enable graphene to become an excellent saturable absorber (Bao et al., 2010; Bonaccorso et al., 2010).

The use of graphene SA for producing *Q*-switched fiber lasers has been demonstrated in many literatures (Cao, Wang, Luo, Luo, & Xu, 2012; J. Liu, Xu, & Wang, 2012; Saidin et al., 2013). For instance, J. Wang et al. (2012) have recently reported a *Q*-switched and mode-locked Erbium-doped fiber laser (EDFL) using an optical deposition technique. The deposition is performed onto a tapered fiber. Cao et al. (2012), deposited graphene which is dispersed in a Dimethylformamide (DMF) solution onto a fiber ferrule using optical deposition. In another work, D Popa et al. (2010) reported a tunable *Q*-switched fiber laser using a graphene SA. In other paper, Wei, Zhou, Fan, and Liu (2012) reported a new graphene *Q*-switched EDFL with low pump threshold, and wide pulse repetition- rate range. The laser has a low pump threshold of 16.9 mW, and a wide range of repetition rate from 31.7 to 236.3 kHz within the pump power range of 18.6-192.6 mW. In this section, a simple and compact *Q*-switched EDFL is demonstrated using graphene solution deposited on end surface of fiber ferrule, which is then incorporated in a ring laser cavity to act as saturable absorber. Compared to the previous works, the proposed EDFL using a Bismuth-based Erbium-doped fiber (EDF) as a gain medium, which only requires 49 cm long fiber for operation in C-band region. The *Q*-switching performance of the laser is investigated for two different graphene saturable absorbers (GSAs).

4.2.1 EXPERIMENTAL SETUP

Fig. 4.1 shows an experimental setup for the deposition of graphene onto the end surface of the ferrule, whereby the optical deposition method proposed by Kashiwagi et al. (2009) and Martinez et al. (2010) was used. In the optical deposition method, injecting amplified light to fiber end will create an optical trapping, thermally driven convection flow

and thermo-diffusion (Nicholson et al., 2007). The interaction of the laser beam and the graphene solution will increase the solution temperature; due to the amplified injected light and therefore will induce optical trapping. The difference in temperature between the fiber ferule and solution creates temperature gradient. The temperature gradient will direct the graphene flakes towards the fiber core. The effect is called thermophoresis. The graphene flakes (in a solution) used in the experiment were supplied by Graphene Research Ltd and prior to deposition, the solution is agitated for 30 minutes using an ultrasonic bath. Optical radiation from 1550 nm laser source is amplified by an optical amplifier up to 30 dBm and then propagated through a fiber pigtail via an optical circulator. The end surface of the pigtail is dipped into the graphene aqueous suspension and the whole deposition process of the graphene to the fiber ferule core is monitored by optical power meter and recorded using GPIB card connected to computer through Labview 7.1 interface. The deposition process is halted when there is a sudden change in power and from the experiment, a rapid increment of the reflected light power is observed after 10 seconds. The light source is turned off after 5 seconds from the sudden change of power which indicates that graphene has been deposited on the ferrule end surface. The fiber is then removed from the solution. After water evaporation, the ferrule is connected to another ferrule to form a fiber compatible graphene saturable absorber (GSA).

Fig. 4.2 shows the experimental setup of the proposed compact *Q*-switched EDFL using the fabricated GSA. A 49 cm long Bismuth-based Erbium-doped fiber (Bi-EDF) with Erbium ion concentration of 3250 ppm (parts per million) and cutoff wavelength of 1450 nm is used as the gain medium. The Bi-EDF used was obtained from Asahi Glass Co. Ltd, Japan and commercially available. It was fabricated using lanthanum/erbium co-doped Bi2O3 – based glass, which was prepared by a melting method. The fiber has an erbium ion

concentration of 3250 ppm with 83 dB/m peak absorption around 1480 nm, a cut-off wavelength of 1450 nm, small mode-field diameter of 6.2 μm at 1550 nm and numerical aperture (N.A) of 2.0. The advantages of Bi-EDF are the broad gain profile coverage from 1530 nm to 1620 nm, high concentration of Erbium ions and fusion-spliceable to silica EDF (Sugimoto, 2008). Due to high concentration of Er3+, a very short length (49 cm) of Bi-EDF can provide the same gain as 14 m of silica EDF. The fiber also presents balance to the high nonlinearity caused by high core refractive index and small mode-field diameter (S.Y. Set, M. Jablonski, et al., 2003). Bi-EDF is more suitable compared to the conventional silica EDF for short pulse amplification because there is no significant pulse and spectrum broadening due to negligible self-phase modulation and dispersion effects on optical pulses because of short length (Ohara, Hasegawa, & Sugimoto, 2005).

In this experiment, the Bi-EDF is forward pumped by a 1480 nm laser diode through a 1480 / 1550 nm wavelength division multiplexer (WDM). Another WDM is placed after the Bi-EDF to remove the excess pump power. The laser output is obtained via a 10 dB optical coupler located after the GSA, which channels out about 10% of the oscillating light from the ring cavity. The output is analyzed by using an optical spectrum analyzer (OSA) of 0.02 nm resolution and a 500 MHz oscilloscope with 6 GHz bandwidth light wave detector. An optical isolator is incorporated after the optical coupler to ensure light propagates in a unidirectional manner. The rest of the cavity is made of SMF-28 single-mode fiber. All components used in the setup are polarization independent, i.e. they support any light polarization. No polarization controller (PC) is included in the laser cavity as it had been observed earlier that a PC did not improve the pulse stability. There is no significant pulse jitter observed through oscilloscope during the experiment. The experiment is carried out for two different GSAs; GSA1 and GSA2. The insertion loss of GSA1 and GSA2 are measured

to be around 0.55 dB and 0.9 dB respectively, while the total length of the cavity is measured to be about 25 m. For GSA2, graphene is deposited on both end surface faces of the ferrules and thus it has a thicker graphene layer compared to that on the GSA1.

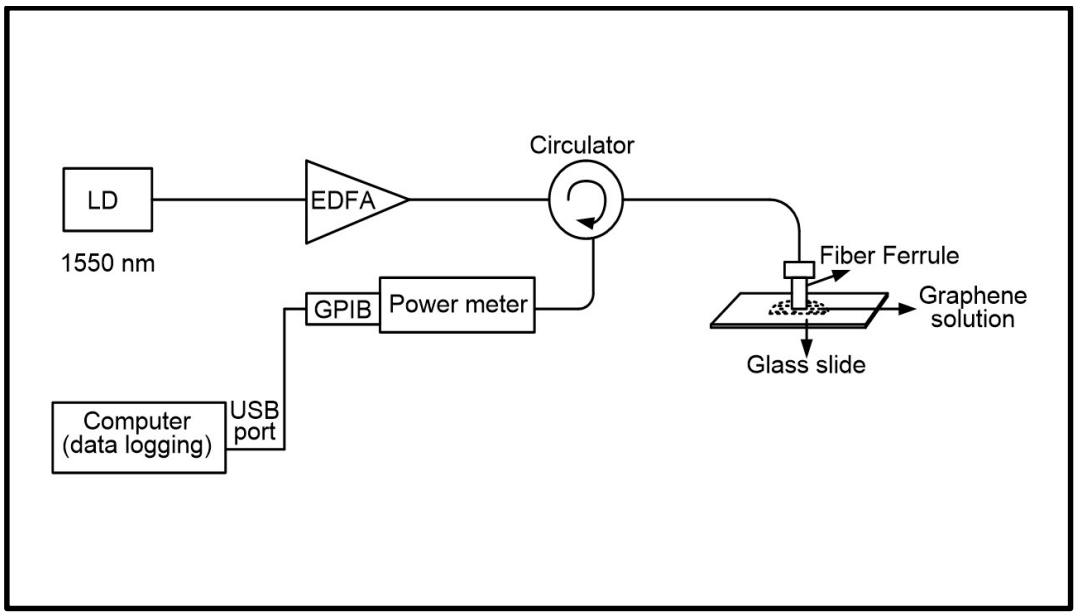

Fig. 4.1: Experimental setup for depositing graphene on the fiber end surface by optical radiation

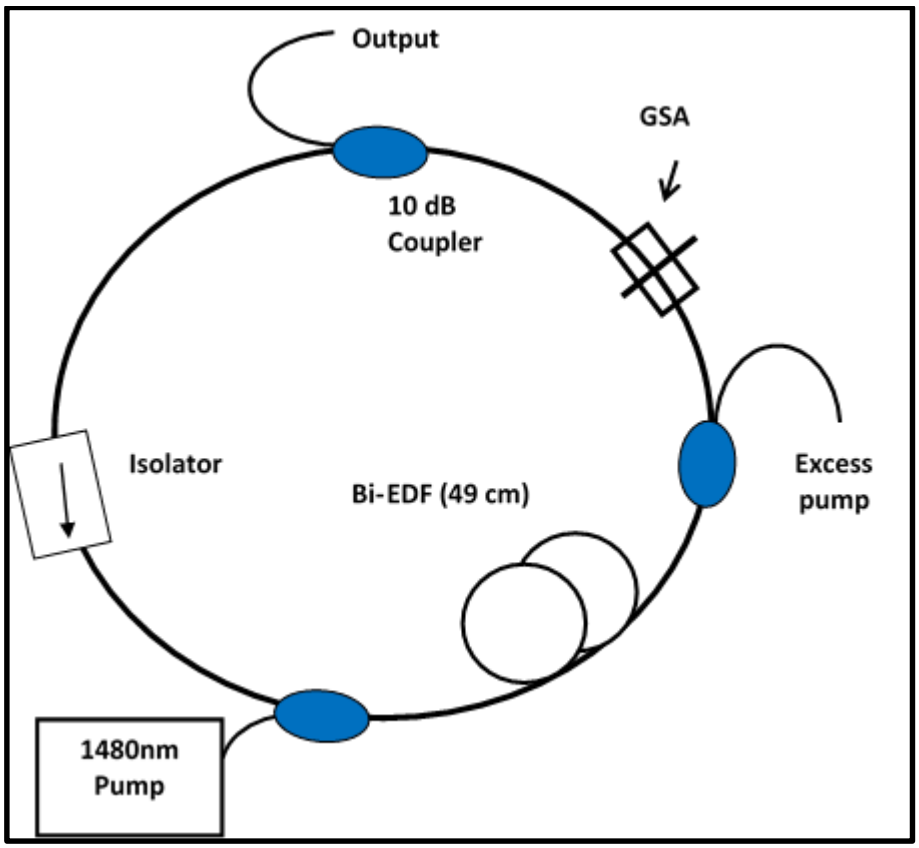

Fig. 4.2: Experimental setup of the proposed graphene based *Q*-switched EDFL.

4.2.2 *Q*-SWITCHING PERFORMANCE

The proposed EDFL started to lase with the passive *Q*-switching mode at the pump power of around 50 mW. The pump threshold was relatively low compared to that of SWNT or SESAM based *Q*-switched EDFL, mainly owing to a lower saturation intensity of the graphene. Fig. 4.3 compares the oscilloscope traces of the *Q*-switched pulse trains for two different GSA when the pump power is fixed at the maximum value of 120 mW. As shown in the figure, the repetition rates of 31.3 kHz and 25 kHz are obtained with GSA1 and GSA2, respectively. Since thicker graphene layer means more absorption, it takes longer time for the GSA2 to bleach and thus its repetition rate is lower than that of GSA1. Unlike mode-locked fiber laser, where the repetition rate is dependent on cavity length, the repetition rate

in *Q*-switched fiber laser varies with pump power. Fig. 4.4 shows the repetition rate as a function of pump power for both cases. As the pump power increases, more gain is provided to saturate the GSA. Since pulse generation relies on saturation, the repetition rate increase with the pump power as shown in Fig. 4.4. For instance, with GSA1, the pulse repetition rate of the *Q*-switched EDFL can be widely tuned from 16.7 kHz to 31.6 kHz by varying the pump power from 55 mW to 120 mW. At every specific repetition rate and pump power, the *Q*-switching pulse output was stable and no significant pulse jitter was observed on the oscilloscope. Fig. 4.5 shows the output spectrum for the proposed *Q*-switched EDFL configured with GSA1 and GSA2. As shown in the figure, the laser operates at around 1560 nm with full-width half maximum of around 0.3 nm.

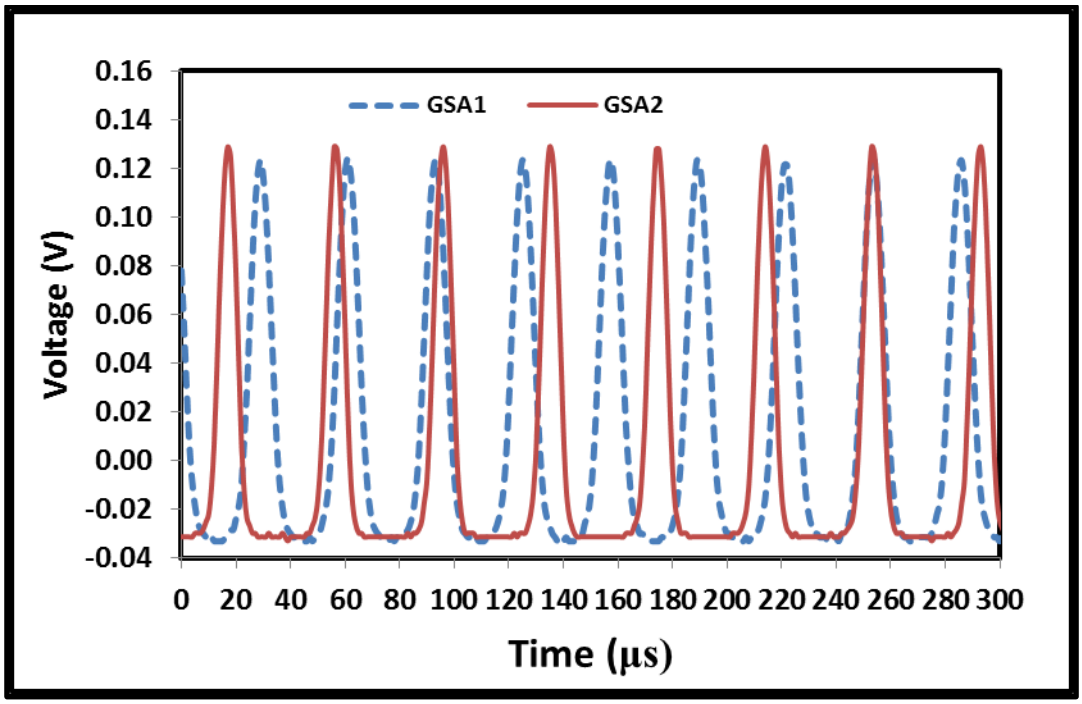

Fig. 4.3: Typical pulse trains for the proposed EDFL configured with GSA1 and GSA2 at a pump power of 120 mW.

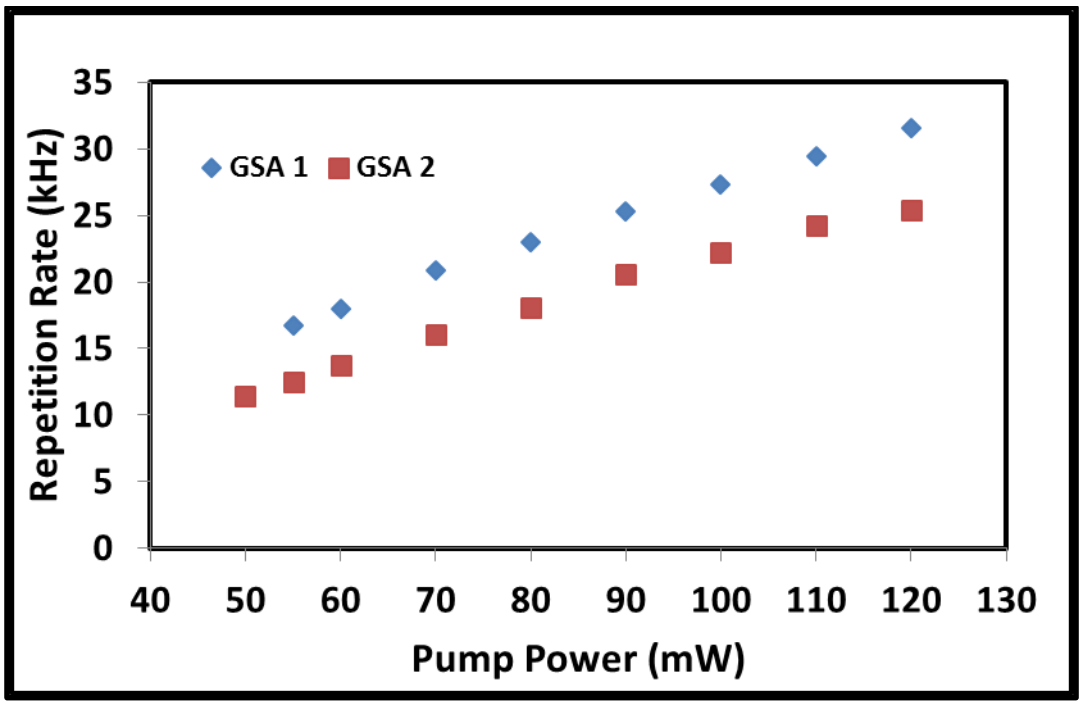

Fig. 4.4: Repetition rate as a function of 1480 nm pump power.

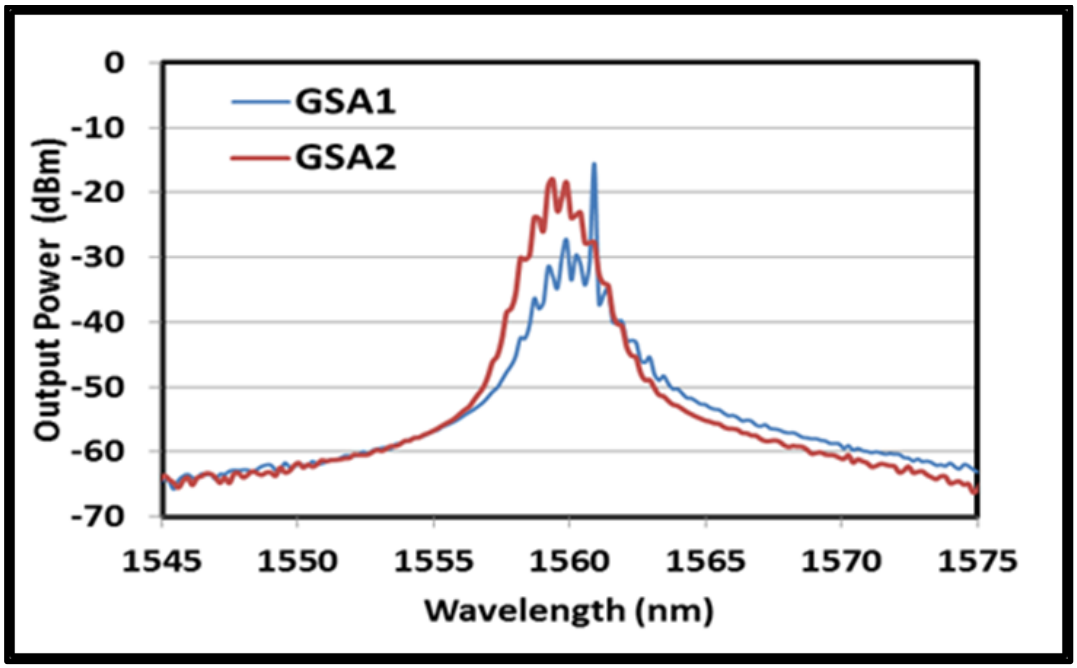

Fig. 4.5: Optical spectrum of the laser at pump power of 120 mW.

Fig. 4.6 shows the pulse width and the pulse energy as a function of the pump power. As seen in the figure, increasing the pump power makes the pulse width narrower and the pulse energy higher for both GSAs. At the pump power of 120 mW, the *Q*-switched EDFL has a pulse width of 7.5 μs and pulse energy of 43.7 nJ with the use of GSA2. A thicker layer of graphene (in GSA2) implies that more atoms are stored in the excited state level and consequently, more stimulated emission occurs when the GSA bleaches. This in turn, generates more output power. This explains why the output energy of GSA2 is significantly higher than that of GSA1. The reason is also linked to the observation where using GSA2 yields lower pulsing threshold. The threshold pump powers for *Q*-switching operation with GSA1 and GSA2 are observed to be 51.3 mW and 47.6 mW, respectively. These results indicate that graphene has a larger potential for better *Q*-switching and saturable absorption compared to conventional light absorbing components when carefully employed in an appropriate laser system. The proposed EDFL requires only a very short length of gain medium and uses a simple technique for GSA fabrication and thus the cost of the laser can be significantly reduced. The simple and low cost laser is suitable for applications in metrology, environmental sensing and biomedical diagnostics.

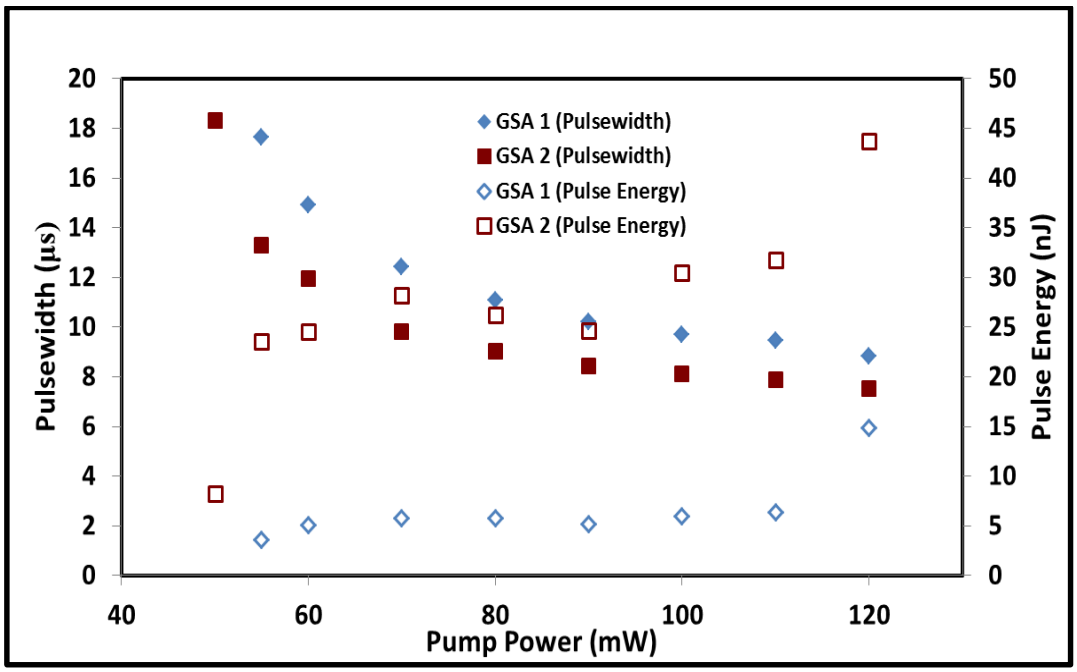

Fig. 4.6: Pulse width and pulse energy as a function of input pump power.

4.3 DEVELOPMENT OF SINGLE LAYER GRAPHENE SATURABLE ABSORBER USING MECHANICAL EXFOLIATION TECHNIQUE

Graphene was first produced by a mechanical exfoliation method in 2004 (Novoselov et al., 2004). In this work, a fresh surface of a layered crystal was rubbed against another surface which left variety of flakes attached to it. Among the resulting flakes, a single layer flake can be found. Despite there are other methods to produce graphene, mechanical exfoliation still gives the best samples in terms of purity, defects, electron mobility and optoelectronic properties. A single-layer graphene saturable absorber has an ultrafast relaxation time, lower scattering loss and it performs better than multilayer graphene saturable absorber in terms of pulse shaping ability, pulse stability and output energy (Bao et al., 2010). However, this method has disadvantages in terms of yield and throughput, and thus it is impractical for large-scale production. Graphene can be optically distinguished,

regardless of being one-atom thick and its transmittance (T) can be expressed in terms of the fine-structure constant. Due to the some properties of graphene such as linear dispersion of the Dirac electrons and Pauli blocking, graphene makes broadband applications and saturable absorption possible. Furthermore, by inducing a bandgap through chemical and physical treatment, graphene can be made luminescence. These properties lead to interesting and ideal photonic and optoelectronic material (Bonaccorso et al., 2010).

In the previous section, a graphene saturable absorber fabricated using an optical deposition technique is used to demonstrate a *Q*-switched fiber laser. However, a mode-locked operation cannot be realized using the SA due to the loss incurred by multilayer graphene. Previously, Martinez et al. (2011) and Chang et al. (2010) have successfully produced few-layers graphene SA using mechanical exfoliation technique. In another work, Bao et al. (2010) demonstrated a mode-locked fiber laser using single-layer graphene SA, but using a more complicated technique, where the monolayer graphene is grown on by chemical vapour deposition (CVD) on copper (Cu) foil before being etched away using $FeCl_3$ solution. The graphene film then transferred to fiber pigtail.

In this section, the preparation of a single-layer graphene SA (GSA) based on mechanical exfoliation technique, also known as the "scotch tape" method is demonstrated. The method is simpler compared to Bao et al. (2010) yet yields a high quality graphene SA. The position of graphene SA on the fiber core can easily be recognized by using a fiber probe.

4.3.1 PREPARATION AND CHARACTERIZATION OF THE GSA

4.3.1.1 RAMAN SPECTRUM

The originating material is commercially available highly ordered pyrolytic graphite (HOPG). The HOPG flakes were inserted on a strip of scotch tape and then were pressed and peeled off repeatedly in-order to optimize the graphene thickness. The resultant graphene sheets were then pressed against the end facet of an optical fiber ferrule. The scotch tape was slowly peeled off and accordingly, a few graphene sheets remained on the end facet of an optical fiber ferrule. Graphical presentation of this technique is explained in detail by Chang et al. (2010) as in Fig. 4.7. The result is inspected using EXFO's FIP-400 fiber inspection probe to ensure that the graphene sheets lays on top of the fiber core. The microscope image of the end surface of the ferrule after coating the graphene is illustrated in Fig. 4.8.

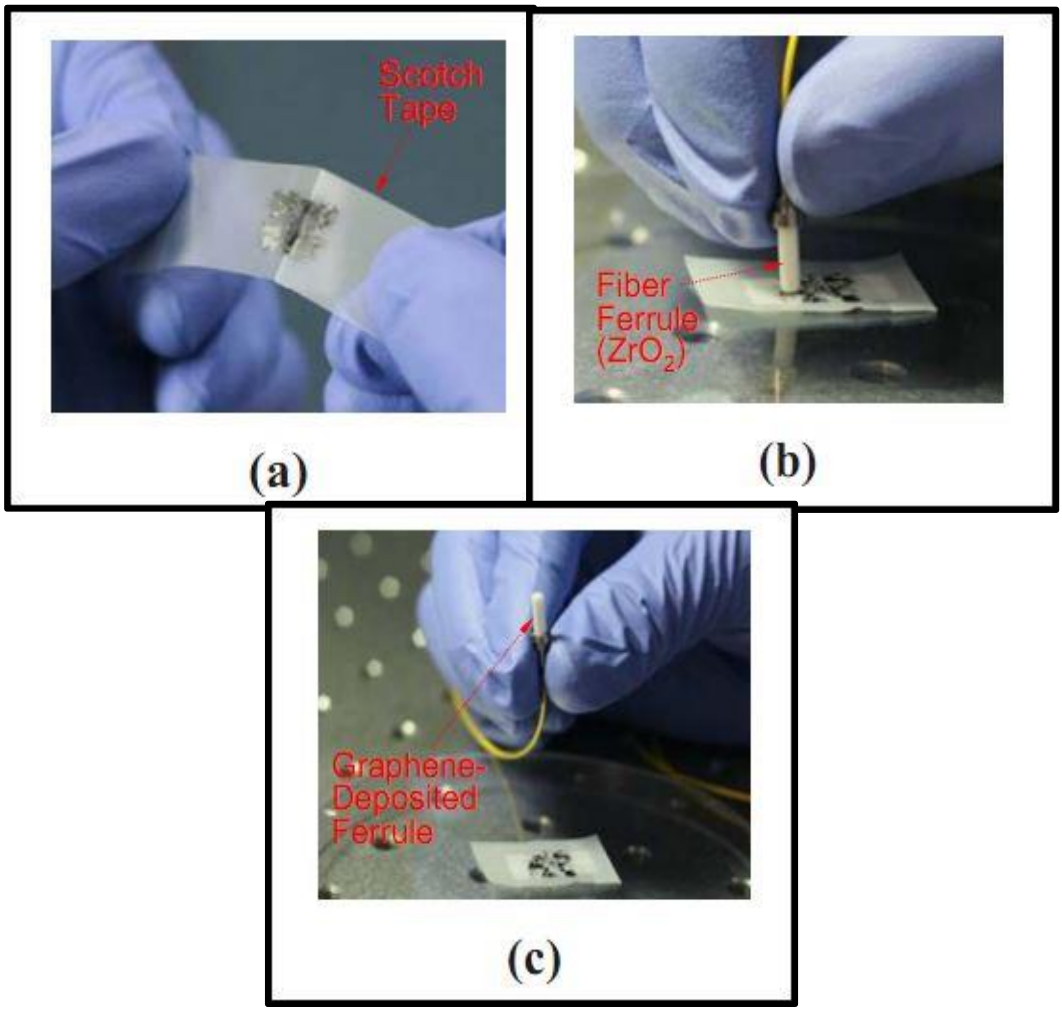

Fig. 4.7: Graphene SA preparation on a fiber ferrule (a) Mechanical exfoliation of highly ordered pyrolitic graphite (HOPG) using scotch tape (b) Graphene is deposited onto a clean fiber ferrule via direct contact (c) Careful separation of the ferrule from the scotch tape (Reproduced from Chang et al., 2010)

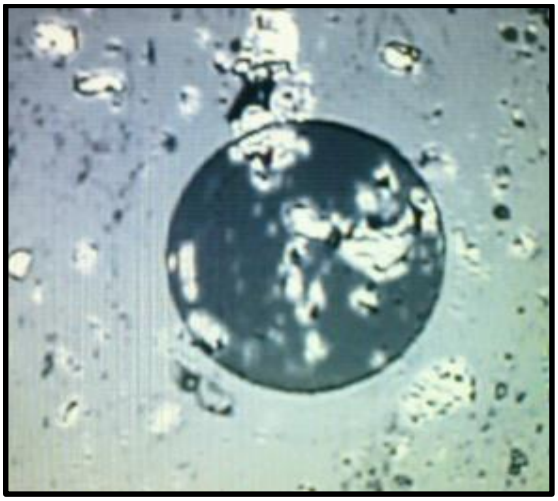

Fig. 4.8: Microscope image of fiber ferrule with graphene.

Raman spectroscopy was performed on the graphene saturable absorber using laser excitation at 532 nm (2.33eV) with 10 s exposure time. The detector is a charge-coupled device camera. The result reveals two prominent peaks as clearly shown in Fig. 4.9. One is located at approximately 1580 cm^{-1}, generally known as the G peak, and the other one is located at approximately at 2700 cm^{-1}, known as the 2-D peak. The width of the 2-D peak can be used to determine the number of graphene layers. As the graphene layer increases, the width also increases (Ferrari et al., 2006). The Raman spectroscopy reveals a sharp and pointy 2-D peak. However the 2-D width is broad. The broadening is because the graphene is mechanically exfoliated from HOPG (Graf et al., 2007). Another method of determining the graphene layers is by calculating the intensity ratio of G /2-D peak. Single-layer graphene has a low intensity ratio, usually lower than 0.5 while multi-layer graphene shows high intensity ratio ($\geq$1) (Chen et al., 2010). In this work, a G/2-D peak ratio of 0.48 is obtained, which indicates that a single-layer graphene saturable absorber has been successfully obtained.

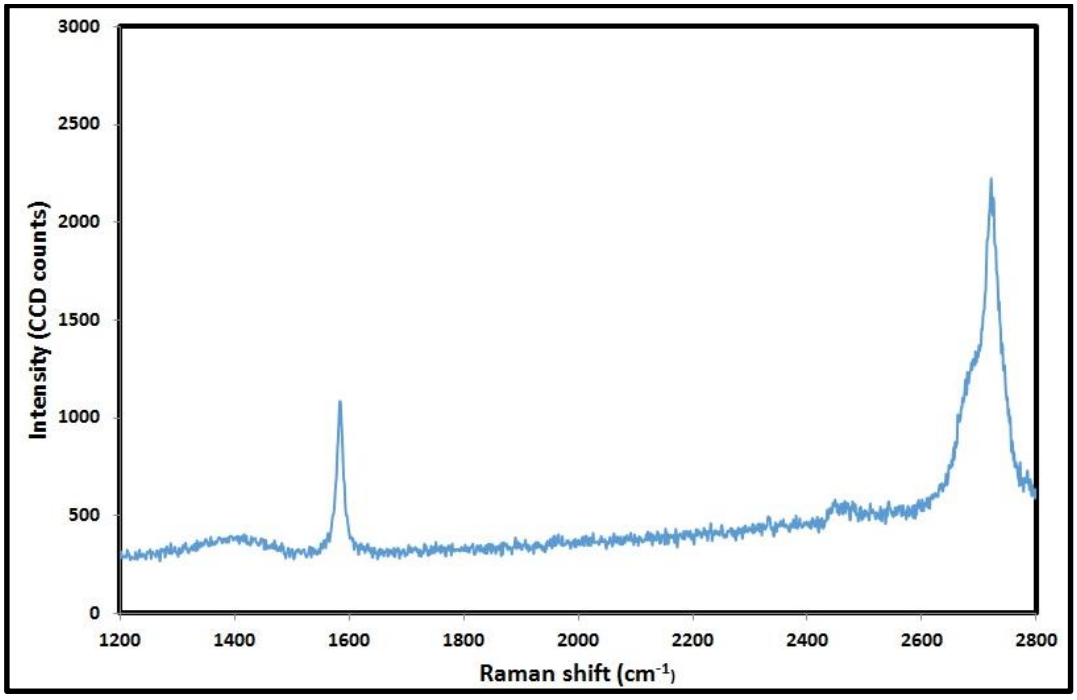

Fig. 4.9: Raman Spectrum of the GSA

4.3.2 DEMONSTRATION OF *Q*-SWITCHED EDFL USING THE GSA

4.3.2.1 EXPERIMENTAL SETUP

4.3.2.1 (a) *Q*-SWITCH

The setup of the proposed *Q*-switched EDFL with the newly developed GSA is similar to the previous section of Fig. 4.2, except for the SA. It is based on unidirectional ring cavity configuration consisting of two wavelength division multiplexer (WDM) coupler, 49 cm long bismuth-based erbium doped fiber (Bi-EDF) as gain medium, 10 dB output coupler and an optical isolator. The WDM is used to launch 1480 nm pump light from a laser diode into the Bi-EDF while another WDM is used for removing excess pump. An optical

isolator is used to force unidirectional propagation of the oscillating laser. The total length of the cavity is ~20 m while all components are polarization independence and connected by fiber pigtails. The laser output is obtained via a 10 dB optical coupler, which channels out about 10% of the oscillating light from the ring cavity. The optical spectrum of the output pulse is analyzed by using an OSA of 0.02 nm resolution and the resultant pulse train is captured by a 500 MHz oscilloscope via 6 GHz bandwidth light wave detector. Since there is no polarizer in the laser cavity, the graphene is the sole responsible mechanism for creating saturable absorption.

The newly developed GSA based on mechanical exfoliation is used for generating the passive *Q*-switched operation in the fiber laser. In the experiment, the continuous wave (CW) lasing threshold was about 30 mW. When the pump power was increased to about 80 mW, the *Q*-switched pulses were observed by introducing physical disturbance to the cavity. Then, the pump power is further increased to the maximum pump power of 130 mW and observed the *Q*-switched operation. Fig. 4.10 shows the output spectrum of the *Q*-switched EDFL at 130 mW pump power. It centers at 1559.4 nm with a 3-dB spectral bandwidth of about 0.66 nm and peak to noise ratio of ~40 dB. A slight spectral broadening is also observed in the optical spectrum which is caused by Self-phase Modulation effect (SPM). In this case, the optical Kerr effect induces a phase shift in the oscillating pulse in the cavity that leads to change in the frequency spectrum. In the anomalous dispersion regime, the "red" portion of the pulse moves backward, while the "blue" portion moves forward. This will create a hole in the spectrum. Correspondingly, the typical *Q*-switched pulse train is presented in Fig. 4.11. As shown in the figure, the peak to peak pulse interval is measured to be around 43.3 μs, which can be translated into repetition rate of 26 kHz. The pulse duration, which was measured directly from a single envelope of the pulse, is about 5.842 μs, as shown in the Fig.

4.12. At 130 mW pump power, the *Q*-switched laser has an average output power of 0.5656 mW, which corresponds to pulse energy of 24.399 nJ.

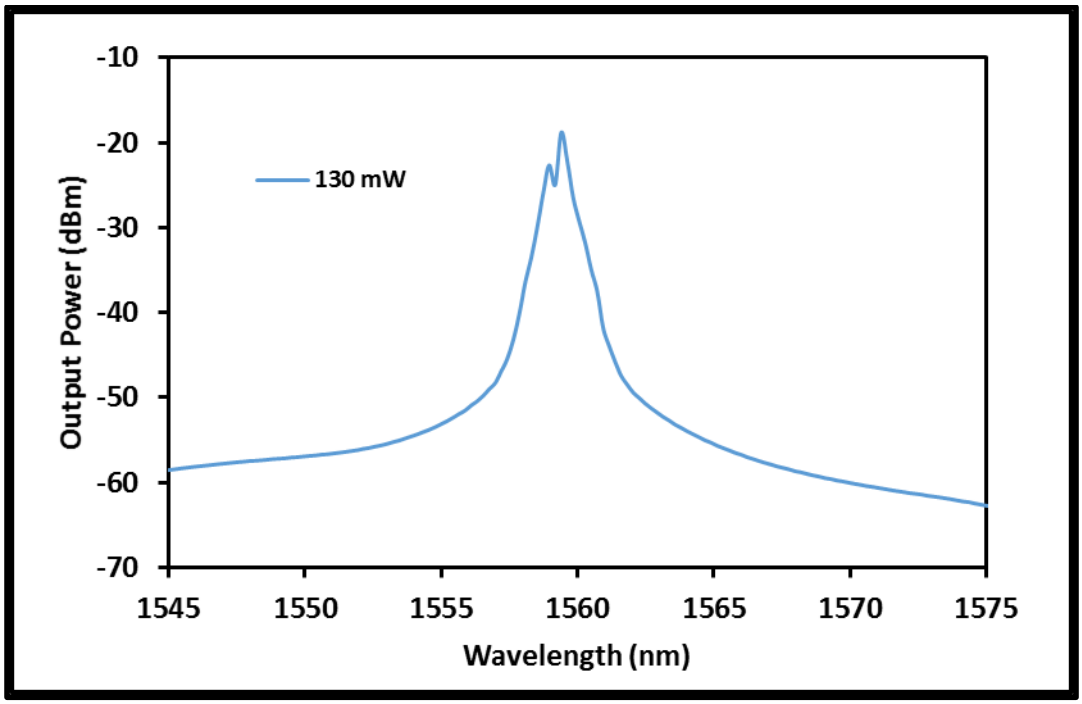

Fig. 4.10: Optical spectrum of the *Q*-switched laser at pump power of 130 mW.

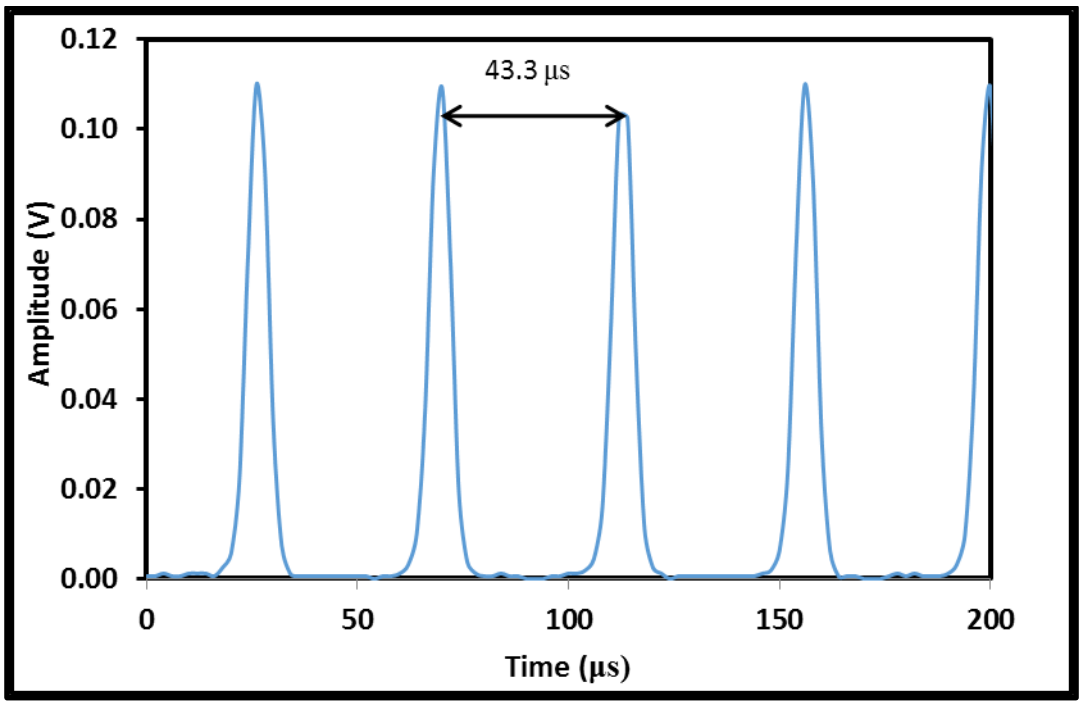

Fig. 4.11: Pulse train of the *Q*-switched laser at 130 mW pump power

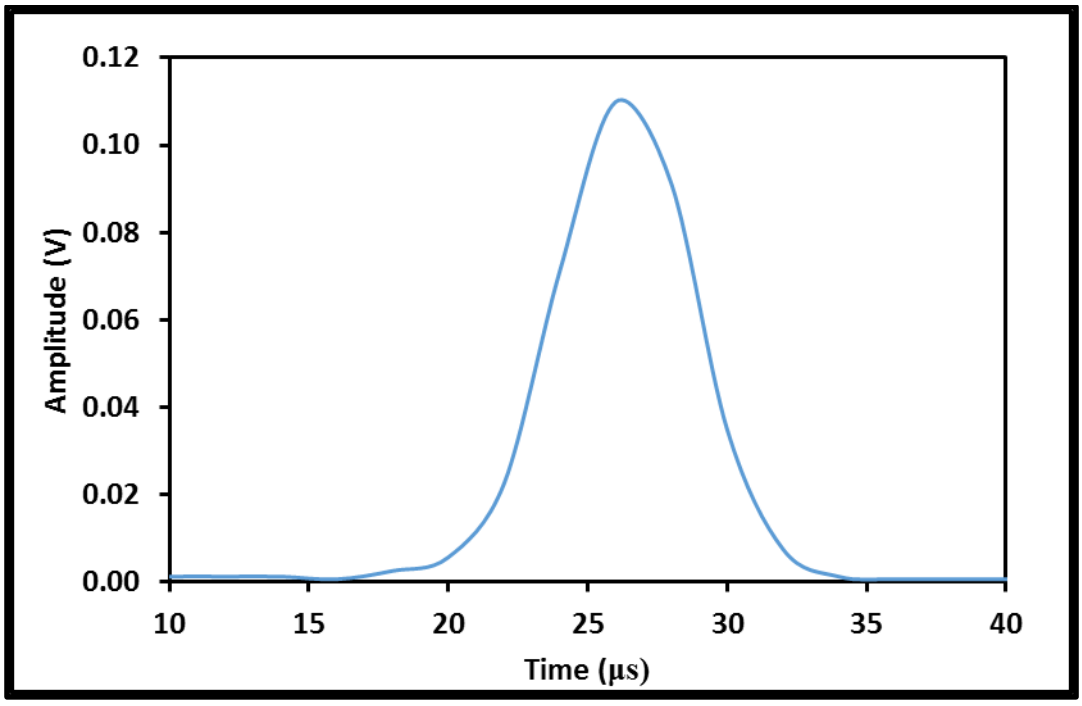

Fig. 4.12: Single-pulse envelope of the *Q*-switched laser at 130 mW pump power

Fig. 4.13 present the pulse repetition rate and the pulse energy of the *Q*-switched fiber laser as a function of the pump power. As shown in the figure, both repetition rate and pulse energy increase almost linearly with the pump power, like a typical *Q*-switched fiber laser. The repetition rate can be tuned from 16.7 kHz to 23.1 kHz by increasing the pump power from 80 mW to 130 mW. The maximum pulse energy was 24.4 nJ with pump power of 130 mW. The attainable energy is lower than the previous *Q*-switched laser with optical deposition technique based GSA. This is attributed to the large modulation depth of the single-layer graphene SA. A large modulation depth implies a large change in absorption for the incident light. Therefore, a lower repetition rate and pulsewidth are achieved with higher modulation depth (Spühler et al., 1999). The pulse width and average output power were also measured as functions of pump power, as shown in Fig. 4.14. The pulsewidth decreased with increasing pump power. This effect is due to gain compression in the *Q*-switched fiber laser. As higher energy being pumped, the time needed to saturate the SA is becoming less and less. Therefore, the pulsewidth is smaller with increasing pump power. In the experiment, the pulse width variation exhibited an almost linear tendency with the pump power, even though it is supposed to decrease nonlinearly with increasing pump power in a *Q*-switched laser. Note that such an almost linear variation of the pulse width with the pump power was also reported previously (F. Wang et al., 2012; Zhang, Zhuo, Wang, & Wang, 2012). The pulse width can be tuned from 10.14 to 5.84 μs by increasing the pump power from 80 mW to 130 mW. The measured maximum average output power was -2.49 dBm at a pump power of 130 mW. It is believed that a further optimization of the cavity parameters together with a higher pump power and higher output coupler ratio could significantly enhance the output power and pulse energy performances.

.

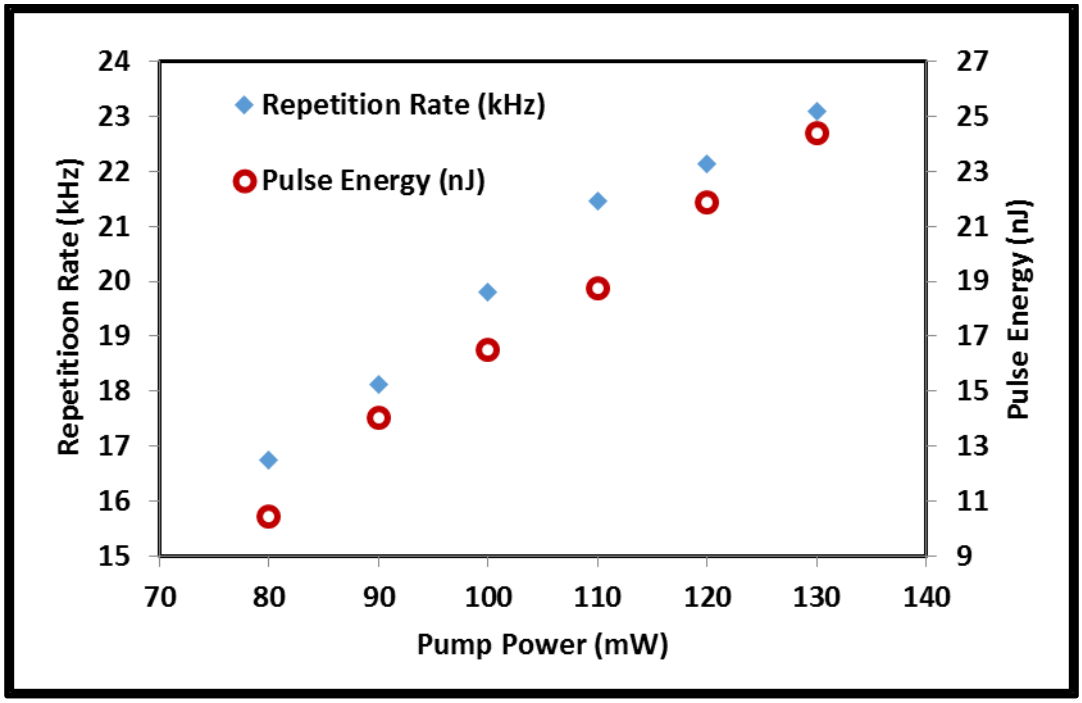

Fig. 4.13: Repetition rate and pulse energy as a function of pump power

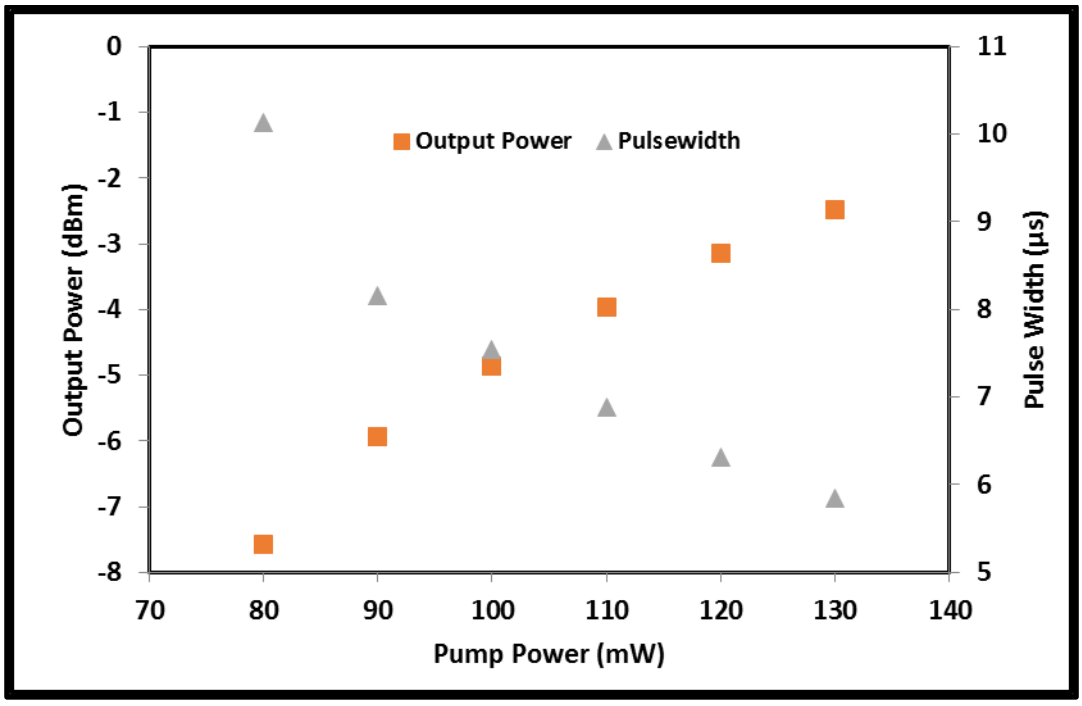

Fig. 4.14: Output power and pulse width as a function of pump power

4.3.3 DEMONSTRATION OF MODE-LOCKED EDFL USING THE GSA

During the previous experiment, any mode locking phenomena was not observed. To produce stable mode-locked pulses from a saturable absorber–incorporated fiber laser cavity, a variety of cavity parameters must be controlled in addition to the modulation depth of a saturable absorber—for example, cavity dispersion, cavity nonlinearity, saturation gain level, and saturation energy level of a saturable absorber. It is well known that at least the following condition needs to be satisfied to obtain stable continuous-wave mode locking without *Q*-switching instabilities (Ursula Keller, 2004).

$$E_p^2 > E_{L,sat} E_{A,sat} \Delta m \qquad \text{(Eq. 4.1)}$$

where E_p is the intracavity pulse energy and Δm is the modulation depth of the saturable absorber. $E_{L,sat}$ and $E_{A,sat}$ represent the effective saturation energy of the gain medium and saturable absorber, respectively. Furthermore, in the case of a fiber laser cavity, fiber dispersion and Kerr nonlinearity play a key role in mode-locked laser formation.

In this section, the cavity design of the previous laser is modified to achieve mode-locking. Fig. 4.15 shows the modified configuration where a longer EDF is used in conjunction with an additional 200 m long SMF-28 to reduce the repetition rate and increase the pulse energy. The new EDF is 1.6 m long with an Erbium ion concentration of 2000 ppm, cut-off wavelength of 970 nm, has a numerical aperture of 0.24 and the absorption at 980 nm is 24 dB/m. The gain medium is forward pumped by using 1480/1550 nm WDM. An isolator is used to ensure uni-directionality so that the back-scattering can be significantly reduced to help in initiating mode-locking (Tamura, Jacobson, Ippen, Haus, & Fujimoto, 1993). The laser output beam is extracted by a 5% output port of a 95:5 fiber coupler. A GSA, which

was fabricated by mechanical exfoliation technique, is placed between the SMF's spool and the output coupler to act as a saturable absorber.

The length of total cavity is about 207 m including 1.6 m EDF, 205.4 m SMF-28 fiber from the WDM, isolator, coupler and additional spool of SMF. The group velocity dispersion (GVD) of EDF and SMF-28 at 1550 nm are about -21.64 ps/nm/km and 17 ps/nm/km, respectively, which are provided by the fiber producer. The small amount of dispersion due to the optical isolator can be neglected. Thus, the net GVD in the cavity was calculated to be 3.457 ps/nm/km, suggesting that the laser was operating at an anomalous dispersion regime. This shows that a soliton effect dominates the mode-lock pulse formation and, the resultant mode-locked pulse train is termed as soliton mode-locking. For the measurements of the laser output, a photodetector with a 800 nm – 1700 nm wavelength range is coupled to a 500 MHz digital oscilloscope was used to measure the pulse train and pulse waveforms. The pulse duration was measured by a two-photon absorption (TPA) autocorrelator. The spectrum of pulse was measure by an OSA with 0.1 nm resolution. The signal-to-noise ratio (SNR) is measured using 7 GHz radio frequency spectrum analyzer (RFSA).

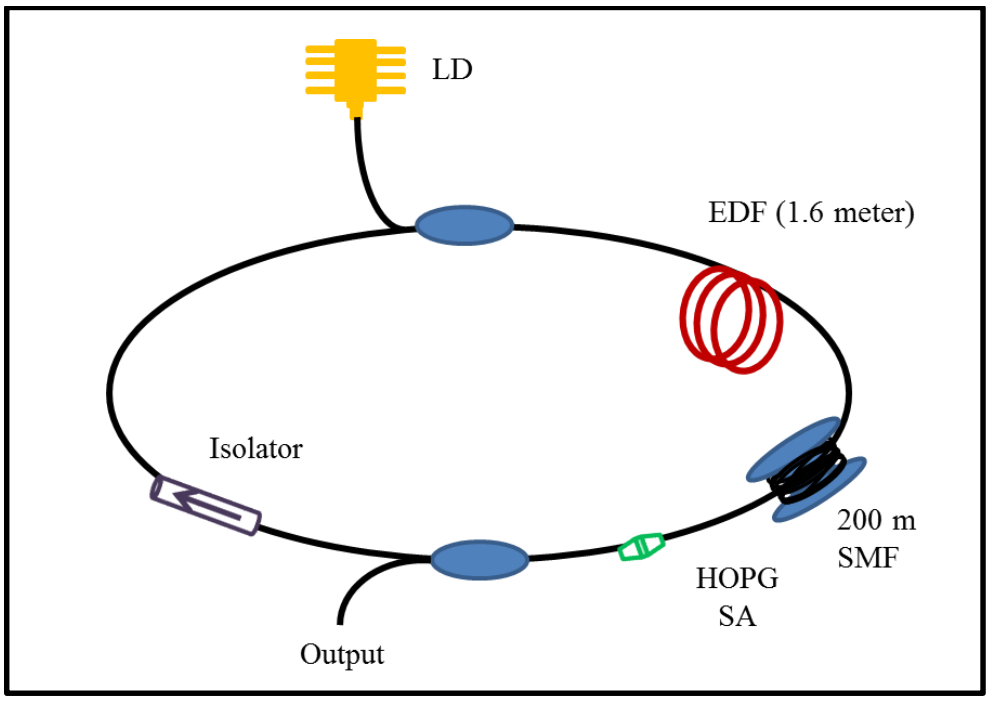

Fig. 4.15: Configuration of the mode-locked EDFL with GSA.

The oscillator started to operate at continuous wave (CW) regime after reaching the launched pump power of about 30 mW. Operation in this regime occurred with a small pump power range. The mode-locking operation is not self-started in proposed setup. Stable mode-locked pulses were observed as shown in Fig. 4.16 by introducing physical disturbance to the SA after increasing the 1480 nm pump power to maximum (130 mW). The mode-locking pulse then disappears when pump power falls below 84.5 mW. As shown in Fig. 4.16, the cavity round-trip time is measured to be 1.034 μs, which corresponds to repetition rate of 967 kHz. The measured repetition rate correspond with the cavity length. Therefore, this value suggest that the oscillators operates with a single-pulse per round trip. The average output power at was measured to be 2.825 mW and the pulse energy was calculated to be 2.921 nJ at the maximum pump power of 130 mW.

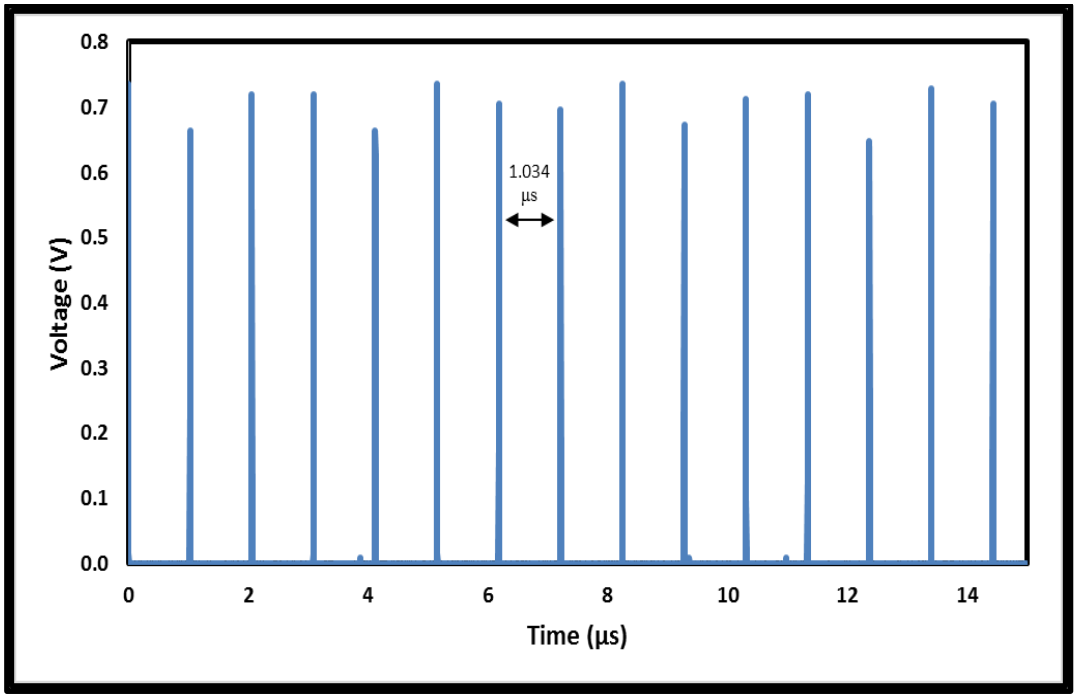

Fig. 4.16: Typical mode-locking pulse train on oscilloscope.

Fig. 4.17 shows the measured optical spectrum of the soliton pulses at the launched pump power of 130 mW with a resolution of 0.02 nm. The central wavelength and FWHM were 1568 nm and 0.912 nm, respectively. The spectral broadening is due to the SPM effect in the cavity. Although the resultant pulse fiber laser is a soliton mode-locked fiber laser, Kelly sidebands are less prominent due to excessive nonlinearity caused by high pump power and cavity length. The sidebands total power is pulse width dependent. In a relatively long pulse width cavity, the sidebands can be suppressed. This is due to the sideband fractional power, which seems to decrease exponentially with increasing pulse width (Dennis & Duling III, 1994). Fig. 4.18 shows the measured interference autocorrelation trace of the mode-locked pulses at a scanning range of 40 ps. The shoulder to peak ratio is 1:9 confirming that the oscillator operated at typical solitary mode-locking regime as well. As shown in Fig. 4.18, the pulse was fitted by a sech^2 -pulse profile very well, and the pulse duration was determined to be 3.41 ps. Consequently, the time-bandwidth time (TBP) was calculated to

be 0.38, which is almost 1.2 times larger than the ideal TBP value (0.315). This is most probably due to the large GVD in the laser cavity and high pump power.

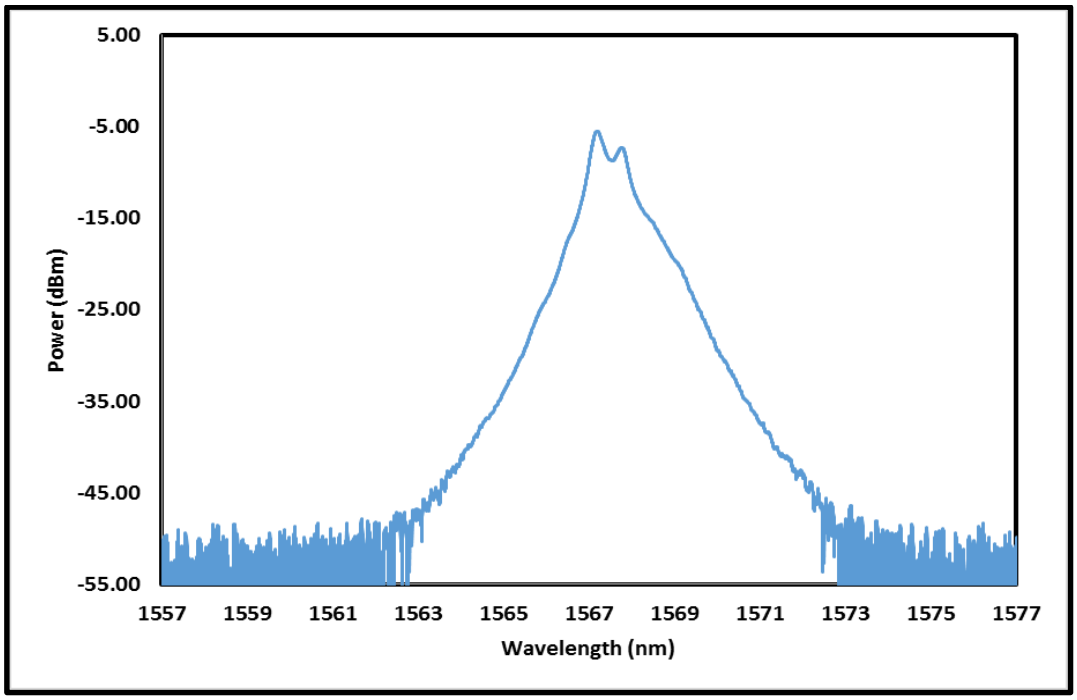

Fig. 4.17: OSA trace of the mode-locked EDFL.

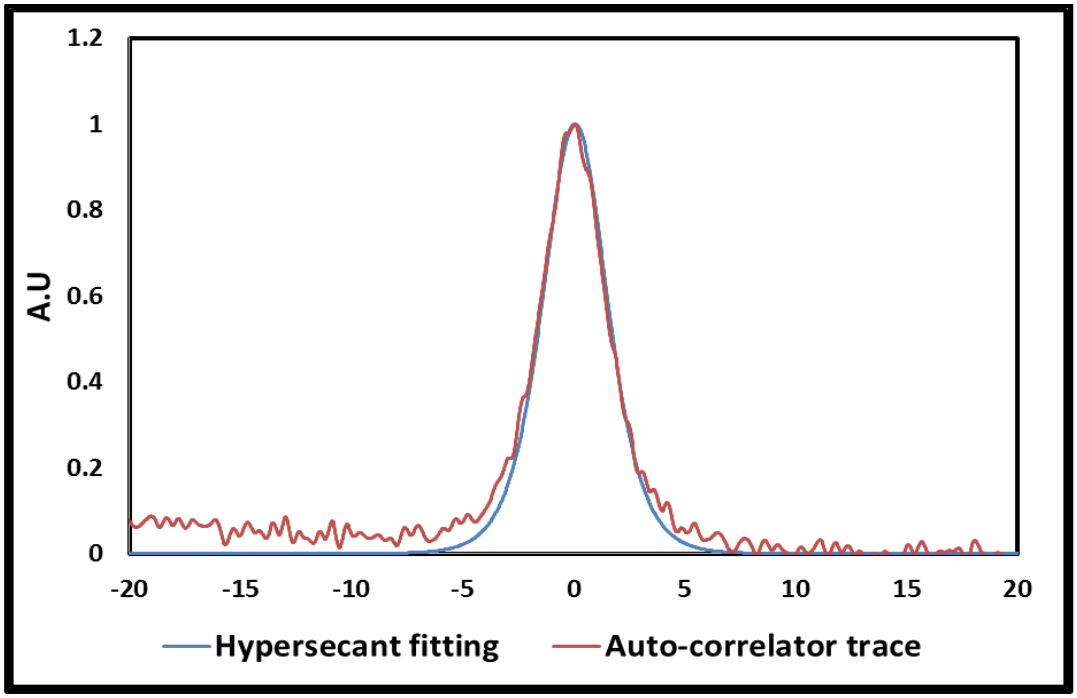

Fig. 4.18: Autocorrelation trace of the mode-locking pulse at launched pump power of 130 mW.

Fig. 4.19 shows the RF spectrum of the output at the launched pump power of 130 mW. The signal noise ratio (SNR) of 62.45 dB indicated that the oscillator operated at stable mode-locking regime. The smooth noise floor also indicated that the oscillator operated with low amplitude noise. To investigate the long-term stability of the mode-locked laser, the soliton mode-locked operation was monitored continuously for 24 hours under laboratory condition. It is found that once the mode locking was achieved, the oscillator can keep the mode-locking state and it was not sensitive to the environmental fluctuations. Additionally, the influence of the passive fiber length on the performance of the oscillator was also investigated. If removing the 200 m long SMF, the soliton pulses cannot be achieved due to insufficient pulse energy that needed to saturate the GSA. This shows that a single-layer graphene has a large modulation depth, as high as 65.9% (Bao et al., 2010).

These results indicate that graphene has a larger potential for better *Q*-switching and saturable absorption compared to conventional light absorbing components when carefully employed in an appropriate laser system. The proposed EDFL requires only a very short length of gain medium and uses a simple technique for GSA fabrication and thus the cost of the laser can be significantly reduced. The simple and low cost laser is suitable for applications in metrology, environmental sensing and biomedical diagnostics.

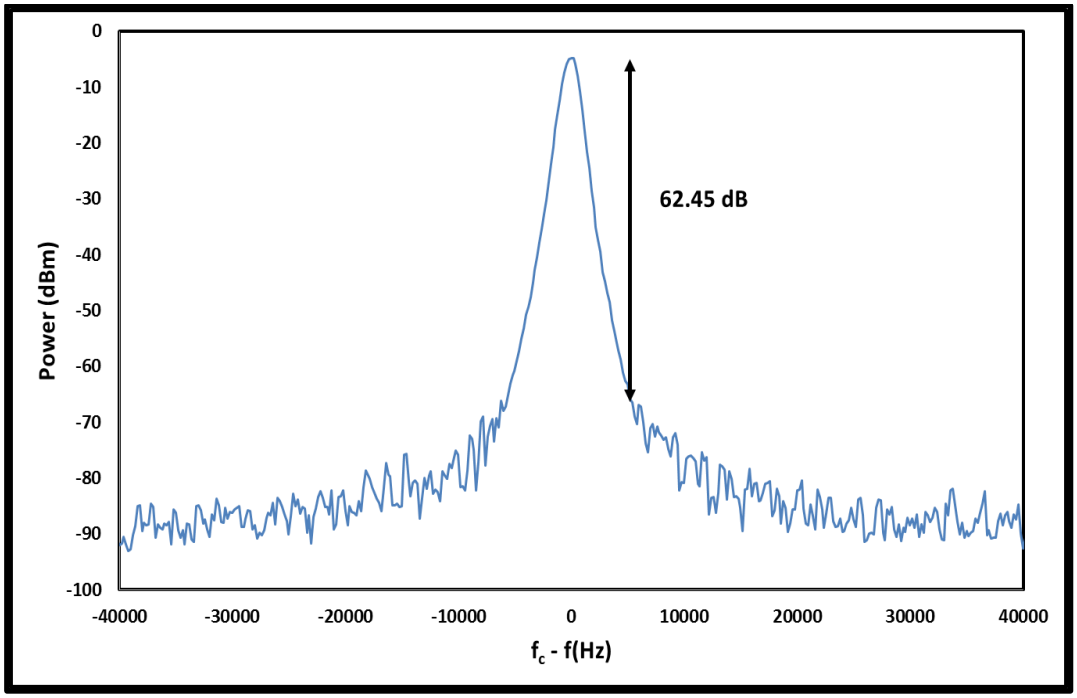

Fig. 4.19: RF spectrum of the mode-locked pulse train

4.3.4 MODE-LOCKED FIBER LASER OPERATING AT 1.9 µm REGION USING THE GSA

Most recent works on the mode-locked fiber lasers are focusing on Ytterbium- and Erbium-doped fiber lasers, which operate at wavelengths around 1 and 1.5 µm, respectively. However, much attention has also been focused on Thulium-doped fiber laser in recent years to provide an integrated

and robust laser source operating at around 2-μm wavelength for many applications in nonlinear optics, medicine, and sensing. To date, few mode-locked oscillators based on Thulium doped fiber have been reported. For instance, Nelson, Ippen, and Haus (1995) demonstrated an additive-pulse mode-locked thulium fiber laser with 500-fs pulses generation. In another work, Sharp, Spock, Pan, and Elliot (1996) used a semiconductor saturable absorber mirror (SESAM) in a Tm fiber laser to achieve 190-fs pulses. More recently, Engelbrecht, Haxsen, Ruehl, Wandt, and Kracht (2008) reported a laser with grating- based dispersion compensation and double-clad thulium-doped fiber. The laser has a pulse energy as high as 4.3 nJ with pulse duration of 1.2 ps pulsewidth at the repetition rate of 41.4 MHz.

As discussed earlier, GSA is an excellent passive mode-locker because of their many advantages such as sub-picosecond recovery time, broad operation range, low saturation intensity, polarization insensitivity, low cost and easy fabrication (Z. Sun et al., 2010). In this section, a mode-locked fiber laser operating at 1.9 μm is demonstrated using Thulium Bismuth co-doped fiber (TBF) in conjunction with a simple and low cost graphene based saturable absorber. The saturable absorber is obtained by implementing mechanical exfoliation technique as described in the previous section. The proposed laser uses a 5 m long TBF, which was obtained through a modified chemical vapor deposition and solution doping processes as the gain medium to achieve a stable pulse train with 16.7 MHz repetition rate and 0.37 ps pulse width operating at 1901.6 nm. The proposed laser is simple and low-cost but has many potential applications especially in sensing and biomedical diagnostics where eye-safe and low-photon-energy light sources are required.

4.3.4.1 EXPERIMENTAL SETUP AND PROCEDURE

A schematic of the experimental laser setup is shown in Fig. 4.20. It consists of a 1552 nm Erbium/Ytterbium fiber laser as a pump source, a 5 m long TBF as a gain medium, a 1550 nm / 2000

nm wavelength division multiplexer (WDM), a polarization insensitive circulator, a fiber Bragg grating, a 10 dB coupler, a polarisation controller and a GSA. The TBF is obtained by drawing a preform, which was fabricated using a deposition of porous layer by the MCVD process in conjunction with solution doping technique. The dopant concentrations (wt%) and compositions inside the core are 0.35 Bi_2O_3, 0.9 Tm_2O_3, 3.0 Al_2O_3 and 4.0 GeO_2. The fiber has a core and cladding diameters of 7.2 and 125 μm, respectively with a NA of 0.23. The WDM is used to inject the 1552 nm pump into the TBF. The circulator is used to allow the reflected light from the FBG to oscillate in the ring cavity as well as to ensure a unidirectional operation of the laser. The FBG used has a center wavelength of 1901.6 nm with a 3 dB bandwidth of 1.5 nm and a reflectivity of 99.6%. The purpose of the FBG is to stabilize the laser, as the mode competition of the laser would render the center wavelength behaves erratically. A polarization controller (PC) is used to adjust the intra-cavity polarization of light. The graphene based SA plays the key role of a passive mode-locker. It is constructed by depositing a single layer graphene on the end facet of the optical fiber ferrule by mechanical exfoliation technique as discussed in the previous section. The dispersion parameter of the gain medium is calculated to be 44.4 ps/nm/km at operating wavelength of 1900 nm, the rest of the cavity uses an SMF-28 fiber. The estimated dispersion parameter of SMF-28 at 1900 nm is 35 ps/nm/km (Wang et al., 2013). The total length of the laser cavity is about 12.5 m. All components are polarization independent and connected by fiber pigtails. Therefore, graphene based SA is the only mechanism responsible for saturable absorption. The laser output is tapped from the 10% port of the output coupler, measured by a power meter and monitored by a photodetector, which is attached to a 500 MHz oscilloscope.

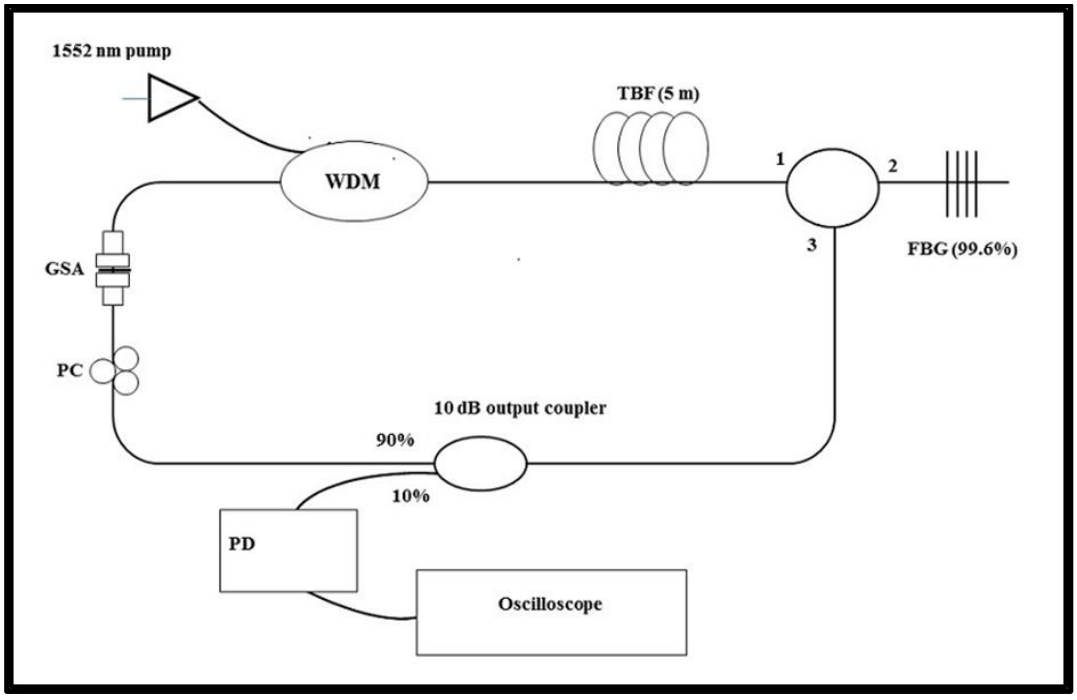

Fig. 4.20: Schematic configuration of the proposed mode-locked TBFL

The pulses formed by the mode-locking process in the resonator were detected using a 6-GHz photo-detector and a 500-MHz digital phosphor oscilloscope. It was observed that the mode-locked laser self-started at 1552 nm pump power of 869 mW without any disturbance to the fiber cavity. The optical spectrum of the passively mode-locked laser is shown in Fig. 4.21. It operates at the center wavelength of 1901.6 nm, which coincides with the FBG wavelength with a few sidebands. The total GVD of the cavity is estimated to be 0.485 ps/nm/km. Hence, the mode-lock fiber laser is operating in the anomalous dispersion region. The presence of Kelly sidebands in the optical spectrum (Fig. 4.21) confirm this. The theory of saturable absorption in graphene was thoroughly discussed by Winzer et al. (2012a). A spectral broadening is also observed, which is most probably due to the soliton effect from the balance between the self-phase modulation (SPM) and group velocity dispersion (GVD) in the cavity. This broadening is not observed without the saturable absorber. The average output power is measured to be around 1.72 mW at 1552 nm pump power of

869 mW. The full width half maximum (FWHM) of the optical spectrum is far below 1 nm due to the use of narrow-band FBG in the cavity.

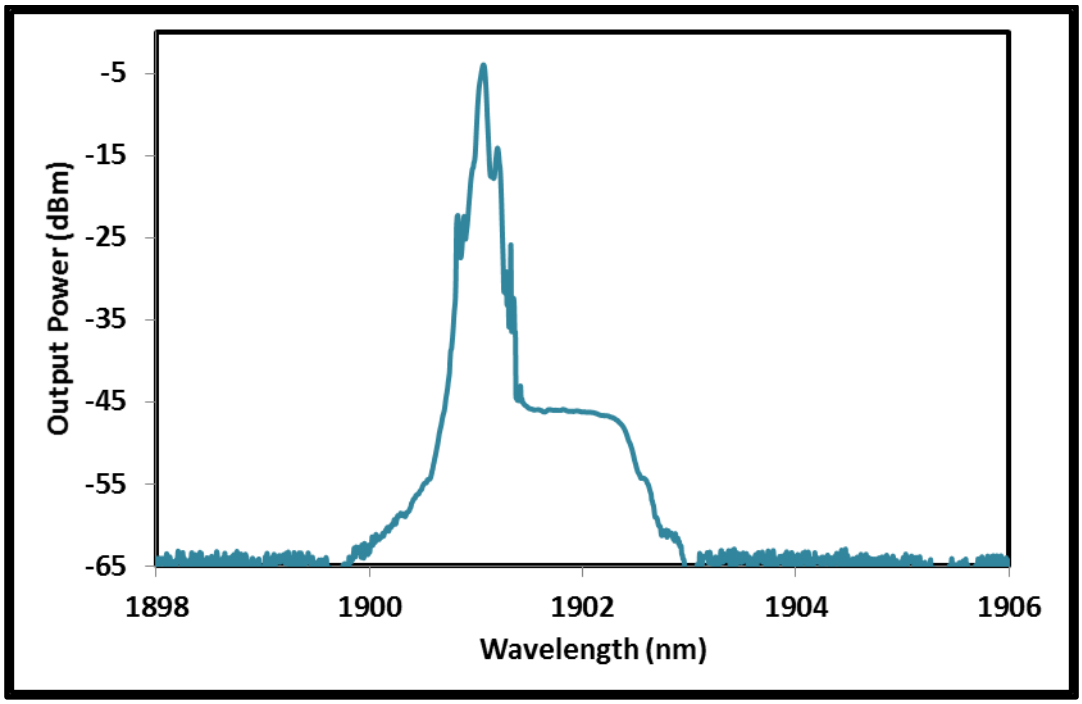

Fig. 4.21: The attenuated output spectrum at pump power at 1552 nm pump power of 869 mW.

Fig. 4.22 shows a pulse train from the mode-locked thulium bismuth co-doped fiber laser (TBFL) recorded by an oscilloscope. As seen, the time interval is measured to be around 60 ns, which corresponds to a repetition rate of 16.7 MHz. Fig. 4.23 shows a plot of a two-photon absorption autocorrelation trace measured using an autocorrelator, which is optimized for 1550 nm region. The estimated pulse duration at its full-width half maximum (FWHM) is about 0.37 ps. The autocorrelation trace reveals that the experimental result does not really follow the sech^2 fitting.

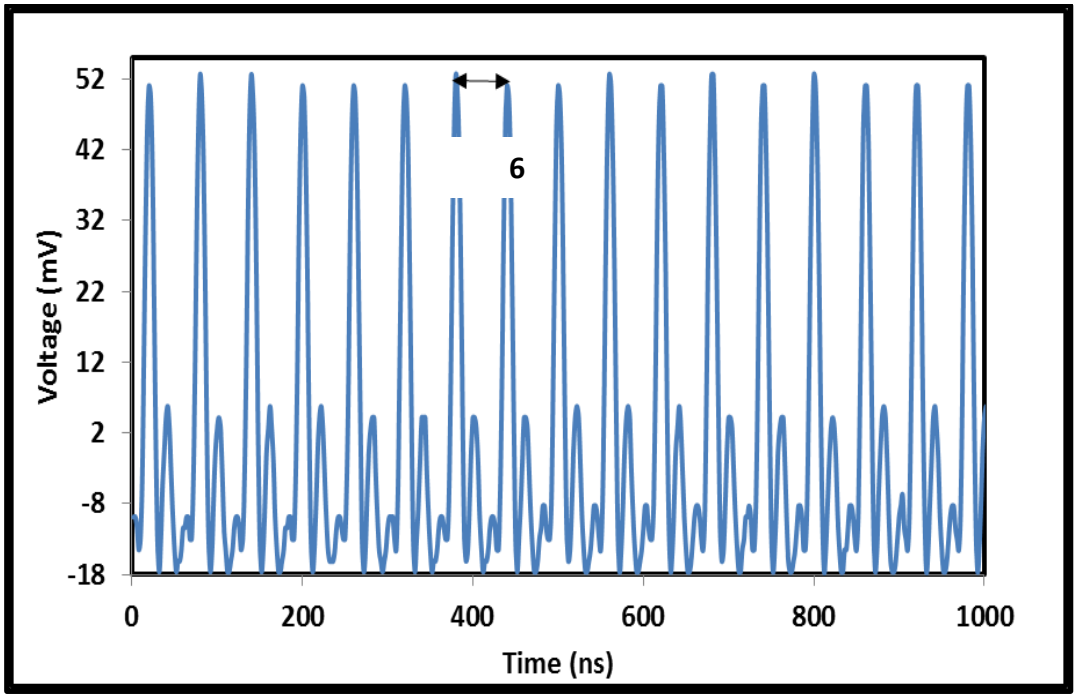

Fig. 4.22: Output pulse train from the mode-locked TBFL.

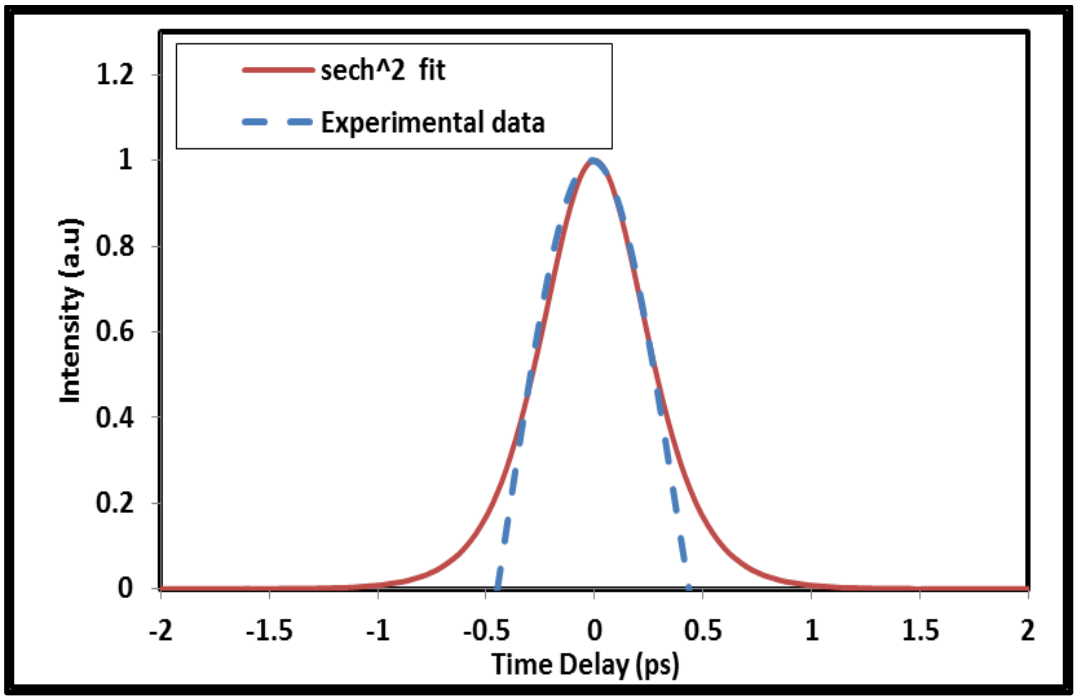

Fig. 4.23: Autocorrelation trace of the mode-locking pulse measured by 1550 nm autocorrelator.

According to the output spectrum shown in Fig. 4.21, the 3 dB bandwidth of the output pulses is not more than 0.1 nm. Assuming that the output pulses possess a transform-limited, secant hyperbolic temporal shape, their temporal width must be ~40 ps at a wavelength of 1901.6 nm. If the pulses have a frequency chirp, their temporal width must be larger than that of the transform limited pulses. There is no theoretical explanation of obtaining 370 fs pulses from the laser setup shown in Fig. 4.20. Furthermore, since the laser setup used a fiber Bragg grating (FBG) with a 3 dB bandwidth of 1.5 nm, the spectral bandwidth of the output pulses cannot exceed the limit. This implies that the output pulse width must be no less than 2.5 ps at 1901.6 nm. If the mode-locked pulses with a temporal width of 370 fs were really obtained, the measured optical spectrum of the output pulses in Fig. 4.21 should have exhibited a spectral 3 dB bandwidth of no less than 10.43 nm. Therefore, it is believed that the autocorrelation trace in Fig. 4.23 gives completely incorrect information. The measured temporal peak might be a coherent spike of a substantial incoherent background noise of the output from the laser. Further investigation cannot be carried out due to unavailability of 2 micron autocorrelator is the laboratory.

Fig. 4.24 shows the radio frequency (RF) spectrum of the mode-locked fiber laser. As seen, the signal-to-floor noise ratio is observed to be more than 60 dB, while the signal-to-noise (SNR) ratio is 46 dB. This indicates that the mode-locked pulse is stable.

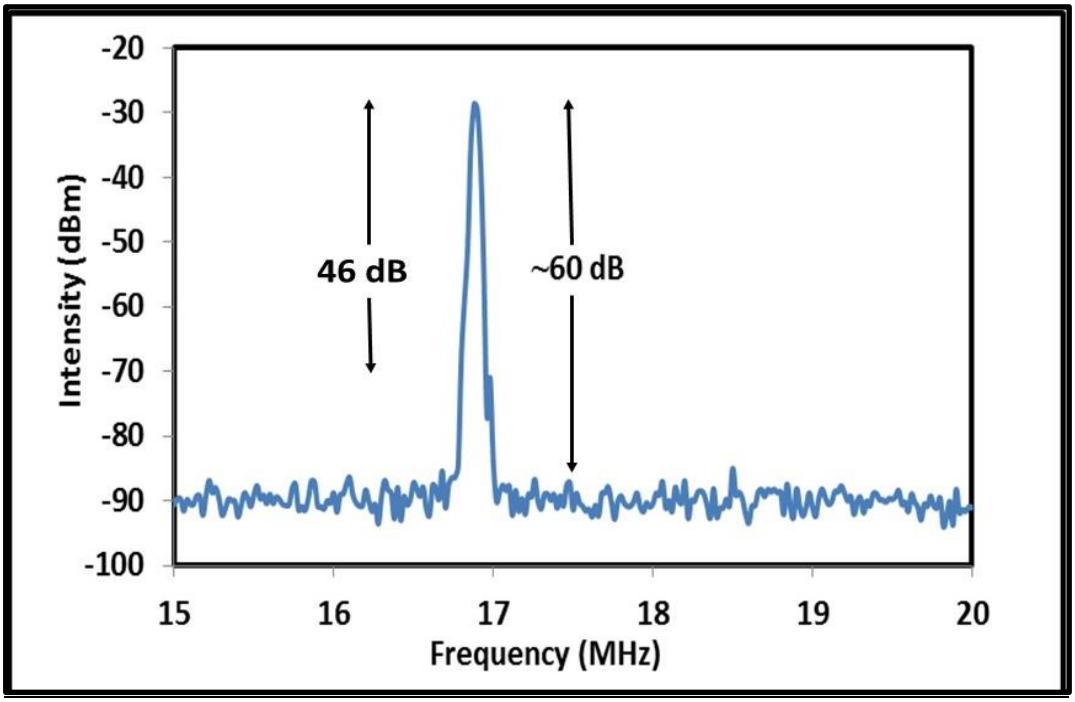

Fig. 4.24: RF spectrum of the mode-locking pulse from the TBDFL.

4.4 SUMMARY

A simple and compact *Q*-switched EDFL is demonstrated using a GSA, which is obtained by depositing graphene solution on the end surface of fiber ferrule. It is found that a thicker layer of graphene produces a *Q*-switched fiber laser with a lower pump threshold and higher energy but smaller repetition rate and pulse width. The EDFL operates at 1560 nm with a repetition rate that varies with the pump power. For instance, the repetition rate of the EDFL configured with GSA1 can be widely tuned from 16.7 kHz to 31.6 kHz by varying the pump power from 55 mW to 120 mW. The EDFL has a pulse width of 7.5 µs and pulse energy of 43.7 nJ with GSA2 at 120 mW pump power.

A single-layer graphene SA presents some advantages as well as disadvantages. A single-layer graphene SA suggest a large modulation depth, lower insertion loss, better pulse

shaping ability, improved pulse stability and higher output energy. However, a single-layer graphene is difficult to produce, and its large modulation depth implies a higher mode-locking threshold. A higher threshold indicates that the laser cavity requires a large pulse energy to bleach the SA, which can be met by adding extra optical fiber or by using a higher pump power. In the case of fiber laser, a longer cavity length would add extra dispersion into the laser cavity and effects its pulsewidth. In the experiment, the resultant mode-locked fiber laser has a repetition rate of 967 kHz, a pulsewidth of 3.41 ps and a TBP of 0.38. Due to the large dispersion presence, the TBP is 1.2 times higher than the ideal value.

A passive and stable mode-locked TBFL operating in 1901.6 nm region using a graphene based SA, which was obtained via mechanical exfoliation technique, has successfully been demonstrated. The SA was fabricated by mechanically exfoliating a single layer graphene using a scotch tape method and transferred the graphene layer onto the end surface of the fiber pigtail. At 1552 nm pump power of 869 mW, the TBFL generates a mode locking pulses with a repetition rate of 16.7 MHz and pulsewidth of 0.37 ps. The single-layer graphene SA can be used in the 2 μm region, owing to its ultra-broadband operating wavelength. Nevertheless, a high pump power is needed to start the mode-locking process. A suitable autocorrelator is also needed to characterize the pulse accurately.

CHAPTER 5

SOLITON MODE-LOCKING BY USING NON-CONDUCTIVE GRAPHENE OXIDE PAPER AS SATURABLE ABSORBER

5.1 INTRODUCTION

Since the discovery of graphene by Novoselov et al. (2004), graphene has been touted as wonder material. The unique electrical and optical properties of graphene originates from its high mobility charged carriers and its hole and electron conical bands that meet at Dirac point (A.K. Geim & Novoselov, 2007). Linear optical absorption and saturable absorption are among the optical properties of graphene. The linear dispersion of the Dirac electrons yield promising broadband applications and saturable absorption property of graphene results from Pauli blocking (Bonaccorso et al., 2010). At high intensity, the photon generated carriers increase in concentration and cause the states near the edge of the conduction and valence bands to fill, thus, blocking further absorption. Band filling occurs because no two electrons can fill the same state. Consequently, saturable absorption is reached due to this Pauli blocking process (Q. Bao et al., 2009). Moreover, the relaxation of carriers in a single layer graphene is ultrafast (200 fs) (Carbone et al., 2011). Other papers have included other factors that enables graphene to be an excellent saturable absorber (Winzer et al., 2012b; Xing, Guo, Zhang, Sum, & Huan, 2010)

Graphite oxide is a compound that composed of carbon, hydrogen and oxygen in variable ratios. The oxygen functional groups of graphite oxide causes the graphite oxide to be hydrophilic; i.e. graphite oxide disperses well in water to produce graphene oxide. Graphite oxide has attracted much attention recently as a cost-effective and large-scale production route (oxidation of graphite followed by reduction of graphene oxide platelets obtained by exfoliation) of graphene (Zhu et al., 2010). A graphene paper is prepared by mixing graphite oxide in water. The oxygen atoms of graphite oxide repel water molecules, thus, undergoing complete exfoliation in water, producing a colloidal suspensions of almost entirely individual graphene oxide sheets. After filtering the exfoliated mixture using through a membrane, these graphene oxide sheets could be made into paper-like material under a directional flow. A free-standing graphene oxide paper is obtained after drying. By changing the oxygen amount on the layers, the material can be an electrical insulator, semi-conductor or conductor. This material is uniform and dark brown in colour. (Dmitriy A Dikin et al., 2007).

In the previous chapters, *Q*-switched and mode-locked fiber lasers have been demonstrated using two types of graphene saturable absorber. Numerous works have also been reported on graphene based mode-locked fiber lasers in literatures (Cao et al., 2012; J. Liu et al., 2011; D. Popa et al., 2011; Z. Sun et al., 2010; J. Xu et al., 2012; S. Yamashita, 2012; H Zhang et al., 2010; Han Zhang et al., 2010). Recently, J. Xu, Liu, Wu, Yang, and Wang (2012) has demonstrated a mode-locked femtosecond erbium-doped fiber lasers (EDFLs) using graphene oxide as a saturable absorber (SA). The SA was prepared by immersing a broadband mirror into a graphene oxide hydrosol. After 48 hour, a thin graphene membrane was formed on top of the broadband reflective mirror. In another work, Sobon et al. (2012) compares the performances of graphene oxide and reduced graphene oxide as SA.

The saturable absorbers were placed on fused silica substrate and inserted between two collimating gradient index (GRIN) lenses to achieve mode-locked fiber lasers.

In this chapter, a femtosecond mode-locked EDFL using a commercially available nonconductive graphene oxide paper as a saturable absorber is successfully demonstrated. The paper is sandwich between two fiber ferrules to function as a SA for initiating a mode-locking. This results in passive mode-locking with 15.62 MHz repetition rate and 680 fs pulse width. The fiber laser is observed to have a low pulsing threshold as well as low damage threshold. Therefore, pulse energy and peak power are 0.0085 nJ and 11.85 W respectively. The easy fabrication of graphene oxide paper will promote its potential in ultrafast photonics applications.

5.2 RAMAN SPECTROSCOPY OF GRAPHENE OXIDE PAPER

Fig. 5.1 below shows the result of Raman spectroscopy on graphene oxide paper. The spectroscopy was performed using 532 nm laser with only 10% power. The exposure time was set to 20 s. From the result, there are two distinctive peaks that can be observed; at 1349 cm^{-1} and 1588 cm^{-1}. These two peak corresponds to D-band and G-band respectively (Yang et al., 2009). The peak at D-band is caused by the hybridized vibrational mode related to graphene edges and it also reveal that there is disorder to the graphene structure. The G-band, also known as the graphite or tangential band, is due to the energy in the sp^2 bonded carbon in planar sheets. The in-plane optical vibration of the bond resulted in Raman spectrum at the frequency (Zhu et al., 2010). A small bump at 2700 cm^{-1}, also known as G' or 2D band, is barely observable because the laser power is low. Because the intensity of G'

band is lower than the G band, it also shows that the GO paper has more than one graphene layer.

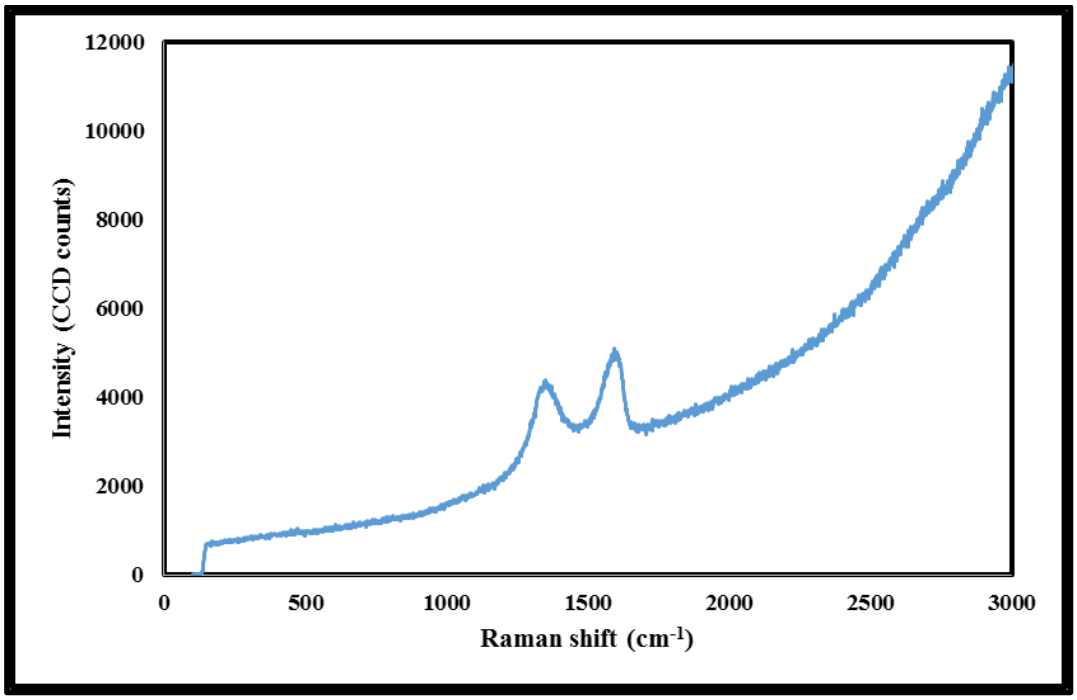

Fig. 5.1: Raman spectroscopy result of graphene oxide paper

5.3 EXPERIMENTAL SETUP

The schematic of the proposed mode-locked EDFL is shown in Fig. 5.2. It was constructed using a simple ring cavity, in which a 1.6 m long Erbium-doped fiber (EDF) with an Erbium ion concentration of 2000 ppm was used for the active medium and the GO paper based SA was used as a mode-locker. The EDF used has numerical aperture of 0.24, cut off wavelength of 930 nm and 24 dB/m absorption at 980 nm. It was forward pumped by a 1480 nm laser diode via a 1480/1550 nm wavelength division multiplexer (WDM). The polarization independent isolator was used to ensure unidirectional light propagation in the cavity and thus facilitate self-starting laser (Tamura et al., 1993). The laser output was

obtained via a 95/5 output coupler located between the isolator and SA, which channeled out about 5% of the oscillating light from the ring cavity. The output was analyzed by using an optical spectrum analyzer (OSA) with a resolution of 0.07 nm and a 350 MHz oscilloscope with 6 GHz bandwidth light wave detector. The pulse width of the output laser was measured using an autocorrelator. All components used in the experimental setup are polarization independent, i.e. they support any light polarization. No polarization controller (PC) was included in the laser cavity as a PC neither improve the pulse stability nor promote self-starting, as observed earlier. There was no significant pulse jitter observed through the oscilloscope during the experiment. The lasing threshold of the laser cavity was approximately 8.3 mW.

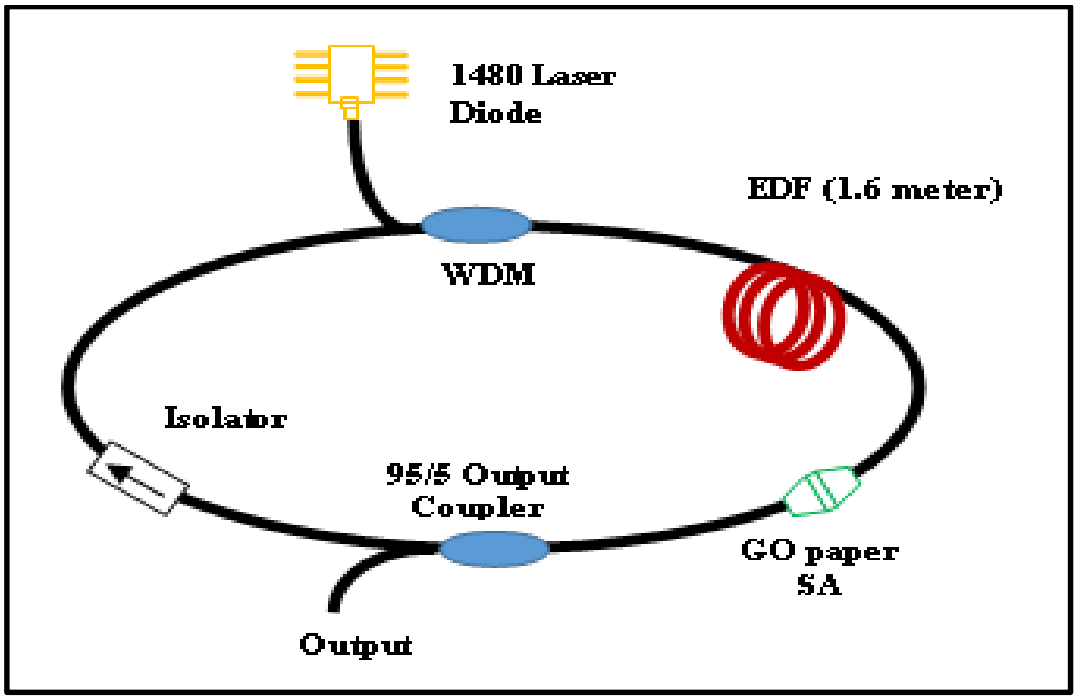

Fig. 5.2: Experimental setup

The SA was fabricated by cutting a small piece (2×2 mm2) of a commercially non-conductive graphene oxide paper ("Graphene Laboratories Inc. ,") and sandwiching it

between two FC/PC fiber connectors, after depositing index-matching gel onto the fiber ends. According to the specification given by manufacturer, the thickness of the GO paper is 10 μm while the measured insertion loss of the SA to be 1.0 dB at 1550 nm. The SA was placed between the gain medium and output coupler in the ring cavity. The total length of the laser cavity was measured to be approximately 12.6 meter, comprising 1.6 m EDF and 11 meter SMF-28 fiber. The Group Velocity Dispersion (GVD) for the EDF and SMF-28 were -21.64 ps/nm/km and 17 ps/nm/km respectively at 1550 nm. Therefore, the resultant total GVD for this mode-locked fiber laser was calculated to be 0.1513 ps/nm/km. This indicated that the proposed mode-locked fiber laser operated in the anomalous dispersion regime and thus it could be classified as a soliton fiber laser.

5.4 MODE-LOCKING PERFORMANCE OF THE LASER

The mode-locked fiber laser had a low self-starting threshold; approximately at 17.5 mW. Before all the modes were locked, multiple pulsing could be seen to occur at pump power as low as 10 mW. Fig. 5.3 shows the spectral profile where the presence of soliton is confirmed. The solitons' central wavelength, λc, is situated at 1563.56 nm and the 3-dB bandwidth (3-dB BW) is approximately 3.77 nm with strong Kelly sidebands at 1554.6 nm and 1573 nm. The spectrum is free from continuous wave (CW) parasitic lasing. The presence of Kelly sidebands confirms that this mode-lock fiber laser is operating in anomalous dispersion regime. Fig. 5.4 shows the pulse train of the passive mode-locked fiber laser obtained at pump power of 18 mW. It has a cavity round trip time of 64 ns, corresponding to a pulse repetition rate 15.6 MHz and a cavity length of 12.6 m.

Fig. 5.5 shows the autocorrelation trace which uses the Two-Photon Absorption (TPA) technique, with the measured pulsewidth of 680 fs at its full-width half maximum (FWHM). The sech² fitting which indicates the generation of the soliton pulse is also included in the figure. The autocorrelation trace reveals that the experimental result follows the sech² fitting closely. A time-bandwidth product (TBP) of 0.315 calculated from the 3-dB bandwidth of the optical spectrum and the acquired pulsewidth. This shows that the pulse is a transform-limited pulse. Since the pulsing threshold is low, the output power for this fiber laser is 0.134 mW. Consequently, the resultant pulse energy and peak power are 0.0085 nJ and 11.85 W respectively.

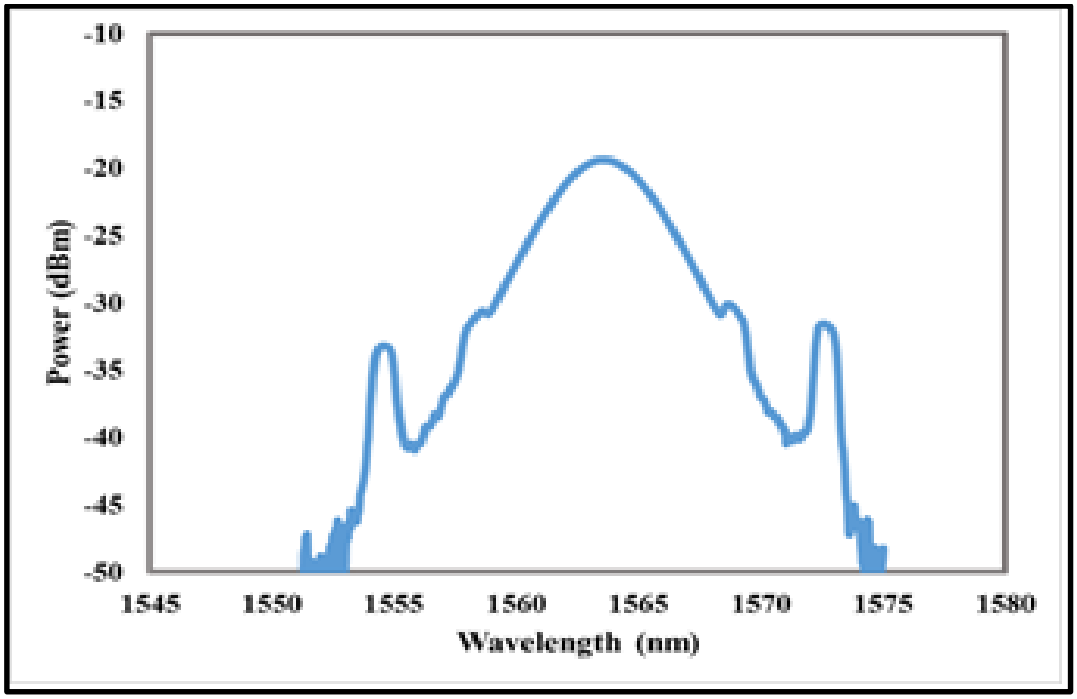

Fig. 5.3: Spectral characteristic of mode-locked fiber laser using GO paper

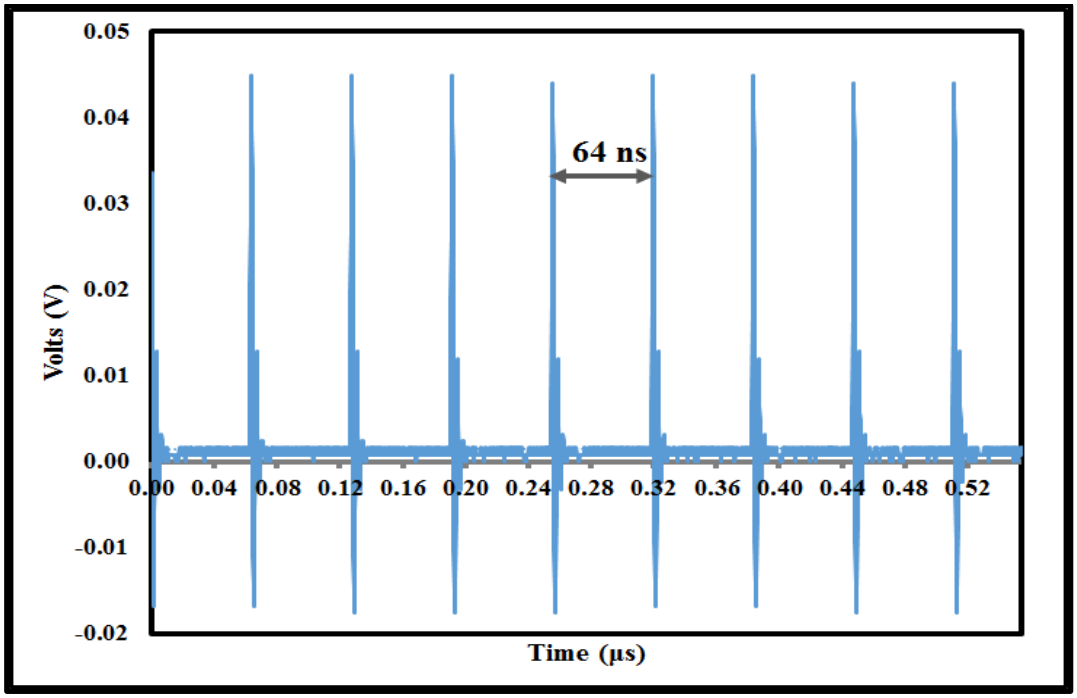

Fig. 5.4: Mode-locked pulse train with cavity round-trip time.

As the data measurements being performed, it is observed that the pulse increasingly expanded and the spectral profile gradually changed from soliton to laser. Therefore, it is suspected that the pulse gradually is destroying the SA. Moreover, at approximately 24.4 mW, the output power was attenuated. Thus, it is concluded that a 1-layer GO paper SA is only effective in a short period of time and has low damage threshold. For the same reason, a satisfactory signal-to-noise (SNR) data using Radio Frequency Spectrum Analyzer (RFSA) is unable to be acquired. Together with low pulsing and damage thresholds, combined with the 5% of the intracavity energy taken out for performing measurements, it seems that the SNR is unable to extend more than 30 dB.

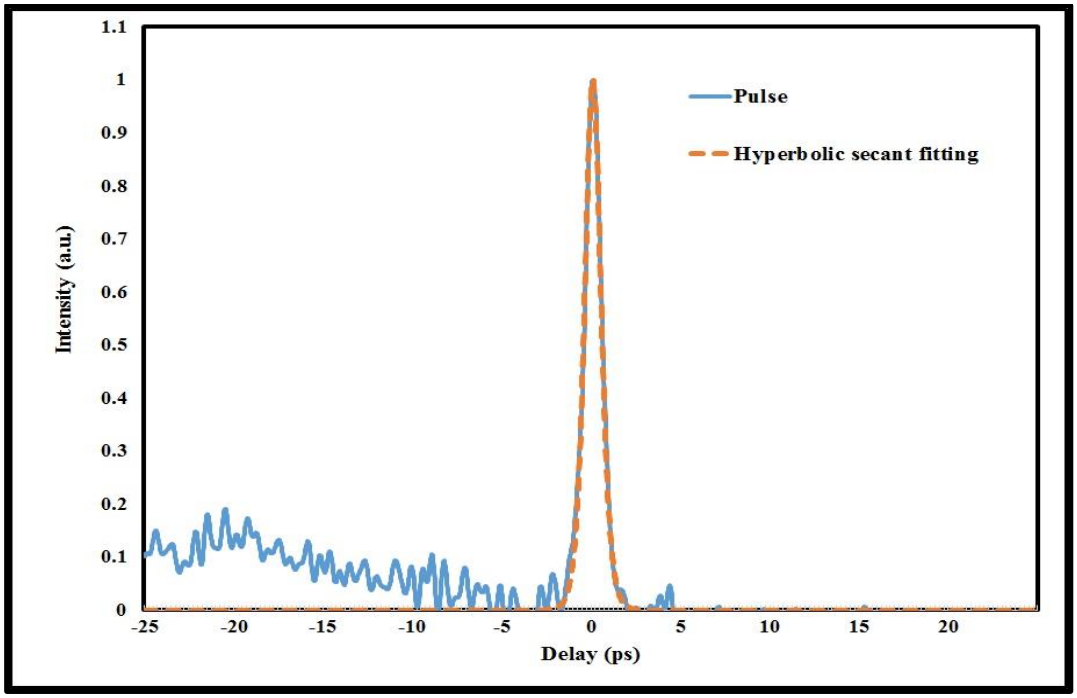

Fig. 5.5: Autocorrelation trace.

5.5 SUMMARY

In summary, the use of nonconductive GO paper as SA for generating transfom limited, soliton mode-locked fiber laser has successfully demonstrated. The resultant soliton mode-locked pulse has a repetition rate of 15.6 MHz with pulsewidth of 680 fs. The TBP value is calculated to be 0.315, which indicates that the mode-locked pulse has the ideal shape. The SA has a relatively low self-starting threshold although susceptible to damage at higher pump power. The SA is only able to withstand pulse operation for a short period of time. Given by the simplicity of preparing a GO paper, this experiment proves that a non-conductive GO paper can be an alternative to existing graphene and GO based SA.

CHAPTER 6

CONCLUSIONS AND FUTURE WORKS

6.1 CONCLUSIONS

Pulsed fiber lasers are simple and compact. These fiber lasers can supply high power, small, easy to integrate and operate. With Ytterbium, Erbium and Thulium as gain mediums, pulsed fiber laser offers a wide operating wavelength. *Q*-switched fiber laser have high peak power and usually operates in nanosecond pulsewidth. These advantages enables the fiber laser to be utilized in various applications such as micromachining, marking and scribing. Mode-locking are has lesser peak power compared to *Q*-switched laser, but shorter pulsewidth. The pulse duration of mode-locked fiber laser varies from ~ps to ~fs. Mode-locked lasers have found its applications in terahertz generation, two-photon microscopy and second-harmonic generation, among others. In this thesis, *Q*-switched and mode-locked fiber lasers are demonstrated using various techniques, most notably, using carbon-based saturable absorbers. We have also shown how we developed passive *Q*-switched and soliton mode-locked fiber lasers from these saturable absorbers.

In the first sub-chapter of chapter 3, *Q*-switched and soliton mode-locked fiber lasers are demonstrated using nonlinear polarization rotation (NPR), semiconductor saturable absorber (SA) and single-walled carbon nanotubes (SWCNT). NPR is a Kerr-effect based technique that changes the polarization states of the propagating light while SA is made of a combination of semiconductor materials with bandgap that corresponds to the laser's operating wavelength. The resultant pulsewidth for NPR and semiconductor SA are 1.11 ps

and 0.58 ps respectively. While both techniques show soliton spectra, the optical spectrum of NPR reveals prominent Kelly sidebands whereas the optical spectrum of a semiconductor SA optical does not feature noticeable Kelly sidebands. This indicates that, although the use of SA in the laser cavity greatly assist the pulse formation and produces shorter pulse, it also alters the nonlinearity of the resultant soliton mode-locked fiber laser. On the other hand, because NPR relies on Kerr effect to generate mode-locked pulse, the technique depends on pump power and fiber length in-order to be effective. Due to this reason, the ensuing pulsewidth is broader because of higher pump power and the need for longer fiber laser cavity entail an increase in dispersion. Ultimately, the time-bandwidth product (TBP) of the soliton mode-locked fiber laser by NPR technique is larger than the one generated using semiconductor SA.

In the second sub-chapter of chapter 3, a simple method of fabricating single-walled carbon nanotubes (SWCNT) SA is demonstrated. A *Q*-switched and soliton mode-locked fiber lasers are successfully demonstrated by using the same SWCNT SA. The novelty of this method is that the same SA not only can generate a *Q*-switched fiber laser, but it can also be used to generate a soliton mode-locked fiber laser. Beforehand, the prevalent methods of fabricating SWCNT SA for generating a mode-locked fiber laser are by creating SWCNT film, optical deposition, and spraying. These methods usually comprise of multiple processes. The proposed method in chapter 3 creates the SWCNT SA only by dripping the SWCNT-SDS solution onto the fiber ferrule. The SWCNT is then allowed to dry overnight in room temperature. The resultant SWCNT SA has an insertion loss of 3.61 dB, which is more than the recommended maximum 3 dB insertion loss. As a result, instead of a mode-locked fiber laser, we obtained a *Q*-switched fiber laser. However, the generation of mode-locked fiber laser does not depend entirely on the insertion loss of the SA. This is a factor

that is often overlooked by most researchers. The design of the fiber laser cavity can also determine the success of creating a mode-locked fiber laser. By increasing the fiber length, and in turn increasing the pulse energy, the SA can be saturated faster. Hence, a mode-locked fiber laser can be created. Therefore, even with the SA's high insertion loss, as long as the high pulse energy is able to saturate the SA, a soliton mode-locked fiber laser can be generated. Hence, in chapter 3, it is proven that the insertion loss can be compensated by changing the design of the fiber laser.

In chapter 4, *Q*-switched and soliton mode-locked Erbium-doped fiber lasers (EDFL) and Thulium-Bismuth doped fiber (TBFL) lasers are successfully demonstrated by using graphene as SA. In the first sub-chapter, a simple and compact *Q*-switched fiber laser is successfully demonstrated. The experiment compares the *Q*-switched performances of two different graphene SA (GSA). The GSAs are created using optical deposition method. From the experiments, it is concluded that a thicker layer of GSA produces a *Q*-switched fiber laser with lower *Q*-switched threshold with higher energy but smaller repetition rate and pulsewidth.

The novelty of the experiment in the second sub-chapter of chapter 4 is that a single-layer graphene is successfully isolated using the mechanical exfoliation technique. The single-layer graphene is originated from a highly ordered pyrolitic graphite (HOPG). Theoretically, a single-layer graphene implies a large modulation depth, lower insertion loss and better pulse shaping ability. A multilayer graphene presents lower modulation depth due to the losses by scattering and non-saturable absorption. A multilayer graphene also has higher insertion loss. Initially, the single-layer graphene SA generates a *Q*-switched fiber laser. The large modulation depth suggest that a high pulse energy is required to saturate the single-layer graphene SA. Even after changing the gain medium from the Bismuth based

Erbium-doped fiber (Bi-EDF) to the normal Erbium-doped fiber (EDF), a soliton mode-locked fiber laser is still out of reach. Only after adding an extra 200 meter of single mode fiber (SMF), the pulse energy becomes high enough to saturate the SA. Therefore, it can be concluded that a single-layer graphene has a very large modulation depth. Due to the lack equipment, the modulation depth of a single-layer graphene is unable to be determined. However, in another scientific publication, the modulation depth of a single-layer graphene is reported to be ~66%. Apart from the very large modulation depth, the resultant mode-locked fiber laser also does not self-start. Taking advantage from the ultra-broadband operating wavelength of graphene SA, a soliton mode-locked Thulium-Bismuth doped fiber laser (TBFL) is also demonstrated. The fiber laser operates at 1901.6 nm region. Suffering from the very large modulation depth of single-layer graphene SA, the solition mode-locked fiber laser self-starts at 869 mW pump power. However, a suitable autocorrelator is needed in order to accurately measure the pulsewidth.

Chapter 5 demonstrates the usability of nonconductive graphene oxide (GO) paper as SA. To the best to our knowledge, this is the first introduction of GO paper as SA. Previous experiments uses GO film as SA. The nonconductive GO paper SA has an advantage of requiring a small pump power to self-start the mode-locking process. The pump power is only slightly higher than the lasing threshold. The experiment also yield a soliton mode-locked pulse with TBP value of 0.315, an ideal TBP value. In spite of this, the disadvantage is that the pulse does not endure for an extended duration because the mode-locked pulse slowly destroys the SA.

To summarize, a variety of techniques to generate mode-locked and *Q*-switched fiber lasers have successfully been demonstrated. New technique and material as SA have also been introduced. Although there are numerous techniques of generating mode-locked pulse,

each technique has their own advantages and disadvantages. NPR works for all wavelength, however, NPR is not reliable. NPR does not guarantee self-starting, and since the technique depends on Kerr effect, the length and pump power needed to generate enough Kerr effect have effects on pulsewidth. Furthermore, the modulation depth of an NPR technique is difficult to measure.

Semiconductor-based SA has many attractive properties. It self-starts and has appropriate modulation depth. Nevertheless, since the operating wavelength depends on the materials, it only works for a narrow band of wavelength. It is expensive, difficult to fabricate and prone to damage if subject to *Q*-switch pulse. Careful operating is required when using semiconductor based SA.

The resonant wavelength of SWCNT varies depending on the tube's diameter. Therefore, the modulation depth also varies according to wavelength. The popular technique of incorporating SWCNT SA into fiber laser is by fabricating it into a film. Fabricating a SWCNT film is easy, however, this technique does not produce consistent properties between one film and another. A film fabricated by one person is different from another film fabricated by another person. Different SWCNT concentration, thickness and other factors that involved when fabricating the film leads different modulation depth, non-saturable losses and mode-lock threshold.

Graphene SA film suffers the same drawbacks as SWCNT SA film. The properties varies between films. The advantage of graphene SA is that it works on an ultra-broadband. The best graphene SA is a single-layer graphene, however, it is notoriously difficult to produce and the modulation depth is very large. To saturate a single-layer graphene SA, a high pulse energy is needed; requiring high pump power and/or long fiber length. These will ultimatley affect the achievable pulse duration and repetition rate. Without the high pulse

energy to saturate the graphene SA, the resultant pulse is a *Q*-switched; instead of mode-locked.

There are many ways of creating a mode-locked fiber laser. The flaw in the SA can be compensated through changing the cavity design. Although the cavity design is not critical in soliton mode-locked laser, to achieve an ultrashort mode-locked pulse, we have to consider numerous factors. Factors such as modulation depth, dispersion, pump power, self-starting ability and overall cavity design need to be taken into account. These factors influence each other and to some extent, they may cancel each other. A large modulation depth may imply better pulse shaping ability, but it also imply a larger pulse energy needed to saturate the SA. A large pulse energy can be met by adding extra length to the fiber laser cavity, but it also means that the dispersion is now increased. An increase in dispersion can lead to broader pulsewidth. In short, there are trade-offs when trying to achieve narrower pulse. Trying to create an ultrashort mode-locked pulse is akin to balancing all these factors. As a result, the ability to produce an ultrashort mode-locked pulse is often very limited.

In *Q*-switched fiber laser, the number of layers of the graphene SA has influence on the performances of the fiber laser. A thicker layer lead to higher insertion loss but produced a fiber laser with lower starting threshold, repetition rate and pulsewidth. As a result, a *Q*-switched fiber laser with higher pulse energy is generated.

6.2 FUTURE WORKS

If we observe the published journal papers regarding mode-locked fiber laser, we would have noticed that the majority of these papers do not have mathematical explanations. Generally, the nonlinear Schrödinger equation is used to describe the mode-locking phenomena. Most of these journal papers are concentrating on shorter pulse width, higher repetition rate, new operating wavelength and new SA materials. While these are nonetheless an important progress in the field of pulse laser, the lack of mathematical explanations indicate that the phenomena is not fully understood. This signals an opportunity for improvement. A detailed and accurate explanations on the factors that influence pulse formation and pulse shaping can make the phenomena more predictable. Furthermore, the existing mathematical equations are derived from experiments using solid-state laser. For fiber laser, the interplay between pump power, dispersion, modulation depth and other factors are yet to be discovered. Additionally, the nonlinear effects are more dominant in fiber laser compared to solid-state laser. It would be interesting to explore the theoretical, mathematical and modelling aspects of mode-locked fiber laser.

The inventions of quantum dots, nanoparticles and metamaterial fibers have the potential to bring mode-locked fiber laser into new directions. These inventions have potential to become new SA and effect other properties of mode-locked pulse; such as repetition rate and pulsewidth. With suitable equipment, we can study the effects of these inventions and find new ways of incorporating them into fiber laser. By utilizing them, we hope to enhance the performance of mode-locked fiber laser.

REFERENCES

Agrawal, G. (2006). *Nonlinear Fiber Optics*: Academic Press.

Ahmad, H, Saat, NK, & Harun, SW. (2005). S-band erbium-doped fiber ring laser using a fiber Bragg grating. *Laser Physics Letters, 2*(7), 369.

Ahmad, H., Paul, M. C., Awang, N. A., Harun, S. W., Pal, M., & Thambiratnam, K. (2012). Four-Wave-Mixing in Zirconia-Yttria-Aluminum Erbium Codoped Silica Fiber. *Journal of the European Optical Society: Rapid Publications, 7*. doi: 10.2971/jeos.2012.12011

Au, J, Kopf, D, Morier-Genoud, F, Moser, M, & Keller, U. (1997). 60-fs pulses from a diode-pumped Nd: glass laser. *Optics letters, 22*(5), 307-309.

Avouris, P., Freitag, M., & Perebeinos, V. (2008). Carbon-nanotube photonics and optoelectronics. *Nature photonics, 2*(6), 341-350.

Avouris, Phaedon, & Chen, Jia. (2006). Nanotube electronics and optoelectronics. *Materials Today, 9*(10), 46-54.

Bachilo, Sergei M, Strano, Michael S, Kittrell, Carter, Hauge, Robert H, Smalley, Richard E, & Weisman, R Bruce. (2002). Structure-assigned optical spectra of single-walled carbon nanotubes. *Science, 298*(5602), 2361-2366.

Bao, Q., Zhang, H., Wang, Y., Ni, Z., Yan, Y., Shen, Z.X., . . . Tang, D.Y. (2009). Atomic-Layer Graphene as a Saturable Absorber for Ultrafast Pulsed Lasers. *Adv. Funct. Mater, 19*, 3077-3083.

Bao, Qiaoliang, Zhang, Han, Ni, Zhenhua, Wang, Yu, Polavarapu, Lakshminarayana, Shen, Zexiang, . . . Loh, Kian Ping. (2010). Monolayer graphene as a saturable absorber in a mode-locked laser. *Nano Research, 4*(3), 297-307. doi: 10.1007/s12274-010-0082-9

Bao, Qiaoliang, Zhang, Han, Wang, Yu, Ni, Zhenhua, Yan, Yongli, Shen, Ze Xiang, . . . Tang, Ding Yuan. (2009). Atomic-Layer Graphene as a Saturable Absorber for Ultrafast Pulsed Lasers. *Advanced Functional Materials, 19*(19), 3077-3083. doi: 10.1002/adfm.200901007

Berger, Claire, Song, Zhimin, Li, Xuebin, Wu, Xiaosong, Brown, Nate, Naud, Cécile, . . . Marchenkov, Alexei N. (2006). Electronic confinement and coherence in patterned epitaxial graphene. *Science, 312*(5777), 1191-1196.

Blake, P., Hill, EW, Castro Neto, AH, Novoselov, KS, Jiang, D., Yang, R., . . . Geim, AK. (2007). Making graphene visible. *Applied Physics Letters, 91*(6), 063124-063124-063123.

Boivin, L., Wegmueller, M., Nuss, M. C., & Knox, W. H. (1999). 110 channels x 2.35 Gb/s from a single femtosecond laser. *Photonics Technology Letters, IEEE, 11*(4), 466-468. doi: 10.1109/68.752550

Bonaccorso, F., Sun, Z., Hasan, T., & Ferrari, AC. (2010). Graphene photonics and optoelectronics. *Nature Photonics, 4*(9), 611-622.

Boyd, Robert W, Raymer, Michael G, & Narducci, Lorenzo M. (1986). Optical instabilities: Cambridge University Press, New York, NY.

Breusing, Markus, Ropers, Claus, & Elsaesser, Thomas. (2009). Ultrafast Carrier Dynamics in Graphite. *Physical Review Letters, 102*(8), 086809.

Brodie, BC. (1860). Sur le poids atomique du graphite. *Ann. Chim. Phys, 59*(7).

Cao, W. J., Wang, H. Y., Luo, A. P., Luo, Z. C., & Xu, W. C. (2012). Graphene-based, 50 nm wide-band tunable passively Q-switched fiber laser. *Laser Physics Letters, 9*(1), 54-58. doi: 10.1002/lapl.201110085

Carbone, F, Aubock, G, Cannizzo, A, Van Mourik, F, Nair, RR, Geim, AK, . . . Chergui, M. (2011). Femtosecond carrier dynamics in bulk graphite and graphene paper. *Chemical Physics Letters, 504*(1), 37-40.

Casiraghi, C., Hartschuh, A., Lidorikis, E., Qian, H., Harutyunyan, H., Gokus, T., . . . Ferrari, AC. (2007). Rayleigh imaging of graphene and graphene layers. *Nano letters, 7*(9), 2711-2717.

Chang, You Min, Kim, Hyungseok, Lee, Ju Han, & Song, Yong-Won. (2010). Multilayered graphene efficiently formed by mechanical exfoliation for nonlinear saturable absorbers in fiber mode-locked lasers. *Applied Physics Letters, 97*(21), 211102. doi: 10.1063/1.3521257

Chen, S., Brown, L., Levendorf, M., Cai, W., Ju, S.Y., Edgeworth, J., . . . Piner, R.R. (2010). Oxidation resistance of graphene-coated Cu and Cu/Ni alloy. *arXiv preprint arXiv:1011.3875*.

Choudhary, Veena, & Gupta, Anju. (2011). *Polymer/Carbon Nanotube Nanocomposites*.

Collins, RJ, & Kisliuk, P. (1962). Control of Population Inversion in Pulsed Optical Masers by Feedback Modulation. *Journal of Applied Physics, 33*(6), 2009-2011.

Cuong, Tran Viet, Pham, Viet Hung, Tran, Quang Trung, Hahn, Sung Hong, Chung, Jin Suk, Shin, Eun Woo, & Kim, Eui Jung. (2010). Photoluminescence and Raman studies of graphene thin films prepared by reduction of graphene oxide. *Materials letters, 64*(3), 399-401.

Dahlström, L. (1972). Passive mode-locking and Q-switching of high power lasers by means of the optical Kerr effect. *Optics Communications, 5*(3), 157-162. doi: http://dx.doi.org/10.1016/0030-4018(72)90055-7

De Souza, E. A., Nuss, M. C., Knox, W. H., & Miller, D. A. B. (1995). Wavelength-division multiplexing with femtosecond pulses. *Optics Letters, 20*(10), 1166-1168. doi: 10.1364/OL.20.001166

Dennis, M.L., & Duling III, I.N. (1994). Experimental study of sideband generation in femtosecond fiber lasers. *Quantum Electronics, IEEE Journal of, 30*(6), 1469-1477.

Diddams, Scott A., Hollberg, L., Ma, Long-Sheng, & Robertsson, Lennart. (2002). Femtosecond-laser-based optical clockwork with instability? less than or equal to 6.3 X 10-16 in 1 s. *Optics Letters, 27*(1), 58-60. doi: 10.1364/OL.27.000058

Diddams, Scott A., Jones, David J., Ye, Jun, Cundiff, Steven T., Hall, John L., Ranka, Jinendra K., . . . Hänsch, T. W. (2000). Direct Link between Microwave and Optical Frequencies with a 300 THz Femtosecond Laser Comb. *Physical Review Letters, 84*(22), 5102-5105.

Digonnet, M.J.F. (2001). *Rare-Earth-Doped Fiber Lasers and Amplifiers, Revised and Expanded*: CRC.

Dikin, Dmitriy A, Stankovich, Sasha, Zimney, Eric J, Piner, Richard D, Dommett, Geoffrey HB, Evmenenko, Guennadi, . . . Ruoff, Rodney S. (2007). Preparation and characterization of graphene oxide paper. *Nature, 448*(7152), 457-460.

Dikin, Dmitriy A., Stankovich, Sasha, Zimney, Eric J., Piner, Richard D., Dommett, Geoffrey H. B., Evmenenko, Guennadi, . . . Ruoff, Rodney S. (2007). Preparation and characterization of graphene oxide paper. *Nature, 448*(7152), 457-460. doi: http://www.nature.com/nature/journal/v448/n7152/suppinfo/nature06016_S1.html

Dössel, Lukas, Gherghel, Lileta, Feng, Xinliang, & Müllen, Klaus. (2011). Graphene Nanoribbons by Chemists: Nanometer-Sized, Soluble, and Defect-Free. *Angewandte Chemie International Edition, 50*(11), 2540-2543.

Duling III, Irl N, & Duling, III. (2006). *Compact sources of ultrashort pulses* (Vol. 18): Cambridge University Press.

Eda, G., Lin, Y.Y., Mattevi, C., Yamaguchi, H., Chen, H.A., Chen, I., . . . Chhowalla, M. (2009). Blue photoluminescence from chemically derived graphene oxide. *Advanced Materials, 22*(4), 505-509.

Eda, Goki, Lin, Yun-Yue, Mattevi, Cecilia, Yamaguchi, Hisato, Chen, Hsin-An, Chen, I, . . . Chhowalla, Manish. (2010). Blue photoluminescence from chemically derived graphene oxide. *Advanced Materials, 22*(4), 505-509.

Eda, Goki, Mattevi, Cecilia, Yamaguchi, Hisato, Kim, HoKwon, & Chhowalla, Manish. (2009). Insulator to semimetal transition in graphene oxide. *The Journal of Physical Chemistry C, 113*(35), 15768-15771.

Einstein, Albert. (1917). On the quantum theory of radiation. *Phys. Z, 18*, 121-128.

Engelbrecht, Martin, Haxsen, Frithjof, Ruehl, Axel, Wandt, Dieter, & Kracht, Dietmar. (2008). Ultrafast thulium-doped fiber-oscillator with pulse energy of 4.3 nJ. *Optics letters, 33*(7), 690-692.

Essig, S, Marquardt, CW, Vijayaraghavan, A, Ganzhorn, M, Dehm, S, Hennrich, F, . . . Bonaccorso, F. (2010). Phonon-assisted electroluminescence from metallic carbon nanotubes and graphene. *Nano letters, 10*(5), 1589-1594.

Fabrikant, VA. (1940). The emission mechanism of a gas discharge. *Trudy (Proceedings) of VEI (the All-Soviet-Union Electro-Technical Institute), Electronic and Ion Devices, 41*, 236-296.

Fermann, M.E., Galvanauskas, A., & Sucha, G. (2002). *Ultrafast lasers: Technology and applications* (Vol. 80): CRC Press.

Fermann, M.E., Galvanauskas, A., Sucha, G., & Harter, D. (1997). Fiber-lasers for ultrafast optics. *Applied Physics B: Lasers and Optics, 65*(2), 259-275.

Fermann, ME, Andrejco, MJ, Silberberg, Y., & Stock, ML. (1993). Passive mode locking by using nonlinear polarization evolution in a polarization-maintaining erbium-doped fiber. *Optics letters, 18*(11), 894-896.

Ferrari, A. C., Meyer, J. C., Scardaci, V., Casiraghi, C., Lazzeri, M., Mauri, F., . . . Geim, A. K. (2006). Raman Spectrum of Graphene and Graphene Layers. *Physical Review Letters, 97*(18), 187401.

Fluck, R., Braun, B., Gini, E., Melchior, H., & Keller, U. (1997). Passively Q-switched 1.34- ?m Nd:YVO4 microchip laser with semiconductor saturable-absorber mirrors. *Optics Letters, 22*(13), 991-993. doi: 10.1364/OL.22.000991

Fluck, R., Weingarten, K. J., Moser, M., Zhang, G., & Keller, U. (1996). Diode-pumped passively mode-locked 1.3- ?m Nd:YVO4 and Nd:YLF lasers by use of semiconductor saturable absorbers. *Optics Letters, 21*(17), 1378-1380. doi: 10.1364/OL.21.001378

French, PMW. (1995). The generation of ultrashort laser pulses. *Reports on Progress in Physics, 58*(2), 169.

Gambling, WA. (2000). The rise and rise of optical fibers. *Selected Topics in Quantum Electronics, IEEE Journal of, 6*(6), 1084-1093.

Gao, Wei, Alemany, Lawrence B, Ci, Lijie, & Ajayan, Pulickel M. (2009). New insights into the structure and reduction of graphite oxide. *Nature Chemistry, 1*(5), 403-408.

Geim, A. K. (2009). Graphene: Status and Prospects. *Science, 324*(5934), 1530-1534. doi: 10.1126/science.1158877

Geim, A.K., & Novoselov, K.S. (2007). The rise of graphene. *Nature materials, 6*(3), 183-191.

Gokus, T., Nair, RR, Bonetti, A., Bohmler, M., Lombardo, A., Novoselov, KS, . . . Hartschuh, A. (2009). Making graphene luminescent by oxygen plasma treatment. *ACS nano, 3*(12), 3963-3968.

González, J., Guinea, F., & Vozmediano, MAH. (1996). Unconventional quasiparticle lifetime in graphite. *Physical review letters, 77*(17), 3589-3592.

Gordon, James P, Zeiger, Herbert J, & Townes, Charles H. (1955). The maser—new type of microwave amplifier, frequency standard, and spectrometer. *Physical Review, 99*(4), 1264.

Graf, D., Molitor, F., Ensslin, K., Stampfer, C., Jungen, A., Hierold, C., & Wirtz, L. (2007). Spatially resolved Raman spectroscopy of single-and few-layer graphene. *Nano letters, 7*(2), 238-242.

Grange, R, Rutz, A, Liverini, V, Haiml, M, Schon, S, & Keller, U. (2005). Nonlinear absorption edge properties of 1.3-μm GaInNAs saturable absorbers. *Applied Physics Letters, 87*(13), 132103-132103-132103.

Graphene Laboratories Inc. .). 2013, from https://graphene-supermarket.com/

Hall, R. N. (1963). Coherent light emission from p-n junctions. *Solid-State Electronics, 6*(5), 405-408. doi: http://dx.doi.org/10.1016/0038-1101(63)90024-8

Hamada, Noriaki, Sawada, Shin-ichi, & Oshiyama, Atsushi. (1992). New one-dimensional conductors: Graphitic microtubules. *Physical Review Letters, 68*(10), 1579.

Hasan, T., Sun, Z., Wang, F., Bonaccorso, F., Tan, P.H., Rozhin, A.G., & Ferrari, A.C. (2009). Nanotube–polymer composites for ultrafast photonics. *Advanced materials, 21*(38-39), 3874-3899.

Hasan, Tawfique, Sun, Zhipei, Wang, Fengqiu, Bonaccorso, Francesco, Tan, Ping Heng, Rozhin, Aleksey G., & Ferrari, Andrea C. (2009). Nanotube–Polymer Composites for Ultrafast Photonics. *Advanced Materials, 21*(38-39), 3874-3899. doi: 10.1002/adma.200901122

Hasegawa, Akira. (1984). Generation of a train of soliton pulses by induced modulational instability in optical fibers. *Optics letters, 9*(7), 288-290.

Haus, H. A., Fujimoto, J. G., & Ippen, E. P. (1991). Structures for additive pulse mode locking. *Journal of the Optical Society of America B, 8*(10), 2068-2076. doi: 10.1364/JOSAB.8.002068

Haus, Herman A. (2000). Mode-locking of lasers. *Selected Topics in Quantum Electronics, IEEE Journal of, 6*(6), 1173-1185.

He, Heyong, Klinowski, Jacek, Forster, Michael, & Lerf, Anton. (1998). A new structural model for graphite oxide. *Chemical Physics Letters, 287*(1), 53-56.

Hellwarth, RW. (1961). Advances in quantum electronics: Columbia Press, New York.

Hideur, Ammar, Chartier, Thierry, Brunel, Marc, Salhi, Mohamed, Özkul, Cafer, & Sanchez, François. (2001). Mode-lock, Q-switch and CW operation of an Yb-doped double-clad fiber ring laser. *Optics communications, 198*(1), 141-146.

Hunsperger, RobertG. (2009). Acousto-Optic Modulators *Integrated Optics* (pp. 201-220): Springer New York.

Ichida, M, Hamanaka, Y, Kataura, H, Achiba, Y, & Nakamura, A. (2002). Ultrafast relaxation dynamics of photoexcited states in semiconducting single-walled carbon nanotubes. *Physica B: Condensed Matter, 323*(1), 237-238.

Iii, IrI N. Duling. (1991). All-fiber ring soliton laser mode locked with a nonlinear mirror. *Opt. Lett., 16*(8), 539-541.

Iijima, S. (1991). Helical microtubules of graphitic carbon. *nature, 354*(6348), 56-58.

International, Opton Laser. (2013). Mode-Locking. Retrieved 29/12/2013, 2013, from http://www.optonlaser.com/spip.php?article51

Ippen, EP. (1994). Principles of passive mode locking. *Applied Physics B: Lasers and Optics, 58*(3), 159-170.

Islam, Mohammed N, Dijaili, SP, & Gordon, James P. (1988). Modulation-instability-based fiber interferometer switch near 1.5 μm. *Optics letters, 13*(6), 518-520.

Izawa, T, Kobayashi, S, Sudo, S, & Hanawa, F. (1977). *Continuous fabrication of high silica fibre preform', C1-1.* Paper presented at the International conference on integrated optics and optical-fibre communication.

Javan, A., Bennett, W. R., & Herriott, D. R. (1961). Population Inversion and Continuous Optical Maser Oscillation in a Gas Discharge Containing a He-Ne Mixture. *Physical Review Letters, 6*(3), 106-110.

Javan, Ali. (1957). Theory of a three-level maser. *Physical Review, 107*(6), 1579.

Jeong, HK, Jin, MH, So, KP, Lim, SC, & Lee, YH. (2009). Tailoring the characteristics of graphite oxides by different oxidation times. *Journal of Physics D: Applied Physics, 42*(6), 065418.

Jorio, A., Pimenta, MA, Souza Filho, AG, Saito, R., Dresselhaus, G., & Dresselhaus, MS. (2003). Characterizing carbon nanotube samples with resonance Raman scattering. *New Journal of Physics, 5*(1), 139.

Jung, ID, Kärtner, FX, Brovelli, LR, Kamp, M, & Keller, U. (1995). Experimental verification of soliton mode locking using only a slow saturable absorber. *Optics letters, 20*(18), 1892-1894.

Kampfrath, Tobias, Perfetti, Luca, Schapper, Florian, Frischkorn, Christian, & Wolf, Martin. (2005). Strongly coupled optical phonons in the ultrafast dynamics of the electronic energy and current relaxation in graphite. *Physical review letters, 95*(18), 187403.

Kao, KC, & Hockham, George A. (1966). Dielectric-fibre surface waveguides for optical frequencies. *Electrical Engineers, Proceedings of the Institution of, 113*(7), 1151-1158.

Kapron, F. P., Keck, D. B., & Maurer, R. D. (1970). Radiation losses in glass optical waveguides. *Applied Physics Letters, 17*(10), 423-425. doi: doi:http://dx.doi.org/10.1063/1.1653255

Kärtner, F. X., & Keller, U. (1995). Stabilization of solitonlike pulses with a slow saturable absorber. *Optics Letters, 20*(1), 16-18. doi: 10.1364/OL.20.000016

Kartner, FX, Jung, ID, & Keller, U. (1996). Soliton mode-locking with saturable absorbers. *Selected Topics in Quantum Electronics, IEEE Journal of, 2*(3), 540-556.

Kashiwagi, Ken, & Yamashita, Shinji. (2009). Deposition of carbon nanotubes around microfiber via evanascent light. *Opt. Express, 17*(20), 18364-18370.

Kashiwagi, Ken, Yamashita, Shinji, & Set, Sze Y. (2009). In-situ monitoring of optical deposition of carbon nanotubes onto fiber end. *Opt. Express, 17*(7), 5711-5715.

Kazaoui, S, Minami, N, Nalini, B, Kim, Y, Takada, N, & Hara, K. (2005). Near-infrared electroluminescent devices using single-wall carbon nanotubes thin flms. *Applied Physics Letters, 87*(21), 211914-211914-211913.

Keller, U. (2003). Recent developments in compact ultrafast lasers. *Nature, 424*(6950), 831-838.

Keller, U., Weingarten, K.J., Kartner, F.X., Kopf, D., Braun, B., Jung, I.D., . . . Aus der Au, J. (1996). Semiconductor saturable absorber mirrors (SESAM's) for femtosecond to nanosecond pulse generation in solid-state lasers. *Selected Topics in Quantum Electronics, IEEE Journal of, 2*(3), 435-453.

Keller, Ursula. (2004). Ultrafast solid-state lasers. *Progress in Optics, 46*, 1-115.

Kim, Keun Soo, Zhao, Yue, Jang, Houk, Lee, Sang Yoon, Kim, Jong Min, Kim, Kwang S, . . . Hong, Byung Hee. (2009). Large-scale pattern growth of graphene films for stretchable transparent electrodes. *Nature, 457*(7230), 706-710.

Kivistö, Samuli, Hakulinen, Tommi, Kaskela, Antti, Aitchison, Brad, Brown, David P., Nasibulin, Albert G., . . . Okhotnikov, Oleg G. (2009). Carbon nanotube films for ultrafast broadband technology. *Opt. Express, 17*(4), 2358-2363.

Koechner, Walter. (2006). Solid-State Laser Engineering (Springer Series in Optical Sciences).

Komarov, A., Leblond, H., & Sanchez, F. (2005). Theoretical analysis of the operating regime of a passively-mode-locked fiber laser through nonlinear polarization rotation. *Physical Review A, 72*(6), 063811.

Kopfermann, H, & Ladenburg, R. (1928). Experimental Proof ofNegative Dispersion.'. *Nature, 122*, 438-439.

Kramers, Hendrik Anthony. (1924). The law of dispersion and Bohr's theory of spectra. *Nature, 113*, 673-674.

Kuizenga, D, & Siegman, A. (1970a). FM and AM mode locking of the homogeneous laser-Part I: Theory. *Quantum Electronics, IEEE Journal of, 6*(11), 694-708.

Kuizenga, D, & Siegman, A. (1970b). FM and AM mode locking of the homogeneous laser-part II: experimental results in a Nd: YAG laser with internal FM modulation. *Quantum Electronics, IEEE Journal of, 6*(11), 709-715.

Kumar, Sunil, Anija, M., Kamaraju, N., Vasu, K. S., Subrahmanyam, K. S., Sood, A. K., & Rao, C. N. R. (2009). Femtosecond carrier dynamics and saturable absorption in graphene suspensions. *Applied Physics Letters, 95*(19), 191911-191913.

Kuppers, D, Lydtin, H, & Meijer, F. (1977). *Preparation methods for optical fibers applied in Philips research.* Paper presented at the Technical Digest, International Conference on Integrated Optics and Optical Fiber Communication, Tokyo.

Ladenburg, Rudolf. (1928). Untersuchungen über die anomale Dispersion angeregter Gase. *Zeitschrift für Physik, 48*(1-2), 15-25. doi: 10.1007/BF01351571

LaGasse, M. J., Liu-Wong, D., Fujimoto, J. G., & Haus, H. A. (1989). Ultrafast switching with a single-fiber interferometer. *Optics Letters, 14*(6), 311-313. doi: 10.1364/OL.14.000311

Lamb, Willis E, & Retherford, Robert C. (1947). Fine structure of the hydrogen atom by a microwave method. *Physical Review, 72*(3), 241-243.

Lasers, World of. (2014). Properties of lasers. Retrieved 4/3/2014, 2014, from http://www.worldoflasers.com/laserproperties.htm

Lazzeri, Michele, Piscanec, S., Mauri, Francesco, Ferrari, A. C., & Robertson, J. (2005). Electron Transport and Hot Phonons in Carbon Nanotubes. *Physical Review Letters, 95*(23), 236802.

Lee, J., Koo, J., Chang, Y.M., Debnath, P., Song, Y.W., & Lee, J.H. (2012). Experimental investigation on a Q-switched, mode-locked fiber laser based on the combination of active mode locking and passive Q switching. *JOSA B, 29*(6), 1479-1485.

Li, Xuesong, Cai, Weiwei, An, Jinho, Kim, Seyoung, Nah, Junghyo, Yang, Dongxing, . . . Tutuc, Emanuel. (2009). Large-area synthesis of high-quality and uniform graphene films on copper foils. *Science, 324*(5932), 1312-1314.

Lin, Yung-Hsiang, Yang, Chun-Yu, Liou, Jia-Hong, Yu, Chin-Ping, & Lin, Gong-Ru. (2013). Using graphene nano-particle embedded in photonic crystal fiber for evanescent wave mode-locking of fiber laser. *Optics Express, 21*(14), 16763-16776. doi: 10.1364/OE.21.016763

Liu, J., Wu, S., Yang, Q., Song, Y., Wang, Z., & Wang, P. (2011). *163 nJ graphene mode-locked Yb-doped fiber laser*.

Liu, Jiang, Xu, Jia, & Wang, Pu. (2012). Graphene-based passively Q-switched 2μm thulium-doped fiber laser. *Optics Communications, 285*(24), 5319-5322. doi: 10.1016/j.optcom.2012.07.063

Liu, Zhi-Bo, Zhao, Xin, Zhang, Xiao-Liang, Yan, Xiao-Qing, Wu, Ying-Peng, Chen, Yong-Sheng, & Tian, Jian-Guo. (2011). Ultrafast dynamics and nonlinear optical responses from sp2-and sp3-hybridized domains in graphene oxide. *The Journal of Physical Chemistry Letters, 2*(16), 1972-1977.

Liu, Zhuang, Robinson, Joshua T, Sun, Xiaoming, & Dai, Hongjie. (2008). PEGylated nanographene oxide for delivery of water-insoluble cancer drugs. *Journal of the American Chemical Society, 130*(33), 10876-10877.

Liverini, Valeria, Schon, S, Grange, Rachel, Haiml, Markus, Zeller, Simon Christian, & Keller, Ursula. (2004). Low-loss GaInNAs saturable absorber mode locking a 1.3-μm solid-state laser. *Applied physics letters, 84*(20), 4002-4004.

Loh, Kian Ping, Bao, Qiaoliang, Eda, Goki, & Chhowalla, Manish. (2010). Graphene oxide as a chemically tunable platform for optical applications. *Nat Chem, 2*(12), 1015-1024.

Lu, Jiong, Yang, Jia-xiang, Wang, Junzhong, Lim, Ailian, Wang, Shuai, & Loh, Kian Ping. (2009). One-Pot Synthesis of Fluorescent Carbon Nanoribbons, Nanoparticles, and Graphene by the Exfoliation of Graphite in Ionic Liquids. *ACS Nano, 3*(8), 2367-2375. doi: 10.1021/nn900546b

Luo, Z. Q., Wang, J. Z., Zhou, M., Xu, H. Y., Cai, Z. P., & Ye, C. C. (2012). Multiwavelength mode-locked erbium-doped fiber laser based on the interaction of graphene and fiber-taper evanescent field. *Laser Physics Letters, 9*(3), 229-233. doi: 10.1002/lapl.201110124

Luo, Z., Vora, P.M., Mele, E.J., Johnson, AT, & Kikkawa, J.M. (2009). Photoluminescence and band gap modulation in graphene oxide. *Applied physics letters, 94*(11), 111909-111909-111903.

Ma, Ying-Zhong, Hertel, Tobias, Vardeny, Zeev Valy, Fleming, Graham R, & Valkunas, Leonas. (2008). Ultrafast spectroscopy of carbon nanotubes *Carbon Nanotubes* (pp. 321-352): Springer.

Ma, Ying-Zhong, Stenger, Jens, Zimmermann, Jörg, Dexheimer, Susan L, Fleming, Graham R, Bachilo, Sergei M, . . . Weisman, R Bruce. (2004). *Ultrafast carrier dynamics in single-walled carbon nanotubes probed by femtosecond spectroscopy.* Paper presented at the International Quantum Electronics Conference.

Maiman, Theodore H. (1960). Stimulated optical radiation in ruby.

Maldonado, Theresa A. (1995). Electro-optic modulators. *Handbook of optics, 2*, 13.11-13.35.

Martinez, Amos, Fuse, Kazuyuki, Xu, Bo, & Yamashita, Shinji. (2010). Optical deposition of graphene and carbon nanotubes in a fiber ferrule for passive mode-locked lasing. *Optics Express, 18*(22), 23054-23061.

Martinez, Amos, Fuse, Kazuyuki, & Yamashita, Shinji. (2011). Mechanical exfoliation of graphene for the passive mode-locking of fiber lasers. *Applied Physics Letters, 99*(12), 121107. doi: 10.1063/1.3641419

McClung, FJ, & Hellwarth, RW. (1962). Giant Optical Pulsations from Ruby. *Applied Optics, 1*(101), 103-105.

Milonni, Peter W., & Eberly, Joseph H. (2010). *Laser Physics (2nd Edition)*. Hoboken, NJ, USA: Wiley.

Misewich, JA, Martel, R, Avouris, Ph, Tsang, JC, Heinze, S, & Tersoff, J. (2003). Electrically induced optical emission from a carbon nanotube FET. *Science, 300*(5620), 783-786.

Moghaddam, M. R. A., Harun, S. W., Akbari, R., & Ahmad, H. (2011). Stable mode-locked fiber laser using 49 cm long bismuth oxide based erbium doped fiber and slow saturable absorber. *Laser Physics, 21*(5), 913-918. doi: 10.1134/s1054660x11090209

Nair, RR, Blake, P., Grigorenko, AN, Novoselov, KS, Booth, TJ, Stauber, T., . . . Geim, AK. (2008). Fine structure constant defines visual transparency of graphene. *Science, 320*(5881), 1308-1308.

Nelson, LE, Ippen, EP, & Haus, HA. (1995). Broadly tunable sub-500 fs pulses from an additive-pulse mode-locked thulium-doped fiber ring laser. *Applied physics letters, 67*(1), 19-21.

Nelson, LE, Jones, DJ, Tamura, K, Haus, HA, & Ippen, EP. (1997). Ultrashort-pulse fiber ring lasers. *Applied Physics B: Lasers and Optics, 65*(2), 277-294.

Neto, AH Castro, Guinea, F, Peres, NMR, Novoselov, Kostya S, & Geim, Andre K. (2009). The electronic properties of graphene. *Reviews of modern physics, 81*(1), 109.

Nicholson, JW, Windeler, RS, & DiGiovanni, DJ. (2007). Optically driven deposition of single-walled carbon-nanotube saturable absorbers on optical fiber end-faces. *Optics Express, 15*(15), 9176-9183.

Novoselov, KS, Geim, AK, Morozov, SV, Jiang, D., Zhang, Y., Dubonos, SV, . . . Firsov, AA. (2004). Electric field effect in atomically thin carbon films. *Science, 306*(5696), 666-669.

Ohara, S., Hasegawa, T., & Sugimoto, N. (2005). *Boron co-doped Bi2O3-based Erbium doped fiber for Short Pulse Amplification*.

Okhotnikov, O., Grudinin, A., & Pessa, M. (2004). Ultra-fast fibre laser systems based on SESAM technology: new horizons and applications. *New journal of physics, 6*(1), 177.

Okhotnikov, OG, Jouhti, T, Konttinen, J, Karirinne, S, & Pessa, M. (2003). 1.5-μm monolithic GaInNAs semiconductor saturable-absorber mode locking of an erbium fiber laser. *Optics letters, 28*(5), 364-366.

Pan, Dengyu, Zhang, Jingchun, Li, Zhen, & Wu, Minghong. (2010). Hydrothermal Route for Cutting Graphene Sheets into Blue-Luminescent Graphene Quantum Dots. *Advanced Materials, 22*(6), 734-738.

Partoens, B., & Peeters, F. (2006). From graphene to graphite: Electronic structure around the K point. *Physical Review B, 74*(7). doi: 10.1103/PhysRevB.74.075404

Paschotta, Dr. Rüdiger. (2013). Haus Master Equation. Retrieved 31/12/2013, 2013, from http://www.rp-photonics.com/haus_master_equation.html?s=ak

Paschotta, R., Häring, R., Gini, E., Melchior, H., Keller, U., Offerhaus, H. L., & Richardson, D. J. (1999). Passively Q-switched 0.1-mJ fiber laser system at 1.53 ?m. *Optics Letters, 24*(6), 388-390. doi: 10.1364/OL.24.000388

Paschotta, R., & Keller, U. (2001). Passive mode locking with slow saturable absorbers. *Applied Physics B: Lasers and Optics, 73*(7), 653-662. doi: 10.1007/s003400100726

Patel, C. K. N. (1965). CW HIGH POWER N2–CO2 LASER. *Applied Physics Letters, 7*(1), 15-17. doi: doi:http://dx.doi.org/10.1063/1.1754233

Popa, D, Sun, Z, Hasan, T, Torrisi, F, Wang, F, & Ferrari, AC. (2010). Graphene Q-switched, tunable fiber laser. *arXiv preprint arXiv:1011.0115*.

Popa, D., Sun, Z., Hasan, T., Torrisi, F., Wang, F., & Ferrari, A. C. (2011). Graphene Q-switched, tunable fiber laser. *Applied Physics Letters, 98*(7), 073106-073103.

Popov, Valentin N. (2004). Carbon nanotubes: properties and application. *Materials Science and Engineering: R: Reports, 43*(3), 61-102.

Reibold, M, Paufler, P, Levin, AA, Kochmann, W, Pätzke, N, & Meyer, DC. (2006). Materials: Carbon nanotubes in an ancient Damascus sabre. *Nature, 444*(7117), 286-286.

Reich, S., Thomsen, C., & Maultzsch, J. (2008). *Carbon Nanotubes: Basic Concepts and Physical Properties*: Wiley.

Renk, Karl F. (2012). Basics of laser physics. *Basics of Laser Physics: For Students of Science and Engineering, Graduate Texts in Physics. ISBN 978-3-642-23564-1. Springer-Verlag Berlin Heidelberg, 2012, 1*.

Richardson, DJ, Laming, RI, Payne, DN, Phillips, MW, & Matsas, VJ. (1991). 320 fs soliton generation with passively mode-locked erbium fibre laser. *Electronics letters, 27*(9), 730-732.

Rozhin, A.G., Sakakibara, Y., Namiki, S., Tokumoto, M., Kataura, H., & Achiba, Y. (2006). Sub-200-fs pulsed erbium-doped fiber laser using a carbon nanotube-

polyvinylalcohol mode locker. *Applied physics letters, 88*(5), 051118-051118-051113.

Rutz, A, Grange, R, Liverini, V, Haiml, M, Schon, S, & Keller, U. (2005). 1.5 μm GaInNAs semiconductor saturable absorber for passively modelocked solid-state lasers. *Electronics Letters, 41*(6), 321-323.

Saidin, N., Zen, D. I. M., Hamida, B. A., Khan, S., Ahmad, H., Dimyati, K., & Harun, S. W. (2013). A Q -switched thulium-doped fiber laser with a graphene thin film based saturable absorber. *Laser Physics, 23*(11), 115102.

Saito, R. (1998). Physical properties of carbon nanotubes (paperback).

Saito, Riichiro, Fujita, Mitsutaka, Dresselhaus, Gene, & Dresselhaus, Mildred S. (1992). Electronic structure of graphene tubules based on C_ {60}. *Physical Review B, 46*(3), 1804.

Sakakibara, Youichi, Rozhin, Aleksey G., Kataura, Hiromichi, Achiba, Yohji, & Tokumoto, Madoka. (2005). Carbon Nanotube-Poly(vinylalcohol) Nanocomposite Film Devices: Applications for Femtosecond Fiber Laser Mode Lockers and Optical Amplifier Noise Suppressors. *Japanese Journal of Applied Physics, 44*(4A), 1621-1625. doi: 10.1143/jjap.44.1621

Sardesai, H. P., Chang, C. C., & Weiner, A. M. (1998). A femtosecond code-division multiple-access communication system test bed. *Lightwave Technology, Journal of, 16*(11), 1953-1964. doi: 10.1109/50.730356

Scardaci, V., Rozhin, AG, Hennrich, F., Milne, WI, & Ferrari, AC. (2007). Carbon nanotube–polymer composites for photonic devices. *Physica E: Low-dimensional Systems and Nanostructures, 37*(1), 115-118.

Scardaci, Vittorio, Sun, Zhipei, Wang, Frank, Rozhin, Aleksey G., Hasan, Tawfique, Hennrich, Frank, . . . Ferrari, Andrea C. (2008). Carbon Nanotube Polycarbonate Composites for Ultrafast Lasers. *Advanced Materials, 20*(21), 4040-4043. doi: 10.1002/adma.200800935

Schön, S, Rutz, A, Liverini, V, Grange, R, Haiml, M, Zeller, SC, & Keller, U. (2005). Dilute nitride absorbers in passive devices for mode locking of solid-state lasers. *Journal of crystal growth, 278*(1), 239-243.

Segal, Michael. (2009). Selling graphene by the ton. *Nat Nano, 4*(10), 612-614.

Seong, NH, & Kim, D.Y. (2002). A new figure-eight fiber laser based on a dispersion-imbalanced nonlinear optical loop mirror with lumped dispersive elements. *Photonics Technology Letters, IEEE, 14*(4), 459-461.

Set, S.Y., Jablonski, M., Kotake, T., Furuki, K., Tojo, M., Tanaka, Y., . . . Kikuchi, K. (2003). *Low nonlinearity Bismuth oxide-based Erbium-doped fiber amplifiers for short pulse amplification*.

Set, S.Y., Yaguchi, H., Jablonski, M., Tanaka, Y., Sakakibara, Y., Rozhin, A.G., . . . Kikuchi, K. (2003). *A noise suppressing saturable absorber at 1550nm based on carbon nanotube technology*. Paper presented at the Optical Fiber Communication Conference.

Set, S.Y., Yaguchi, H., Tanaka, Y., & Jablonski, M. (2004a). Laser mode locking using a saturable absorber incorporating carbon nanotubes. *Journal of lightwave technology, 22*(1), 51.

Set, S.Y., Yaguchi, H., Tanaka, Y., & Jablonski, M. (2004b). Ultrafast fiber pulsed lasers incorporating carbon nanotubes. *Selected Topics in Quantum Electronics, IEEE Journal of, 10*(1), 137-146.

Set, SY, Yaguchi, H., Tanaka, Y., Jablonski, M., Sakakibara, Y., Tokomuto, M., . . . Kikuchi, K. (2003). *A dual-regime mode-locked/Q-switched laser using a saturable absorber incorporating carbon nanotubes (SAINT).* Paper presented at the Lasers and Electro-Optics, 2003. CLEO'03. Conference on.

Set, Sze Y, Yaguchi, Hiroshi, Tanaka, Yuichi, Jablonski, Mark, Sakakibara, Yoichi, Rozhin, Alex, . . . Kikuchi, Kazuro. (2003). *Mode-locked fiber lasers based on a saturable absorber incorporating carbon nanotubes.* Paper presented at the Optical Fiber Communications Conference, 2003. OFC 2003.

Shah, Jagdeep. (1999). *Ultrafast spectroscopy of semiconductors and semiconductor nanostructures* (Vol. 115): Springer.

Sharp, RC, Spock, DE, Pan, N, & Elliot, J. (1996). 190-fs passively mode-locked thulium fiber laser with a low threshold. *Optics letters, 21*(12), 881-883.

Shen, Yan, Yang, Songbo, Zhou, Peng, Sun, Qingqing, Wang, Pengfei, Wan, Li, . . . Zhang, David Wei. (2013). Evolution of the band-gap and optical properties of graphene oxide with controllable reduction level. *Carbon, 62*(0), 157-164. doi: http://dx.doi.org/10.1016/j.carbon.2013.06.007

Shioda, Tatsutoshi, Mori, Takayoshi, Sugimoto, Tatsuya, Tanaka, Yosuke, & Kurokawa, Takashi. (2009). High-resolution spectroscopy based on optical phase modulator and optical frequency comb. *Optics Communications, 282*(14), 2909-2912. doi: http://dx.doi.org/10.1016/j.optcom.2009.03.065

Sobon, Grzegorz, Sotor, Jaroslaw, Jagiello, Joanna, Kozinski, Rafal, Zdrojek, Mariusz, Holdynski, Marcin, . . . Abramski, Krzysztof M. (2012). Graphene Oxide vs. Reduced Graphene Oxide as saturable absorbers for Er-doped passively mode-locked fiber laser. *Optics Express, 20*(17), 19463-19473.

Song, Yong-Won, Jang, Sung-Yeon, Han, Won-Suk, & Bae, Mi-Kyung. (2010). Graphene mode-lockers for fiber lasers functioned with evanescent field interaction. *Applied Physics Letters, 96*(5), 051122-051123.

Song, Yong-Won, Morimune, Keiyo, Set, Sze Y., & Yamashita, Shinji. (2007). Polarization insensitive all-fiber mode-lockers functioned by carbon nanotubes deposited onto tapered fibers. *Applied Physics Letters, 90*(2), 021101-021103.

Spuhler, G. J., Golding, P. S., Krainer, L., Kilburn, I. J., Crosby, P. A., Brownell, M., . . . Keller, U. (2003). Multi-wavelength source with 25 GHz channel spacing tunable over C-band. *Electronics Letters, 39*(10), 778-780. doi: 10.1049/el:20030501

Spühler, GJ, Paschotta, R, Fluck, R, Braun, B, Moser, M, Zhang, G, . . . Keller, U. (1999). Experimentally confirmed design guidelines for passively Q-switched microchip lasers using semiconductor saturable absorbers. *JOSA B, 16*(3), 376-388.

Stetser, DA, & Demaria, AJ. (1966). Optical Spectra of Ultrashort Optical Pulses Generated by Mode-Locked GLASS: Nd Lasers. *Applied Physics Letters, 9*, 118-120.

Stewart, Derek A, & Mkhoyan, K Andre. (2012). Graphene Oxide: Synthesis, Characterization, Electronic Structure, and Applications *Graphene Nanoelectronics* (pp. 435-464): Springer.

Stöhr, Rainer J., Kolesov, Roman, Pflaum, Jens, & Wrachtrup, Jörg. (2010). Fluorescence of laser-created electron-hole plasma in graphene. *Physical Review B, 82*(12), 121408.

Stolen, RH, Botineau, J, & Ashkin, A. (1982). Intensity discrimination of optical pulses with birefringent fibers. *Optics Letters, 7*(10), 512-514.

Subrahmanyam, KS, Kumar, Prashant, Nag, Angshuman, & Rao, CNR. (2010). Blue light emitting graphene-based materials and their use in generating white light. *Solid State Communications, 150*(37), 1774-1777.

Sugimoto, Naoki. (2008). Erbium doped fiber and highly non-linear fiber based on bismuth oxide glasses. *Journal of Non-Crystalline Solids, 354*(12), 1205-1210.

Sun, Xiaoming, Liu, Zhuang, Welsher, Kevin, Robinson, Joshua Tucker, Goodwin, Andrew, Zaric, Sasa, & Dai, Hongjie. (2008). Nano-graphene oxide for cellular imaging and drug delivery. *Nano research, 1*(3), 203-212.

Sun, Z., Hasan, T., & Ferrari, AC. (2012). Ultrafast lasers mode-locked by nanotubes and graphene. *Physica-Section E, 44*(6), 1082.

Sun, Z., Hasan, T., Torrisi, F., Popa, D., Privitera, G., Wang, F., . . . Ferrari, A.C. (2010). Graphene mode-locked ultrafast laser. *Acs Nano, 4*(2), 803-810.

Sun, Zhipei, Popa, Daniel, Hasan, Tawfique, Torrisi, Felice, Wang, Fengqiu, Kelleher, Edmund J. R., . . . Ferrari, Andrea C. (2010). A stable, wideband tunable, near transform-limited, graphene-mode-locked, ultrafast laser. *Nano Research, 3*(9), 653-660. doi: 10.1007/s12274-010-0026-4

Sun, Zhipei, Popa, Daniel, Hasan, Tawfique, Torrisi, Felice, Wang, Fengqiu, Kelleher, EdmundJ R., . . . Ferrari, AndreaC. (2010). A stable, wideband tunable, near

transform-limited, graphene-mode-locked, ultrafast laser. *Nano Research, 3*(9), 653-660. doi: 10.1007/s12274-010-0026-4

Svelto, Orazio, & Hanna, David C. (1976). *Principles of lasers*: Springer.

Tamura, K, Haus, HA, & Ippen, EP. (1992). Self-starting additive pulse mode-locked erbium fibre ring laser. *Electronics Letters, 28*(24), 2226-2228.

Tamura, K, Jacobson, J, Ippen, EP, Haus, HA, & Fujimoto, JG. (1993). Unidirectional ring resonators for self-starting passively mode-locked lasers. *Optics letters, 18*(3), 220-222.

Tang, D. Y., Zhao, L. M., Zhao, B., & Liu, A. Q. (2005). Mechanism of multisoliton formation and soliton energy quantization in passively mode-locked fiber lasers. *Physical Review A, 72*(4), 043816.

Tang, DY, Zhao, LM, & Lin, F. (2005). Numerical studies of routes to chaos in passively mode-locked fiber soliton ring lasers with dispersion-managed cavity. *EPL (Europhysics Letters), 71*(1), 56.

Tatsuura, Satoshi, Furuki, Makoto, Sato, Yasuhiro, Iwasa, Izumi, Tian, MINQUAN, & Mitsu, Hiroyuki. (2003). Semiconductor carbon nanotubes as ultrafast switching materials for optical telecommunications. *Advanced Materials, 15*(6), 534-537.

Träger, Frank. (2007). *Springer handbook of lasers and optics*: Springer.

Travers, JC, Morgenweg, J., Obraztsova, ED, Chernov, AI, Kelleher, EJR, & Popov, SV. (2011). Using the E22 transition of carbon nanotubes for fiber laser mode-locking. *Laser Physics Letters, 8*(2), 144-149.

Tsuchiya, Takashi, Terabe, Kazuya, & Aono, Masakazu. (2013). In Situ and Non-volatile Bandgap Tuning of Multilayer Graphene Oxide in an All-Solid-State Electric Double-Layer Transistor. *Advanced Materials*.

Uchida, S., Martinez, A., Song, Y.W., Ishigure, T., & Yamashita, S. (2009). Carbon nanotube-doped polymer optical fiber. *Optics letters, 34*(20), 3077-3079.

Udem, Th, Holzwarth, R., & Hansch, T. W. (2002). Optical frequency metrology. *Nature, 416*(6877), 233-237.

Wang, Fengqiu, Torrisi, Felice, Jiang, Zhe, Popa, Daniel, Hasan, Tawfique, Sun, Zhipei, . . . Ferrari, Andrea C. (2012). *Graphene passively Q-switched two-micron fiber lasers.* Paper presented at the CLEO: Science and Innovations.

Wang, Jinzhang, Luo, Zhengqian, Zhou, Min, Ye, Chenchun, Fu, Hongyan, Cai, Zhiping, . . . Qi, Wei. (2012). Evanescent-light deposition of graphene onto tapered fibers for passive Q-switch and mode-locker. *Photonics Journal, IEEE, 4*(5), 1295-1305.

Wang, QingQing, Chen, Tong, Zhang, Botao, Li, Mingshan, Lu, Yongfeng, & Chen, Kevin P. (2013). All-fiber passively mode-locked thulium-doped fiber ring laser using

optically deposited graphene saturable absorbers. *Applied Physics Letters, 102*(13), -. doi: doi:http://dx.doi.org/10.1063/1.4800036

Warner, Jamie H, Schaffel, Franziska, Rummeli, Mark, & Bachmatiuk, Alicja. (2012). *Graphene: Fundamentals and emergent applications*: Access Online via Elsevier.

Wei, Li, Zhou, Da-Peng, Fan, Helen Y, & Liu, Wing-Ki. (2012). Graphene-based-switched erbium-doped fiber laser with wide pulse-repetition-rate range. *Photonics Technology Letters, IEEE, 24*(4), 309-311.

Welford, D. (2003). Passively Q-switched lasers. *Circuits and Devices Magazine, IEEE, 19*(4), 31-36.

Wilder, Jeroen WG, Venema, Liesbeth C, Rinzler, Andrew G, Smalley, Richard E, & Dekker, Cees. (1998). Electronic structure of atomically resolved carbon nanotubes. *Nature, 391*(6662), 59-62.

Winzer, Torben, Knorr, Andreas, Mittendorff, Martin, Winnerl, Stephan, Lien, Miao-Bin, Sun, Dong, . . . Malic, Ermin. (2012a). Absorption saturation in optically excited graphene. *Applied Physics Letters, 101*(22), 221115.

Winzer, Torben, Knorr, Andreas, Mittendorff, Martin, Winnerl, Stephan, Lien, Miao-Bin, Sun, Dong, . . . Malic, Ermin. (2012b). Absorption saturation in optically excited graphene. *Applied Physics Letters, 101*(22), 221115-221115-221114.

Xing, Guichuan, Guo, Hongchen, Zhang, Xinhai, Sum, Tze Chien, & Huan, Cheng Hon Alfred. (2010). The Physics of ultrafast saturable absorption in graphene. *Optics Express, 18*(5), 4564-4573.

Xu, J., Wu, S., Liu, J., Wang, Q., Yang, Q.H., & Wang, P. (2012). Nanosecond-pulsed erbium-doped fiber lasers with graphene saturable absorber. *Optics Communications*.

Xu, Jia, Liu, Jiang, Wu, Sida, Yang, Quan-Hong, & Wang, Pu. (2012). Graphene oxide mode-locked femtosecond erbium-doped fiber lasers. *Optics Express, 20*(14), 15474-15480.

Xu, Zhihua, Wu, Yue, Hu, Bin, Ivanov, Ilia N, & Geohegan, David B. (2005). Carbon nanotube effects on electroluminescence and photovoltaic response in conjugated polymers. *Applied Physics Letters, 87*(26), 263118-263118-263113.

Yamamoto, Y., Yoshida, E., Tamura, K. R., Yonenaga, K., & Nakazawa, M. (2000). 640-Gbit/s optical TDM transmission over 92 km through a dispersion-managed fiber consisting of single-mode fiber and "reverse dispersion fiber". *Photonics Technology Letters, IEEE, 12*(3), 353-355. doi: 10.1109/68.826938

Yamashita, S. (2012). A Tutorial on Nonlinear Photonic Applications of Carbon Nanotube and Graphene. *Lightwave Technology, Journal of, 30*(4), 427-447.

Yamashita, S., Inoue, Y., Maruyama, S., Murakami, Y., Yaguchi, H., Jablonski, M., & Set, SY. (2004). Saturable absorbers incorporating carbon nanotubes directly synthesized

onto substrates and fibers and their application to mode-locked fiber lasers. *Optics letters, 29*(14), 1581-1583.

Yamashita, Shinji, Inoue, Yusuke, Maruyama, Shigeo, Murakami, Youichi, Yaguchi, Hiroshi, Kotake, Tomoharu, & Set, Sze Y. (2006). Mode-Locked Fiber Lasers Using Adjustable Saturable Absorption in Vertically Aligned Carbon Nanotubes. *Japanese Journal of Applied Physics, 45*(1), L17-L19. doi: 10.1143/jjap.45.l17

Yang, Dongxing, Velamakanni, Aruna, Bozoklu, Gülay, Park, Sungjin, Stoller, Meryl, Piner, Richard D, . . . Ventrice Jr, Carl A. (2009). Chemical analysis of graphene oxide films after heat and chemical treatments by X-ray photoelectron and micro-Raman spectroscopy. *Carbon, 47*(1), 145-152.

Yoshitomi, Dai, Kobayashi, Yohei, Takada, Hideyuki, Kakehata, Masayuki, & Torizuka, Kenji. (2005). 100-attosecond timing jitter between two-color mode-locked lasers by active-passive hybrid synchronization. *Optics letters, 30*(11), 1408-1410.

Zayhowski, J. J., & Dill Iii, C. (1994). Diode-pumped passively Q-switched picosecond microchip lasers. *Opt. Lett., 19*(18), 1427-1429.

Zayhowski, J. J., & Kelley, P. L. (1991). Optimization of <e1>Q</e1>-switched lasers. *Quantum Electronics, IEEE Journal of, 27*(9), 2220-2225. doi: 10.1109/3.135181

Zayhowski, JJ, & Kelley, PL. (1991). Optimization of Q-switched lasers. *Quantum Electronics, IEEE Journal of, 27*(9), 2220-2225.

Zeller, Simon C, Krainer, Lukas, Spühler, Gabriel J, Paschotta, Rüdiger, Golling, Matthias, Ebling, D, . . . Keller, U. (2004). Passively modelocked 50 GHz Er: Yb: glass laser. *Electronics Letters, 40*(14), 875-877.

Zhang, H, Tang, DY, Zhao, LM, Bao, QL, Loh, KP, Lin, B, & Tjin, SC. (2010). Compact graphene mode-locked wavelength-tunable erbium-doped fiber lasers: from all anomalous dispersion to all normal dispersion. *Laser Physics Letters, 7*(8), 591-596.

Zhang, Han, Tang, Dingyuan, Knize, RJ, Zhao, Luming, Bao, Qiaoliang, & Loh, Kian Ping. (2010). Graphene mode locked, wavelength-tunable, dissipative soliton fiber laser. *Applied Physics Letters, 96*(11), 111112-111112-111113.

Zhang, LQ, Zhuo, Z, Wang, JX, & Wang, YZ. (2012). Passively Q-switched fiber laser based on graphene saturable absorber. *Laser Physics, 22*(2), 433-436.

Zhu, Yanwu, Murali, Shanthi, Cai, Weiwei, Li, Xuesong, Suk, Ji Won, Potts, Jeffrey R, & Ruoff, Rodney S. (2010). Graphene and graphene oxide: synthesis, properties, and applications. *Advanced materials, 22*(35), 3906-3924.

APPENDIX

A selection of published works are attached in this section.

Quantum Electronics Letters

Soliton Mode-Locked Erbium-Doped Fiber Laser Using Non-Conductive Graphene Oxide Paper

Mohd Afiq Ismail, Harith Ahmad, and Sulaiman Wadi Harun

***Abstract*— A femtosecond mode-locked soliton erbium-doped fiber laser (EDFL) is demonstrated using a commercially available nonconductive graphene oxide paper as a saturable absorber. The paper that is sandwiched between two fiber ferrules acts as a mode-locker. The EDFL generates a soliton mode-locked pulse train with a repetition rate of 15.62 MHz and pulsewidth of 680 fs. It is observed that the fiber laser has a low pulsing threshold as well as low damage threshold. The pulse energy and peak power are 0.0085 nJ and 11.85 W, respectively. The easy fabrication of graphene oxide paper should promote its potential application in ultrafast photonics.**

***Index Terms*— Fiber lasers, laser mode locking, nanophotonics, optical pulses, optical solitions, ring lasers, ultrafast optics.**

I. Introduction

GRAPHENE is an atomic-thin nano-scale material, which has unique electrical and optical properties that opens a new field of research in solid state physics and material science [1]. It also exhibits linear optical absorption and saturable absorption properties, which are useful in generating ultra-short laser pulses [2]. The linear dispersion of the Dirac electrons in graphene promises broadband applications while its saturable absorption property is the result of Pauli blocking [3]. At high intensity, the photo-generated carriers increase in concentration and cause the states near the edge of the conduction and valence bands to fill, thus, blocking further absorption. Band filling occurs because no two electrons can fill the same state. Consequently, saturable absorption is reached due to this Pauli blocking process [4]. Moreover, the relaxation of carriers in a single layer graphene is ultrafast (200 fs) [5]. Other papers have included other factors that enable graphene to become an excellent saturable absorber [6], [7].

Graphite oxide is a compound that is composed of carbon, hydrogen and oxygen in variable ratios. It has attracted much attention recently as a cost-effective and large-scale production route (oxidation of graphite followed by reduction of graphene oxide platelets obtained by exfoliation) of graphene [8]. A graphene paper is prepared by mixing graphite oxide in water. The oxygen atoms of graphite oxide repel water molecules, thus, undergoing complete exfoliation in water, producing colloidal suspensions of almost entirely individual graphene oxide sheets. After filtering the exfoliated mixture using a membrane, these graphene oxide sheets could be fashioned into paper-like material under a directional flow. A free-standing graphene oxide paper is obtained after drying. By changing the oxygen amount in the layers, the material can be an electrical insulator, semi-conductor or conductor. This material is uniform and dark brown in colour. [9].

Using graphene saturable absorber for producing Q-switched and mode-locked fiber lasers has been demonstrated in many literatures [10]–[17]. For instance, in 2012, Xu et al. [18] demonstrated a mode-locked femtosecond erbium-doped fiber lasers (EDFLs) using graphene oxide as saturable absorber. A broadband mirror was immersed into a graphene oxide hydrosol. After 48 hour, a thin graphene membrane was formed on top of the broadband reflective mirror. Sobon et al. [19] compared the performances of graphene oxide and reduced graphene oxide as saturable absorber. The saturable absorbers were placed on fused silica substrate and inserted between two collimating gradient index (GRIN) lenses. In this letter, a soliton mode-locked Erbium-doped fiber laser (EDFL) is demonstrated using a commercially available graphene oxide (GO) paper as a saturable absorber (SA) for the first time. The SA is constructed by sandwiching the graphene oxide paper between two fiber connectors.

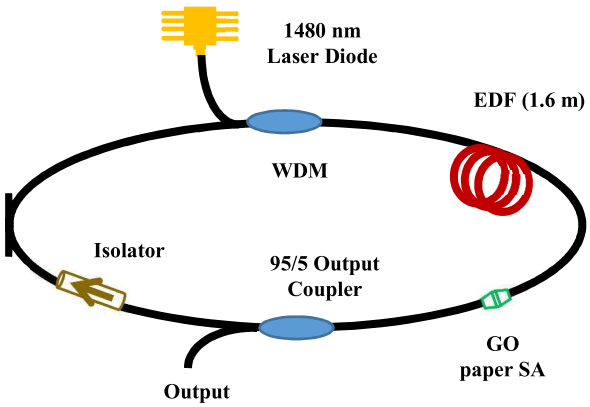

Fig. 1. Experimental setup of the proposed soliton EDFL based on GO paper SA.

II. Experiment

The schematic of the proposed mode-locked EDFL is shown in Fig. 1. It was constructed using a simple ring cavity, in which a 1.6 m long Erbium-doped fiber (EDF) with an Erbium ion concentration of 2000 ppm was used for the active medium and the GO paper based SA was used as a mode-locker. The EDF used has numerical aperture of 0.24, cut off wavelength of 930 nm and 24 dB/m absorption at 980 nm. It was forward pumped by a 1480 nm laser diode via a 1480/1550 nm wavelength division multiplexer (WDM). The polarization independent isolator was used to ensure unidirectional light propagation in the cavity and thus facilitate self-starting laser [20]. The laser output was obtained via a 95/5 output coupler located between the isolator and SA, which channeled out about 5% of the oscillating light from the ring cavity. The output

Manuscript received October 3, 2013; revised November 25, 2013; accepted December 3, 2013. Date of publication December 17, 2013; date of current version December 31, 2013. This work was supported in part by University Malaya Research under Grants RP008C-13AET and RU002/2013 and in part by High Impact Research under Grant HIR000009-16001.

M. A. Ismail is with the Department of Electrical Engineering, Faculty of Engineering, University of Malaya, Kuala Lumpur 50603, Malaysia (e-mail: afiq.ismail@siswa.um.edu.my).

H. Ahmad is with the Photonics Research Center, University of Malaya, Kuala Lumpur 50603, Malaysia (e-mail: harith@yahoo.com).

S. W. Harun is with the Department of Electrical Engineering, Faculty of Engineering, University of Malaya, Kuala Lumpur 50603, Malaysia, and also with the Photonics Research Center, University of Malaya, Kuala Lumpur 50603, Malaysia (e-mail: swharun@um.edu.my).

Color versions of one or more of the figures in this letter are available online at http://ieeexplore.ieee.org.

Digital Object Identifier 10.1109/JQE.2013.2295199

0018-9197 © 2013 IEEE. Personal use is permitted, but republication/redistribution requires IEEE permission.
See http://www.ieee.org/publications_standards/publications/rights/index.html for more information.

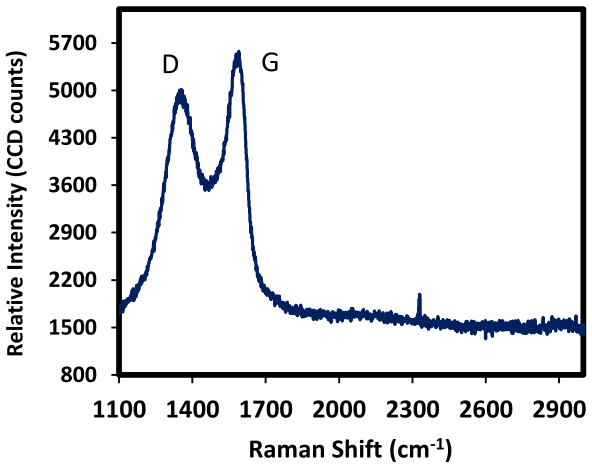

Fig. 2. Raman spectrum of the GO paper.

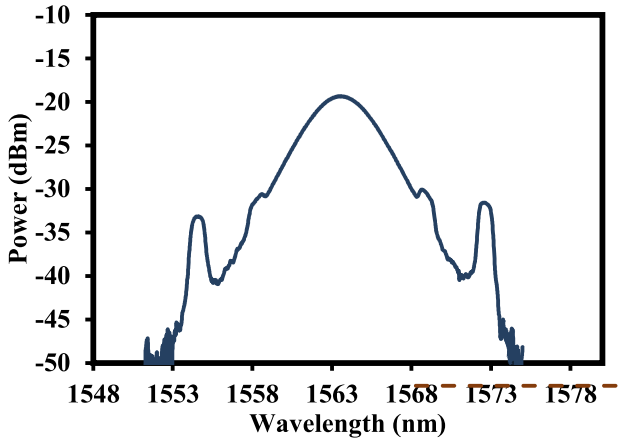

Fig. 3. Spectral characteristic of mode-locked fiber laser using GO paper.

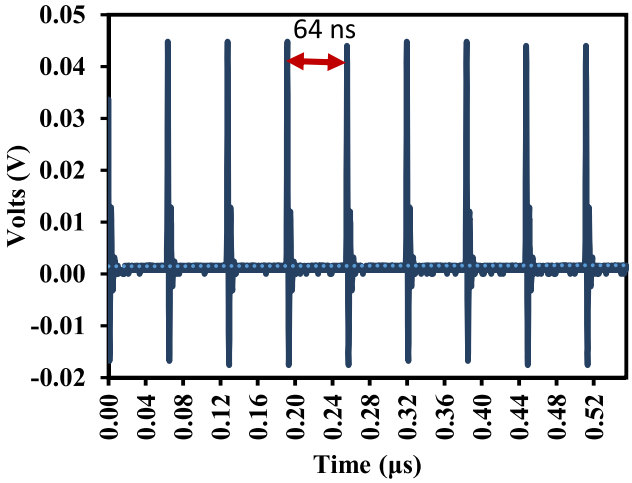

Fig. 4. Mode-locked pulse train with cavity round-trip time of 64 ns, corresponding to a pulse repetition rate 15.6 MHz.

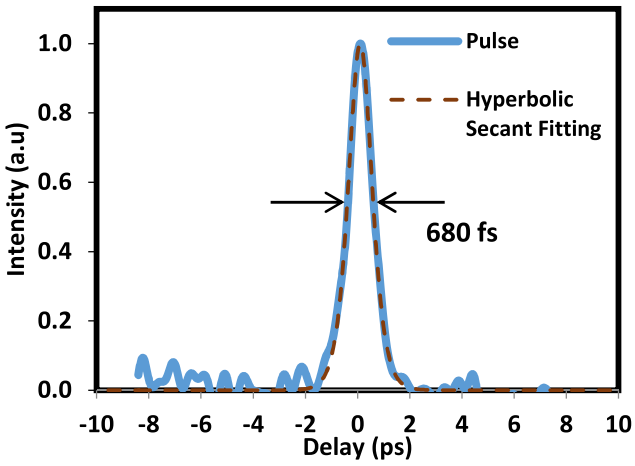

Fig. 5. Autocorrelation traces of the experimental data (solid curves) and $sech^2$–shaped fit (dashed curves).

was analyzed by using an optical spectrum analyzer (OSA) with a resolution of 0.07 nm and a 350 MHz oscilloscope with 6 GHz bandwidth light wave detector. The pulse width of the output laser was measured using an auto-correlator. All components used in our setup were polarization independent, i.e. they support any light polarization. No polarization controller (PC) was included in the laser cavity as we had observed earlier that a PC did not improve our pulse stability. There was no significant pulse jitter observed through the oscilloscope during the experiment. The lasing threshold was approximately 8.3 mW.

The SA was fabricated by cutting a small piece (2×2 mm^2) of a commercially non-conductive graphene oxide paper [21] and sandwiching it between two FC/PC fiber connectors, after depositing index-matching gel onto the fiber ends. The thickness of the GO paper was measured to be around 10 μm while the insertion loss of the SA was 1.0 dB at 1550 nm. The SA was placed between the gain medium and output coupler in the ring cavity. The total length of the laser cavity was measured to be approximately 12.6 meter, comprising 1.6 m EDF and 11 meter SMF-28 fiber. The Group Velocity Dispersion (GVD) for the EDF and SMF-28 were –21.64 ps/nm/km and 17 ps/nm/km respectively at 1550 nm. Therefore, the resultant total GVD for this mode-locked fiber laser was estimated to be 0.1513 ps/nm/km. This indicated that the proposed mode-locked fiber laser operated in the anomalous dispersion regime and thus it could be classified as a soliton fiber laser.

Raman spectroscopy was performed to confirm the presence of graphene layer in the GO paper using laser excitation at 532 nm (2.33eV) with an exposure time of 10 s. The detector was a charge-coupled device (CCD) camera. Fig. 2 shows the two prominent peaks in the Raman spectrum, which are located at approximately 1378 cm^{-1} and 1594 cm^{-1}, generally known as the D and G band, respectively. G band contributes to an E_{2g} mode of graphite and is related to the in-plane vibration of sp^2-bonded carbon atoms, while D band is associated with the vibrations of carbon atoms with sp^3 electronic configuration of disordered graphite. The relatively weak D band indicates a low density of defects and high crystallinity of the graphene.

III. Results and Discussion

The mode-locked fiber laser had a low self-starting threshold; approximately at 17.5 mW. Before all the modes were locked, multiple pulsing could be seen to occur at pump power as low as 10 mW. Fig. 3 shows the spectral profile where the presence of soliton is confirmed. The solitons' central wavelength, λc, is situated at 1563.56 nm and the 3 dB bandwidth is approximately 3.77 nm with strong Kelly sidebands at 1554.6 nm and 1573 nm. The spectrum is free from continuous wave (CW) parasitic lasing. The presence of Kelly sidebands confirms that this mode-lock fiber laser is operating in anomalous dispersion regime. Fig. 4 shows the pulse train of the

passive mode-locked fiber laser obtained at pump power of 18 mW. It has a cavity round trip time of 64 ns, corresponding to a pulse repetition rate 15.6 MHz and a cavity length of 12.6 m.

Fig. 5 shows the second harmonic generation (SHG) autocorrelation trace, with the estimated pulse duration of 680 fs at its full-width half maximum (FWHM). The sech^2 fitting which indicates the generation of the soliton pulse is also included in the figure. The autocorrelation trace reveals that the experimental result follows the sech^2 fitting closely. A time-bandwidth product (TBP) calculated from the 3 dB bandwidth of the optical spectrum and the FWHM of the pulse is around 0.315, which indicates that we obtained the bandwidth limited pulse. Since the pulsing threshold is low, the output power for this fiber laser is 0.134 mW. Consequently, the resultant pulse energy and peak power are 0.0085 nJ and 11.85 W respectively. We believe that the pulsewidth can be further reduced by shortening the cavity length. It is also expected that the output power can be improved by optimizing the output coupler.

We also observed that as we were performing data measurements, the pulse increasingly expanded and the spectral profile gradually changed from soliton to laser. Therefore, we suspect that the pulse is destroying the SA. Moreover, at approximately 24.4 mW, the output power was attenuated. Thus, we conclude that a 1-layer GO paper SA is only effective in a short period of time and has low damage threshold. For the same reason, we were unable to acquire a satisfactory data via Radio Frequency Spectrum Analyzer (RFSA). Together with low pulsing and damage thresholds, combined with the 5% of the intracavity energy taken out for performing measurements, it seems that the SNR is unable to extend more than 30 dB.

IV. Conclusion

In conclusion, we have successfully demonstrated the use of nonconductive GO paper as SA for generating soliton mode-locked fiber laser. The SA has a relatively low self-starting threshold although susceptible to damage at higher pump power. The SA is only able to withstand pulse operation for a short period of time. Given by the simplicity of preparing a GO paper, this experiment proves that a nonconductive GO paper can be an alternative to existing graphene and GO based SA.

References

[1] K. Novoselov, A. Geim, S. Morozov, D. Jiang, Y. Zhang, S. Dubonos, *et al.*, "Electric field effect in atomically thin carbon films," *Science*, vol. 306, pp. 666–669, Oct. 2004.

[2] A. K. Geim and K. S. Novoselov, "The rise of graphene," *Nature Mater.*, vol. 6, pp. 183–191, Mar. 2007.

[3] F. Bonaccorso, Z. Sun, T. Hasan, and A. Ferrari, "Graphene photonics and optoelectronics," *Nature Photon.*, vol. 4, no. 9, pp. 611–622, 2010.

[4] Q. Bao, H. Zhang, Y. Wang, Z. Ni, Y. Yan, Z. X. Shen, *et al.*, "Atomic-layer graphene as a saturable absorber for ultrafast pulsed lasers," *Adv. Funct. Mater*, vol. 19, no. 19, pp. 3077–3083, 2009.

[5] F. Carbone, G. Aubock, A. Cannizzo, F. Van Mourik, R. Nair, A. Geim, *et al.*, "Femtosecond carrier dynamics in bulk graphite and graphene paper," *Chem. Phys. Lett.*, vol. 504, nos. 1–3, pp. 37–40, 2011.

[6] G. Xing, H. Guo, X. Zhang, T. C. Sum, and C. H. A. Huan, "The physics of ultrafast saturable absorption in graphene," *Opt. Exp.*, vol. 18, no. 5, pp. 4564–4573, 2010.

[7] T. Winzer, A. Knorr, M. Mittendorff, S. Winnerl, M.-B. Lien, D. Sun, *et al.*, "Absorption saturation in optically excited graphene," *Appl. Phys. Lett.*, vol. 101, no. 22, pp. 221115-1–221115-4, 2012.

[8] Y. Zhu, S. Murali, W. Cai, X. Li, J. W. Suk, J. R. Potts, *et al.*, "Graphene and graphene oxide: Synthesis, properties, and applications," *Adv. Mater.*, vol. 22, no. 35, pp. 3906–3924, 2010.

[9] D. A. Dikin, S. Stankovich, E. J. Zimney, R. D. Piner, G. H. Dommett, G. Evmenenko, *et al.*, "Preparation and characterization of graphene oxide paper," *Nature*, vol. 448, pp. 457–460, Jul. 2007.

[10] W. J. Cao, H. Y. Wang, A. P. Luo, Z. C. Luo, and W. C. Xu, "Graphene-based, 50 nm wide-band tunable passively Q-switched fiber laser," *Laser Phys. Lett.*, vol. 9, no. 1, pp. 54–58, 2012.

[11] D. Popa, Z. Sun, T. Hasan, F. Torrisi, F. Wang, and A. C. Ferrari, "Graphene Q-switched, tunable fiber laser," *Appl. Phys. Lett.*, vol. 98, no. 7, pp. 073106-1–073106-3, 2011.

[12] J. Liu, S. Wu, Q. Yang, Y. Song, Z. Wang, and P. Wang, "163 nJ graphene mode-locked Yb-doped fiber laser," in *Proc. CLEO*, 2011, pp. 1–2.

[13] J. Xu, S. Wu, J. Liu, Q. Wang, Q. H. Yang, and P. Wang, "Nanosecond-pulsed erbium-doped fiber lasers with graphene saturable absorber," *Opt. Commun.*, vol. 285, no. 21, pp. 4466–4469, 2012.

[14] Z. Sun, T. Hasan, F. Torrisi, D. Popa, G. Privitera, F. Wang, *et al.*, "Graphene mode-locked ultrafast laser," *Acs Nano*, vol. 4, no. 2, pp. 803–810, 2010.

[15] S. Yamashita, "A tutorial on nonlinear photonic applications of carbon nanotube and graphene," *J. Lightw. Technol.*, vol. 30, no. 4, pp. 427–447, Feb. 15, 2012.

[16] H. Zhang, D. Tang, R. Knize, L. Zhao, Q. Bao, and K. P. Loh, "Graphene mode locked, wavelength-tunable, dissipative soliton fiber laser," *Appl. Phys. Lett.*, vol. 96, no. 11, pp. 111112-1–111112-3, 2010.

[17] H. Zhang, D. Tang, L. Zhao, Q. Bao, K. Loh, B. Lin, *et al.*, "Compact graphene mode-locked wavelength-tunable erbium-doped fiber lasers: From all anomalous dispersion to all normal dispersion," *Laser Phys. Lett.*, vol. 7, no. 8, pp. 591–596, 2010.

[18] J. Xu, J. Liu, S. Wu, Q.-H. Yang, and P. Wang, "Graphene oxide mode-locked femtosecond erbium-doped fiber lasers," *Opt. Exp.*, vol. 20, no. 14, pp. 15474–15480, 2012.

[19] G. Sobon, J. Sotor, J. Jagiello, R. Kozinski, M. Zdrojek, M. Holdynski, *et al.*, "Graphene oxide vs. reduced graphene oxide as saturable absorbers for Er-doped passively mode-locked fiber laser," *Opt. Exp.*, vol. 20, no. 17, pp. 19463–19473, 2012.

[20] K. Tamura, J. Jacobson, E. Ippen, H. Haus, and J. Fujimoto, "Unidirectional ring resonators for self-starting passively mode-locked lasers," *Opt. Lett.*, vol. 18, no. 3, pp. 220–222, 1993.

[21] Graphene Laboratories Inc., Calverton, NY, USA. (2013, Dec. 24). *Graphene Supermarket* [Online]. Available: https://graphene-supermarket.com/

[22] K. Kashiwagi and S. Yamashita, "Deposition of carbon nanotubes around microfiber via evanascent light," *Opt. Exp.*, vol. 17, no. 20, pp. 18364–18370, 2009.

[23] R. R. Xu, Y. Tian, M. Wang, L. L. Hu, and J. J. Zhang, "Spectroscopic properties of 1.8 μm emission of thulium ions in germanate glass," *Appl. Phys. B*, vol. 102, no. 1, pp. 109–116, 2011.

Q-switched and Soliton Pulses Generation Based on Carbon Nanotubes Saturable Absorber

Sulaiman Wadi Harun, Harith Ahmad
Photonics Research Center,
University of Malaya,
50603, Kuala Lumpur, Malaysia
e-mail: swharun@um.edu.my

Mohd Afiq Ismail, Fauzan Ahmad
Department of Electrical Engineering,
University of Malaya,
50603, Kuala Lumpur, Malaysia

Abstract ─**This paper presents Q-switched and soliton mode-locked fiber lasers using a single-walled carbon nanotubes (SWCNT) based saturable absorber (SA). The SA is fabricated by dripping the SWCNT sodium dedocyl sulfate (SDS) solution onto the fiber ferrule, which is then mated to another clean ferrule before it is incorporated into a ring Erbium-doped fiber laser (EDFL) cavity. The laser Q-switched and mode-locked pulses as the cavity length is fixed at 23 m and 223 m, respectively. The Q-switched laser is self-started to produce a pulse with repetition rate that can be widely tuned from 10.25 kHz to 41.87 kHz by varying the pump power from 30 mW to 129 mW. At the pump power of 129 mW, the Q-switched EDFL has a pulse width of 10.92 μs and pulse energy of 5.2 nJ. The mode-locked EDFL produces a self-started soliton pulses with a repetition rate of 907 kHz, pulse duration of 2.52 ps and signal-to-noise ratio (SNR) of more than 53 dB.**

Keywords ─ Single-walled carbon nanotubes, passive saturable absorber, Q-switching, mode-locking .

I. INTRODUCTION

Passively Q-switched and mode-locked erbium-doped fiber lasers (EDFLs) have been applied in many areas ranging from basic research to telecommunications, medicine, and material processing because of their simple and compact design and high quality pulse generation [1-2]. The Q-switched fiber lasers are generally used for generating high-energy pulses at relatively low repetition rates while the mode-locked fiber lasers usually have high repetition rate (~MHz to ~GHz) and shorter pulse duration (~ps to ~fs). Both pulsed lasers are normally realized using passive method based on nonlinear characteristic of the material [3] or saturable absorber [4]. Both techniques can generates shorter pulses compared to that of the active method since the loss modulation is faster.

Recently, a simple and cost-effective alternative using single walled carbon nanotubes (CNT) has gained recognition owing to its advantages, such as ultrafast recovery time, large saturable absorption, ease of fabrication, and low cost. Several methods of incorporating CNT based SA into fiber laser have also been developed such as spraying [5], optical deposition [6], polymer composite [7] and film [8]. Many research works have been focused on demonstrating a dual-regime fiber lasers that can operates in both mode-locking and Q-switching regimes [9]. In this paper, a switchable Q-switched and soliton mode-locked fiber laser is demonstrated using a CNT-based SA. The SA is fabricated by simply depositing single-walled CNT sodium dedocyl sulfate (SDS) solution onto fiber ferrule. The ferrule is then mated to another clean ferrule so that it can be incorporated in the laser cavity for generating the switchable fiber laser by means of cavity tuning.

II. EXPERIMENTAL SETUP

The SA is fabricated using single-walled CNT SDS solution, which was prepared in our laboratory. Firstly, a homogeneous suspension solution was prepared by mixing 250 mg single-walled CNTs (99% pure, diameter of 1-2 nm and length of 3-30 μm) with 400 ml 1% SDS solution in deionized water and then ultrasonicating it for 30 minutes at 50 W. The solution was centrifuged at 1000 rpm to remove large particles of undispersed CNT to obtain dispersed suspension that is stable for months. The CNT SA was fabricated by dripping a CNT-SDS solution onto a fiber ferrule using a pipette, which was then allowed to dry overnight at room temperature. The SA is constructed by mating the ferrule to another clean ferrule connector so that it could be easily spliced in the cavity of the fiber laser. The insertion loss of the SA is measured to be approximately 3.61 dB.

Fig. 2 shows the experimental setup of the proposed all fiber Q-switched EDFL using the fabricated CNT-based SA as a mode-locker. As shown in Fig. 2, a 4 m long Erbium-doped fiber (EDF) with an Erbium concentration of 2000 ppm acts as the gain medium. It was pumped by a 1480 nm laser diode via a 1480/1550nm wavelength division multiplexer (WDM). Another WDM is used after the gain medium to dispose excess power from the laser diode. An isolator is placed at the end of the EDF to maintain unidirectional laser operation. The laser output is obtained via a 20 dB optical coupler located after the isolator, which channels out about 1% of the oscillating light from the ring cavity. The output is analyzed by using an optical spectrum

978-1-4673-6195-8/13/$31.00 ©2013 IEEE

analyzer (OSA) with a resolution of 0.02 nm and a 500 MHz oscilloscope with 6 GHz bandwidth light wave detector. All components used in our setup are polarization independent, i.e. they support any light polarization. No polarization controller (PC) is included in the laser cavity as we had observed earlier that a PC did not improve our pulse stability. There was no significant pulse jitter observed through the oscilloscope during the experiment. The total length of the laser cavity is estimated to be around 23m. Except for the EDF, all other fiber used in the cavity is a standard single mode fiber (Corning SMF-28).

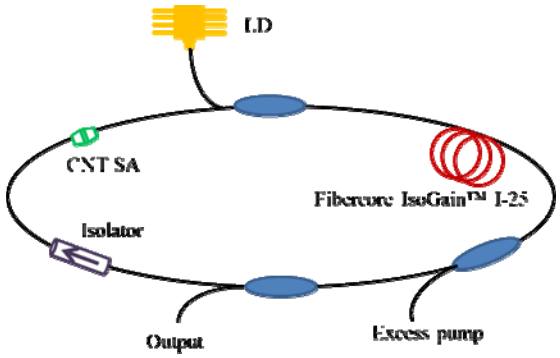

Fig. 2: Configuration of the proposed Q-switched EDFL. The operating mode of the laser is converted from Q-switching to mode-locking by adding an additional 200 m long SMF in the cavity.

The Q-switched EDFL is converted into mode-locked laser by incorporating an additional 200 m long SMF in the setup. The total dispersion of the EDF and SMF are -21.64 ps/nm.km and 17 ps/nm.km, respectively at 1550 nm. The total cavity length for the mode-locked EDFL is around 223 meter with a total Group Velocity Dispersion (GVD) of 3.6364 ps nm^{-1} km^{-1}. Therefore, the proposed mode-locked fiber laser is predicted to produce a soliton pulse output. For pulse duration measurement, an autocorrelator with 25 fs resolution was used. The signal to noise ratio (SNR) is measured using Anritsu MS2667C Radio Frequency Spectrum Analyzer (RFSA).

III. RESULTS AND DISCUSSION

It is observed that the proposed EDFL started to lase with the passive Q-switching mode at the pump power of around 30 mW. Fig. 3 shows the repetition rate and pulse duration as a function of pump power. As the pump power increases, more gain is provided to saturate the CNT-based SA. Since pulse generation relies on saturation, the repetition rate increases with the pump power as shown in Fig. 3. For instance, the pulse repetition rate of the Q-switched EDFL can be widely tuned from 10.25 kHz to 41.87 kHz by varying the pump power from 30 mW to 129 mW. At every specific repetition rate and pump power, the Q-switching pulse output was stable and no significant pulse jitter was observed on the oscilloscope.

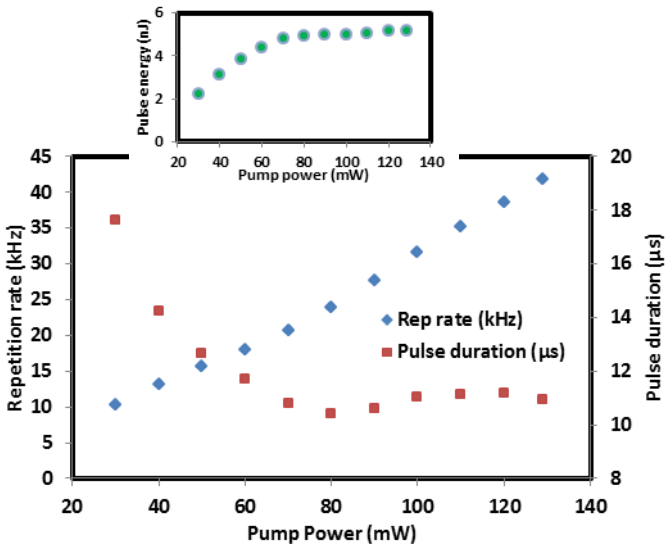

Fig. 3: Repetition rate and pulse duration as a function of pump power. Inset shows the pulse energy characteristic against the pump power.

On the other hand, the pulse width becomes narrower as the pump power increases from 30 mW to 80 mW. The pulse width is maintained at around 11 µs as the pump power further increases up to 129 mW. Inset of Fig. 4 shows the pulse energy characteristic showing that increasing the pump power makes the pulse energy higher especially at pump power region below 80 mW. At the pump power of 129 mW, the Q-switched EDFL has a pulse width of 10.92 µs and pulse energy of 5.2 nJ. The lowest pulse duration of 10.24 µs is achieved at pump power of 80 mW. Based on the minimum attainable pulse duration, the modulation depth of the SWCNT SA is calculated to be ≈3.7%.

It is observed that sufficient intra-cavity power and high pulse energy are important for initiating mode-locking without any Q-switching instability. Reducing repetition rate by increasing cavity length will increase pulse energy that can help to initiate mode-locking pulse generation. Therefore, in this work, we use 20-dB optical coupler and added 200 m long SMF to maintain most of the power inside the cavity as well as increasing pulse energy. Only 1% of the total power is extracted for data measurements. Given the group velocity dispersion (GVD) of 4m long EDF is -21.64 ps ps/nm.km at 1550 nm and 219 meter SMF-28 is 17 ps/nm.km, total cavity dispersion in the proposed mode-locked EDFL is calculated to be 3.64 ps/nm. Hence, the fiber laser is expected to operate in the anomalous dispersion regime. The pulses formed by the mode-locking process in the resonator were detected using a 6-GHz photodetector and a 500-MHz digital phosphor oscilloscope.

The mode-locking operation is observed to self-start at the pump power of as low as 56.8 mW without Q-switching instabilities. It is observed that the pulse state diminishes into continuous-wave (CW) when we lower the pump power

below 30 mW. Fig. 4 shows the oscilloscope trace of the mode-locked pulse trains for the proposed EDFL incorporating a CNT-based SA at the maximum available pump power of 129 mW. It has a time interval of 1.1 µs between the pulses, which can be translated to a pulse repetition rate of 907 kHz, corresponding to 223 m cavity length. Fig. 5 shows a plot of a typical output second harmonics generation (SHG) autocorrelation trace for the mode-locked laser. By applying sech^2 fitting for the output curve, the pulse duration at its full-width half maximum (FWHM) is estimated to be about 2.52 ps.

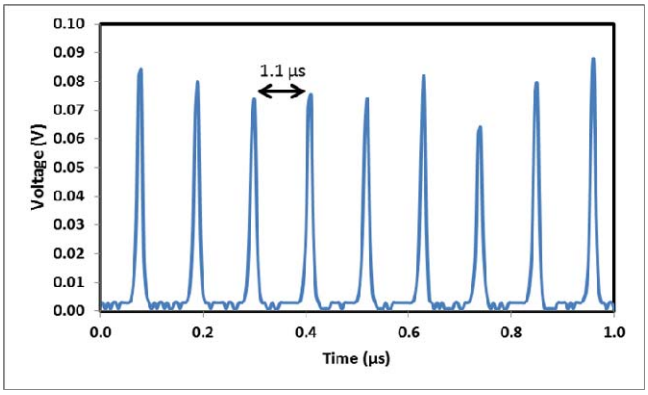

Fig. 4: Oscilloscope trace of the mode-locked fiber laser

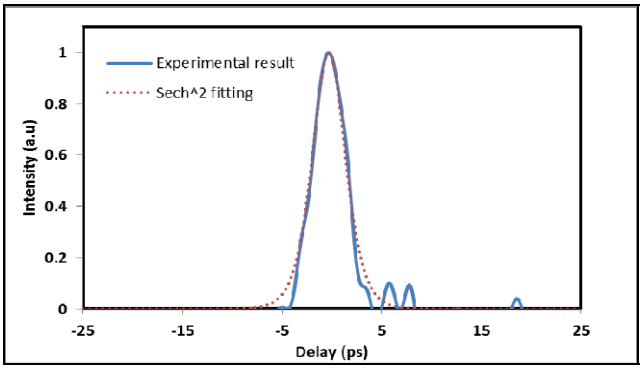

Fig. 5: Autocorrelation trace of the mode-locked fiber laser at pump power of 129 mW.

Fig. 6 shows the radio frequency (RF) spectrum of the mode-locked fiber laser. As seen, the signal to noise ratio is observed to be more than 53 dB, which indicates the pulsing behavior is quite stable. The output power of the soliton laser is measured to be 6.54 dBm. Inset of Fig. 6 shows the optical spectrum of the passively mode-locked laser, which operates at the center wavelength of 1570.5 nm. It has a 3-dB bandwidth of 4.7 nm, which gives a Time Bandwidth Product (TBP) of 1.4345. Compared to sech^2 transform limited value of 0.315, this indicates that the pulse is slightly chirped. When comparing between the leading edge and the trailing edge of the pulse from autocorrelation trace, the leading edge shows significant loss from the saturable absorber. On the contrary, the pulse trailing edge has negligible loss because the saturable absorber is fully saturated. This shows that the SWCNT absed SA is a slow SA.

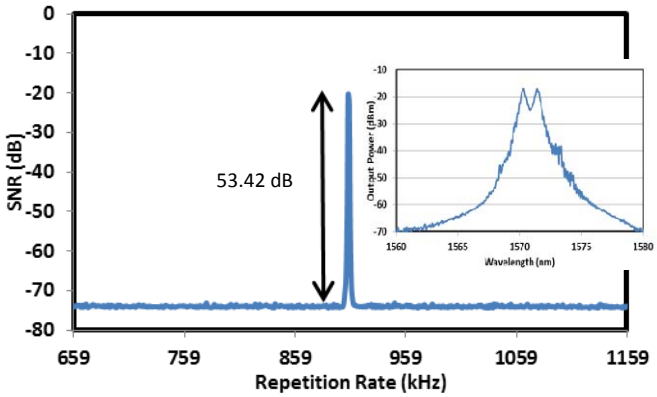

Fig. 6: RF spectrum of the mode-locked fiber laser at 129 mW. Inset shows the output spectrum.

IV. CONCLUSIONS

A switchable Q-switched and soliton mode-locked fiber laser is demonstrated using a SWCNT-based SA. The Q-switched EDFL is self-started in a 23 m long laser cavity to produce a pulse with repetition rate that can be widely tuned from 10.25 kHz to 41.87 kHz by varying the pump power from 30 mW to 129 mW. It has a pulse width of 10.92 µs and pulse energy of 5.2 nJ at the maximum pump power of 129 mW. A 200 m long SMF is incorporated in the laser cavity to switch the EDFL into a self-started mode-locked fiber laser. The mode-locked EDFL produces a soliton pulse train with a repetition rate of 907 kHz, pulse duration of 2.52 ps and signal-to-noise ratio (SNR) of more than 53 dB.

REFERENCES

[1] D. Welford, "Passively Q-switched lasers," Circuits and Devices Magazine, IEEE, vol. 19(4), pp. 31-36, (2003).

[2] A. Hamzah, M. C. Paul, N. A. Awang, H. Ahmad, M.Pal, S. Das, M. A. Ismail, , S. W. Harun, "Passively mode-locked erbium doped zirconia fiber laser using a nonlinear polarisation rotation technique," Optics and Laser Technology, vol. 47, pp. 22-25, (2013)

[3] S. W. Harun, R. Akbari, H. Arof, H. Ahmad, "Mode-locked bismuth-based erbium-doped fiber laser with stable and clean femtosecond pulses output," Laser Physics Letters, vol. 8, pp. 449 – 452, (2011).

[4] M. A. Ismail, S. J. Tan, N. S. Shahabuddin, S. W. Harun, H. Arof and H. Ahmad, "Performance Comparison of Mode-Locked Erbium-Doped Fiber Laser with Nonlinear Polarization Rotation and Saturable Absorber Approaches," Chin. Phys. Lett., vol. 29(5), pp. 54216, (2012)

[5] S.Y. Set, H. Yaguchi, Y. Tanaka, M. Jablonski, "Laser mode locking using a saturable absorber incorporating carbon nanotubes," Journal of lightwave technology, vo.l. 22(1), pp. 51. (2004)

[6] K. Kashiwagi, S. Yamashita, S.Y. Set, "In-situ monitoring of optical deposition of carbon nanotubes onto fiber end," Opt. Express, vol. 17(7), pp. 5711-5715, (2009)

[7] J.W. Nicholson, R.S. Windeler, D.J. DiGiovanni, “Optically driven deposition of single-walled carbon-nanotube saturable absorbers on optical fiber end-faces,” Optics Express, vol. 15(15), pp. 9176-9183, (2007

[8] T. Hasan, Z. Sun, F. Wang, F. Bonaccorso, P.H. Tan, A.G. Rozhin, A.C. Ferrari, “Nanotube–polymer composites for ultrafast photonicst photonics”, Advanced materials, vol. 21(38-39), pp. 3874-3899, (2009).

[9] Set, SY, Yaguchi, et al., “A dual-regime mode-locked/Q-switched laser using a saturable absorber incorporating carbon nanotubes (SAINT),” Paper presented at the Lasers and Conference of Laser and Electro-Optics (CLEO), (2003)

CHIN. PHYS. LETT. Vol. 29, No. 5 (2012) 054216

Performance Comparison of Mode-Locked Erbium-Doped Fiber Laser with Nonlinear Polarization Rotation and Saturable Absorber Approaches *

M. A. Ismail[1], S. J. Tan[1], N. S. Shahabuddin[1], S. W. Harun[1,2**], H. Arof[1], H. Ahmad[2]

[1]*Department of Electrical Engineering, Faculty of Engineering, University of Malaya, 50603 Kuala Lumpur, Malaysia*
[2]*Photonics Research Center, Department of Physics, University of Malaya, 50603 Kuala Lumpur, Malaysia*

(Received 29 December 2011)

A mode-locked erbium-doped fiber laser (EDFL) is demonstrated using a highly concentrated erbium-doped fiber (EDF) as the gain medium in a ring configuration with and without a saturable absorber (SA). Without the SA, the proposed laser generates soliton pulses with a repetition rate of 12 MHz, pulse width of 1.11 ps and energy pulse of 1.6 pJ. By incorporating SA in the ring cavity, the optical output of the laser changes from soliton to stretched pulses due to the slight change in the group velocity dispersion. With the SA, a cleaner pulse is obtained with a repetition rate of 11.3 MHz, a pulse width of 0.58 ps and a pulse energy of 2.3 pJ.

PACS: 42.55.Wd, 42.60.Fc, 42.65.Re, 42.65.Tg DOI: 10.1088/0256-307X/29/5/054216

Fiber lasers are made possible by incorporating trivalent rare-earth ions such as neodymium, erbium and thulium into glass hosts. Since the 1980s, erbium-doped fiber lasers (EDFLs) have gained widespread interest because the lasing wavelength at 1.55 μm, falls within the low-loss window of optical fiber, which is suitable for optical fiber communications.[1,2] They have numerous advantages such as simple doping procedures, low loss, compact, high reliability and high-output power. We have also observed growing interest in mode-locked EDFLs due to their many applications in communication systems for time-division multiplexing (TDM),[3] code-division multiple access (CDMA)[4] and wavelength division-multiplexing (WDM).[5,6] They can also find applications in high-resolution spectroscopy, THz pulse generation, optical clockworks, absolute distance measurements and many others.[7–10]

Recently, a high concentration erbium-doped fiber (EDF), IsoGain^{TM}, was commercially developed by FiberCore Co. Ltd. to provide the ultimate in cost-effectiveness for the EDF amplifier (EDFA), with typical C-band gain-lengths of only a few meters.[11] This fiber is actually more suited to reducing the exceptionally long doped fiber lengths required for effective L-band amplification. In this Letter, a mode-locked EDFL is demonstrated using a simple ring cavity structure with the IsoGain^{TM} EDF as the gain medium. The performance of the laser is investigated for two different mode-locking techniques; nonlinear polarization rotation (NPR) and saturable absorber (SA). Since the gain medium is only a piece of 2.5-m-long EDF, the cavity length of the EDFL is considered short and therefore stable clean pulses can be generated with a higher repetition frequency. The super-mode noise can also be suppressed effectively because the EDF has a very high nonlinearity.

Figure 1 shows the configuration of the proposed laser, which is an all-fiber setup using commercially available components. It consists of a piece of 2.5-m-long EDF, wavelength division multiplexers (WDMs), an isolator, a polarization controller (PC), a saturable absorber (SA) and a 3-dB output coupler. The total length of the cavity is about 14.5 m, which comprises a 2.5-m-long EDF and a 12-m-long single mode fiber (SMF) used in the other components. The EDF has an erbium ion concentration of 2000 ppm, cut-off wavelength of 910 nm, a pump absorption rate of 24 dB/m at 980 nm and a dispersion coefficient of -21.64 ps/nm·km at $\lambda = 1550$ nm. It is forward pumped using a 1480 nm laser diode via the WDM to provide amplification in the C-band region. The other part of the ring cavity uses a standard single mode fiber (SMF-28) with a dispersion coefficient of 17 ps/nm·km at $\lambda = 1545$ nm. A semiconductor SA is used for the initiation and stabilization of mode-locking at around the 1550 nm region. The SA is designed for transmission application and has a modulation depth ΔR of 15%, saturation fluence of 300 μJ/cm^2, nonsaturable loss of 10% and relaxation time constant of 2 ps. An isolator is used to ensure a unidirectional operation of the laser and acts as a polarizer. A PC is used to rotate the polarization state and allows continuous adjustment of the birefringence within the cavity to balance the gain and loss for laser pulse generation. The experiment is also repeated without the SA wherein the mode locking mechanism is based on the NPR technique.

Figure 2 shows the output spectrum of the mode locked EDFL with and without the SA in the ring

*Supported by the Ministry of Higher Education under PRGS under Grant No PR003-2011A, and HIRG under Grant No HIR-MOHE D000009-16001.
**Email: swharun@um.edu.my
© 2012 Chinese Physical Society and IOP Publishing Ltd

cavity. As shown in the figure, the output of the laser changes from soliton to stretched pulses as the SA is incorporated in the cavity. The anti-resonant SA is incorporated in the laser cavity to exploit its nonlinear optical property of an intensity dependent absorption for reducing the pulse width of the laser. Without the SA, the proposed laser generates mode-locked pulses using the NPR effect in the cavity. The NPR relies on the Kerr effect in an EDF in conjunction with an optical isolator to produce artificial saturable absorber action. By setting the initial polarization ellipse and phase bias properly, pulse shortening can be attained. The NPR can occur in an optical fiber when the initial polarization state is elliptical. This elliptical state can be resolved into right- and left-hand circular polarization components of different intensities. These two circular components then experience different nonlinear phase shifts related to the intensity dependence of the refractive index.[12,13] By properly choosing the linear cavity phase delay bias, which corresponds to appropriately selecting the orientations of the polarization controllers, soliton operation can be always obtained. With a fixed linear cavity phase delay bias but different values of gain, as long as the generated soliton pulse peak power is weaker than that of the polarization switching power of the cavity, stable uniform soliton pulse train is always achievable.

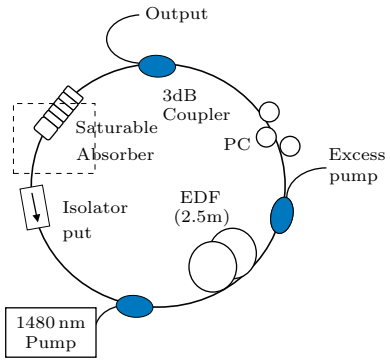

Fig. 1. Experimental setup for mode-locked fiber laser.

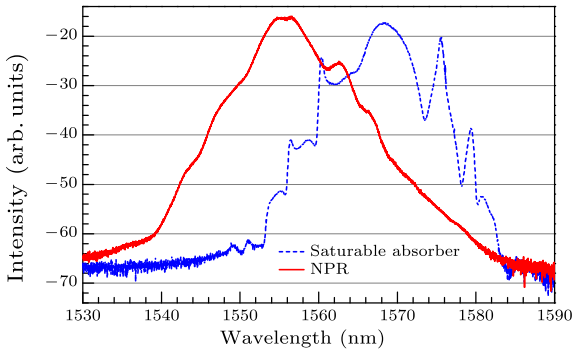

Fig. 2. Output spectrum of the proposed EDFL with NPR and SA operations.

SA is an optical component that has a certain optical loss at a certain optical intensity. As the intensity increases, the optical loss decreases. The incorporation of an anti-resonant SA leads to a high-repetition-rate cavity and improves the mode-locking operation. The total group velocity dispersion (GVD) in the ring cavity will determine whether the fiber laser is a soliton or stretched-pulse. If the total GVD is negative, the fiber laser operates in the soliton regime whereas if the total GVD is positive, the resulting fiber laser is a stretched-pulse. In a stretched-pulse laser, the use of large positive- and negative-dispersion fibers causes the pulses to be alternately stretched and compressed as they circulate in the cavity. Figure 2 reaffirms the fact that the incorporation of SA in the cavity converts the laser output from soliton to stretched pulses. This is attributed to the GVD, which becomes slightly positive with the incorporation of SA. Spectral broadening occurs in the doped fiber as a result of the positive dispersion with SPM.[13] As observed in Fig. 2, the output spectrum peaks at 1568.2 nm and 1556.6 nm for the respective NPR and SA operations. The 3-dB bandwidths of the output spectrum are obtained at 17.0 nm and 19.8 nm for NPR- and SA-based operation respectively. With maximum pump power of 136 mW, the average maximum output of 1.4 mW was achieved with the SA.

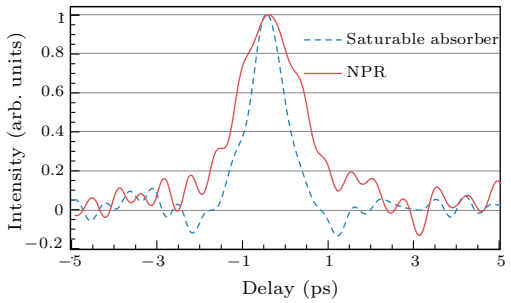

Fig. 3. Autocorrelation trace of the output pulse from both mode-locked EDFLs with SA and NPR approaches.

Figure 3 illustrates the autocorrelation trace of the output pulse of the laser with SA and NPR operations. By applying such function fitting for both output curves, the pulse width of the laser is estimated to be 0.58 ps and 1.11 ps for the SA- and NPR-operation, respectively. The pulse width of the NPR laser is nearly twice as broad as that of the pulse width of the SA laser. An important aspect of the stretched-pulse generation is the presence of alternating positive- and negative-dispersion in the resonator which causes a periodically varying $k(\omega)$ that reduces the phase-matched coupling to resonant sidebands.[14] Consequently, the spectra are cleaner and less dispersive radiation is noticeable between pulses as indicated in Fig. 3. Figure 4 shows the oscilloscope traces for both lasers. The repetition rate for the SA operation is determined at 11.3 MHz while the repetition rate for NPR operation is 12 MHz. Adding an SA to the

fiber ring brings an extra length to the existing experimental setup. As a result, the repetition rate for the SA operation is slightly more than that of the NPR operated laser. Figure 4 also illustrates that the pulse shape of the laser with SA is cleaner than the one generated by the NPR laser. The pulse energy when adding SA to the experimental setup is 2.3 pJ while the pulse energy for the NPR laser is 1.6 pJ.

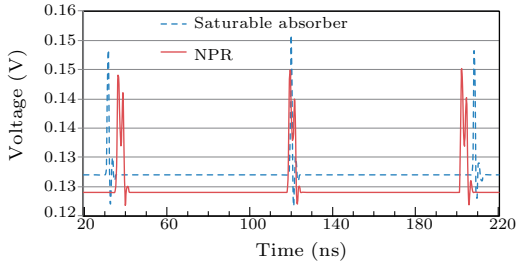

Fig. 4. Repetition rate observed from an oscilloscope for both SA and NPR lasers.

In conclusion, mode-locked fiber lasers are successfully achieved using a commercially available 2.5-meter Fibercore IsoGain I-25 as a gain medium. Two techniques were demonstrated to generate the mode-locked fiber laser, namely the NPR technique and another technique formulated by adding an SA to the experimental setup. By incorporating an SA to the ring cavity, the output laser changes from soliton to stretched pulses with a cleaner pulse shape. Correspondingly, the pulse-width and pulse energy are also improved from 1.11 ps to 0.58 ps and 1.6 pJ to 2.3 pJ, respectively.

References

[1] Tamura K, Haus H A and Ippen E P 1992 *Electron. Lett.* **28** 2226
[2] Ahmad H, Saat N K and Harun S W 2005 *Laser Phys. Lett.* **2** 369
[3] Ahmad H, Saat N K and Harun S W 2000 *IEEE Photon. Technol. Lett.* **12** 353
[4] Sardesai H P, Chang C C and Weiner A M 1998 *J. Lightwave Technol.* **16** 1953
[5] De Souza E A, Nuss M C, Knox W H and Miller D A B 1995 *Opt. Lett.* **20** 1166
[6] Boivin L, Wegmueller M, Nuss M C and Knox W H 1999 *IEEE Photon. Technol. Lett.* **11** 466
[7] Udem T, Holzwarth R and Hansch T W 2002 *Nature* **416** 233
[8] Diddams S, Hollberg L, Ma L and Robertsson L 2002 *Opt. Lett.* **27** 58
[9] Diddams S A, Jones D J, Ye J, Cundiff S T, Hall J L, Ranka J K, Windler R S, Holzwarth R, Udem T and Hansch T W 2000 *Phys. Rev. Lett.* **84** 5102
[10] Shioda T, Mori T, Sugimoto T, Tanaka Y and Kurosawa T 2009 *Opt. Commun.* **282** 2909
[11] Harun S W, Abd Rahman F, Dimyati K and Ahmad H 2006 *Laser Phys. Lett.* **3** 536
[12] Stolen R H, Botineau J and Ashkin A 1982 *Opt. Lett.* **7** 512
[13] Nelson L E, Jones D J, Tamura K, Haus H A and Ippen E P 1997 *Appl. Phys. B: Lasers Opt.* **65** 277
[14] Tamura K, Nelson L E, Haus H A and Ippen E P 1994 *Appl. Phys. Lett.* **64** 149

Mode-locked thulium–bismuth codoped fiber laser using graphene saturable absorber in ring cavity

D. I. M. Zen,[1,2] N. Saidin,[2,3] S. S. A. Damanhuri,[2,3] S. W. Harun,[2,3,*] H. Ahmad,[2] M. A. Ismail,[2,3] K. Dimyati,[1] A. Halder,[4] M. C. Paul,[4] S. Das,[4] M. Pal,[4] and S. K. Bhadra[4]

[1]Department of Electrical and Electronic Engineering, National Defense University of Malaysia, Kem Sungai Besi, Kuala Lumpur 57000, Malaysia

[2]Photonics Research Centre, University of Malaya, Kuala Lumpur 50603, Malaysia

[3]Department of Electrical Engineering, Faculty of Engineering, University of Malaya, Kuala Lumpur 50603, Malaysia

[4]Fiber Optics and Photonics Division, Central Glass & Ceramic Research Institute, CSIR, Kolkata 700032, India

*Corresponding author: swharun@um.edu.my

Received 19 December 2012; revised 18 January 2013; accepted 18 January 2013; posted 22 January 2013 (Doc. ID 182105); published 15 February 2013

We demonstrate mode locking of a thulium–bismuth codoped fiber laser (TBFL) operating at 1901.6 nm, using a graphene-based saturable absorber (SA). In this work, a single layer graphene is mechanically exfoliated using the scotch tape method and directly transferred onto the surface of a fiber pigtail to fabricate the SA. The obtained Raman spectrum characteristic indicates that the graphene on the core surface has a single layer. At 1552 nm pump power of 869 mW, the mode-locked TBFL self starts to generate an optical pulse train with a repetition rate of 16.7 MHz and pulse width of 0.37 ps. This is a simple, low-cost, stable, and convenient laser oscillator for applications where eye-safe and low-photon-energy light sources are required, such as sensing and biomedical diagnostics. © 2013 Optical Society of America

OCIS codes: 060.3510, 140.3538.

1. Introduction

Mode-locked fiber lasers currently attract great interest due to their extensive applications in telecommunication, imaging, spectroscopy, and medicine [1–3]. In this laser, the random phases of oscillating modes are phase locked to produce a single pulse [4], which can be realized by two main methods: active and passive. For the active method, a modulator has to be used, which increases the complexity of the laser structure. Compared to active method, the passive method possesses many advantages, including compactness, low cost, flexibility, and simplicity of design. Nonlinear polarization rotation (NPR) and semiconductor saturable absorber mirror (SESAM) are normally used to provide amplitude modulation in passively mode-locked fiber lasers [5]. However, these two techniques have drawbacks. NPR requires additional elements in the cavity, including a polarizer and polarization controllers (PCs). Furthermore, fiber lasers mode locked with NPR will generally not be environmentally stable. SESAMs have recently become readily available, but tend to get damaged easily when used in fiber lasers, perhaps due to insufficient modulation depth. Recently, alternative saturable absorbers (SAs) based on single-walled carbon nanotubes and graphene have been investigated [6]. Graphene-based SAs are excellent passive mode lockers because of their subpicosecond recovery time, broad operation range, low saturation intensity, polarization insensitivity, low cost, and easy fabrication [7].

Most recent works on the mode-locked fiber lasers focus on ytterbium- and erbium-doped fiber lasers, which operate at wavelengths around 1 and 1.5 μm, respectively. However, much attention has also been

1559-128X/13/061226-04$15.00/0
© 2013 Optical Society of America

focused on thulium-doped fiber lasers in recent years to provide an integrated and robust laser source operating at around 2 μm wavelength for many applications in nonlinear optics, medicine, and sensing. To date, few mode-locked oscillators based on thulium-doped fiber have been reported. For instance, Nelson *et al.* demonstrated NPR-based mode-locked thulium fiber laser with 500 fs pulses generation [8]. In another work, Sharp *et al.* used a semiconductor SESAM in a Tm fiber laser to achieve 190 fs pulses [9]. More recently, Engelbrecht *et al.* reported a laser with grating-based dispersion compensation and double-clad thulium-doped fiber. The laser operates in the stretched pulse regime [10] with pulse energy as high as 4.3 nJ and dechirped pulse duration around 300 fs. Thulium-doped, mode-locked fiber lasers have also been demonstrated recently using a graphene-based SA [11–13].

In our earlier work, a thulium–bismuth codoped fiber (TBF) is used to generate a broadband amplified spontaneous emission source operating in an 1880 nm wavelength region [14]. In this paper, a mode-locked TBF laser (TBFL) is demonstrated for the first time using a similar TBF in conjunction with a simple and low-cost, graphene-based SA. The SA is obtained by implementing mechanical exfoliation technique. The proposed laser uses a 5 m long TBF, which was obtained through a modified chemical vapor deposition (MCVD) and solution-doping processes as the gain medium to achieve a stable pulse train with 16.7 MHz repetition rate and 0.37 ps pulse width operating at 1901.6 nm. The proposed laser is simple and low cost but has many potential applications, especially in sensing and biomedical diagnostics, where eye-safe and low-photon-energy light sources are required.

2. Experimental Setup and Procedure

A schematic of the experimental laser setup is shown in Fig 1. It consists of a 1552 nm erbium/ytterbium fiber laser as a pump source, a 5 m long TBF as a gain medium, a wavelength division multiplexer (WDM), a polarization-insensitive circulator, a fiber Bragg grating (FBG), a 10 dB coupler, a PC, and a graphene-based SA. The TBF is obtained by drawing a preform, which was fabricated using a deposition of porous layer by the MCVD process in conjunction with solution-doping technique. The dopant concentrations (wt. %) and compositions inside the core are $0.35\,Bi_2O_3$, $0.9\,Tm_2O_3$, $3.0\,Al_2O_3$, and $4.0\,GeO_2$. The fiber has core and cladding diameters of 7.2 and 125 μm, respectively, with a NA of 0.23. The WDM is used to inject the 1552 nm pump into the TBF. The circulator is used to allow the reflected light from the FBG to oscillate in the ring cavity, as well as to ensure a unidirectional operation of the laser. The FBG used has a center wavelength of 1901.6 nm with a 3 dB bandwidth of 1.5 nm and a reflectivity of 99.6%. A PC is used to adjust the intracavity polarization of light.

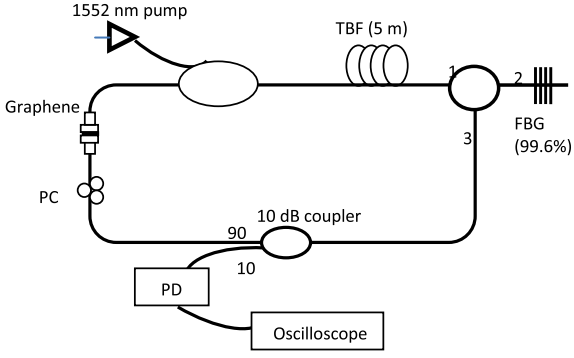

Fig. 1. (Color online) Schematic configuration of the proposed mode-locked TBFL.

The graphene-based SA plays the key role of a passive mode locker. It is constructed by depositing a single layer graphene on the end facet of the optical fiber ferrule by mechanical exfoliation technique. The original graphene material is a commercially available highly ordered pyrolytic graphite (HOPG). The HOPG flakes are pasted onto a strip of scotch tape and then pressed and peeled off repeatedly in order to optimize the graphene thickness. The resulting graphene strip is then pressed against the end facet of an optical fiber ferrule. The scotch tape is slowly peeled off and accordingly the graphene layer remains on the end facet of the optical fiber ferrule. The ferrule is then mated to another clean ferule by a connector to form a graphene-based SA. The total length of the laser cavity is about 16.8 m. All components are polarization independent and connected by fiber pigtails. The laser output is tapped from the 10% port of the output coupler, measured by a power meter, and monitored by a photodetector, which is attached to an oscilloscope. The pulse width of the laser is measured by an autocorrelator.

3. Result and Discussion

Raman spectroscopy was performed to confirm the presence of single-layer graphene using laser excitation at 532 nm with an exposure time of 10 s. Figure 2 shows the measured Raman spectrum from the graphene-deposited fiber ferrule. It clearly shows

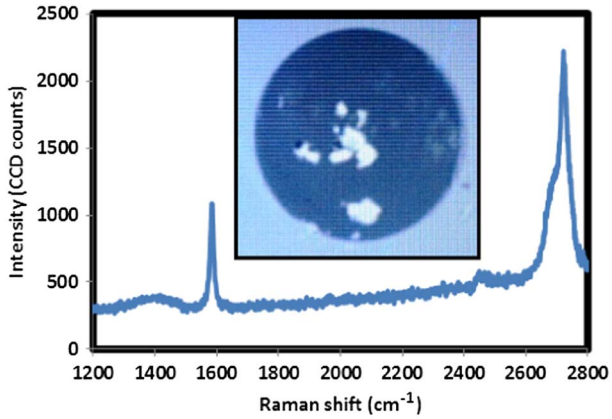

Fig. 2. (Color online) Raman spectrum from the graphene-based SA. Inset shows an image of the fiber ferrule with graphene layer deposited on it.

two prominent peaks; one is located at approximately 1580 cm^{-1}, generally known as the *G* peak, and the other is located at approximately 2700 cm^{-1}, known as the 2-D peak. The width of the 2-D peak can be used to determine the number of graphene layers. As the graphene layer increases, the width also increases [15]. The Raman spectroscopy reveals a sharp and pointy 2-D peak. However the 2-D width is broad since the graphene was mechanically exfoliated from HOPG [16]. Another method of determining the graphene layers is by calculating the intensity ratio between the *G* and 2-D peaks. It was reported that single-layer graphene has a low intensity ratio, usually lower than 0.5, while multilayer graphene shows higher intensity ratio (≥1) [17]. In our work, we obtain a *G*/2-D peak ratio of 0.48, which indicates that we have successfully obtained a single-layer graphene on the proposed SA. The inset of Fig. 2 shows the microscope image of the graphene layer on a fiber ferrule, which indicates that a single-layer graphene is properly attached to the fiber core.

The pulses formed by the mode-locking process in the resonator were detected using a 6 GHz photodetector and a 500 MHz digital phosphor oscilloscope. It was observed that the mode-locked laser self-started at 1552 nm pump power of 869 mW without the requirement to introduce any disturbance to the intracavity fiber. The optical spectrum of the passively mode-locked laser is shown in Fig. 3. It operates at the center wavelength of 1901.6 nm, which coincides with the FBG wavelength with a few sidebands. The Kelly sidebands indicate that the pulse is soliton, which is generated due to the graphene SA. The theory of saturable absorption in graphene was thoroughly discussed in [18]. A spectral broadening is also observed, which is most probably due to the soliton effect from the balance between the self-phase modulation and group velocity dispersion in the cavity. This broadening is not observed without the SA. The average output power is measured to be around 1.72 mW at 1552 nm pump power of 869 mW. The full width half-maximum (FWHM) of the optical spectrum is far below 1 nm due to the use of narrowband FBG in the cavity.

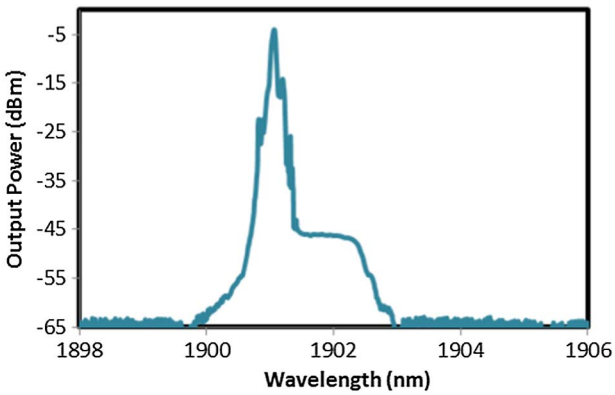

Fig. 3. (Color online) The attenuated output spectrum at pump power at 1552 nm pump power of 869 mW.

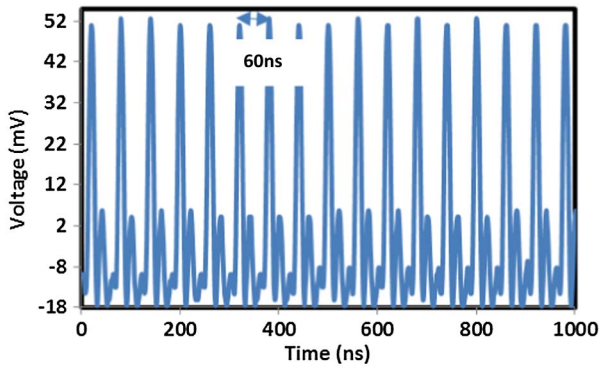

Fig. 4. (Color online) Output pulse train from the mode-locked TBFL.

Figure 4 shows a pulse train from the mode-locked TBFL recorded by an oscilloscope. As seen, the time interval is measured to be around 60 ns, which corresponds to a repetition rate of 16.7 MHz. Multiple solitons are generated as identified in the pulse train, which is due to the energy quantization. The high repetition rate obtained is due to the multiple pulses circulating inside the cavity that generate harmonics mode-locked fiber laser. The major factors in creating this phenomenon are interrelated with the peak power limiting effect of the laser cavity besides the gain competition between the multiple solitons. This proves that the proposed graphene-based SA is able to operate efficiently in the ring TBFL. Figure 5 shows a plot of a typical output second harmonics generation autocorrelation trace. The estimated pulse duration at its FWHM is about 0.37 ps. The autocorrelation trace reveals that the experimental result follows the $sech^2$ fitting. However, at lower intensity, the experimental curve does not fit well due to the noise from the detector used. The inset of Fig. 5 shows the radio frequency spectrum of the mode-locked fiber laser. As seen, the signal to noise ratio is observed to be more than 60 dB, which indicates the pulsing behavior is quite stable. The time-bandwidth product is calculated to be about 418, which shows that the output pulse is highly chirped.

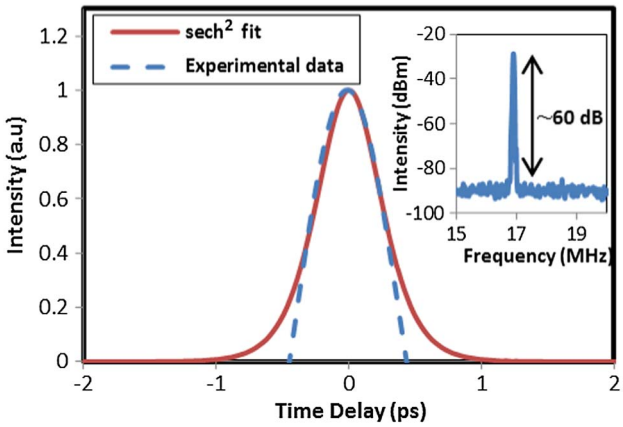

Fig. 5. (Color online) Autocorrelation trace. Inset shows the output RF spectrum of the mode-locked TBFL.

4. Conclusion

We have demonstrated a passive and stable, mode-locked TBFL operating in the 1901.6 nm region using a graphene-based SA, which was obtained via a mechanical exfoliation technique. The SA was fabricated by mechanically exfoliating a single layer of graphene using a scotch tape method and transferring the graphene layer onto the end surface of the fiber pigtail. At 1552 nm pump power of 869 mW, the TBFL generates mode-locking pulses with a repetition rate of 16.7 MHz and pulse width of 0.37 ps. Besides showing good performance in the mid-IR operation, the SA is easy to fabricate and low in cost.

References

1. F. Wang, A. G. Rozhin, V. Scardaci, Z. Sun, F. Hennrich, I. H. White, W. I. Milne, and A. C. Ferrari, "Wideband-tuneable, nanotube mode-locked, fibre laser," Nat. Nanotechnol. **3**, 738–742 (2008).
2. M. A. Ismail, S. J. Tan, N. S. Shahabuddin, S. W. Harun, H. Arof, and H. Ahmad, "Performance comparison of mode-locked erbium-doped fiber laser with nonlinear polarization rotation and saturable absorber approaches," Chin. Phys. Lett. **29**, 054216 (2012).
3. S. W. Harun, R. Akbari, H. Arof, and H. Ahmad, "Mode-locked bismuth-based erbium-doped fiber laser with stable and clean femtosecond pulses output," Laser Phys. Lett. **8**, 449–452 (2011).
4. F. Träger, *Springer Handbook of Lasers and Optics* (Springer-Verlag, 2007).
5. H. A. Haus, "Mode-locking of lasers," IEEE J. Sel. Top. Quantum Electron. **6**, 1173–1185 (2000).
6. A. Martinez, K. Kazuyuki, B. Xu, and S. Yamashita, "Optical deposition of graphene and carbon nanotubes in a fiber ferrule for passive mode-locking lasing," Opt. Express **18**, 23054–23061 (2010).
7. Z. Sun, T. Hasan, F. Bonaccorso, F. Torrisi, D. M. Basko, D. Popa, and A. C. Ferrari, "Graphene mode-locked ultrafast laser," ACS Nano **4**, 803–810 (2010).
8. L. E. Nelson, E. P. Ippen, and H. A. Haus, "Broadly tunable sub-500 fs pulses from an additive-pulse mode-locked thulium-doped fiber ring laser," Appl. Phys. Lett. **67**, 19–21 (1995).
9. R. C. Sharp, D. E. Spock, N. Pan, and J. Elliot, "190 fs passively mode-locked thulium fiber laser with a low threshold," Opt. Lett. **21**, 881–883 (1996).
10. M. Engelbrecht, F. Haxsen, A. Ruehl, D. Wandt, and D. Kracht, "Ultrafast thulium-doped fiber-oscillator with pulse energy of 4.3 nJ," Opt. Lett. **33**, 690–692 (2008).
11. J. Liu, S. Wu, J. Xu, Q. Wang, Q. Yang, and Pu Wang, "Mode-locked 2 μm thulium-doped fiber laser with graphene oxide saturable absorber," in *CLEO/Europe and EQEC 2011 Conference Digest*, OSA Technical Digest (CD) (Optical Society of America, 2012), paper JW2A.76.
12. M. Zhang, E. J. R. Kelleher, F. Torrisi, Z. Sun, T. Hasan, D. Popa, F. Wang, A. C. Ferrari, S. V. Popov, and J. R. Taylor, "Tm-doped fiber laser mode-locked by graphene-polymer composite," Opt. Express **20**, 25077–25084 (2012).
13. M. Jung, J. Koo, P. Debnath, Y. W. Song, and J. H. Lee, "A mode-locked 1.91 μm fiber laser based on interaction between graphene oxide and evanescent field," Appl. Phys. Express **5**, 112702 (2012).
14. A. Halder, M. C. Paul, S. W. Harun, S. M. M. Ali, N. Saidin, S. S. A. Damanhuri, H. Ahmad, S. Das, M. Pal, and S. K. Bhadra, "1880 nm broadband ASE generation with bismuth–thulium codoped fiber," IEEE Photon. J. **4**, 2176–2181 (2012).
15. A. C. Ferrari, J. C. Meyer, V. Scardaci, C. Casiraghi, M. Lazzeri, F. Mauri, S. Piscanec, D. Jiang, K. S. Novoselov, S. Roth, and A. K. Geim, "Raman spectrum of graphene and graphene layers," Phys. Rev. Lett. **97**, 187401 (2006).
16. D. Graf, F. Molitor, K. Ensslin, C. Stampfer, A. Jungen, C. Hierold, and L. Wirtz, "Spatially resolved Raman spectroscopy of single-and few-layer graphene," Nano Lett. **7**, 238–242 (2007).
17. S. Chen, L. Brown, M. Levendorf, W. Cai, S.-Y. Ju, J. Edgeworth, X. Li, C. W. Magnuson, A. Velamakanni, R. D. Piner, J. Kang, J. Park, and R. S. Ruoff, "Oxidation resistance of graphene-coated Cu and Cu/Ni alloy," ACS Nano **5**, 1321–1327 (2011).
18. T. Winzer, A. Knorr, M. Mittendorff, S. Winnert, M.-B. Lien, D. Sun, T. B. Norris, M. Helm, and E. Malic, "Absorption saturation in optically excited graphene," Appl. Phys. Lett. **101**, 221115 (2012).

IOPscience iopscience.iop.org

Home Search Collections Journals About Contact us My IOPscience

A *Q*-switched erbium-doped fiber laser with a graphene saturable absorber

This article has been downloaded from IOPscience. Please scroll down to see the full text article.

2013 Laser Phys. Lett. 10 025102

(http://iopscience.iop.org/1612-202X/10/2/025102)

View the table of contents for this issue, or go to the journal homepage for more

Download details:
IP Address: 161.142.24.130
The article was downloaded on 15/02/2013 at 07:13

Please note that terms and conditions apply.

Laser Phys. Lett. **10** (2013) 025102 (4pp) doi:10.1088/1612-2011/10/2/025102

LETTER

A *Q*-switched erbium-doped fiber laser with a graphene saturable absorber

M A Ismail[1], F Ahmad[1], S W Harun[1,2], H Arof[1] and H Ahmad[2]

[1] Faculty of Engineering, Department of Electrical Engineering, University of Malaya, 50603 Kuala Lumpur, Malaysia
[2] Photonics Research Center, Physics Department, University of Malaya, 50603 Kuala Lumpur, Malaysia

E-mail: swharun@um.edu.my

Received 9 April 2012, in final form 13 November 2012
Accepted for publication 15 November 2012
Published 8 January 2013
Online at stacks.iop.org/LPL/10/025102

Abstract
We demonstrate a simple, compact and low cost *Q*-switched erbium-doped fiber laser (EDFL) exploiting a graphene saturable absorber (GSA) for possible applications in metrology, sensing and medical diagnostics. The EDFL operates at 1560 nm with repetition rates of 31.3 kHz and 25 kHz with GSA1 and GSA2, respectively, at pump power of 120 mW. The repetition rate is smaller with a lower pump power. It has a pulse width of 7.5 μs and pulse energy of 43.7 nJ with GSA2 at 120 mW pump power. It is also observed that a thicker layer of graphene produces a *Q*-switched fiber laser with a lower pump threshold and a higher output energy, but smaller repetition rate and pulse width.

(Some figures may appear in colour only in the online journal)

1. Introduction

Q-switched fiber lasers are of great interest because of their versatile applications to remote sensing, range finding, medicine, material processing and telecommunications [1, 2]. They can be obtained through active [3] or passive techniques [4]. Compared to the active technique, passively *Q*-switched fiber lasers possess the attractive advantages of compactness, simplicity and flexibility in design. They have been intensively investigated using different kinds of saturable absorbers (SAs) [5–7] such as transition-metal-doped crystals [8], semiconductor saturable absorber mirrors (SESAMs) [9] and single-wall carbon nanotubes (SWCNTs) [10]. Saturable absorbers are materials whose absorptions decrease with increasing irradiances. In saturable absorbers, the molecules absorb radiation so strongly that substantial numbers of atoms can be excited to upper levels and significant changes occur in the absorption rates of the materials. When the ground and excited state populations are almost equal, the absorption becomes very small and the material is said to be 'bleached', or 'saturated'. An increase in irradiance leads to further bleaching until the material switches from absorbing to transmitting, thereby allowing the formation of a very intense and short (a few nanoseconds) pulse [11–13].

Recently, graphene has gained tremendous attention for SA applications. This is due to the gapless linear dispersion of Dirac electrons in graphene, which allows a broadband operation. The graphene is a flat monolayer of carbon atoms tightly packed into a two-dimensional (2D) honeycomb lattice. It can be stacked to form 3D graphite, rolled to form 1D nanotubes and wrapped to form 0D fullerenes [14]. Nair *et al* [15] have demonstrated that, despite being only one atom thick, graphene absorbs a significant ($\pi\alpha = 2.3\%$) fraction of incident white light due to its unique electronic structure. The optical absorption is also found to be frequency independent and proportional to the number of layers [16]. Boe *et al* [17] have recently reported that graphene can provide outstanding saturable absorption, where it has a much lower saturation intensity, larger saturable-absorption modulation depth and a higher damage threshold compared to SWCNTs. Therefore, many techniques have been developed

 © 2013 Astro Ltd Printed in the UK & the USA

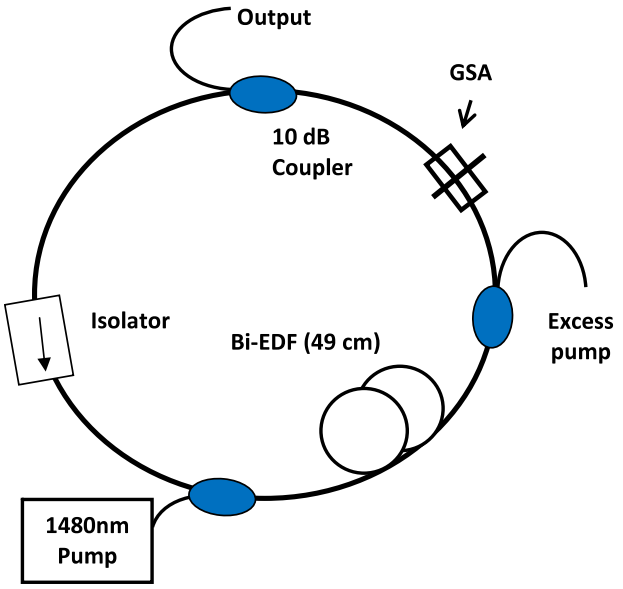

Figure 1. Experimental setup of the proposed graphene based *Q*-switched EDFL.

to integrate graphene into fiber devices to construct SAs for passive pulse construction [17], which are mostly based on graphene mode-locked fiber lasers. In this letter, we demonstrate a simple and compact *Q*-switched EDFL using a graphene solution deposited on the end surface of a fiber ferrule, which is then incorporated in a ring laser cavity to act as a saturable absorber. The *Q*-switching performance of the laser is investigated for two different graphene saturable absorbers (GSAs).

2. Experiment

Figure 1 shows an experimental setup for the deposition of graphene onto the end surface of the ferrule, whereby the optical deposition method proposed by Kashiwagi *et al* [18] and Martinez *et al* [19] was used. In the optical deposition method, injecting amplified light to the fiber end will create optical trapping, thermally driven convection flow and thermo-diffusion [20]. The interaction of the laser beam and graphene composite is developed by optical trapping and this will increase the solution temperature due to amplified injected light. The difference in temperature between the fiber ferrule and heated solution creates a thermo-diffusion effect where the graphene flakes are attracted to the cooler fiber ferrule. The graphene flakes (in solution) used in the experiment are supplied by Graphene Research Ltd, and prior to deposition the solution is agitated for 30 min using an ultrasonic bath. Optical radiation from a 1550 nm laser source is amplified by an optical amplifier to 30 dBm and then propagated through a fiber pigtail via an optical circulator. The end surface of the pigtail is dipped into the graphene aqueous suspension and the whole deposition process of the graphene on the fiber ferrule core is monitored by an optical power meter and recorded using a GPIB card connected to a computer through a LabVIEW 7.1 interface. The deposition

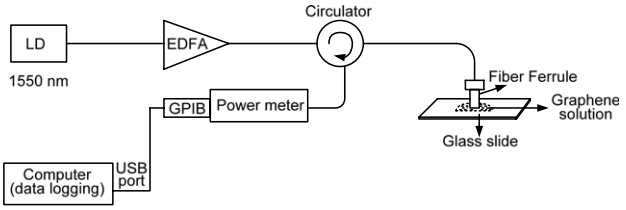

Figure 2. Experimental setup for depositing graphene on the fiber end surface by optical radiation.

process is halted when there is a sudden change in power, and from the experiment a rapid increment of the reflected light power is observed after 10 s. The light source is turned off 5 s after the sudden change of power, which indicates that graphene has been deposited on the ferrule end surface. The fiber is then removed from the solution. After water evaporation, the ferrule is connected to another ferrule to form a fiber compatible graphene saturable absorber (GSA).

Figure 2 shows the experimental setup of the proposed compact *Q*-switched EDFL using the fabricated GSA as a passive *Q*-switcher. A 49 cm long bismuth based erbium-doped fiber (Bi–EDF) with erbium ion concentration of 3250 ppm and cutoff wavelength of 1450 nm is used as the gain medium. The Bi–EDF is forward pumped by a 1480 nm laser diode through a 1480/1550 nm wavelength division multiplexer (WDM). Another WDM is placed after the Bi–EDF to remove the excess pump power. The laser output is obtained via a 10 dB optical coupler located after the GSA, which channels out about 10% of the oscillating light from the ring cavity. The output is analyzed using an optical spectrum analyzer (OSA) of 0.02 nm resolution and a 500 MHz oscilloscope with a 6 GHz bandwidth lightwave detector. An optical isolator is incorporated after the optical coupler to ensure that light propagates in a unidirectional manner. The rest of the cavity is made of SMF-28 single-mode fiber. All components used in our setup are polarization independent, i.e. they support any light polarization. No polarization controller (PC) is included in our cavity as we had observed earlier that a PC did not improve our pulse stability. There is no significant pulse jitter observed through the oscilloscope during the experiment. The experiment is carried out for two different GSAs: GSA1 and GSA2. The insertion loss of GSA1 and GSA2 are determined to be around 0.5 dB while the total length of the cavity is measured to be about 25 m. For GSA2, graphene is deposited on both end surface faces of the ferrules and thus it has a thicker graphene layer compared to that on the GSA1.

3. Result and discussion

The proposed EDFL started to lase with the passive *Q*-switching mode at the pump power of around 50 mW. The pump threshold was relatively low compared to that of an SWNT or SESAM based *Q*-switched EDFL, mainly owing to a lower saturation intensity of the graphene. Figure 3 compares the oscilloscope traces of the *Q*-switched pulse trains for two different GSAs when the pump power is fixed

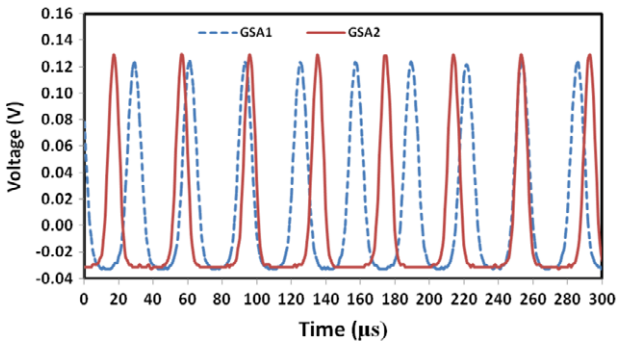

Figure 3. Typical pulse trains for the proposed EDFL configured with GSA1 and GSA2 at a pump power of 120 mW.

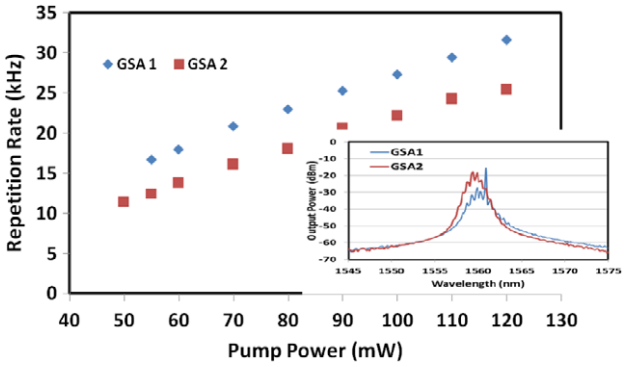

Figure 4. Repetition rate as a function of 1480 nm pump power. The inset shows the optical spectrum of the laser at a pump power of 120 mW.

at the maximum value of 120 mW. As shown in the figure, repetition rates of 31.3 and 25 kHz are obtained with GSA1 and GSA2, respectively. Since a thicker graphene layer means more absorption, it takes a longer time for the GSA2 to bleach and thus its repetition rate is lower than that of GSA1. Unlike a mode-locked fiber laser, where the repetition rate is dependent on cavity length, the repetition rate in a *Q*-switched fiber laser varies with pump power. Figure 4 shows the repetition rate as a function of pump power for both cases. As the pump power increases, more gain is provided to saturate the GSA. Since pulse generation relies on saturation, the repetition rate increases with the pump power as shown in figure 4. For instance, with GSA1, the pulse repetition rate of the *Q*-switched EDFL can be widely tuned from 16.7 to 31.6 kHz by varying the pump power from 55 to 120 mW. At every specific repetition rate and pump power, the *Q*-switching pulse output was stable and no significant pulse jitter was observed on the oscilloscope. The inset of figure 4 shows the output spectrum for the proposed *Q*-switched EDFL configured with FSA1 and GSA2. As shown in the figure, the laser operates at around 1560 nm with a full width at half maximum of around 0.3 nm.

Figure 5 shows the pulse width and the pulse energy as a function of the pump power. As seen in the figure, increasing the pump power makes the pulse width narrower and the pulse energy higher for both GSAs. At the pump power of 120 mW, the *Q*-switched EDFL has a pulse width of 7.5 μs

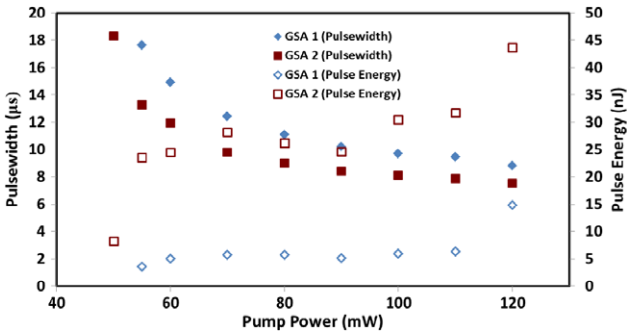

Figure 5. Pulse width and pulse energy as a function of input pump power.

and pulse energy of 43.7 nJ using GSA2. A thicker layer of graphene (in GSA2) implies that more atoms are stored in the excited state level, and consequently more stimulated emission occurs when the GSA bleaches. This in turn generates more output power. This explains why the output energy of GSA2 is significantly higher than that of GSA1. The reason is also linked to the observation that using GSA2 yields a lower pulsing threshold. The threshold pump powers for *Q*-switching operation with GSA1 and GSA2 are observed to be 51.3 and 47.6 mW, respectively. These results indicate that graphene has a larger potential for better *Q*-switching and saturable absorption compared to conventional light absorbing components when carefully employed in an appropriate laser system. The proposed EDFL is simple, low in cost and suitable for metrology, environmental sensing and biomedical diagnostics.

4. Conclusion

A simple and compact *Q*-switched EDFL is demonstrated using a GSA, which is obtained by depositing the graphene solution on the end surface of a fiber ferrule. It is found that a thicker layer of graphene produces a *Q*-switched fiber laser with a lower pump threshold and higher energy but smaller repetition rate and pulse width. The EDFL operates at 1560 nm with a repetition rate that varies with the pump power. For instance, the repetition rate of the EDFL configured with GSA1 can be widely tuned from 16.7 to 31.6 kHz by varying the pump power from 55 to 120 mW. The EDFL has a pulse width of 7.5 μs and pulse energy of 43.7 nJ with GSA2 at 120 mW pump power.

Acknowledgments

This project was funded by the Ministry of Higher Education under PRGS (grant no PR003-2011A) and HIRG (grant no HIR-MOHE D000009-16001).

References

[1] Koechner W 1996 *Solid-State Laser Engineering* 4th edn (Berlin: Springer)
[2] Skorczakowski M *et al* 2010 *Laser Phys. Lett.* **7** 498–504
[3] Andrés M V, Cruz J L, Díez A, Pérez-Millán P and Delgado-Pinar M 2008 *Laser Phys. Lett.* **5** 93–9

[4] Garnov S V *et al* 2007 *Laser Phys. Lett.* **4** 648
[5] Krylov A A, Kryukov P G, Dianov E M and Okhotnikov O G 2009 *Quantum Electron.* **39** 882
[6] Solodyankin M A, Obraztsova E D, Lobach A S, Chernov A I, Tausenev A V, Konov V I and Dianov E M 2008 *Opt. Lett.* **33** 1336
[7] Kurkov A S 2011 *Laser Phys. Lett.* **8** 335–42
[8] Pan L, Utkin I and Fedosejevs R 2007 *IEEE Photon. Technol. Lett.* **19** 1979
[9] Huang J Y, Huang W C, Zhuang W Z, Su K W, Chen Y F and Huang K F 2009 *Opt. Lett.* **34** 2360
[10] Zhou D P, Wei L, Dong B and Liu W K 2010 *IEEE Photon. Technol. Lett.* **22** 9
[11] Luo A, Luo Z and Xu W 2011 *Laser Phys.* **21** 395
[12] Harun S W, Akbari R, Arof H and Ahmad H 2011 *Laser Phys. Lett.* **8** 449
[13] Moghaddam M R A, Harun S W, Akbari R and Ahmad H 2011 *Laser Phys.* **21** 913
[14] Geim A K 2009 *Science* **324** 1530–4
[15] Nair R R, Blake P, Grigorenko A N, Novoselov K S, Booth T J, Stauber T, Peres N M R and Geim A K 2008 *Science* **320** 1308
[16] Yamashita S 2012 *J. Lightwave Technol.* **30** 427–47
[17] Bao Q L, Zhang H, Wang Y, Ni Z, Yan Y, Shen Z X, Loh K P and Tang D Y 2009 *Adv. Funct. Mater.* **19** 3077
[18] Kashiwagi K, Yamashita S and Set S Y 2009 *Opt. Express* **17** 5711–5
[19] Martinez A, Fuse K, Xu B and Yamashita S 2010 *Opt. Express* **18** 23054–61
[20] Kim H, Cho J, Jang S-Y and Song Y-W 2011 *Appl. Phys. Lett.* **98** 021104

IOPscience iopscience.iop.org

Home Search Collections Journals About Contact us My IOPscience

A Q-Switched Erbium-Doped Fiber Laser with a Carbon Nanotube Based Saturable Absorber

This article has been downloaded from IOPscience. Please scroll down to see the full text article.

2012 Chinese Phys. Lett. 29 114202

(http://iopscience.iop.org/0256-307X/29/11/114202)

View the table of contents for this issue, or go to the journal homepage for more

Download details:
IP Address: 161.142.24.130
The article was downloaded on 28/11/2012 at 05:44

Please note that terms and conditions apply.

CHIN. PHYS. LETT. Vol. 29, No. 11 (2012) 114202

A Q-Switched Erbium-Doped Fiber Laser with a Carbon Nanotube Based Saturable Absorber *

S. W. Harun[1,2**], M. A. Ismail[1], F. Ahmad[1], M. F. Ismail[1], R. M. Nor[3], N. R. Zulkepely[3], H. Ahmad[2]

[1]*Department of Electrical Engineering, University of Malaya 50603 Kuala Lumpur, Malaysia*
[2]*Photonics Research Center, Department of Physics, University of Malaya, 50603 Kuala Lumpur, Malaysia*
[3]*Department of Physics, University of Malaya, 50603 Kuala Lumpur, Malaysia*

(Received 13 June 2012)

We demonstrate a simple, compact and low cost Q-switched erbium-doped fiber laser (EDFL) using single-wall carbon nanotubes (CNTs) as a saturable absorber for possible applications in metrology, sensing, and medical diagnostics. The EDFL operates at around 1560 nm with repetition rates of 16.1 kHz and 6.4 kHz with saturable absorbers SA1 and SA2 at a pump power of 120 mW. The absorbers are constructed by optically driven deposition and normal deposition techniques. It is observed that the optical deposition method produces a Q-switched EDFL with a lower threshold of 70 mW and better Q-switching performance compared to that of the normal deposition method. The EDFL also has pulse energy of 90.3 nJ and pulse width of 11.6 μs at 120 mW pump power.

PACS: 42.60.Da, 42.60.Fc DOI: 10.1088/0256-307X/29/11/114202

Research interest on fiber lasers has grown after the introduction of doped fibers as the gain medium, resulting in an intrinsically excellent beam quality.[1,2] They can be designed to operate in either continuous-wave or pulsed mode. Q-switched fiber lasers are generally used for generating high-energy pulses at relatively low repetition rates.[3] They have attracted much interest due to their versatile applications in remote sensing, range finding, medicine, material processing, and telecommunications.[3–5] They can be constructed via active[3] or passive techniques.[4] Compared to those fabricated using the active technique, passively Q-switched fiber lasers are advantageous in terms of compactness, simplicity, and flexibility in design. They have been intensively investigated using different kinds of saturable absorbers (SAs) such as transition metal doped crystals[6] and semiconductor saturable absorber mirrors (SESAMs).[7] However, these SAs are complex and expensive to be fabricated. Furthermore, they are not compatible with many optical fibers, which limits their widespread application.

Recently, single-wall carbon nanotubes (SWCNTs) have shown promising potential in mode locked fiber laser systems due to its intrinsic saturable absorption properties, ultrafast recovery time and wide absorption wavelength bandwidth.[8,9] In this Letter, we demonstrate a simple and compact Q-switched erbium-doped fiber laser (EDFL) using a CNT-based saturable absorber (CNT-SA) with good compatibility with optical fibers. The SA is constructed by optically controlling the deposition of CNTs onto the end of fiber ferrules. The relative performance of the Q-switched EDFL is also investigated by comparing it with another CNT-SA which was obtained using a normal deposition technique.

The fabrication process starts by preparing a homogeneous suspension by mixing approximately 0.5 mg SWCNTs (95% pure, diameter of 1–2 nm and length of 5–10 μm) with 1 ml of dimethylformamide (DMF) solvent and then sonicated for one hour. The suspension was centrifuged at 1000 rpm for one hour to remove large particles of undispersed SWCNT to obtain dispersed suspension that is stable for weeks. Then optical deposition method proposed by Kashiwagi *et al.*[10] and Martinez *et al.*[11] was employed to deposit SWCNTs onto optical fiber end with ferrule to be used as an SA. In this method, an amplified light is injected into the fiber ferrule end to create an optical trapping, thermally driven convection flow and thermo-diffusion.[12] The interaction between the laser beam and CNTs is initiated by the optical trapping that increases the solution temperature by the amplified injected light. The difference in temperature between the fiber ferule and heated solution creates thermo-diffusion effect where the CNTs are attracted to the cooler fiber ferule. In the experiment, a 1550 nm laser source was amplified at around 25 dBm and launched into a fiber FC/PC connector via an optical circulator. Then the end surface of the fiber ferrule of the connector was immersed into a droplet of the prepared CNTs solution and the reflected light from the connector was monitored by an optical power meter. The deposition process was halted when there was a sudden change in the reflected light power which indicates that the CNTs have been sufficiently deposited on the ferrule end surface. The connector with CNTs was then mated to another clean connector to construct an SA1 that could be easily spliced to the

*Supported by University of Malaya PPP under Grant No PV029/2011B.
**Corresponding author. Email: swharun@um.edu.my
© 2012 Chinese Physical Society and IOP Publishing Ltd

cavity of the fiber laser. The insertion loss of the SA1 was measured to be about 1.8 dB.

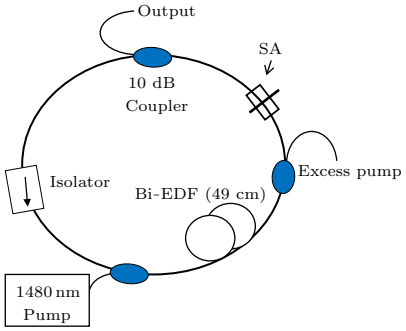

Fig. 1. Experimental setup of the proposed CNT-based Q-switched EDFL.

Figure 1 shows the experimental setup of the compact Q-switched EDFL proposed using the fabricated SA as a passive Q-switcher. A 49-cm-long bismuth-based erbium-doped fiber (Bi-EDF) with erbium ion concentration of 3250 ppm and cutoff wavelength of 1450 nm is used as the gain medium. This fiber is an advanced erbium doped fiber, which is based on bismuth oxide host glass and thus allows both compactness and great broadband transmission capability.[13] The Bi-EDF is forward pumped by a 1480 nm laser diode through a 1480/1550 nm wavelength division multiplexer (WDM). Another WDM is placed after the Bi-EDF to remove the excess pump power. The laser output is extracted from a 10 dB optical coupler located after the SA, which releases about 10% of the oscillating light from the ring cavity. The output is analyzed by an optical spectrum analyzer (OSA) of 0.02 nm resolution and a 500 MHz oscilloscope with 6 GHz bandwidth lightwave detector. An optical isolator is incorporated after the optical coupler to ensure that light propagates unidirectionally. The rest of the cavity is made of SMF-28 single-mode fiber. All components used in our setup are polarization independent, i.e. they support any light polarization. No polarization controller (PC) is included in our cavity as we had observed earlier that a PC did not improve our pulse stability. There was no significant pulse jitter observed through oscilloscope during the experiment. The experiment was also carried out using another SA (SA2), which was obtained by the normal deposition method for comparison. In this technique, the deposition of CNTs on the fiber ferrule is carried out by dropping a droplet of the prepared CNTs solution to the end of fiber ferrule using micropipette. After that, the fiber ferrule was left at room temperature to let the solution evaporate for one hour. The SA2 has an insertion loss of about 2.0 dB.

Figure 2 compares the oscilloscope traces of the Q-switched pulse trains of the proposed EDFL using the two fabricated CNT-SAs (SA1 and SA2) while the pump power was fixed at the maximum value of 120 mW. As stated earlier, the SA1 and SA2 were developed using the optical and normal deposition method, respectively. As seen in the figure, the repetition rates of 16.1 kHz and 6.4 kHz are obtained for the SA1 and SA2 setup, respectively. It is believed that the normal deposition method allows more CNTs to be deposited on the fiber. This is evident from the microscope image of the ferrule end of SA2, which is observed to be darker at the core area compared to that of SA1. Since thicker CNTs layer means more absorption, it takes a bit longer time for the SA2 to bleach and thus its repetition rate is lower than that of the SA1. It is also observed that the proposed EDFLs start to lase with the passive Q-switching mode at the pump power of around 70 mW and 110 mW for the SA1 and SA2, respectively. The pump threshold of the EDFL with SA2 is higher compared to that of SA1, mainly due to higher absorption of the thicker CNTs layer. Since the CNTs layer is not uniformly distributed on the core surface of the SA2, the Q-switching performance of the laser is affected.

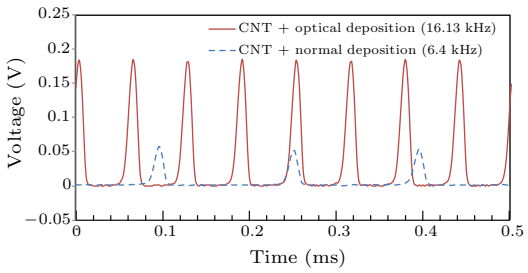

Fig. 2. Typical pulse trains for the proposed EDFL configured with SA1 and SA2 at a pump power of 120 mW.

Figure 3 shows the output spectrum of the proposed Q-switched EDFL constructed using the SA1 and SA2. As shown in the figure, the laser operates at around 1559.2 nm and 1557.8 nm respectively. The laser operating wavelength is shorter for the one with SA2 compared to that with SA1. This is attributed to the SA2, having a larger loss and thus decreasing the oscillating wavelength to acquire a higher gain for compensating the loss. The full-width half maximum (FWHM) of more than 1.0 nm is obtained with SA1, which is so much larger than that of the SA2. This indicates that SA1 produces a better Q-switching pulse compared the one generated by the SA2. Unlike the mode-locked fiber laser wherein the repetition rate is dependent on cavity length, the repetition rate of the Q-switched fiber laser varies with pump power. The inset of Fig. 3 shows the repetition rate as a function of pump power for the EDFL configured with SA1. As the pump power increases, more gain is provided to saturate the SA. Since pulse generation relies on saturation, the repetition rate increases with the pump power as shown in the figure. The pulse repetition rate of the Q-switched EDFL can be widely tuned from 8.2 kHz to 16.1 kHz by varying the pump power

from 70 mW to 120 mW. At every specific repetition rate and pump power, the Q-switching pulse output was stable and no significant pulse jitter was observed on the oscilloscope.

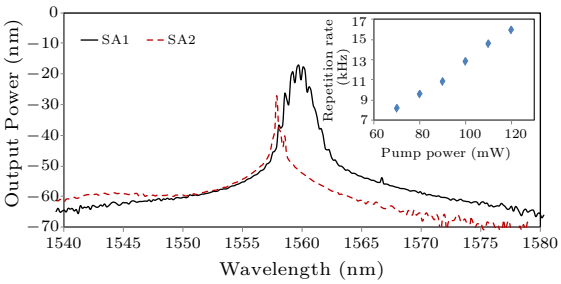

Fig. 3. Optical spectra of the Q-switched EDFL with SA1 and SA2 at pump power of 120 mW. Inset: the repetition rate as a function of 1480 nm pump power.

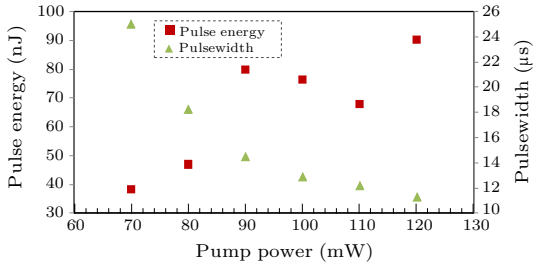

Fig. 4. Pulse energy and pulse width as a function of input pump power.

Figure 4 shows the pulse energy and the pulse width as a function of the pump power for the proposed EDFL with SA1. As seen in the figure, raising the pump power increases the pulse energy and reduces the pulse width. It is also observed that the pulse energy shows a drop of around 110 mW in pump power, which is most probably due to the mode competition inside the laser cavity which slightly changes the operating wavelength. This phenomenon exists for both SAs and the incorporation of a band-pass filter in the laser cavity is expected to improve the laser output energy. At the pump power of 120 mW, the Q-switched EDFL has a pulse energy of 90.3 nJ and pulse width of 11.3 μs as depicted in Fig. 4. With SA2, the pulse energy and pulse width are obtained at 5.5 nJ and 11.6 μs, respectively, for 1480 nm pumping of 120 mW. A thicker and rough layer of CNTs in SA2 increases the cavity loss, causing unbalanced dispersive and nonlinear characteristic properties in the laser cavity. Consequently, it degrades both the attainable pulse energy and pulse width. These results indicate that CNTs have a larger potential for better Q-switching and saturable absorption compared to conventional light absorbing components when carefully employed in an appropriate laser system. The proposed EDFL is simple, low in cost and suitable for metrology, environmental sensing and biomedical diagnostics.

In conclusion, a simple and compact Q-switched EDFL is demonstrated using a CNT-SA, which is obtained by depositing the prepared CNTs solution on the end surface of fiber ferrule. It is found that the optical deposition method achieves a Q-switched fiber laser with a lower pump threshold and higher energy compared to that of normal deposition technique. The EDFL operates at around 1560 nm with repetition rates of 16.1 kHz and 6.4 kHz at the pump power of 120 mW and threshold pump powers of 70 mW and 110 mW, respectively. The repetition rate and pulse energy of the EDFL increase with the rise in pump power, but its pulse width reduces with the pump power. With the optical deposition method, the EDFL achieves a pulse energy of 90.3 nJ and pulse width of 11.6 μs at 120 mW pump power.

References

[1] Dong X Y, Tam H Y, Guan B O, Kai G Y and Dong X Y 2002 *Chin. Phys. Lett.* **19** 1296
[2] Wang R and Shen K 2001 *Chin. Phys.* B **10** 711
[3] Svelin O 1998 *Principles of Lasers* 4th edn (New York: Plenum) chap 8 p 311
[4] Tsai T Y and Fang Y C 2009 *Opt. Express* **17** 1429
[5] Yap Y K, Richard M De La Rue, Pua C H, Harun S W and Ahmad H 2012 *Chin. Opt. Lett.* **10** 041405
[6] Pan L, Utkin I and Fedosejevs R 2007 *IEEE Photon. Technol. Lett.* **19** 1979
[7] Huang J Y, Huang W C, Zhuang W Z, Su K W, Chen Y F and Huang K F 2009 *Opt. Lett.* **34** 2360
[8] Sun Z, Rozhin A G, Wang F, Hasan T, Popa D, O'Neill W and Ferrari A C 2009 *Appl. Phys. Lett.* **95** 253102
[9] Wang X Q, Wang M, Li Z H and Liu Z Y 2004 *Acta Phys. Sin.* **53** 2254 (in Chinese)
[10] Kashiwagi K, Yamashita S and Set S Y 2009 *Opt. Express* **17** 571
[11] Martinez A, Fuse K, Xu B and Yamashita S 2010 *Opt. Express* **18** 23054
[12] Kim H, Cho J, Jang S Y and Song Y W 2011 *Appl. Phys. Lett.* **98** 021104
[13] Cheng X S, Parvizi R, Ahmad H and Harun S W 2009 *IEEE Photon. J.* **1** 259